

IMPACTS OF CLIMATE NONSTATIONARITIES ON  
HYDROCLIMATOLOGICAL VARIABLES IN TURKEY

A THESIS SUBMITTED TO  
THE GRADUATE SCHOOL OF NATURAL AND APPLIED SCIENCES  
OF  
MIDDLE EAST TECHNICAL UNIVERSITY

BY

RIZWAN AZIZ

IN PARTIAL FULFILLMENT OF THE REQUIREMENTS  
FOR  
THE DEGREE OF DOCTOR OF PHILOSOPHY  
IN  
CIVIL ENGINEERING

AUGUST 2018



Approval of the thesis:

**IMPACTS OF CLIMATE NONSTATIONARITIES ON  
HYDROCLIMATOLOGICAL VARIABLES IN TURKEY**

submitted by **RIZWAN AZIZ** in partial fulfillment of the requirements for the degree of **Doctor of Philosophy in Civil Engineering Department, Middle East Technical University** by,

Prof. Dr. Halil Kalıpçılar  
Dean, Graduate School of **Natural and Applied Sciences** \_\_\_\_\_

Prof. Dr. İsmail Özgür Yaman  
Head of Department, **Civil Engineering** \_\_\_\_\_

Prof. Dr. İsmail Yücel  
Supervisor, **Civil Engineering Dept., METU** \_\_\_\_\_

Assoc. Prof. Dr. Ceylan Talu Yozgatlıgil  
Co-supervisor **Statistics Dept., METU** \_\_\_\_\_

**Examining Committee Members:**

Prof. Dr. Elçin Kentel Erdoğan  
Civil Engineering Dept., METU \_\_\_\_\_

Prof. Dr. İsmail Yücel  
Civil Engineering Dept., METU \_\_\_\_\_

Assoc. Prof. Dr. Koray K. Yılmaz  
Geological Engineering Dept., METU \_\_\_\_\_

Prof. Dr. Ömer Lütfi Şen  
Eurasia Institute of Earth Sciences, ITU \_\_\_\_\_

Prof. Dr. Cemal Saydam  
Environmental Engineering Dept., Hacettepe University \_\_\_\_\_

**Date:** \_\_\_\_\_ 29/08/2018

**I hereby declare that all information in this document has been obtained and presented in accordance with academic rules and ethical conduct. I also declare that, as required by these rules and conduct, I have fully cited and referenced all material and results that are not original to this work.**

Name, Last Name : Rizwan Aziz  
Signature :

## **ABSTRACT**

# **IMPACTS OF CLIMATE NONSTATIONARITIES ON HYDROCLIMATOLOGICAL VARIABLES IN TURKEY**

Aziz, Rizwan

Ph.D., Department of Civil Engineering

Supervisor: Prof. Dr. İsmail Yücel

Co-supervisor: Assoc. Prof. Dr. Ceylan Talu Yozgatlıgil

August 2018, 257 pages

Using multiple nonstationary frequency distributions, this study investigated the impacts of nonstationarities on yearly and seasonal extremes of hydroclimatological variables for observations and CORDEX projected data of period 2050-2100 in Turkey. Future streamflow is generated using the calibrated HBV-light hydrological model. Evaluation of CORDEX models suggests that for precipitation RCMs originated from GCMs EC-EARTH and HadGEM2-ES and for temperature GCM HadGEM2-ES coupled with RCM CCLM4-8-17 showed better agreement with observations. GEV distribution fits observation better than other distributions for all variables. During historical period generally in Turkey, and particularly in the eastern part, nonstationarity impacts are positive on yearly as well as seasonal temperature maxima (up to 5°C) and minima (up to 10°C). These impacts are amplified during the projection period. For observed precipitation, positive impacts (up to 50%) are recorded for yearly maxima but many stations, particularly in South-Eastern Anatolia, Central Anatolia, and Eastern Anatolia, exhibited negative impacts (up to 40%). Mostly positive impacts are found during the projection period for

yearly and seasonal precipitation maxima. Some reversal in the impact type also appeared from the current to the future period. In Upper Euphrates basin, for annual high flows, four sub-basins showed positive impacts (up to 12%) and four sub-basins showed negative impacts (up to 30%) however mostly positive impacts are obtained for annual and seasonal maxima of low flows. Bias-adjusted RCMs tend to lose the nonstationarity signal for precipitation. It is suggested that in the operational and planning strategies of existing and new hydraulic structures, the nonstationarity approach should be taken into account to be in the safe side and economical scale. More precautions should be given to water conservation as milder minimum temperatures might contribute to less snowpack in mountainous regions.

**Keywords:** Nonstationarities, Temperature, Precipitation, Streamflow, GCM/RCM,

**ÖZ**

**TÜRKİYE ÜZERİNDEKİ HİDROKLİMATOLOJİK  
DEĞİŞKENLERE İKLİM DURAĞANSIZLIKLARININ  
ETKİLERİ**

Aziz, Rizwan

Doktora, İnşaat Mühendisliği Bölümü

Tez Yöneticisi: Prof. Dr. İsmail Yücel

Ortak Tez Yöneticisi: Doç. Dr. Ceylan Talu Yozgatlıgil

Ağustos 2018, 257 sayfa

Çoklu durağansız dağılım fonksiyonları kullanılarak, bu çalışma da Türkiye deki hidroklimatolojik değişkenlerin yıllık ve mevsimlik ekstremlerdeki durağansızlık etkileri gözlem ve 2050-2100 CORDEX periyodu için araştırılmıştır. Gelecek dönem akımı kalibre edilmiş HBV-Light hidrolojik modeli kullanılarak üretilmiştir. CORDEX modellerinin değerlendirmesine göre yağış için EC-EARTH ve HadGEM2-ES den üretilen RCM ler ve sıcaklık için CCLM4-8-17RCM modeli ile birleştirilmiş GCM HadGEM2-ES modeli gözlemler ile daha iyi bir yakınlık göstermiştir. Bütün değişkenler için, GEV dağılımı diğer dağılımlardan gözlemlere daha iyi uygundur. Gözlem periyodu süresince genellikle Türkiye de, ve özellikle doğu kısmında, durağansızlık etkileri hem yıllık hemde mevsimsel en yüksek (+5 °C e kadar) ve en düşük sıcaklık (+10 °C e kadar) lar için pozitifdir. Bu etkiler gelecek dönemde güçlenmektedir. Gözlenmiş yağışlar da, pozitif etkiler (%50 e kadar) yıllık maksimum için kaydedilmiştir fakat çoğu istasyon, özellikle Güney-Doğu Anadolu, Orta Anadolu, ve Doğu Anadolu da negatif etkiler (%40 a kadar) göstermiştir. Gelecek dönem süresince hem yıllık hemde mevsimsel yağış maksimumu için çoğukez pozitif etkiler

bulunmuştur. Şuandan gelecek zamana etki tipinde bazı ters dönüşümler de görülmüştür. Yukarı Fırat Havzasında, yıllık yüksek akımlar için, dört alt-havza pozitif etkiler gösterdi (+12 e kadar) ve dört alt-havza negatif etkiler (-30 e kadar) göstermiştir. Fakat, daha çok pozitif etkiler düşük akımların yıllık ve mevsimlik maksimumları için elde edilmiştir. Düzeltilmiş RCM ler yağış için durağansızlık sinyalini kaybetme eğilimindedir. Mevcut ve yeni hidrolik yapıların planlama aşamalarında ve işletilmelerinde, durağansızlık yaklaşımının ekonomik açıdan ve tedbirli olmak için dikkate alınması önerilir. Daha ılıman düşük sıcaklıklar dağlık bölgelerde kar toplanmasını azaltırken suyun korunmasına karşı daha fazla önlem verilmelidir

**Anahtar Kelimeler:** Durağansızlık, Sıcaklık, Yağış, Akım, GCM/RCM

**To**  
**My Sister Saima Aziz**  
**and**  
**My Brother Ahsan Aziz**

## ACKNOWLEDGEMENTS

Firstly, I would like to express my profound gratitude to my supervisor Prof. Dr. İsmail Yücel for his guidance, precious ideas, and tremendous motivation throughout my Ph.D. study. I appreciate his contribution of ideas and time, which enlightened my way to make this study more productive. Besides my advisor, I would also like to extend my gratitude to my Co-supervisor Assoc. Prof. Dr. Ceylan Talu Yozgatlıgil for her valuable help and advice. My sincere thanks to our academic and supporting staff of METU as well.

I cordially acknowledge the scholarship received towards my PhD from the Higher Education Commission, Pakistan.

I am extremely grateful to my friend M. Uzair Ahsan & Amjad Iqbal for their continuous and valuable help throughout this thesis. Sincere thanks to my labmates Faisal Baig, Anil Y. Poyraz, Mehdi Afshar, and Hüseyin N. Karaaslan with whom I have spent great time. My sincere appreciation also goes to my friends Ishfaq Bashir, S. Tanvir Shah, Bakht Z. Afridi, M. Saad Arshad, Saeed A. Khan, Mohsin Ali, Qanbar A. Shah, and Usman Hassan. Their amazing company have been a great support to me during this whole period.

Heartfelt gratitude to my brothers Asim Aziz & Ahsan Aziz, my sisters Saima Aziz & Asma Aziz and my cousin Aroosa Asim for providing me with much needed moral support and motivation. I owe the deepest thanks to my parents Abdul Hamid and Surriya Begum, whom I admire as great role models. Their never-ending support, unconditional love, prayers, and guidance have been with me in whatever I pursue. I thank you immensely.

And thank you Turkey for being a great host.

## TABLE OF CONTENTS

ABSTRACT .....	v
ÖZ.....	vii
ACKNOWLEDGEMENTS.....	x
TABLE OF CONTENTS .....	xi
LIST OF TABLES.....	xiv
LIST OF FIGURES .....	xvii
ABBREVIATIONS .....	xxix
CHAPTERS.....	1
1. INTRODUCTION .....	1
1.1. Background and Motivation .....	1
1.2. Problem Definition.....	3
1.3. Literature Review.....	5
1.3.1. Historical Overview of Nonstationary Frequency Analyses .....	5
1.3.2. Historical Overview of Status of Climate Change in Turkey .....	8
1.4. Goals and Objectives .....	15
1.5. Thesis Description .....	16
2. STUDY AREA AND DATA .....	19
2.1. Study Area .....	19
2.2. Data Used.....	24
2.2.1. Observational Data.....	24
2.2.2. CORDEX Data.....	29
3. METHODOLOGY .....	31

3.1. Stationary and Nonstationary Distributions .....	32
3.2. Hydrological Modeling .....	39
3.3. CORDEX Performance Evaluation .....	45
3.3.1. Root Mean Square Error .....	46
3.3.2. Mean Absolute Error .....	47
3.3.3. Mean Bias Error .....	47
3.3.4. Correlation Coefficient .....	48
3.4. Bias Corrected CORDEX RCMs .....	49
3.4.1. Distribution Based Scaling (DBS Method) .....	50
3.4.2. Cumulative Distribution Function Transform (CDF-transform Method) .....	53
4. CORDEX PERFORMANCE EVALUATION .....	55
4.1. Results .....	55
4.1.1. Precipitation Evaluation .....	55
4.1.2. Temperature Evaluation .....	79
4.2. Discussion .....	102
5. NONSTATIONARITY ANALYSES OF PRECIPITATION .....	105
5.1. Results .....	105
5.1.1. Distribution Fitting Under Stationary and Nonstationary Conditions ....	105
5.1.2. Nonstationarity Impacts During Historical Time Period (1971-2015)...	109
5.1.3. Nonstationarity Impacts During Projection Time Period (2050-2100) ..	120
5.2. Discussion .....	133
6. NONSTATIONARITY ANALYSES OF TEMPERATURE .....	137
6.1. Results .....	137
6.1.1. Distribution Fitting Under Stationary and Nonstationary Conditions ....	137
6.1.2. Nonstationarity Impacts During Historical Time Period (1971-2015)...	142
6.1.3. Nonstationarity Impacts During Projection Time Period (2050-2100) ..	158
6.2. Discussion .....	181

7. NONSTATIONARITY ANALYSES OF STREAMFLOW .....	185
7.1. Results .....	185
7.1.1. Hydrological Modelling .....	185
7.1.2. Impacts of Nonstationarities on Observed Streamflow .....	191
7.1.3. Impacts of Nonstationarities for Projected Streamflow (2050-2100) .....	200
7.2. Discussion .....	204
8. ANALYSES OF BIAS-ADJUSTED CORDEX RCMS .....	209
8.1. Results .....	210
8.1.1. Precipitation Analyses .....	210
8.1.2. Temperature Analyses .....	220
8.2. Discussion .....	230
9. SUMMARY AND CONCLUSIONS .....	233
9.1. Summary .....	233
9.2. Conclusions .....	237
9.3. Recommendations .....	238
REFERENCES .....	241
APPENDICES .....	251
A. PROGRAMING CODES .....	251
B. MISSING DATA .....	255
CURRICULUM VITAE.....	257

## LIST OF TABLES

### TABLES

Table 2-1 Information about meteorology stations of the Black Sea region .....	25
Table 2-2 Information about meteorology stations of the Marmara region.....	25
Table 2-3 Information about meteorology stations of the Central Anatolia region..	26
Table 2-4 Information about meteorology stations of the East Anatolia region.....	26
Table 2-5 Information about meteorology stations of the Aegean region .....	27
Table 2-6 Information about meteorology stations of the South-Eastern Anatolia region.....	27
Table 2-7 Information about meteorology stations of the Mediterranean region .....	27
Table 2-8 Information about the selected streamflow stations of Upper Euphrates basin and their relevant geographical information.....	28
Table 2-9 GCM-RCM matrix of CORDEX ensemble members .....	29
Table 3-1 Information about precipitation series used for nonstationary impact assessment.....	38
Table 3-2 Information about temperature series used for nonstationary impact assessment.....	38
Table 3-3 Information about streamflow series used for nonstationary impact assessment.....	39
Table 3-4 HBV parameters and range (Seibert, 1997).....	44

Table 4-1 Performance statistics summary of precipitation for the Marmara region	58
Table 4-2 Performance statistics summary of precipitation for the Aegean region ..	61
Table 4-3 Performance statistics summary of precipitation for the Mediterranean region .....	64
Table 4-4 Performance statistics summary of precipitation for the Central Anatolia region .....	67
Table 4-5 Performance statistics summary of precipitation for the Black Sea region .....	70
Table 4-6 Performance statistics summary of precipitation for the Eastern Anatolia region .....	73
Table 4-7 Performance statistics summary of precipitation for South-Eastern Anatolia .....	76
Table 4-8 Performance statistics summary of temperature for the Marmara region	81
Table 4-9 Performance statistics summary of temperature for the Aegean region. .	84
Table 4-10 Performance statistics summary of temperature for the Mediterranean region .....	87
Table 4-11 Performance statistics summary of temperature for the Central Anatolia region. ....	90
Table 4-12 Performance statistics summary of temperature for the Black Sea region .....	93
Table 4-13 Performance statistics summary of temperature for the Eastern Anatolia region. ....	96

Table 4-14 Performance statistics summary of temperature for the South-Eastern Anatolia region.....	99
Table 7-1 Information about fractional areas of land covers in sub-basin 2133.....	188
Table 7-2 Information about fractional areas of land covers in sub-basin 2157.....	188
Table 7-3 Information about fractional areas of land covers in sub-basin 2165.....	189
Table 7-4 Values of the goodness of fit indices for observed and simulated daily streamflow obtained from calibrated HBV-light model using Nash-Sutcliffe as the objective function.....	190
Table 7-5 Values of the goodness of fit indices for observed and simulated daily streamflow obtained from calibrated HBV-light model using log Nash-Sutcliffe as the objective function.....	190
Table 8-1 Performance Evaluation Statistics of Original and Bias-Adjusted RCM for precipitation.....	212
Table 8-2 Performance evaluation statistics of original and bias-adjusted RCM....	217
Table 8-3 Performance evaluation statistic of original and bias-adjusted RCM ....	222
Table 8-4 Performance evaluation statistics of original and bias-adjusted RCM...	227

## LIST OF FIGURES

### FIGURES

- Figure 1.1 Schematic diagram depicting the design flood “ $zq_0$ ” in addition to constant values of exceeding “ $p$ ” and non-exceeding “ $q = 1 - p$ ” probabilities throughout years 1 to  $t$  (stationary condition). ..... 7
- Figure 1.2 Schematic diagram depicting the design flood values “ $zq_0$ ” in addition to exceeding “ $pt$ ” and non-exceeding “ $qt = 1-pt$ ” probabilities as they vary through years 1 to  $t$  (the nonstationary case with increasing flood extremes)..... 8
- Figure 2.1 Map of Turkey showing the surrounding countries with international borders, the national capital Ankara. Downloaded from <https://turkeyfile.com/> ... 20
- Figure 2.2 Geographical regions of Turkey Downloaded from <https://www.mapsofworld.com/turkey/geography/> ..... 20
- Figure 2.3 Elevation map of Turkey, the location of the meteorological stations used along with identification of Upper Euphrates basin as a dark red polygon..... 22
- Figure 2.4 Elevation map of Upper Euphrates basin, the stream network, location of streamflow stations and identification of three selected watersheds (2133,2157 and 2164) for hydrological modeling..... 23
- Figure 2.5 EURO-CORDEX domain area surrounded by the inner square ..... 30
- Figure 3.1 Flowchart of Methodology..... 32
- Figure 3.2 The model structure and parameter description (left panel) and flow chart (right panel) of HBV model..... 43
- Figure 4.1 Comparison of regionally averaged mean daily observed and RCM precipitation for the Marmara region of Turkey..... 57

Figure 4.2 Comparison of regionally averaged mean daily observed and RCM precipitation for the Aegean region of Turkey.....	60
Figure 4.3 Comparison of regionally averaged mean daily observed and RCM precipitation for the Mediterranean region of Turkey.....	63
Figure 4.4 Comparison of regionally averaged mean daily observed and RCM precipitation for the Central Anatolia region of Turkey. ....	66
Figure 4.5 Comparison of regionally averaged mean daily observed and RCM precipitation for the Black Sea region of Turkey.....	69
Figure 4.6 Comparison of regionally averaged mean daily observed and RCM precipitation for the Eastern Anatolia region of Turkey. ....	72
Figure 4.7 Comparison of regionally averaged mean daily observed and RCM precipitation for South-Eastern Anatolia region of Turkey. ....	75
Figure 4.8 Summary of regional evaluation of CORDEX RCMs for precipitation. ....	78
Figure 4.9 Comparison of regionally averaged mean daily observed and RCM temperature for the Marmara region of Turkey. ....	80
Figure 4.10 Comparison of regionally averaged mean daily observed and RCM temperature for the Aegean region of Turkey.....	83
Figure 4.11 Comparison of regionally averaged mean daily observed and RCM temperature for the Mediterranean region of Turkey.....	86
Figure 4.12 Comparison of regionally averaged mean daily observed and RCM temperature for the Central Anatolia region of Turkey. ....	89
Figure 4.13 Comparison of regionally averaged mean daily observed and RCM temperature for the Black Sea region of Turkey.....	92

Figure 4.14 Comparison of regionally averaged mean daily observed and RCM temperature for the Eastern Anatolia region of Turkey.....	95
Figure 4.15 Comparison of regionally averaged mean daily observed and RCM temperature for the South-Eastern Anatolia region of Turkey.....	98
Figure 4.16 Summary of regional evaluation of CORDEX RCMs for temperature.....	101
Figure 5.1 Comparison of Negative Log-Likelihood of distributions for Yearly AMPs of observed data.....	106
Figure 5.2 Comparison of Negative Log-Likelihood of stationary and nonstationary distributions for (a) Winter (b) Spring (c) Summer and (d) Autumn AMPs of observed data .....	107
Figure 5.3 Comparative plots of probability density functions of GEV, Gumbel, Normal, and Lognormal distributions for annual maximum precipitation of Ankara. ....	108
Figure 5.4 Comparative plots of cumulative probability density functions of GEV, Gumbel, Normal, and Lognormal distributions for annual maximum precipitation of Ankara. ....	108
Figure 5.5 QQ-plots of GEV, Gumbel, Normal, and Lognormal distributions for annual maximum precipitation of Ankara. ....	109
Figure 5.6 Percentage Difference between 100-year stationary and nonstationary return levels for annual precipitation maxima using GEV, gumbel, normal and lognormal distributions.....	111
Figure 5.7 Percentage Difference between 100-year stationary and nonstationary return levels for annual precipitation maxima during winter using GEV, gumbel, normal and lognormal distributions.....	113

Figure 5.8 Percentage Difference between 100-year stationary and nonstationary return levels for annual precipitation maxima during spring using GEV, gumbel, normal and lognormal distributions ..... 115

Figure 5.9 Difference between 100-year stationary and nonstationary return levels for annual precipitation maxima during summer using GEV, gumbel, normal and lognormal distributions. .... 117

Figure 5.10 Percentage Difference between 100-year stationary and nonstationary return levels for annual precipitation maxima during autumn using GEV, gumbel, normal and lognormal distributions. .... 119

Figure 5.11 Ensemble mean and ensemble median of the percentage difference between 100-year stationary and nonstationary return levels for yearly AMPs of projected precipitation..... 121

Figure 5.12 Boxplots containing nonstationary impact values of 12 individual CORDEX ensemble members at gridded stations for yearly AMPs. Ensemble mean pointer (black asterisk) and ensemble median pointer (red asterisk) are also given 122

Figure 5.13 Ensemble mean and ensemble median of the percentage difference between 100-year stationary and nonstationary return levels for winter AMPs of projected precipitation..... 123

Figure 5.14 Boxplots containing nonstationary impact values of 12 individual CORDEX ensemble members at gridded stations for winter AMPs. Ensemble mean pointer (black asterisk) and ensemble median pointer (red asterisk) are also given 124

Figure 5.15 Ensemble mean and ensemble median of the percentage difference between 100-year stationary and nonstationary return levels for spring AMPs of projected precipitation..... 125

Figure 5.16 Boxplots containing nonstationary impact values of 12 individual CORDEX ensemble members at gridded stations for spring AMPs. Ensemble mean

pointer (black asterisk) and ensemble median pointer (red asterisk) are also given. .....	126
Figure 5.17 Ensemble mean and ensemble median of the difference between 100-year stationary and nonstationary return levels for summer AMPs of projected precipitation. ....	127
Figure 5.18 Boxplots containing nonstationary impact values of 12 individual CORDEX ensemble members at gridded stations for summer AMPs. Ensemble mean pointer (black asterisk) and ensemble median pointer (red asterisk) are also given. ....	128
Figure 5.19 Ensemble mean and ensemble median of the percentage difference between 100-year stationary and nonstationary return levels for autumn AMPs of projected precipitation. ....	129
Figure 5.20 Boxplots containing nonstationary impact values of 12 individual CORDEX ensemble members at gridded stations for autumn AMPs. Ensemble mean pointer (black asterisk) and ensemble median pointer (red asterisk) are also given. .....	130
Figure 5.21 Boxplots describing the intra-model variability of nonstationarity impact prediction .....	132
Figure 6.1 Comparison of Negative Log-Likelihood of distributions for Yearly AMTmax and AMTmin of observed data. ....	138
Figure 6.2 Comparison of Negative Log-Likelihood of stationary and nonstationary distributions for (a) Winter (b) Spring (c) Summer and (d) Autumn AMTmax and AMTmin of observed data.....	139
Figure 6.3 Comparative plots of probability density functions of GEV, Gumbel, Normal and Lognormal distributions .....	140

Figure 6.4 Comparative plots of cumulative probability density functions of GEV, Gumbel, Normal and Lognormal distributions .....	141
Figure 6.5 QQ-plots of GEV, Gumbel, Normal and Lognormal distributions .....	141
Figure 6.6 Difference ( $^{\circ}\text{C}$ ) between 100-year stationary and nonstationary return levels for annual temperature maxima using GEV, gumbel and normal distributions. ....	144
Figure 6.7 Difference ( $^{\circ}\text{C}$ ) between 100-year stationary and nonstationary return levels for annual temperature minima using GEV, gumbel and normal distributions. ....	145
Figure 6.8 Difference ( $^{\circ}\text{C}$ ) between 100-year stationary and nonstationary return levels for annual temperature maxima during winter using GEV, gumbel and normal distributions.....	147
Figure 6.9 Difference ( $^{\circ}\text{C}$ ) between 100-year stationary and nonstationary return levels for annual temperature minima during winter using GEV, gumbel and normal distributions.....	148
Figure 6.10 Difference ( $^{\circ}\text{C}$ ) between 100-year stationary and nonstationary return levels for annual temperature maxima during spring using GEV, gumbel and normal distributions.....	150
Figure 6.11 Difference ( $^{\circ}\text{C}$ ) between 100-year stationary and nonstationary return levels for annual temperature minima during spring using GEV, gumbel and normal distributions.....	151
Figure 6.12 Difference ( $^{\circ}\text{C}$ ) between 100-year stationary and nonstationary return levels for annual temperature maxima during summer using GEV, gumbel and normal distributions. ....	153

Figure 6.13 Difference (°C) between 100-year stationary and nonstationary return levels for annual temperature minima during summer using GEV, gumbel and normal distributions.....	154
Figure 6.14 Difference (°C) between 100-year stationary and nonstationary return levels for annual temperature maxima during autumn using GEV, gumbel and normal distributions.....	156
Figure 6.15 Difference (°C) between 100-year stationary and nonstationary return levels for annual temperature minima during autumn using GEV, gumbel and normal distributions.....	157
Figure 6.16 Ensemble mean (top) and ensemble median (bottom) of the difference (°C) between 100-year stationary and nonstationary return levels for yearly AMTmax (left) and AMTmin (right). ....	159
Figure 6.17 Boxplots containing nonstationary impact values of 12 individual CORDEX ensemble members at gridded stations for Yearly AMTmax. Ensemble mean pointer (black asterisk) and ensemble median pointer (red asterisk) are also given. ....	160
Figure 6.18 Boxplots containing nonstationary impact values of 12 individual CORDEX ensemble members at gridded stations for Yearly AMTmin. Ensemble mean pointer (black asterisk) and ensemble median pointer (red asterisk) are also given .....	161
Figure 6.19 Ensemble mean (top) and ensemble median (bottom) of the difference (°C) between 100-year stationary and nonstationary return levels for AMTmax (left) and AMTmin (right) during winter. ....	163
Figure 6.20 Boxplots containing nonstationary impact values of 12 individual CORDEX ensemble members at gridded stations for winter AMTmax. Ensemble mean pointer (black asterisk) and ensemble median pointer (red asterisk) are also given. ....	164

Figure 6.21 Boxplots containing nonstationary impact values of 12 individual CORDEX ensemble members at gridded stations for winter AMTmin. Ensemble mean pointer (black asterisk) and ensemble median pointer (red asterisk) are also given.....165

Figure 6.22 Ensemble mean (top) and ensemble median (bottom) of the difference (°C) between 100-year stationary and nonstationary return levels for AMTmax (left) and AMTmin (right) during spring. ....167

Figure 6.23 Boxplots containing nonstationary impact values of 12 individual CORDEX ensemble members at gridded stations for spring AMTmax. Ensemble mean pointer (black asterisk) and ensemble median pointer (red asterisk) are also given.....168

Figure 6.24 Boxplots containing nonstationary impact values of 12 individual CORDEX ensemble members at gridded stations for spring AMTmin. Ensemble mean pointer (black asterisk) and ensemble median pointer (red asterisk) are also given.....169

Figure 6.25 Ensemble mean (top) and ensemble median (bottom) of the difference (°C) between 100-year stationary and nonstationary return levels for AMTmax (left) and AMTmin (right) during summer. ....171

Figure 6.26 Boxplots containing nonstationary impact values of 12 individual CORDEX ensemble members at gridded stations for summer AMTmax. Ensemble mean pointer (black asterisk) and ensemble median pointer (red asterisk) are also given.....172

Figure 6.27 Boxplots containing nonstationary impact values of 12 individual CORDEX ensemble members at gridded stations for summer AMTmin. Ensemble mean pointer (black asterisk) and ensemble median pointer (red asterisk) are also given.....173

Figure 6.28 Ensemble mean (top) and ensemble median (bottom) of the difference (°C) between 100-year stationary and nonstationary return levels for AMTmax (left) and AMTmin (right) during autumn.....	175
Figure 6.29 Boxplots containing nonstationary impact values of 12 individual CORDEX ensemble members at gridded stations for autumn AMTmax. Ensemble mean pointer (black asterisk) and ensemble median pointer (red asterisk) are also given. ....	176
Figure 6.30 Boxplots containing nonstationary impact values of 12 individual CORDEX ensemble members at gridded stations for autumn AMTmin. Ensemble mean pointer (black asterisk) and ensemble median pointer (red asterisk) are also given. ....	177
Figure 6.31 Boxplots describing the intra-model variability of nonstationarity impact prediction for yearly AMTmax.....	179
Figure 6.32 Boxplots describing the intra-model variability of nonstationarity impact prediction for yearly AMTmin .....	180
Figure 7.1 CONUS land use Maps of a) sub-basin 2133, b) sub-basin 2164 and c) sub-basin2157 before and after classification. ....	186
Figure 7.2 Hypsometric curve of sub-basin a) 2133 b) 2164 and c) 2157 .....	187
Figure 7.3 Comparison of daily observed and simulated streamflow at the station a)- 2133, b)- 2157 and c)- 2164. Daily total precipitation is also given at the right-hand side y-axis. ....	191
Figure 7.4 Comparative plots of probability density functions of GEV, Gumbel, Normal and Lognormal distributions .....	192
Figure 7.5 Comparative plots of cumulative probability density functions of GEV, Gumbel, Normal and Lognormal distributions.....	193

Figure 7.6 QQ-plots of GEV, Gumbel, Normal and Lognormal distributions .....	193
Figure 7.7 Comparison of stationary and nonstationary design discharges obtained from yearly AMFs of observed data at eight streamflow stations using GEV distribution (left column), gumbel distribution (middle column) and normal distribution (right column). .....	195
Figure 7.8 Percentage difference between 100-year stationary and nonstationary return levels for Yearly AMFs during the observation period. ....	196
Figure 7.9 Percentage difference between 100-year stationary and nonstationary return levels for seasonal AMFs during the observation period. ....	197
Figure 7.10 Percentage difference between 100-year stationary and nonstationary return levels for seasonal ALFs during the observation period. ....	198
Figure 7.11 Percentage difference between 100-year stationary and nonstationary return levels for seasonal ALFs during the observation period. ....	199
Figure 7.12 Boxplots of stationary and nonstationary return levels at three selected watersheds obtained from yearly AMFs of CORDEX driven streamflow projections. In each boxplot “—” refers to ensemble median while green and red lines represent .....	200
Figure 7.13 Boxplots of the percentage difference between 100-year stationary and nonstationary return levels obtained from yearly and seasonal AMFs of CORDEX driven streamflow projections for three watersheds (2133,2157 and 2164) using GEV distribution. ....	201
Figure 7.14 Boxplots of stationary and nonstationary return levels at three selected watersheds obtained from yearly ALFs of CORDEX driven streamflow projections. ....	203
Figure 7.15 Boxplots of the percentage difference between 100-year stationary and nonstationary flows obtained from yearly and seasonal ALFs of CORDEX driven	

streamflow projections for three watersheds (2133,2157 and 2164) using GEV distribution.....	203
Figure 8.1 Comparison of observed daily mean precipitation with those of original and bias-adjusted RCM ( CNRM-CERFACS-CNRM-CM5—CCLM4-8-7 (BDS Method) ) .....	211
Figure 8.2 Comparison of nonstationarity impacts obtained from original and the bias-adjusted RCM for Yearly AMPs .....	213
Figure 8.3 Comparison of nonstationarity impact values at gridded stations obtained using original and bias-adjust RCM for yearly AMPs .....	214
Figure 8.4 Comparison of observed mean daily precipitation with original and bias-adjusted RCM.....	216
Figure 8.5 Comparison of nonstationarity impacts obtained from original and bias-adjusted RCM for Yearly AMPs .....	218
Figure 8.6 Bar charts of nonstationarity impact value at gridded stations obtained using original and bias-adjusted RCM for yearly AMPs .....	219
Figure 8.7 Comparison of observed mean daily temperature with original and bias-adjusted RCM.....	221
Figure 8.8 Comparison of nonstationarity impacts obtained using original and bias-adjusted RCM for Yearly AMTmax.....	223
Figure 8.9 Bar chart of nonstationarity impact values at gridded stations obtained from original and bias-Adjusted RCM for AMTmax.....	224
Figure 8.10 Comparison of observed mean daily temperature with original and bias-adjusted RCM.....	226
Figure 8.11 Comparison of nonstationarity impacts obtained using original and the bias-adjusted RCM for AMTmax.....	228

Figure 8.12 Bar charts of nonstationarity impact values at gridded stations obtained using original and bias-adjusted RCM for AMTmax .....229

## ABBREVIATIONS

ALF	Annual Low Flow Series
AMTmax	Annual Maximum Temperature Series
AMTmin	Annual Minimum Temperature Series
AMP	Annual Maximum Precipitation Series
AMF	Annual Maximum Flow Series
CLMcom	Climate Limited-area Modelling Community
CNRM	Météo-France/Centre National de Recherches Météorologiques
CORDEX	Coordinated Regional Climate Downscaling Experiment
CORR	Correlation Coefficient
EC-Earth	European community Earth-System Model
GCM	General Circulation Model/Global Climate Model
GDM	General Directory of Meteorology
GDSHW	General Directory of State Hydraulic Works
GEV	Generalized Extreme Value Distribution
HadGEM	Hadley Centre Global Environmental Model
HBV	Hydrologiska Byråns Vattenbalansavdelning
ICHEC	Irish Centre for High-End Computing
IPCC	Intergovernmental Panel on Climate Change
IPSL	Institut Pierre-Simon Laplace
KNMI	Royal Netherlands Meteorological Institute
MAE	Mean Absolute Error
MBE	Mean Bias Error
MGM	Turkish State Meteorological Service
MOHC	Met Office Hadley Centre
RCM	Regional Climate Model
RMSE	Root Mean Square Error
SMHI	Swedish Meteorological and Hydrological Institute



## **CHAPTER 1**

### **INTRODUCTION**

#### **1.1. Background and Motivation**

Weather and climate are two important terms used in meteorology, atmospheric sciences as well as other closely related fields like hydrology and water resources. Weather and climate define the behavior of atmosphere in response to many factors among solar radiation being one of the most important ones. Weather is the behavior of atmosphere over short scales of time and space. Weather can vary from very short time scale like minutes and hours to few months. On the other hand, climate defines the persistent behavior of atmosphere over the relatively large scale of time and space. Weather is a combination of different components like sunshine and temperature, precipitation and its type, flooding patterns, cloud covers, and its types, wind direction and speed etc. Persistence of these components over longer periods throughout a region governs the climate of that region. Weather forecasting is done primarily, to know the condition of atmospheric behavior in near future from a few minutes, hours, days to seasons and it requires more accuracy and reliability. Climate predictions are done to know the overall picture of weather conditions after a longer duration like fifty or hundred years and usually, global circulation models are used for this purpose.

Long-term change in weather is called climate change. These persistent changes may occur in one or more components (like temperature, precipitation and wind speed

etc.) of weather. Solar radiation is one of the major governing factor affecting the world's climate. The overall balance of incoming-outgoing radiation (longwave radiations) has been disturbed because of increased concentration levels of aerosols and greenhouse gases (IPCC, 2013; WEB1). Human activities, for example, modifying the land use patterns by cutting forests alter the carbon dioxide (CO<sub>2</sub>) emission levels and surface albedo which results into variations in the amount of longwave radiations from earth's surface (Salvati et al., 2013; IPCC, 2013). It is also interesting to know that the regions, which contribute least towards greenhouse emissions, are going to be most impacted by climate change. Climate change can be observed as variations (increasing or decreasing trends) in average values or changes in extreme events. Because of climate change, the overall global surface temperature has been increased and the past decade (2000-2010) has been recorded as the warmest decade in the last two centuries. Since 1850, an increase of 1°C was estimated (WEB2). Glacier cover and thickness have been reduced in Greenland, Alaska, and Arctic Canada (Dowdeswell et al., 1997; Aniya, 1999). Snowfall decreased, and snow cover narrowed where winter temperatures increased (Karl et al., 1993). Similarly, precipitation patterns have been changes, especially increases have been found in precipitation amount in mid-latitudes of the northern hemisphere (Givati and Rosenfeld, 2013). Globally, there has been an increase in frequencies and intensities of hydroclimatological extreme events as the number of cold and hot days increased during the period between 1951 and 2010. The frequency of intense heat waves, floods, droughts, and precipitations has increased in the last century (Mirza, 2003; Linnenluecke et al., 2011). The recent magnitude and rate of climate-related changes are more in at least past 2000 years while the spatial extents of these changes are claimed to be more in at least last 1000 years (IPCC, 2007). The rate with which our Earth's environment changes is unprecedented and the risks of natural hazards related to these changes are greater than ever (Montanari and Koutsoyiannis, 2014).

These continuous changes in frequencies and intensities of hydroclimatological extremes (like minimum and maximum temperatures, precipitation and streamflow

extremes) invalidate the assumption of stationarity in hydroclimatological records. With the passage of time, there is a potential for further widening the range between extremes.

Climate plays a very important role and any change in climate can have an impact on every component of the hydrological cycle. According to IPCC (2007), climate change can have its impacts on the hydrological cycle in different ways. Under changing climate, overall water vapor in the atmosphere is increased and precipitation patterns (intensities and extremes) are changed. On the other hand, widespread melting of ice also reduced overall snow cover. Changes in soil moisture and runoff patterns are also observed. The observed data shows that overall global surface temperature has increased considerably (IPPC, 2007). In a warming climate, extreme precipitation events are expected to intensify due to moistening of the atmosphere (Donat et al., 2016; Fischer and Knutti, 2015; Pendergrass et al., 2016). Using observational records, a review of the literature suggests a dependency between mean and extreme precipitation on temperature (O’Gorman, 2015). The increased water-holding capacity of warmer air, as governed by the Clausius–Clapeyron (C–C) relation intensifies heavy rainfall at a rate of approximately 7–8 % per 1°C of warming (Hardwick et al., 2010; Lenderink and van Meijgaard, 2008; O’Gorman and Schneider, 2008). Emission based simulations suggested that the global surface temperature will continue to increase in future, which will eventually end up with adding more and more nonstationarities in hydroclimatological variables. Presence of climate change and land use conditions may change the probabilities of hydrological extreme events, which further means that the parameters (of location, shape, and scale) of underlying distributions may change with the passage of time and assumption of stationarity becomes invalid.

## **1.2. Problem Definition**

Recent developments (IPPC, 2007; Milly et al., 2008; Katz et al., 2002; Salas and Obeysekera, 2014; Mehmetcik Bayazit, 2015) in time series analyses of hydroclimatological variables have led us to the opinion that impacts of

nonstationarities are significant enough to reconsider the idea of traditional stationary approaches. Stationarity is dead and cannot be revived even with most aggressive plans to mitigate the continuous warming (Milly et al., 2008) and one of the main reason is believed to be substantial anthropogenic changes in our earth's climate. The anthropogenic activities change the means and extremes of temperature, precipitation and streamflow rates (IPPC, 2007; Milly et al., 2008). Traditional frequency analyses methods for different hydroclimatological variables are inherent to the assumption of stationarity, i.e. the parameters of underlying distribution and probability density functions (pdf) of a variable is independent of time (Katz, 1992; Katz et al., 2002; Salas and Obeysekera, 2014; Mehmetcik Bayazit, 2015). The nonstationarities are bound to alter the frequencies and magnitude of hydroclimatological extremes which are very important in design and planning procedures. So, it is very important to estimate the impacts of nonstationarities and incorporate these nonstationarities impacts in design and decision-making process, like estimation of return levels for given return periods etc. This can be achieved by using nonstationary frequency analysis where parameters of distributions are time-dependent. In addition to well-known distributions of GEV and Gumbel used in nonstationarity analyses, this thesis study also contributes to the methodology of nonstationarity approach by adding two more distributions namely; normal and lognormal first time. The impacts of nonstationarities can be estimated by comparing the nonstationary return levels to the stationary return levels at any given return period. Although, many of the previous studies about hydroclimatological variables have shed light about the presence of nonstationarities however there are not many studies in the context of quantifying the impacts of nonstationarities in yearly as well as seasonal hydroclimatological extremes and identification of regions wherein these impacts are more significant. So, it is found important and much needed to fill this scientific gap. Furthermore, to understand the impacts and implications of nonstationarities in a longer term, it is important to evaluate these impacts in future projected hydroclimatological extremes obtained from a multi-member ensemble of regional climate model (RCM) simulations.

### **1.3. Literature Review**

#### **1.3.1. Historical Overview of Nonstationary Frequency Analyses**

Planning and developments of water-related structures like dams, barrages, and flood control structures need time series data of temperature, precipitation, and streamflow. These data contain randomness. One of the major causes for this randomness is that the hydroclimatological processes are natural and it is almost impossible to understand these processes completely. Probability distribution methods are used to analyze the problems caused by this randomness. For planning and management of water resources, tails of distributions are the most important because upper tails are related to floods while lower tails are related to droughts (Robert M. Hirsch, 2010). Most of the literature regarding the probabilistic methods in designing and planning of water resources follows the basic assumption that extreme hydrological events are stationary. It might be untrue that the professional involves never accepted the presence nonstationarity in hydrological processes, however, they have opted for the stationary assumption as a reasonable method to represent the estimates of future states of the system from the historical data (Webb and White, 2010). In recent past, many studies (Katz et al., 2002; Milly et al., 2008; Read and Vogel, 2015) have been done, stating the fact that in many areas this assumption of stationarity, (i.e. the concept of average return periods) can be problematic because of climate change. They emphasized the need for new methods to incorporate inherent nonstationarity of hydrological extremes in future studies of hydrology and water resources for a better understanding of extreme conditions. For time series analysis, nonstationary methods can be more helpful especially in the areas we experience changes in hydroclimatological conditions (Milly et al., 2008; Webb and White, 2010). There can be many other causes for the presence of nonstationarity in hydrological records for example urbanization, change in agricultural patterns and deforestation etc.

The concept of return period is of vital importance in the analysis of extreme events like droughts and floods. This statistical evaluation is based on the Extreme Value Theory (EVT hereafter), which exists since the mid-20th century, including two main families of methods. On the one hand, extreme events can be defined as maxima per given blocks of time (e.g. a year, a season or a month), described by the Generalized Extreme Value (GEV hereafter) distribution. On the other hand, in Peak-Over-Threshold method, extremes are retained values over a properly chosen high threshold. Return period in streamflow studies can be defined as the time interval between flood events exceeding a given threshold (Gumbel, 1941). For example, any flood control structure like a levee can be designed to protect the vicinity against the *t-year* flood, where the *t-year* flood is the flood, which occurs once in *t-years*. In this type of problems, we are interested to know the probability of occurrence of the flood, which would overtop the designed structure. This definition of return period follows the assumption that occurrences probability of an extreme hydrological event will remain same (stationary) and occurrences are independent (Leadbetter, 1983), that is, the return periods for a given design flood calculated from observed time series of streamflow will also remain the same in the future.

Many researchers (Wigley, 1988; Castillo, 1988; Olsen et al., 1998 and Du et al., 2015) used the definition of return period as expected waiting time to the first occurrence of an extreme event. Katz (1992) studied the hydrological extreme events under changing climate and concluded that climate change can influence the location and scale parameters, which consequently can change the tail distribution. This change can 1) increase extreme events 2) decrease extreme events or 3) randomly shift the extreme events.

This change in hydroclimatological extreme events, like extreme precipitation, temperature, floods, and droughts can be a matter of big concern for the decision makers. So, the recent literature has suggested using every possible method for better understanding of extremes which are changing over time. Salas and Obeysekera (2014) stated that these methods can be a) probability distribution

having trend component b) probabilistic models with considerations of pattern shifting c) using covariates and d) use of probability distributions with mixed components. Moglen (2003) used a pragmatic approach for tackling nonstationary behavior of hydrological processes by adjusting the peaks of nonstationary discharges by considering the temporal and spatial variations of land use through means of hydrological model. Salas and Obeysekera (2014) proposed a procedure which can be used for designing the flood-related structures under nonstationary conditions. They extended the geometric distribution to allow for changing exceedance probability (probability of failure) with the passage of time. Previous studies have explained that return period estimation using stationary assumption can be quite different than the return period calculated by considering nonstationarity. The return period is the inverse of the probability of failure. Under nonstationary conditions, the probability of failure changes with time so as the return period. If the probability of failure increases with time, the expected waiting time before failure or return period will be less (Olsen et al., 1998). Salas and Obeysekera (2014) explained these changes in design flood in the presence of nonstationarities (a case of increasing flood extremes over time) in Figure 1.1 and Figure 1.2.

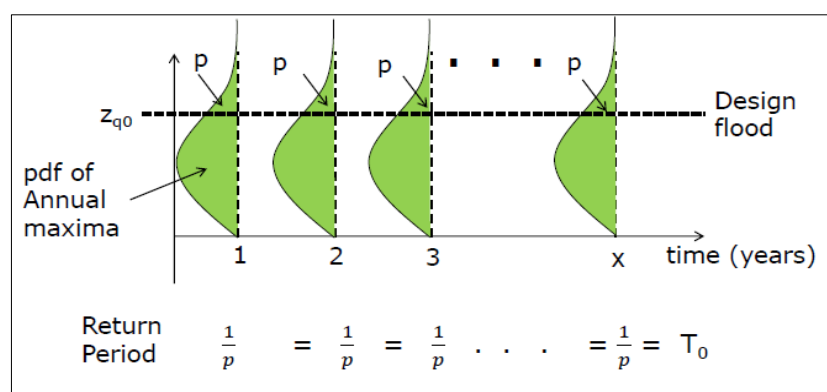


Figure 1.1 Schematic diagram depicting the design flood “ $z_{q_0}$ ” in addition to constant values of exceeding “ $p$ ” and non-exceeding “ $q = 1 - p$ ” probabilities throughout years 1 to  $t$  (stationary condition).

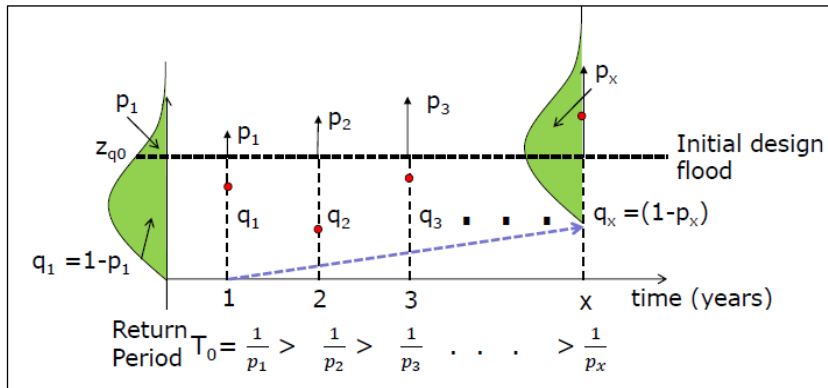


Figure 1.2 Schematic diagram depicting the design flood values “zq0” in addition to exceeding “pt” and non-exceeding “qt = 1-pt” probabilities as they vary through years 1 to t (the nonstationary case with increasing flood extremes)

Salas and Obeysekera (2014) used nonstationary GEV distribution for a case where floods are increasing every year. They have shown that values of return periods obtained under nonstationary consideration were less than the return periods under the stationary assumption.

The basic idea behind the frequency analysis under nonstationary conditions is to use nonstationary frequency models which can account for time-dependent changes in one or more parameters of a distribution. For example, an upward or downward trend in temperature extremes can better be represented using a time-dependent location parameter which is normally associated with the mean. Similarly, changing variabilities of precipitation series can be modeled by using time-dependent scale parameter of the parameter that is normally associated with the variance distribution.

### 1.3.2. Historical Overview of Status of Climate Change in Turkey

In section 1.1, the relationship between climate change and nonstationarity as well as the historical developments about investigating the impacts of nonstationarity have

been discussed. Since climate change and nonstationarities in hydroclimatological variables are linked, it is important to review the climate change status in Turkey. For this purpose, a brief review of the literature was done and highlights of a literature review about climate change studies are presented in the following paragraphs.

Türkeş (1996) analyzed the long-term trends and variability in runs of dry and wet years to examine the spatiotemporal characteristics of annual rainfall in Turkey for a period of 1930-1993. The author claimed an all-around slight decrease in area-averaged annual rainfall in Turkey, particularly in the Mediterranean and the Black Sea regions. Although, no significant trends in area-averaged rainfall series were recorded using Mann-Kendall tests however low-frequency fluctuations were recorded in annual rainfall at many stations.

Kadioğlu (1997) used the Mann-Kendall test to evaluate the trends in annual and seasonal mean, maximum and minimum surface air temperature in Turkey for a period of 1939-1989. The findings of this study suggest an increase in mean annual temperature for period 1939-1989. They found relatively more significance in increases of minimum temperature in winter and spring than the maximum temperature. The author attributed these warming trends in minimum temperatures to the urban heat island (UHI) effect.

Türkeş et al. (2002) studied the trends in mean, minimum and maximum temperature series throughout Turkey for period 1929-1999. Warming trends were recorded in annual as well as winter and spring mean temperatures, however, stations located in the northern part of Turkey and continental inner regions exhibited decreasing trends. Furthermore, they found increasing trends in minimum temperatures in different seasons. However, decreasing trends were recorded in most of the stations located in the Black Sea, Marmara and Eastern Anatolia region of Turkey in minimum temperatures of winter and autumn seasons.

Kahya and Kalayci (2004) used four non-parametric trend tests (Mann-Kendall, Seasonal Kendall, Spearman's Rho and Sen's T) to investigate the trends in monthly streamflow series of 26 basins over Turkey. According to their findings, stations located in the western part of Turkey exhibited a general decreasing trend at significant at 0.05 or lower level. However, basins located in the eastern part of Turkey did not show any significant trend.

Dalfes et al. (2007) investigated the climate trends during the 20th century in Turkey as well as for future scenarios. In their study, they found some short time trends in precipitation and thought that these short-term trends can be related to long-term variability in precipitation patterns. They opted for the Mann-Kendall test to investigate the trends in seasonal rainfall. Their findings suggested increases in fall precipitation in northern areas of Anatolia, however, they also found decreases in winter precipitation in most of the western part of Turkey. In the same study, they also found considerable streamflow decreases at stations located in the western part of Turkey but significant increases at a number of stations located in northern parts of Anatolia were also reported.

Ezber et al. (2007) applied the Mann-Kendall test to minimum temperatures to study the climate impacts of urbanization in Istanbul. According to their findings, a significant trend was found in minimum temperatures. They also used a mesoscale atmospheric model to explore the effects of urbanization on the atmosphere. They also claimed the presence of more significant increasing trends in minimum temperatures at urban stations than rural stations. The results went on to suggest that during summer, these urbanization effects are more influential.

Harmancıoğlu et al. (2007) investigated the impacts of climate change on runoffs in two selected river basins (Büyük Menderes and Gediz) during the period 1960-2000. According to their findings, significant decreases were found in the runoffs of streams in these basins. Therefore, they warned about the potential dwindle of the problems related to water scarcity and water allocation the study area already facing.

According to their model simulations, summer and winters are expected to be warmer while the precipitation is expected to decrease during all months of the year.

Aksoy et al. (2008) analyzed the precipitation, air temperature, and streamflow data from the European part of Turkey from a climate change perspective. They investigated randomness, trends, jump as well as the determined the best-fit distribution for hydroclimatological data. According to their findings, there were no significant trends or jumps found time series of streamflow data. Based on global circulation models (GCMs) ECHAM4, HadCM2 and HadCM3, signals of higher air temperature and lower precipitation were recorded in the 21st century. The authors also warned about potential spatiotemporal increases in the frequency and magnitudes of extremes events like floods and drought in the region.

Fujihara et al. (2007) investigated the potential climate change impacts on water resources in the Seyhan River Basin of Turkey. They used the dynamic downscaling method to generate the high-resolution data from GCMs for hydrological modeling purpose. The models suggested 2-2.7°C increases in average annual temperature while decreases (157–182 mm until 2070) in annual precipitation were estimated. However, they claimed that as long as the water demand remains the same, the study area is not expected to experience the water scarcity.

Tayanç et al. (2009) used the Mann-Kendall test to investigate the trends in temperature and precipitations for a period of 1950-2004 in selected cities of Turkey. They found a cooling period from 1960-1993 and warming trend in the last decade. Their study suggests lowest temperatures in the year 1992-1993 and highest temperatures in history were recorded in 2000-2002. The results of their study were also evident of the presence of larger variability in urban precipitation series than the rural one and they mentioned the possibility of more frequent severe droughts and floods at urban stations. Spatial analysis of their results suggests a significant increasing trend in temperature of southern and southeastern part of Turkey. The results of this study also hinted significant decreases in total precipitation in the

western part of Turkey. However, some stations in the northern part of Turkey exhibited increases in precipitation.

Türkeş et al. (2009) investigated the long-term spatiotemporal variability of monthly, seasonal and annual precipitation total series over Turkey. For this purpose, the Mann–Kendall correlation test and principal component analysis test was used for period 1930-2002. A general decreasing trend was recorded in winter precipitation totals and these decreases were found to be more significant in the Mediterranean and the Mediterranean transition regions. However, their study found evidence of increasing trends during summer, autumn and spring seasons.

ÖnoI and Semazzi (2009) studied the potential impacts of global warming on modulating the future climate over the eastern Mediterranean. A significant increase (10%–50%) in winter precipitation over the Carpathian Mountains, the coast of the Black Sea, Kackar Mountains, and the Caucasus Mountains were revealed from regional model simulations. They also found evidence of significant decreases and increases of precipitation and temperature respectively over south-eastern Turkey.

Yılmaz and Yazıcıgil (2011) reviewed the potential impact of climate change on water resources of Turkey. They divided the studies about climate change into two major groups. 1) Studies investigating the degree of climate change reflected in observed records and 2) studies investigating potential future impacts of climate change on water resources. Their review for most of the studies suggested warming trends since the 1990s. According to this review, the most significant changes were recorded in the Mediterranean region where temperature and precipitation are increased and decreased respectively.

Huseyin Toros (2012) applied homogeneity and Mann-Kendall test to investigate the spatiotemporal variability of maximum and minimum temperatures throughout Turkey for the period of 1961-2008. Overall, the results of their study suggest significant increasing trends in annual maximum temperature as well as annual

minimum temperature series. The author also claimed that temperature started increasing in the early 1980s. Furthermore, it was observed that comparatively more increases were observed in period 1985-2008 than the period 1961-1984 in nine selected stations in different geographic regions of Turkey.

Bozkurt and Sen (2013) studied the potential climate change impacts in the Euphrates–Tigris Basin with the help of different GCMs and emission scenarios. The results of their study suggested increases in winter precipitation in the study area and these increases were more apparent in the highlands of northern regions. Winter surface temperatures are also found to be increasing in the study area. They claimed that the study area in Turkey and Syria within this basin is most vulnerable to climate change owing to decreases in annual surface runoff. They also warned about possible effects of climate change on dam reservoirs and hydropower plants in the area.

Önol et al. (2014) investigated the human-induced climate change over the Eastern Mediterranean–Black Sea region for the 21<sup>st</sup> century through regional climate model simulations forced from three different global circulation models (GCMs). The authors stated that winter runoff increases in second half of the 21<sup>st</sup> century over mountainous regions of Turkey. These regions are an important source of water for the Euphrates and Tigris rivers. The authors also stated that the most probable reason for these winter increases is the acceleration of the snowmelt process because of temperature increases.

Ertürk et al. (2014) investigated the potential climate change impacts on the groundwater resources in a small watershed Köyceğiz-Dalyan Mediterranean region. For this purpose, they quantified the potential climate change impacts on the water budget components. A combination climate change and land-use scenarios were used to investigate the climate change impacts on water budget in the watershed. According to their findings, almost all the components water budget equation showed decreases which might be problematic for future agriculture.

Kum and Çelik (2014) investigated the potential impacts of Global Climate Change in the Adana province of Mediterranean region by using Mann-Kendall and Humidex index to carry out trend analysis in temperature, precipitation and humidity data of the study area. According to their findings, the strong increasing trend was found in average and minimum temperatures. In the case of humidity variables, both strongly negative and strongly positive trends were recorded. Authors also claimed the possibility of increases in frequency and magnitudes of heat waves. However, the findings suggested small decreases in precipitation during the winter season.

Yucel et al. (2015) studied the potential climate change impacts on snowmelt runoff of mountainous transboundary basins of Eastern Anatolia. Their study suggested significant increases (average 1.3 °C across the stations) in temperature during period 1970-2010. The findings of the study also suggested increases in annual precipitation (average 7.5% across the stations) but the increases are not significant, in general. The results of this study found evidence of earlier spring melting of snow packs since the streamflow timings were found to be shifted to earlier days in the year (9-days on average). Authors linked this time shifting with rising temperature in recent years. High emissions scenario-based climate change simulations suggested a decline (10-30%) in annual surface runoffs of Aras, Euphrates and Tigris basins in the region. Authors also discussed the possibility of progression of shifting the timings of peak flows in future as well.

Ozturk et al. (2015) studied the projections of climate change in the Mediterranean Basin using downscaled global climate model outputs and investigated the future projected changes in mean air temperature and precipitation climatology and inter-annual variability. They investigated the future changes in annual as well as seasonal means for projection period (2070-2100) and compared the same with the historical period (1970-2000). According to their findings, future surface mean air temperature of the Mediterranean basin increases. These increases in mean temperature were most significant during summer and least significant increases were recorded in winter. The results of their study also suggested decreases in precipitation amounts

in all seasons. They also claimed that probability density functions of future data were shifted and flattened for projected data as compared to the reference data. According to authors, this is linked with the indication of high intensities and higher frequencies of extreme temperatures as well as precipitation events.

Bozkurt et. al (2015) analyzed the projected river discharge in the Euphrates-Tigris Basin using a hydrological model forced with RCM and GCM outputs. The authors found that low-resolution GCMs outputs are not good at reproducing the seasonal cycle of discharge as compared to the GCMs output with higher resolutions. The authors also claimed about the significant temporal shifts of discharges towards early days of the year.

Türkeş et al. (2016) investigated the regional climate change signals based on statistical analysis of two consecutive time periods, 1950-1980 and 1981-2010. Analysis was made on precipitation totals and mean, minimum and maximum temperatures throughout Turkey. They used K-means and hierarchical clustering methods to obtain surface air temperature and precipitation patterns in Turkey for both consecutive time periods. Furthermore, to investigate any potential change in mean and variance of the series in the transition from one period to the other, Pitman-Morgan (P-M) t-test and Paired-samples Student's t-test (paired t-test) was applied. The results of their study revealed that all three air temperature series (mean, maximum and minimum) increased after 1980. However, the more significant changes occurred in precipitations as precipitation totals were increased in the eastern and northern parts of Turkey after 1980, however, decreases in precipitation amounts were recorded in southern, central and western regions.

#### **1.4. Goals and Objectives**

The main goal of the study is to quantify the impacts of nonstationarities on yearly and seasonal hydroclimatological extremes for observation period using observed data and future projected data using a multi-member ensemble of regional climate

models through the application of four different nonstationary frequency distributions. This goal is achieved by addressing the following scientific questions.

- How much and what type of impacts nonstationarities have on hydroclimatological variables in Turkey during the historical period? (*for precipitation and temperature throughout Turkey and streamflows of Upper Euphrates Basin*).
- How similar or different nonstationarity impacts are, as obtained using different probability distributions? Especially using Normal and Lognormal as compared to the conventionally used GEV and Gumbel distributions for nonstationarity impact assessment.
- How similar or different nonstationarity impacts are, as obtained using historical and projected data using an ensemble approach?
- How well are ensemble members for their ability to reproduce historical data?
- How well bias-adjusted RCMs preserve the nonstationarity signals?
- What are the implications and potential consequences of nonstationarity impacts?

## **1.5. Thesis Description**

The 1<sup>st</sup> chapter provides a brief introduction, historical background, and definition of the problem, a historical overview of climate change studies in Turkey, objectives, and goals of the study. The 2<sup>nd</sup> chapter describes the study area and data used in this study. The 3<sup>rd</sup> chapter outlines the methodology adopted for the CORDEX model performance evaluation, stationary and nonstationary frequency analysis as well as information about hydrological modeling. The 4<sup>th</sup> chapter includes results and discussion about CORDEX performance evaluation. Results and discussions about

nonstationarity impacts on temperature, precipitation, and streamflow are presented in chapter 5, 6 and 7, respectively. The 8<sup>th</sup> chapter contains the results and discussion about the comparison of performance evaluation as well as the ability of bias-adjusted CORDEX RCMs to preserve the nonstationarity signals. Thesis summary, conclusions, and recommendations are provided in Chapter 9.



## CHAPTER 2

### STUDY AREA AND DATA

#### 2.1. Study Area

The impacts of nonstationarities on annual and seasonal minimum-maximum temperature as well as precipitation are investigated throughout Turkey during the observation period (1971-2016). For projection period (2051-2100), impacts of nonstationarities are investigated for gridded stations (a gridded station is the representative grid of observation station on CORDEX mesh) located in that part of Turkey which is enclosed within CORDEX EUR-11 domain. The geographical position of Turkey and its surroundings are shown in Figure 2.1. Owing to the location, diversity of landscapes, irregular topography and the presence of mountain ranges spread parallel to the sea coasts, the climate of Turkey exhibits significant variations from one region to the other. Based on these characteristics, Turkey is generally divided into seven broader geographical regions and they can be seen in Figure 2.2. These regions are described as 1) Mediterranean region 2) Black Sea region 3) Marmara region 4) Aegean region 5) Central Anatolia region 6) Eastern Anatolia region 7) South-Eastern Anatolia region.



Figure 2.1 Map of Turkey showing the surrounding countries with international borders, the national capital Ankara.  
 Downloaded from <https://turkeyfile.com/>



Figure 2.2 The Geographical regions of Turkey  
 Downloaded from <https://www.mapsofworld.com/turkey/geography/>

Most of the precipitation in Turkey occurs during the winter season when there is very less evaporation since the mean temperature is less than 5°C. Usually, the summer precipitation is less in an amount which is not considered enough to remove

water deficit in summer due to increased temperature and evaporation. Climate is milder in coastal areas while inland plateau of Anatolia experiences limited precipitation, cold winter, and warm summer. Inland plateau of Anatolia is categorized as steppe climate while receives a limited amount of rainfall as rain clouds are stopped by the Taurus Mountains. Owing to this blockage, most of the rain clouds drop their water in the coastal areas. Hence rain clouds approaching the Central Anatolia contain very less water, so they have no significant water to produce rain. The average temperature of  $-2^{\circ}\text{C}$  and  $23^{\circ}\text{C}$  is observed during winter and summer season respectively (Sensoy, 2016). Because of higher elevation in the eastern part of Turkey particularly in Eastern Anatolia, bitter cold and long winter with an average temperature of  $-13^{\circ}\text{C}$  and  $17^{\circ}\text{C}$  during winter and summer respectively (Sensoy, 2016). Snow cover lies on the ground for more than 120 days (November until April) in the year. The minimum temperatures of  $-30^{\circ}\text{C}$  to  $-38^{\circ}\text{C}$  are experienced in some areas. The climate of South-Eastern Anatolia region is attributed to hot and dry summer and the temperature is above  $30^{\circ}\text{C}$  in summer. Although the climate in spring and autumn season is generally mild, the occurrences of sudden cold and hot spells during these seasons are also attributed to this region. Generally, coastal areas of the Black Sea region receive the greatest amount of precipitation and categorized as wet and humid where the average temperature of  $7^{\circ}\text{C}$  and  $23^{\circ}\text{C}$  is observed during winter and summer respectively (Sensoy,2016). Most of the eastern part of Black sea region receives rainfall throughout the year which reaches to the annual total of 2200 mm. The coasts of the Mediterranean and Aegean region experience cool and rainy winter, however, the summers are hot and moderately dry. The climate of Marmara regions is moderate where the average temperature is  $4^{\circ}\text{C}$  and  $27^{\circ}\text{C}$  during winter and summer season respectively, however, the minimum temperature can drop below  $0^{\circ}\text{C}$  in winter (Sensoy, 2016).

Analyses were done for 77 meteorological stations obtained from General Directory of Meteorology (GDM) throughout Turkey. The locations of these stations along with Stations IDs are shown in Figure 2.3.

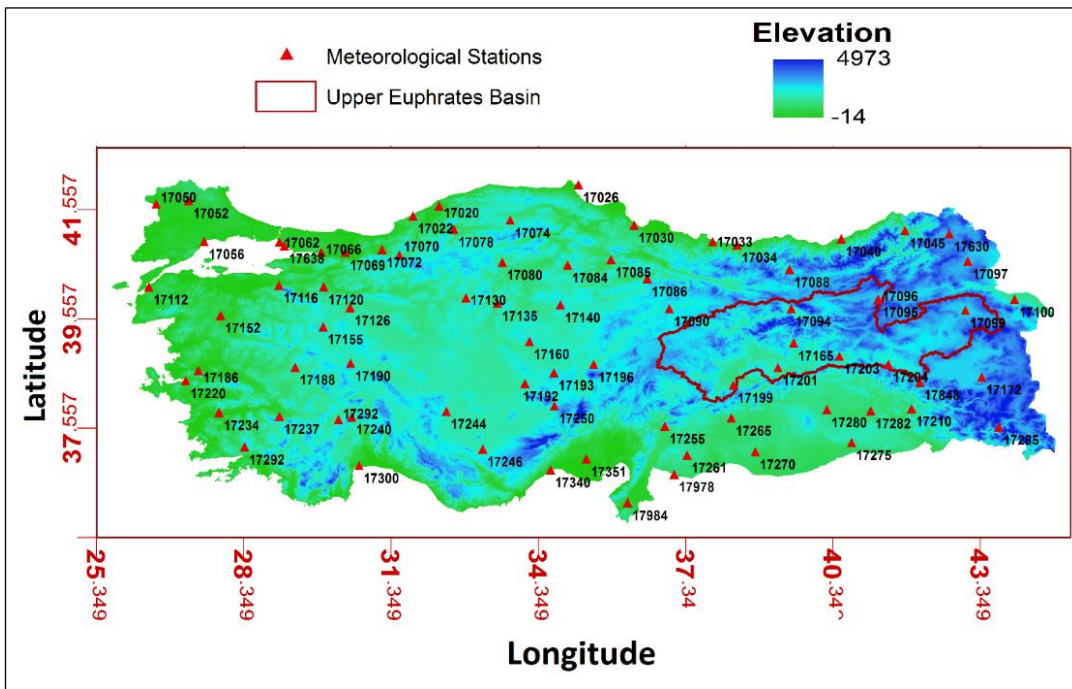


Figure 2.3 Elevation map of Turkey, the location of the meteorological stations used along with identification of Upper Euphrates basin as a dark red polygon.

For streamflow extremes of the observation period, the analysis was done for the stream gauge stations of Upper Euphrates basin whose location is also shown in Figure 2.3. To investigate the nonstationarity impacts for future projection periods (2051-2100), three sub-basins were selected where daily streamflow was generated using CORDEX RCMs projections of temperature and precipitations into calibrated HBV-light model. The study area for streamflow analysis (Upper Euphrates basin) is characterized by a high and mountainous topography (Figure 2.4). Elevation usually exceeds 2000 m. The North Anatolia and Caucasus Mountains in the north and the Taurus Mountains in the south hold the rain clouds, and therefore the study area is under the influence of the continental climate with long and very cold winter, and frequent heavy snowfall which remains on the ground from. Because of its high elevation, the ratio of precipitation falling as snow versus rain is higher than that in the other regions of Turkey. The study area constitutes the upper part of Euphrates

River basin which is an important source of water for a number of water resources development projects at different downstream locations, including the Southeastern Anatolia Project, to produce energy and to irrigate large semi-arid plains to the south of the region.

The study is conducted for eight unregulated streamflows (with standard watershed ID 2102,2122,2124,2133,2145,2156,2157 and 2164) of the Upper Euphrates river basin shown in Figure 2.4. Watersheds with small reservoirs whose effect is less than 10% on the downstream streamflow can be assumed as unregulated (Kahya and Karabörk, 2001). In the selection of streamflow stations in the region, the length of the records and the continuous nature of the data are also considered.

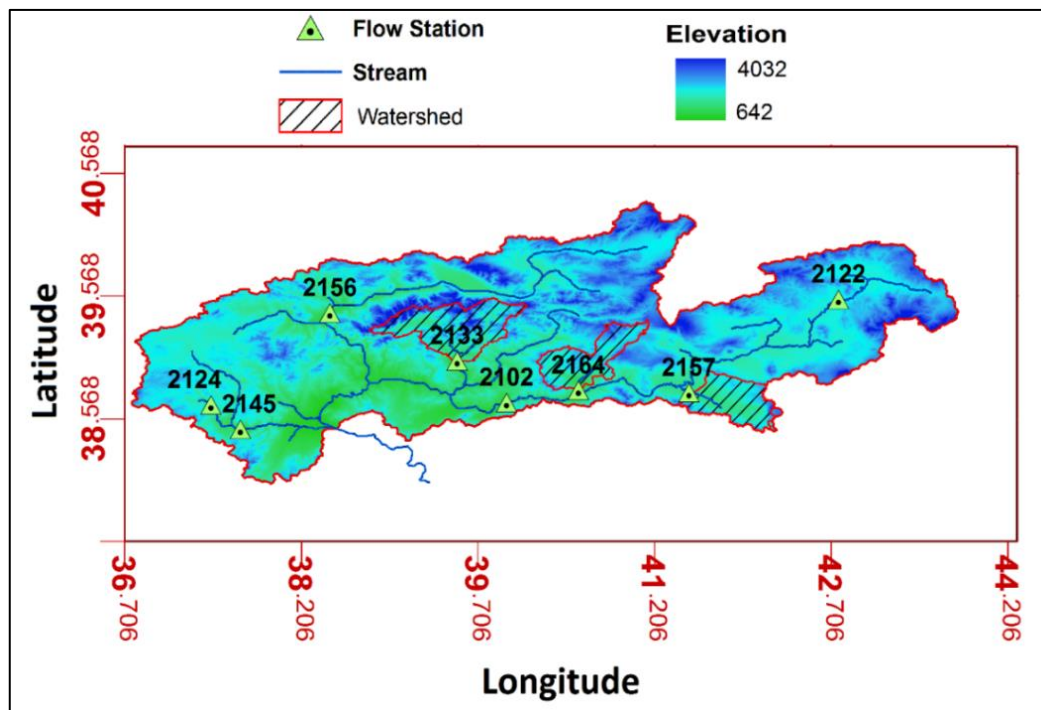


Figure 2.4 Elevation map of Upper Euphrates basin, the stream network, location of streamflow stations and identification of three selected watersheds (2133,2157 and 2164) for hydrological modeling.

## **2.2. Data Used**

Nonstationarity impacts analysis were performed for minimum and maximum temperature, precipitation, and streamflow for observation and projection periods.

### **2.2.1. Observational Data**

The observed precipitation and temperature data were taken for a period 1971-2016 from meteorological stations across Turkey from the GDM. The stations with missing data more than 5 consecutive years were excluded. The stations with missing values were replaced with the average value. The information about stations with missing data is provided in Appendix B. Finally, 77 stations were selected to be included in the study. Region wise information about Station IDs, Station names, latitude and longitude are given in Table 2-1 to Table 2-7. For nonstationary analysis of streamflow of Upper Euphrates basin, streamflow data was obtained from General Directory of State Hydraulic Works (GDSHW) for gauge stations across the basin. The analyses were performed for selected eight unregulated stations. Information about the identification number, name, record length and elevation of the selected streamflow stations are given in Table 2-8.

Table 2-1 Information about meteorology stations of the Black Sea region

<b>Station ID</b>	<b>Station Name</b>	<b>Latitude</b>	<b>Longitude</b>
17020	BARTIN	41.63	32.33
17022	ZONGULDAK	41.45	31.80
17026	SINOP	42.02	35.17
17030	SAMSUN	41.28	36.30
17033	ORDU	40.98	37.90
17034	GIRESUN	40.92	38.40
17040	RIZE	41.03	40.52
17045	ARTVIN	41.18	41.82
17070	BOLU	40.73	31.52
17072	DUZCE	40.83	31.17
17074	KASTAMONU	41.37	33.78
17078	KARABUK	41.20	32.63
17084	CORUM	40.55	34.95
17085	AMASYA	40.65	35.83
17086	TOKAT	40.30	36.57
17088	GUMUSHANE	40.47	39.47
17089	BAYBURT	40.25	40.23

Table 2-2 Information about meteorology stations of the Marmara region

<b>Station ID</b>	<b>Station Name</b>	<b>Latitude</b>	<b>Longitude</b>
17050	EDIRNE	41.67	26.57
17052	KIRKLARELI	41.73	27.23
17056	TEKIRDAG	40.98	27.55
17062	GOZTEPE-ISTANBUL	40.97	29.08
17066	KOCAELI	40.78	29.93
17069	SAKARYA	40.78	30.42
17112	CANAKKALE	40.15	26.42
17116	BURSA	40.18	29.07
17120	BILECIK	40.15	29.98
17152	BALIKESIR	39.63	27.88
17638	KARTAL-IST	37.27	35.07

Table 2-3 Information about meteorology stations of the Central Anatolia region

<b>Station ID</b>	<b>Station Name</b>	<b>Latitude</b>	<b>Longitude</b>
17080	CANKIRI	40.60	33.62
17090	SIVAS	39.75	37.02
17126	ESKISEHIR	39.77	30.52
17130	ANKARA	39.95	32.88
17135	KIRIKKALE	39.85	33.52
17140	YOZGAT	39.82	34.80
17160	KIRSEHIR	39.15	34.17
17192	AKSARAY	38.38	34.08
17193	NEVSEHIR	38.58	34.67
17196	KAYSERI	38.73	35.48
17244	KONYA	37.87	32.48
17246	KARAMAN	37.18	33.22
17250	NIGDE	37.97	34.68

Table 2-4 Information about meteorology stations of the East Anatolia region

<b>Station ID</b>	<b>Station Name</b>	<b>Latitude</b>	<b>Longitude</b>
17094	ERZINCAN	39.75	39.50
17096	ERZURUM	39.92	41.27
17097	KARS	40.62	43.10
17099	AGRI	39.72	43.05
17100	IGDIR	39.92	44.05
17165	TUNCELI	39.12	39.55
17172	VAN	38.50	43.38
17199	MALATYA	38.35	38.32
17201	ELAZIG	38.67	39.23
17203	BINGOL	38.88	40.48
17204	MUS	38.73	41.48
17285	HAKKARI	37.58	43.73
17046	ARDAHAN	41.12	42.72
17848	BITLIS	38.40	42.12

Table 2-5 Information about meteorology stations of the Aegean region

<b>Station ID</b>	<b>Station Name</b>	<b>Latitude</b>	<b>Longitude</b>
17155	KUTAHYA	39.42	29.97
17186	MANISA	38.62	27.43
17188	USAK	38.68	29.40
17190	AFYON	38.75	30.53
17220	IZMIR	38.43	27.17
17234	AYDIN	37.85	27.85
17237	DENIZLI	37.78	29.08
17292	MUGLA	37.22	28.37

Table 2-6 Information about meteorology stations of the South-Eastern Anatolia region

<b>Station ID</b>	<b>Station Name</b>	<b>Latitude</b>	<b>Longitude</b>
17210	SIIRT	37.92	41.95
17261	GAZIANTEP	37.07	37.38
17265	ADIYAMAN	37.75	38.28
17270	SANLIURFA	37.13	38.77
17275	MARDIN	37.30	40.73
17280	DIYARBAKIR	37.90	40.23
17282	BATMAN	37.88	41.12
17978	KILIS	36.72	37.12

Table 2-7 Information about meteorology stations of the Mediterranean region

<b>Station ID</b>	<b>Station Name</b>	<b>Latitude</b>	<b>Longitude</b>
17238	BURDUR	37.72	30.28
17240	ISPARTA	37.77	30.55
17255	KAHRAMANMARAS	37.60	36.93
17300	ANTALYA	36.88	30.70
17340	MERSIN	36.80	34.60
17351	ADANA	37.00	35.33
17984	ANTAKYA	36.20	36.17

Table 2-8 Information about the selected streamflow stations of Upper Euphrates basin and their relevant geographical information

<b>Station ID</b>	<b>Station Name</b>	<b>Longitude (°E)</b>	<b>Latitude (°N)</b>	<b>Altitude (m)</b>	<b>Area (km<sup>2</sup>)</b>	<b>Data Length</b>
<b>2102</b>	MURAT NEHRİ PALU	39.95	38.7	859	25447.2	1971-2010
<b>2122</b>	MURAT NEHRİ TUTAK	42.77	39.54	1552	5882.4	1971-2010
<b>2124</b>	TOHMA SUYU YAZIKÖY	37.44	38.68	1100	1336.4	1971-2010
<b>2133</b>	MUNZUR ÇAYI MELEKBAHÇE	39.53	39.04	940	3284.8	1971-2010
<b>2145</b>	TOHMA SUYU HİSARCIK	37.69	38.48	935	5822	1971-2010
<b>2156</b>	FIRAT NEHRİ BAĞIŞTAŞ	38.45	39.43	865	15562	1971-2010
<b>2157</b>	KARASU KARAKÖPRÜ	41.5	38.78	1250	2098.4	1971-2007
<b>2164</b>	GÖYNÜK ÇAYI ÇAYAĞZI	40.56	38.8	498	2232	1971-2010

GDSHW and GDM follow the same basic principles of the data quality control introduced by the World Meteorological Organization (WMO). Information about such quality control methods applied to data can be found in Sönmez (2013) and Gokturk et al. (2008). All measured data (streamflow, precipitation, and temperature) used in this study have a record length of forty years (1971-2010) except streamflow station 2157 for which thirty-seven years (1971-2007) of continuous data was available. Further three watersheds (2133, 2157 and 2164) were selected for hydrological modeling to evaluate the ensemble nonstationary impacts on CORDEX driven streamflow projections. The selection of sub-basins for hydrological modeling was made considering the availability of representative temperature and precipitation data stations which are either within the watershed or very close to the streamflow station.

### 2.2.2. CORDEX Data

The CORDEX (Coordinated Regional Downscaling Experiment) is initiative of World Climate Research Program (WCRP) which aims to create a coordinated framework for evaluating and improving regional climate downscaling techniques and creating a new framework of high resolution downscaled climate projections for different identified domain worldwide. The EURO-CORDEX ( <http://www.euro-cordex.net/> ) is the branch of CORDEX initiative which provides future projection data for European domain with two different spatial resolutions, the general coarser resolution of 0.44 degree (EUR-44, ~50 km) and the finer resolution of 0.11 degree (EUR-11, ~12.5km). For future nonstationarity analysis, a series of future projections were obtained from a 12-member ensemble of CORDEX projected precipitation and temperature from the EUR-11 domain. Information about each individual CORDEX data members used is provided in Table 2-9. The future projected data (2050-2100) of temperature and precipitation is also used to obtain future projected streamflow at three selected sub-basins of Upper Euphrates basin using calibrated HBV-light model. All the RCMs used are with Representative Concentration Pathways 8.5 (RCP 8.5).

Table 2-9 GCM-RCM matrix of CORDEX ensemble members

<b>Member ID</b>	<b>GCM</b>	<b>RCM</b>
<b>1 1</b>	ICHEC-EC-EARTH	HIRHAM5
<b>1 2</b>		CCLM4-8-17
<b>1 3</b>		RACMO22E
<b>1 4</b>		RCA4
<b>2 1</b>	CNRM-CERFACS-CNRM-CM5	ALADIN53
<b>2 2</b>		CCLM4-8-17
<b>2 3</b>		RCA4
<b>3 1</b>	MOHC-HadGEM2-ES	CCLM4-8-17
<b>3 2</b>		RACMO22E
<b>3 3</b>		RCA4
<b>4 1</b>	IPSL-IPSL-CM5A-MR	RCA4
<b>4 2</b>		WRF331F

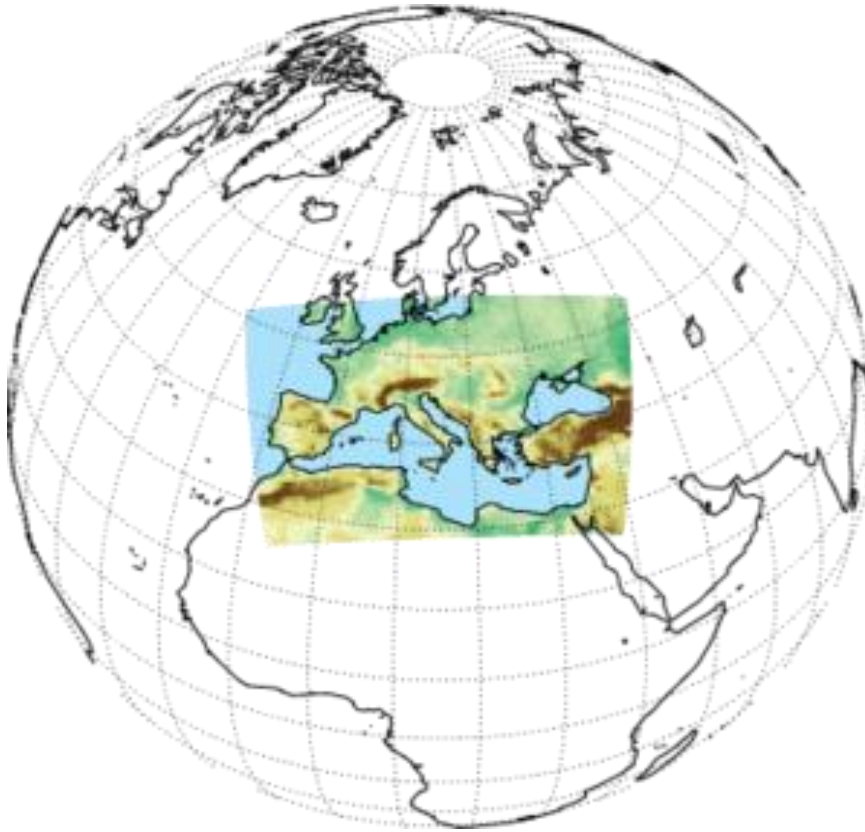


Figure 2.5 EURO-CORDEX domain area surrounded by the inner square

For nonstationary analysis of temperature and precipitation throughout Turkey (within the EURO-CORDEX domain, see Figure 2.5) as well as streamflow generation at three selected sub-basins, the data are extracted from the most representative grids for each of the observation stations. From now on, these representative grids will be stated as a gridded station. The gridded stations are obtained using the nearest neighborhood method. In addition to these 12 RCMs, two bias-adjusted RCMs for precipitation and temperature are also used to evaluate the performance improvement and the effects of bias correction on nonstationarity signals of RCM data.

## **CHAPTER 3**

### **METHODOLOGY**

Impacts of nonstationarities are estimated using stationary and nonstationary probability distributions. Four distributions (GEV, Gumbel, normal and lognormal) are used for precipitation analyses. For analyses of temperature and streamflow, three distribution functions (generalized extreme value (GEV), gumbel and normal) are applied. Analyses of temperature and precipitation for the historical period, observation data is used while CORDEX based projections are used for future projection period. Before using CORDEX data, the performance of data has been evaluated. Streamflow projections are made using calibrated HBV-light model with CORDEX forcing of temperature and precipitation. This chapter includes information about methodology adapted for CORDEX performance evaluation, formulation of stationary and nonstationary probability distribution used as well as hydrological modeling. Information about data series (min-max temperature, high and low flows as well as maximum precipitation) is also present in this chapter. An explanatory flowchart of the methodology adopted in this thesis is provided in Figure 3.1.

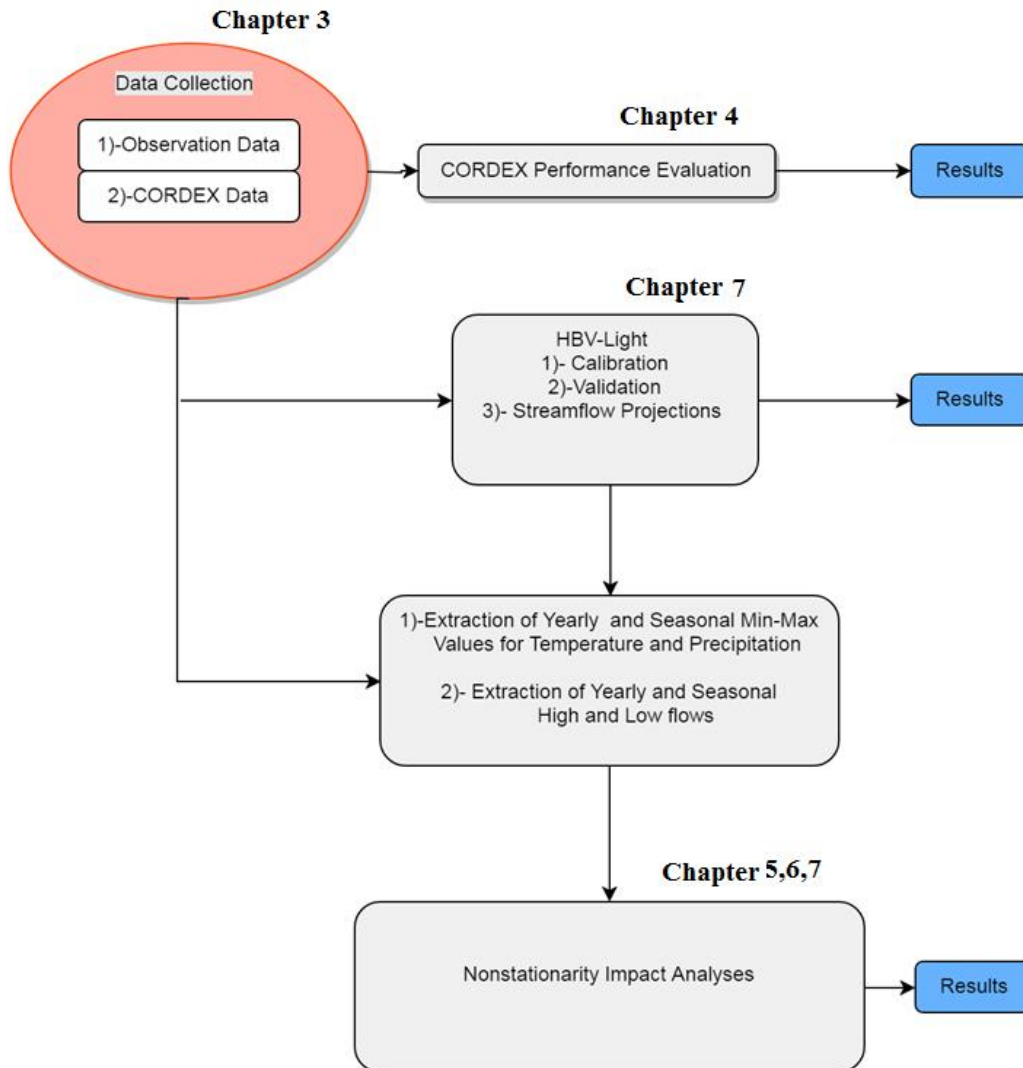


Figure 3.1 Flowchart of Methodology

### 3.1. Stationary and Nonstationary Distributions

In hydrology and water resources, extreme value distributions are used to analyze the probabilistic behavior of extreme events like floods and droughts. Cooley (2013)

explained how return levels (*The return level is stated as a value that is expected to be equaled or exceeded on average once every interval of time (T) with a probability of 1/T*) and return periods can change under non-stationary climate conditions. Gumbel and generalized extreme value (GEV) distributions are well known for their applications in evaluating the frequencies of extreme events. To use these distributions in nonstationary conditions, parameters of the distribution are made time-dependent by incorporating time as a covariate. In this study, stationary and nonstationary forms of GEV, gumbel, normal and lognormal distributions are used.

The cumulative distribution function of GEV incorporates a location parameter, a scale parameter, and the tail shape parameter as given in equation 3.1a (Salas and Obeysekera, 2014; Katz, 2013).

$$F(z, \theta) = \exp \left\{ - \left[ 1 + \varepsilon \left( \frac{z - \mu}{\sigma} \right) \right]^{\frac{-1}{\varepsilon}} \right\} \quad 3.1a$$

Where,  $\theta$  represents a set of parameters which includes location ( $\mu$ ), scale ( $\sigma$ ) and shape ( $\varepsilon$ ) parameters. Nonstationary form of GEV distribution incorporates nonstationary by using time  $t$  dependent location  $\mu_t$ , scale  $\sigma_t$  as given in equation 3.11b (Salas and Obeysekera, 2014); Katz, 2013).

$$F(z, \theta_t) = \exp \left\{ - \left[ 1 + \varepsilon \left( \frac{z - \mu_t}{\sigma_t} \right) \right]^{\frac{-1}{\varepsilon}} \right\} \quad 3.1b$$

where  $\theta_t$  is a time-dependent set of GEV parameters which includes time dependent location  $\mu_t$ , scale  $\sigma_t$  and a constant shape parameter  $\varepsilon$ . So, in case of nonstationary distributions, location parameter becomes  $\mu_t = \mu_1 + \mu_2 * t$  and scale parameter become  $\sigma_t = \sigma_1 + \sigma_2 * t$ . Here,  $\mu_1$  ( $\mu_2$ ) and  $\sigma_1$  ( $\sigma_2$ ) are intercept (slope) values for location and scale parameters, respectively Also, “ $t$ ” represents explanatory covariate of time that

makes  $\mu_t$  and  $\sigma_t$  nonstationary for a given duration. The time “ $t$ ” is given as number of years which varies from 1 to the total number (i.e.,  $x$ ) in Figure 1.2) of data years. In other words, “ $t$ ” represents the time span (in years) during which we are interested to estimate the impacts of nonstationarity. For example, in Figure 1.2, a value of  $t=1,2, 3\dots(x)$  years will give the impacts of nonstationarities in 1,2, 3...( $x$ ) years, respectively. To estimate the impacts of nonstationarity for whole data period, the whole span of data duration (in years) is used in this analysis.

The shape parameter  $\varepsilon$  is difficult to estimate reliably and for this reason, it is normally modeled as a constant (Coles, 2001; Katz, 2013). Maximum likelihood estimation is one of the most widely used parameter estimation methods where parameters of distributions are estimated by maximizing the log-likelihood function. The likelihood functions for a stationary and nonstationary form of GEV distribution can be expressed as Equation 3.2a and Equation 3.2b respectively.

$$l(\mu, \sigma, \varepsilon; x) = -m \log \sigma - \left(\frac{1}{\varepsilon} + 1\right) \sum_{i=1}^m \log \left[1 + \varepsilon \left(\frac{x_i - \mu}{\sigma}\right)\right] - \sum_{i=1}^m \log \left[1 + \varepsilon \left(\frac{x_i - \mu}{\sigma}\right)\right]^{\frac{-1}{\varepsilon}} \quad 3.2a$$

$$l(\mu_t, \sigma_t, \varepsilon; x) = -m \log \sigma - \left(\frac{1}{\varepsilon} + 1\right) \sum_{i=1}^m \log \left[1 + \varepsilon \left(\frac{x_i - \mu_t}{\sigma_t}\right)\right] - \sum_{i=1}^m \log \left[1 + \varepsilon \left(\frac{x_i - \mu_t}{\sigma_t}\right)\right]^{\frac{-1}{\varepsilon}} \quad 3.2b$$

Once we obtain the exceedance probability under the nonstationary condition it is very easy to calculate the return period of any designed quantile and vice versa. Exceedance probabilities corresponding to design quantile  $z_{qo}$  for stationary ( $p$ ) and nonstationary ( $p_t$ ) cases are given as Equations 3.3a and 3.3b respectively.

$$p = 1 - \exp \left\{ - \left[ 1 + \varepsilon \left( \left( \frac{z_{q0} - \mu}{\sigma} \right) \right)^{\frac{-1}{\varepsilon}} \right] \right\} \quad 3.3a$$

$$p_t = 1 - \exp \left\{ - \left[ 1 + \varepsilon \left( \left( \frac{z_{q0} - \mu_t}{\sigma_t} \right) \right)^{\frac{-1}{\varepsilon}} \right] \right\} \quad 3.3b$$

When  $\varepsilon$  approaches to zero, the GEV distribution becomes two parameter gumbel distribution.

GEV and gumbel distribution have been widely used under the nonstationary framework. GEV is considered to be better especially for extreme value analyses. However, in this study, performances of two additional distributions were tested with nonstationary assumption. The normal distribution is applied for temperature, precipitation and streamflow analyses. In addition to GEV, gumbel and normal distribution, for precipitation analyses, lognormal distribution is also applied. The cumulative distribution function of the normal distribution is given by equation 3.4a.

$$F(z, \theta) = \frac{1}{2} \left[ 1 + \operatorname{erf} \left( \frac{x - \mu}{\sigma \sqrt{2}} \right) \right] \quad 3.4a$$

When introducing nonstationarity, the cumulative distribution function of the normal distribution can be formulated as equation 3.4b.

$$F(z, \theta_t) = \frac{1}{2} \left[ 1 + \operatorname{erf} \left( \frac{x - \mu_t}{\sigma_t \sqrt{2}} \right) \right] \quad 3.4b$$

Where the term “erf(x)” is referred as error function and is defined as the probability of a random variable with the normal distribution of mean 0 and variance 1/2 falling in the range [-x, x]. The log-likelihood function of stationary and nonstationary normal distribution can be written as equation 3.5a and equation 3.5b respectively.

$$l(\mu, \sigma, ; x) = -\frac{n}{2}\ln(2\pi) - \frac{n}{2}\ln(2\pi\sigma^2) - \frac{1}{2\sigma^2}\sum_{i=1}^m(x_j - \mu)^2 \quad 3.5a$$

$$l(\mu_t, \sigma_t, ; x) = -\frac{n}{2}\ln(2\pi) - \frac{n}{2}\ln(2\pi\sigma_t^2) - \frac{1}{2\sigma_t^2}\sum_{i=1}^m(x_j - \mu_t)^2 \quad 3.5b$$

The cumulative distribution function of the lognormal distribution is given by equation 3.6a.

$$F(z, \theta) = \frac{1}{2} \left[ 1 + \operatorname{erf} \left( \frac{\ln(x) - \mu}{\sigma\sqrt{2}} \right) \right] \quad 3.6a$$

When introducing nonstationarity, the cumulative distribution function of lognormal distribution can be formulated as equation 3.6b.

$$F(z, \theta_t) = \frac{1}{2} \left[ 1 + \operatorname{erf} \left( \frac{\ln(x) - \mu_t}{\sigma_t\sqrt{2}} \right) \right] \quad 3.6b$$

The log-likelihood function of stationary and nonstationary lognormal distribution can be written as equation 3.7a and equation 3.7b respectively.

$$l(\mu, \sigma, ; x) = -\frac{n}{2} \ln(2\pi\sigma^2) - \sum_{i=1}^m \ln(x_i) - \frac{\sum_{i=1}^m \ln(x_i)^2}{2\sigma^2} + \frac{\sum_{i=1}^m \ln(x_i)\mu}{\sigma^2} - \frac{n\mu^2}{2\sigma^2} \quad 3.7a$$

$$l(\mu_t, \sigma_t, ; x) = -\frac{n}{2} \ln(2\pi\sigma_t^2) - \sum_{i=1}^m \ln(x_i) - \frac{\sum_{i=1}^m \ln(x_i)^2}{2\sigma_t^2} + \frac{\sum_{i=1}^m \ln(x_i)\mu_t}{\sigma_t^2} - \frac{n\mu_t^2}{2\sigma_t^2} \quad 3.7b$$

The parameters of GEV and gumbel distributions were estimated using maximum likelihood method using “ismev” (Heffernan and Stephenson, 2012) package in R programming can be found at <https://cran.r-project.org/web/packages/ismev/>. The same procedure was adapted for parameter estimation of normal and lognormal distribution. The R codes for Normal and Lognormal distributions are provided in Appendix A. Optimization was done using the Nelder-Mead algorithm. Once parameters of each distribution were estimated, the return values corresponding to given return levels were calculated. Impacts of nonstationarities for precipitation and streamflow are quantified in terms of percentage differences between 100-year stationery and nonstationary return values as given in equation 3.8.

$$Percentage\ Difference = \left[ \left( \frac{Nonstationary\ return\ level - stationary\ return\ level}{Stationary\ return\ level} \right) \right] * 100 \quad 3.8$$

Impacts of nonstationarities for temperature are quantified in terms of differences between 100-year stationary and nonstationary return values as given in equation 3.9.

$$Difference = (Nonstationary\ return\ level - stationary\ return\ level) \quad 3.9$$

The values of percentage difference may take positive or negative sign. The positive value will express that nonstationary design discharge values or design levels are higher than the stationary ones and vice versa. From now on, positive values will be stated as positive impacts while negative values will be stated as negative impacts throughout the discussion. Stationary and nonstationary forms of GEV, gumbel, normal and lognormal distributions are applied to analyze the impacts of

nonstationarities for yearly and seasonal precipitation series (Table 3-1). Similarly, Stationary and nonstationary forms of GEV, gumbel, normal distributions are applied to analyze the impacts of nonstationarities for ten types of yearly and seasonal temperature (Table 3-2) and streamflow series (Table 3-3).

Table 3-1 Information about precipitation series used for nonstationary impact assessment

Type	Precipitation Series Name and Abbreviation
<b>Maximum Precipitation</b>	Annual maximum precipitation, yearly AMP
	Annual maximum precipitation during Winter (December-February), Winter AMP
	Annual maximum precipitation during Spring (March–May), Spring AMP
	Annual maximum precipitation during Summer (June–August), Summer AMP
	Annual maximum precipitation during Autumn (September–November), Autumn AMP

Table 3-2 Information about temperature series used for nonstationary impact assessment

Type	Temperature Series Name and Abbreviation
<b>Maximum Temperature</b>	Annual maximum temperature, yearly AMTmax
	Annual maximum temperature during Winter (December-February), Winter AMTmax
	Annual maximum temperature during Spring (March–May), Spring AMTmax
	Annual maximum temperature during Summer (June–August), Summer AMTmax
	Annual maximum temperature during Autumn (September–November), Autumn AMTmax
<b>Minimum Temperature</b>	Annual minimum temperature, yearly AMTmin
	Annual minimum temperature during Winter (December-February), Winter AMTmin
	Annual minimum temperature during Spring (March–May), Spring AMTmin
	Annual minimum temperature during Summer (June–August), Summer AMTmin
	Annual minimum temperature during Autumn (September–November), Autumn AMTmin

Table 3-3 Information about streamflow series used for nonstationary impact assessment

<b>Flow Type</b>	<b>Flow Series Name and Abbreviation</b>
<b>High Flow</b>	Annual maximum flow, yearly AMF
	Annual maximum flow during Winter (December-February), Winter AMF
	Annual maximum flow during Spring (March-May), Spring AMF
	Annual maximum flow during Summer (June-August), Summer AMF
	Annual maximum flow during Autumn (September-November), Autumn AMF
<b>Low Flow</b>	Annual 35th Percentile Value flow, yearly ALF
	Annual 35th Percentile Value flow during Winter (December-February), Winter ALF
	Annual 35th Percentile Value flow during Spring (March-May), Spring ALF
	Annual 35th Percentile Value flow during Summer (June-August), Summer ALF
	Annual 35th Percentile Value flow during Autumn (September-November), Autumn ALF

### 3.2. Hydrological Modeling

"Hydrologiska Byråns Vattenbalansavdelning" or simply HBV is a model developed by the SMHI (Swedish Meteorological and Hydrological Institute). The HBV is the multi-tank, semi-distributed runoff simulation model and has been widely used in Sweden and other parts of Europe (Bergström, 1976; 1990; 1992) in recent. There are many modified versions of HBV present which has been used in around 30 countries across the globe. HBV-light is relatively newer version developed based on same water balance equations used in original HBV. However, HBV-light is relatively more flexible to use due to its inbuilt automatic calibration algorithms. Streamflow projections at three selected sub-basins (2133,2157 and 2164) of Upper Euphrates basin are made by using regional climate model projections of precipitation and temperature as inputs into calibrated HBV-light model. The model can be used in semi-distributed form by dividing the land use/land cover of the

whole basin into four different classes. Furthermore, the model has the capability to simulate runoff based on different elevation zones. The model runs on the daily timescale.

Data required to calibrate the model for runoff simulation are

- 1)-Observed daily temperature
- 2)-Observed daily precipitation
- 3)- Observed Streamflow data
- 4)-Land use data and classifications of the basin
- 5)-Elevation data of the basin
- 6)-Estimated monthly average potential evapotranspiration (estimated by Thornthwaite method)

Observed daily temperature and precipitation data were obtained from the GDM. Streamflow data were obtained from the GDSHW. The 25 land cover class of The USGS Land Cover Institute (LCI) was downloaded from <https://landcover.usgs.gov/landcoverdata.php>. Elevation data with a 90-meter resolution of Shuttle Radar Topography Mission (SRTM) was used in this study which was downloaded from <http://srtm.csi.cgiar.org/>. Potential evapotranspiration was estimated using the Thornthwaite method.

### **Thornthwaite's Method for Estimation of Potential Evapotranspiration**

A noncorrected potential evapotranspiration can be estimated using Thornthwaite's Equation as follows,

$$PET_{Uncorrected} = 16 * \left(\frac{10t}{I}\right)^\alpha \quad 3.10a$$

Where “*t*” is the *monthly average temperature* and “*I*” is the *Annual Heat Index*.  $\alpha$  and “*I*” can be estimated using Equation 3.10b and Equation 3.10c, respectively.

$$\alpha = (6.75 * 10^{-7})I^3 - 7.71 * 10^{-5} * I^2 + 1.792 * 10^{-5} * I + 0.49239 \quad 3.10b$$

$$I = \sum_{i=1}^{12} i \quad 3.10c$$

Where “*i*” is the known as *Monthly Heat Index* and can be estimated using Equation 3.10d.

$$i = \left(\frac{t}{5}\right)^{1.514} \quad 3.10d$$

Equation 2.10a gives the uncorrected estimate of potential evapotranspiration in mm which considers 30-day long month and duration of 12 hours of sunshine in a day. Finally, the corrected potential evapotranspiration is calculated for each month using the actual number of days in month (*d*) and actual average sunshine-hours per day (*N*) in a required month using equation 3.10e.

$$PET = PET_{Uncorrected} * \frac{N}{12} * \frac{d}{30} \quad 3.10e$$

The model structure (left panel) of HBV with a description of parameters and model flowchart (right panel) is provided in Figure 3.2. During the simulation, the model categorizes the precipitation into snow (Ps) and rain (Pr). Precipitation is simulated as snow if the temperature is below a threshold temperature and a snow correction factor (SF<sub>CF</sub>) is used. Similarly, if the temperature is above a threshold temperature, the precipitation is simulated as rainfall. For snowmelt calculation, HBV uses the degree-day method. Water stored in accumulated snowpack is calculated in each elevation zone depending upon the temperature of that elevation zone. Snow melting is related to degree-day factor (DDF) and the difference between air temperature (T<sub>a</sub>) and melting air temperature (T<sub>m</sub>). Soil moisture routine includes runoff generation by considering the changes in soil moisture state and the soil moisture routine process are defined by different parameters like soil moisture state where evaporation reaches at its potential rate (LP), soil moisture storage capacity (FC). After soil moisture routine, there are upper and lower storage zones. Upper zone accumulates the rain and this rainwater leaves the upper zone in three different ways as 1) surface runoff depending upon recession parameter 2) interflow of percolated water from the upper zone to lower and 3) slow and gradual base flow of percolated water from lower zone.

HBV-light software includes automatic calibration using Monte Carlo approach or by using a genetic algorithm. Parameters are estimated within the given range. The range of HBV-light parameters is given in Table 3-4. The HBV-light is calibrated in a semi-distributed way by dividing the basin area into different elevation and land use classes. Original SRTM 90-meter elevation map was divided into ten equal elevation zones. Similarly, the initially obtained land use map was divided into four major land use classes described as 1) urban area and barren rocks 2) agricultural area and other small vegetation 3) forests 4) lakes and open water bodies.



Table 3-4 HBV parameters and range (Seibert, 1997)

Parameter	Explanation	Minimum	Maximum	Unit
<b>Snow routine</b>				
<i>TT</i>	Threshold temperature	-2.5	2.5	°C
<i>CFMAX</i>	Degree-day factor	1	10	mm °C <sup>-1</sup> d <sup>-1</sup>
<i>SFCF</i>	Snowfall correction factor	0.4	1	-
<i>CWH</i>	Water holding capacity	0	0.2	-
<i>CFR</i>	Refreezing coefficient	0	0.1	-
<b>Soil and evaporation routine</b>				
<i>FC</i>	Maximum SM	50	500	mm
<i>LP</i>	SM threshold for reduction of evaporation	0.3	1	
<i>BETA</i>	Shape coefficient	1	6	
<b>Groundwater and response routine</b>				
<i>K<sub>0</sub></i>	Recession coefficient	0.05	0.5	d <sup>-1</sup>
<i>K<sub>1</sub></i>	Recession coefficient	0.01	0.3	d <sup>-1</sup>
<i>K<sub>2</sub></i>	Recession coefficient	0.001	0.1	d <sup>-1</sup>
<i>UZL</i>	Threshold for K <sub>0</sub> -outflow	0	100	mm
<i>PERC</i>	Maximal flow from upper to lower GW-box	0	6	mm d <sup>-1</sup>
<i>MAXBAS</i>	Routing, length of weighting function	1	5	d

Two objective functions 1)- *Nash–Sutcliffe Model Efficiency Coefficient* (NS) and 1)- *Log Nash–Sutcliffe Model Efficiency Coefficient* (LNS) are used for parameter estimations (as suggested in Seibert, 1997). Formulation of NS and LNS are given in Equation 3.11 and Equation 3.12, respectively.

$$NS = 1 - \frac{\sum(Q_{obs} - Q_{sim})^2}{\sum(Q_{obs} - \overline{Q_{sim}})^2} \quad 3.11$$

$$NS = 1 - \frac{\sum(\ln Q_{obs} - \ln Q_{sim})^2}{\sum(\ln Q_{obs} - \overline{\ln Q_{sim}})^2} \quad 3.12$$

Where variable  $Q_{obs}$  is observed daily streamflow and  $Q_{sim}$  is model simulated daily streamflow. The objection functions for NS and LNS can take value in range of  $-\infty$  to 1, and value of 1 depicts the perfect agreement between observation and simulation. HBV-Light is calibrated twice for each basin. For high flow analyses calibration was done using the objective function of NS while LNS was used to calibrate model for the low flow analyses. Alongside the values of objection functions, the model also provides some other performance indicators like *Coefficient of Determination* and *Kling-Gupta Efficiency* after each simulation run.

### **3.3. CORDEX Performance Evaluation**

The 12-members of ensemble CORDEX RCMs for precipitation and temperature data are used to investigate the status of nonstationarities in future projections. A prerequisite before using regional climate model data is to perform evaluation of these models (Luhunga et al., 2016) as these simulations are subjected to a number of uncertainties because of boundary conditions, formulation of GCMs and RCMs as well as size of integration domain (Min et al., 2013). Performance evaluation of RCMs can be done by using different performance evaluation indicators however combined use of these techniques provide more comprehensive information about model's ability to mimic observation data (Flato et al., 2013). Some of the World Meteorological Organization (WMO) recommended techniques for model performance evaluation statistics include *root mean square error* (RMSE), *mean bias error* (MBE), and *correlation coefficient* (CORR) as reported by Luhunga et al. (2016) and Gordon and Shaykewich (2000). Comparative plots of daily average values of observation and model simulation, as used in Kara et al. (2016) are helpful to visualize the ability of the model to emulate the observations especially the annual cycle of a variable.

For this purpose, data from RCMs were compared with the observations and the evaluation and quantification of errors in these RCMs were done using different performance evaluation indicators. In this study, the performance evaluation was done for each of the seven geographical regions of Turkey. This is achieved by making a comparison between regionally averaged observed data and RCM-derived gridded data (data from the grids containing the observation stations). For performance evaluation of precipitation, mean daily precipitation (*daily evaluation*) and mean monthly totals (*monthly evaluation*) are used for a CORDEX reference period of 1971-2005. Similarly, for temperature, mean daily temperature (*daily evaluation*) and mean monthly temperature (*monthly evaluation*) are used to investigate and quantify the errors attached to each of the individual members of CORDEX ensemble. A brief explanation of the model performance indicators used in this study is presented here.

Common Variables:

$M$  = predicted data values

$O$  = observed data values

$n$  = number of data values

$\sigma_m$  = standard deviation of model data values

$\sigma_o$  = standard deviation of observed data values

### **3.3.1. Root Mean Square Error**

The *Root Mean Square Error* (RMSE) is defined as the square root of the variance of the residuals and it is calculated by using the Equation 3.13. It explains the absolute fit of the model to the data i.e., how close are the model predicted data values to the observed data values.

$$\text{Root Mean Square Error} = \sqrt{\frac{\sum_1^n (M_n - O_n)^2}{n}} \quad 3.13$$

RMSE can take values in the range from 0 to  $\infty$ . Lower the values of RMSE, better the fit of the model to the data. RMSE has the same units as of the response variables, and it is considered as one of the most important criteria to evaluate the accuracy of a model.

### 3.3.2. Mean Absolute Error

The Mean Absolute Error (MAE) is another criterion used to evaluate the model performance and is calculated by using the Equation 3.14. MAE is a simple measure and is defined as the mean of the absolute difference between model predicted values and the observed values.

$$\text{Mean Absolute Error} = \frac{1}{n} \sum_1^n |M_n - O_n| \quad 3.14$$

MAE provides an average magnitude of the errors in a set of prediction in comparison to a set of observation, without considering their direction. MAE can take values in the range from 0 to  $\infty$ . Lower the values of MAE, better the fit of the model to the data.

### 3.3.3. Mean Bias Error

The *Mean Bias Error* (MBE) is a simple measure to explain the overall model biases and is calculated by using Equation 3.15. MBE is defined as the mean of the

difference between model predicted values and the observed values. In the case of MBE, signs of the errors are not removed.

$$\text{Mean Bias Error} = \frac{1}{n} \sum_1^n (M_n - O_n) \quad 3.15$$

MBE explains the direction of the error bias. MBE can take values in the range from  $-\infty$  to  $\infty$ . A negative MBE value indicates that the predictions are smaller than observations. Similarly, positive MBE value indicates that the predictions are larger than observations

### 3.3.4. Correlation Coefficient

*Correlation Coefficients* (CORR) is a measure to explain the strength of a relationship between model and observation. CORR can be calculated by using the Equation 3.16.

$$\text{Correlation Coefficient} = \frac{1}{(n-1)} \sum_1^n \left( \left( \frac{O_n - \bar{O}}{\sigma_o} \right) * \left( \frac{M_n - \bar{M}}{\sigma_m} \right) \right) \quad 3.16$$

CORR can take values in the range from -1(for a perfect negative relationship) to 1(for a perfect positive relationship). Closer the values to 1, the stronger positive relationship is observed between model and observation data. Similarly, the stronger negative relationship is present if the CORR value is close to -1. A CORR with zero value indicates no relationship at all between model and observation data.

Once the values of RMSE, CORR, and MAE was calculated for daily and monthly evaluation at each region separately, initially each model was ranked (model with a rank value of 1 being the best) based on RMSE, CORR and MAE as  $N_1$ ,  $N_2$  and  $N_3$ ,

respectively. Then averaged rank was calculated by taking the average of all these ranks for daily and monthly evaluation as given in Equation 3.17.

$$\text{Average Rank} = \text{Average} ((N_1, N_2, N_3)_d, (N_1, N_2, N_3)_m) \quad 3.17$$

Where subscript “*d*” and “*m*” denote daily and monthly evaluations, respectively.

### **3.4. Bias Corrected CORDEX RCMs**

Climate impact models need to have finer resolution with minimum biases. However, GCMs and RCMs generally contain uncertainties and bias. CORDEX provides the downscaled data at much finer resolutions (for example Eur-11 with approximately 12km resolution). But still, CORDEX models contain uncertainties and biases when compared to the observation data because the errors available in GCMs are transferred to RCMs through the boundary and initial conditions. Analysis based on multi-member ensemble approach is one way to reduce the effects of these uncertainties and biases. However, many users (i.e. Sunyer et al., 2015) of climate model data apply some form of bias correction and further downscaling to get better agreement between simulation and observation data. Maraun (2016) critically reviewed the different bias correction methods and discussed the possibility of alteration of climate change trends and nonstationarity signals after bias correction.

However, a couple of bias correction methods are thought to be preserving the long-term nonstationarity signals. *Distribution Based Scaling* (DBS) is thought to preserve future climate variability produced by regional climate models (Yang, 2010) thus improving the usability of RCM data for climate change impact studies.

Another method *Cumulative Distribution Function-Transformation* (CDF-transformation) also considered to be preserving the long-term nonstationarity signals (Vrac et al., 2012; WEB3). As one of the objectives of this thesis study, bias-adjusted CORDEX RCM data is evaluated for their ability to reproduce nonstationarity signals as obtained originally from RCMs.

Two bias-adjusted precipitation models (one with DBS correction method and other with CDF method) and two bias-adjusted temperature models (both with BDS method) were evaluated in this study. Bias correction was not applied as part of this study since the readily available bias-adjusted RCM data were obtained and used, however, a brief description of these bias correction methods is provided here for understanding.

### **3.4.1. Distribution Based Scaling (DBS Method)**

The distribution-based scaling (DBS) method (Yang, 2010) was developed to adjust temperature and precipitation from RCMs to better match with observation.

#### **a) Precipitation Correction**

The DBS method of precipitation correction involves two steps.

1)- Spurious drizzles removal to obtain the corrected percentage of wet days. Percentage of wet days is obtained by introducing a threshold value for each season. Days with precipitation amount larger than the threshold value are considered as wet days and all other days as dry days.

2)- Transformation of remaining precipitation to match observed frequency distribution. There are various theoretical distributions available to describe the

probability distribution function (PDF) of precipitation intensities. A commonly used distribution is the gamma distribution (Equation 3.18), because of its ability to represent the typically asymmetrical and positively skewed.

$$f(x) = \frac{(x/\beta)^{\alpha-1} \exp(-x/\beta)}{\beta \Gamma(\alpha)} \quad x, \alpha, \beta > 0 \quad 3.18$$

where  $\alpha$  is the shape parameter,  $\beta$  is the scale parameter and  $\Gamma(x)$  is the inverse gamma function. The distribution parameters were estimated using maximum likelihood

estimation (MLE). Since the distribution of daily precipitation is heavily skewed towards low-intensity values, the distribution parameters might not capture the properties of extremes. To tackle this issue, the distribution of daily precipitation is partitioned into two parts separated by 95<sup>th</sup> percentile value hence making it double gamma distribution as the Equation 3.19.

$$\begin{cases} P_{DBS} = F^{-1}(\alpha_{Obs}, \beta_{Obs}, F^{-1}(P, \alpha_{CTL}, \beta_{CTL})) & \text{if } P < 95^{\text{th}} \text{ percentile value} \\ P_{DBS} = F^{-1}(\alpha_{Obs,95}, \beta_{Obs,95}, F^{-1}(P, \alpha_{CTL,95}, \beta_{CTL,95})) & \text{if } P \geq 95^{\text{th}} \text{ percentile value} \end{cases} \quad 3.19$$

Two sets of parameters are estimated as  $(\alpha, \beta)$  and  $(\alpha_{95}, \beta_{95})$  from observation as well as RCM in reference and then in turn used to correct the precipitation for projection period. Where *Obs* denotes parameters estimated from observations and *CTL* denotes parameters estimated from the RCM output in the control period. *F* represents the gamma probability distribution. To take seasonality into account, parameters are optimized for each season.

## b) Temperature Correction

Since temperature values are more symmetrically distributed, the normal distribution is used for temperature with mean  $\mu$  and standard deviation  $\sigma$  as Equation 3.20.

$$f(x) = \frac{1}{\sigma\sqrt{2\pi}} e^{-\left(\frac{x-\mu}{\sqrt{2}\sigma}\right)^2} \quad 3.20$$

Mean and standard deviation of temperature are smoothed over reference period with a 15-day moving average window. Temperature time series is conditioned by the dry and wet state of day to account for dependence between temperature and precipitation and seasonal mean and seasonal standard deviation of temperature are smoothed using five harmonics of *Fourier Series* as Equation 3.21 and Equation 3.22.

$$\mu(\dot{t}_{\text{Dry/Wet}}) = \frac{a_{0,\text{Dry/Wet}}}{2} + \sum_{k=1}^K (a_{k,\text{Dry/Wet}} \cdot \cos(kwt^*) + b_{k,\text{Dry/Wet}} \cdot \sin(kwt^*)) \quad 3.21$$

$$\sigma(\dot{t}_{\text{Dry/Wet}}) = \frac{c_{0,\text{Dry/Wet}}}{2} + \sum_{k=1}^K (c_{k,\text{Dry/Wet}} \cdot \cos(kwt^*) + d_{k,\text{Dry/Wet}} \cdot \sin(kwt^*)). \quad 3.22$$

where  $a_0$ ,  $a_k$ ,  $b_k$ ,  $c_0$ ,  $c_k$ , and  $d_k$  are the Fourier coefficients,  $t^*$  is the day of the year,  $w$  equals  $2\pi/n$ , where  $n$  is the time units per cycle and  $k$  stands for the  $n^{\text{th}}$  harmonic used for describing the annual cycle of adjusted daily temperature,  $T_{\text{DBS}}$ . The DBS parameters for temperature were calculated for both observations and RCM-simulated data series. They are denoted  $\mu_{\text{Obs}}$ ,  $\sigma_{\text{Obs}}$ , and  $\mu_{\text{CTL}}$ ,  $\sigma_{\text{CTL}}$  and are used to scale the daily temperature using Equation 3.23.

$$T_{\text{DBS}} = F^{-1}(\sigma_{\text{Obs}}, \mu_{\text{Obs}}, F^{-1}(T_{\text{RCA}}, \sigma_{\text{CTL}}, \mu_{\text{CTL}})) \quad 3.23$$

### 3.4.2. Cumulative Distribution Function Transform (CDF-transform Method)

The main idea behind this approach is to relate the cumulative distribution function (CDF) of a variable (temperature, precipitation etc.) at a large scale (RCM) to the CDF of that variable at the station or local scale. CDF-t approach involves the application of the mathematical transformation to the large-scale CDF and creates a new CDF which is supposed to be as close as possible to the CDF of measured station variable.  $F_{Gh}$  and  $F_{Sh}$  describe the CDFs of the variable of interest from the GCM/RCM and observation, respectively, over a historical calibration period  $h$ . It is assumed that transformation  $T$  allows going from  $F_{Gh}$  to  $F_{Sh}$  using Equation 3.24.

$$T(F_{Gh}(x)) = F_{Sh}(x) \quad 3.24$$

Replacing  $x$  by  $F_{Gh}^{-1}(u)$ , where  $u$  is any probability in  $[0,1]$ , the following can be obtained

$$T(u) = F_{Sh}(F_{Gh}^{-1}(u)) \quad 3.25$$

which provides a simple definition of  $T$ . Assuming  $T$  is stationary in time, the transformation can be applied to  $F_{Gf}$ , the large-scale CDF of the climate variable over a validation or future period  $f$ , to generate  $F_{Sf}$ , the CDF at the station location for the same period  $f$ .

$$T(F_{Gf}(x)) = F_{Sf}(x) \quad 3.26$$

Which can be written as

$$F_{Sf}(x) = F_{Sh}(F_{Gh}^{-1}(F_{Gf}(x))) \quad 3.27$$



## CHAPTER 4

### CORDEX PERFORMANCE EVALUATION

Global circulation models (GCMs) are very useful tools for analysis of climate change and its variability. GCMs have generally the ability to simulate the general circulation of the atmosphere at the continental scale (i.e.,  $1^\circ$ ) but they may not be able to assess the climate change and its variability at regional and smaller scale (10-50 km) (Giorgi et al., 2009; Rummukainen, 2010). Because of the coarser grid resolution, magnitudes and intensity of extreme events (like heavy precipitation) are usually not realistically captured at a smaller scale (Endris et al., 2013). To provide a solution for these problems, regional climate models (RCMs) are mostly used which are available at much finer grids. Before using data from these CORDEX RCMs it is very important to assess their accuracy to represent the actual climate conditions. Different performance evaluation indicators are used for this purpose. In this chapter, the results of performance evaluation of 12 different CORDEX RCMs are presented and discussed for precipitation and temperature.

#### 4.1. Results

##### 4.1.1. Precipitation Evaluation

The performance of each individual RCM is evaluated by different performance evaluation indicators (RMSE, MAE, MBE, and CORR) on a regional scale using

regionally lumped observed and CORDEX precipitation data for CORDEX reference period (1971-2005). Comparisons are made for mean daily precipitation obtained from models as well as observations. Plots obtained from the same GCM, but different RCMs are grouped together to analyze the performance of each of individual GCM. Along with graphical comparisons, summary tables of model evaluation statistics-based on mean daily and monthly total precipitation are given here. In each summary table, green flag, red flag and yellow brick show models with good, bad and average performance.

### 1) Marmara Region

Regionally averaged mean daily precipitation from individual RCM gridded stations against observed mean daily precipitation is plotted for the Marmara region in Figure 4.1. Model performance statistics are given in Table 4-1. Visual inspection of Figure 4.1 shows that all the RCMs originated from GCMs EC-EARTH (i.e. CORDEX RCMs 11,12,13, and 14) and HadGEM2-ES (i.e. CORDEX RCMs 13,23, and 33) were able to emulate the seasonal variation of precipitation in comparison to the observations. The correlation coefficient as given in Table 4-1 for mean daily precipitation, as well as successive monthly precipitation, was also better for these RCMs. The models 21, 22 and 42 overestimated precipitation during the late spring and early days of summer as can be seen from plots. The models 23 and 41 were able to reproduce the seasonal variations of precipitation like the observed ones. The mean bias error values for mean daily precipitation as well as successive monthly precipitation explain that RCMs 11, 14, 31 and 41 have shown slight underestimation while RCMs with 21, 22, 32 and 42 have a tendency to overestimate the precipitation. RCMs 21, 22, 32 and 42 have given more RMSE and MAE values. Based on the average rank values, RCM 13 (EC-EARTH-RACMO22E) and RCM 21(CNRM-CM5-ALADIN53) were found to be the best and worst models for Marmara Region of Turkey, respectively.

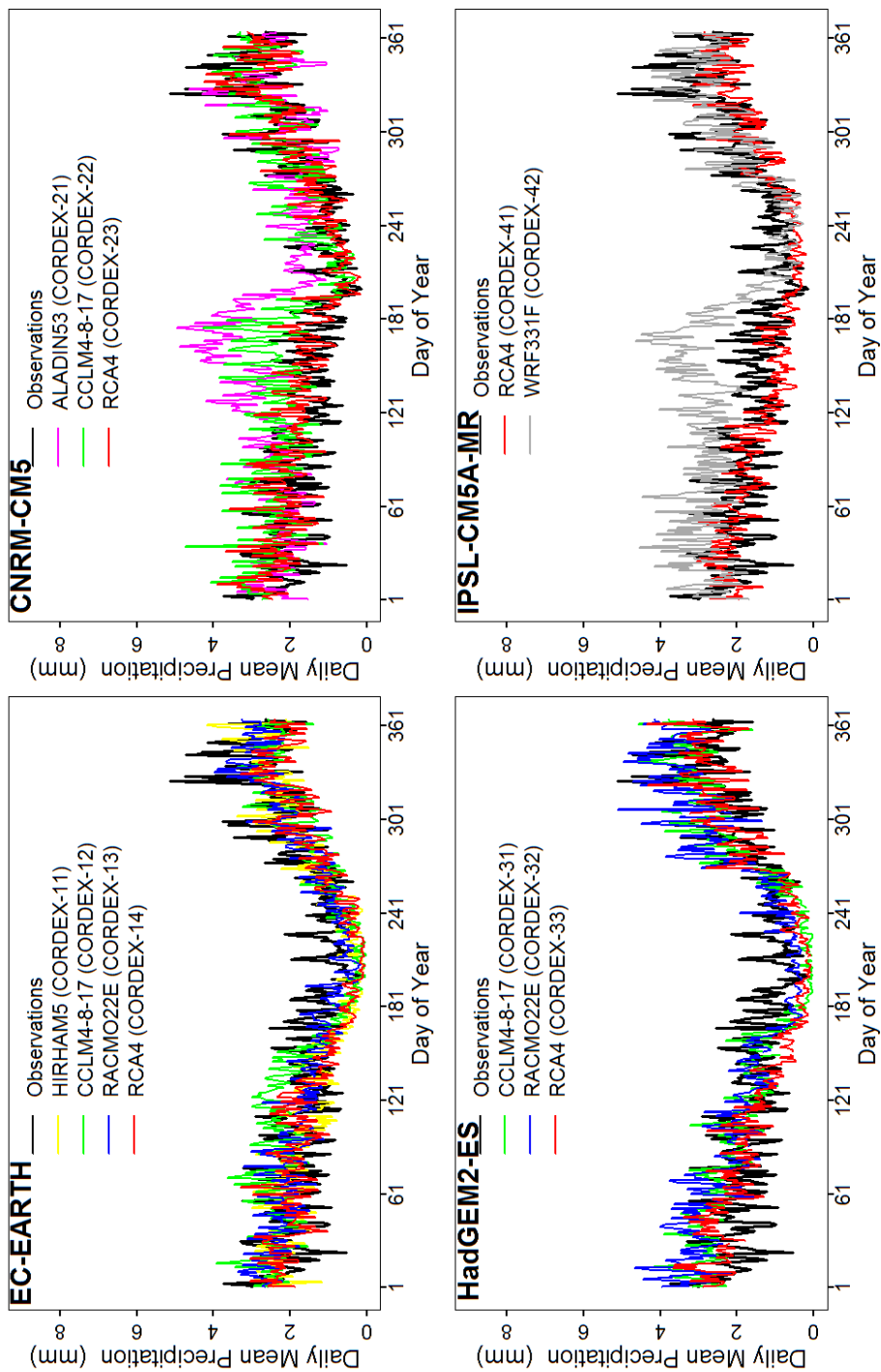


Figure 4.1 Comparison of regionally averaged mean daily observed and RCM precipitation for the Marmara region of Turkey.

Table 4-1 Performance statistics summary of precipitation for the Marmara region

CORDEX ID	Mean Daily Precipitation				Successive Monthly Total Precipitation				Average Rank
	RMSE (mm)	MAE (mm)	MBE (mm)	CORR	RMSE (mm)	MAE (mm)	MBE (mm)	CORR	
<b>11</b>	0.83	0.65	-0.18	0.58	38.30	29.71	-1.22	0.37	6.6
<b>12</b>	0.84	0.65	-0.04	0.56	37.80	28.86	-0.03	0.37	6
<b>13</b>	0.71	0.55	-0.01	0.66	38.05	29.19	3.87	0.35	<b>2.8</b>
<b>14</b>	0.79	0.63	-0.30	0.62	34.51	25.72	-5.31	0.40	3.2
<b>21</b>	1.34	1.05	0.66	0.08	56.54	44.05	22.37	-0.08	<b>12</b>
<b>22</b>	1.04	0.81	0.50	0.45	45.82	35.92	12.94	0.22	10
<b>23</b>	0.76	0.58	0.10	0.60	40.62	31.65	5.57	0.28	5.4
<b>31</b>	0.89	0.73	0.13	0.67	39.44	30.92	3.49	0.46	6.2
<b>32</b>	1.02	0.78	0.40	0.65	41.56	32.08	12.94	0.50	8
<b>33</b>	0.81	0.64	-0.14	0.66	36.55	28.55	-1.53	0.45	3.8
<b>41</b>	0.77	0.59	-0.31	0.62	35.74	27.11	-4.78	0.35	3
<b>42</b>	1.22	0.98	0.67	0.42	54.20	43.47	24.55	0.16	11

## 2) Aegean Region

Regionally averaged mean daily precipitation from individual RCM gridded stations against observed mean daily precipitation is plotted for Aegean region in Figure 4.2. Model performance statistics are given in Table 4-2. Visual inspection of plots given in Figure 4.2 suggests that all the RCMs (except CORDEX RCM 12 which underestimated/overestimated the winter and spring precipitation, respectively) originated from GCMs, EC-EARTH and HadGEM2-ES were able to reproduce the seasonal variability of precipitation better than the RCMs originated from other two GCMs, CNRM-CM5 and IPSL-CM5A-MR. So, these RCMs have shown higher correlations as compared to other two GCM groups as given in Table 4-2. All three RCMs originated from GCM of CNRM-CM5 have shown clear overestimation during late spring and early summer however during autumn and winter these three RCMs have shown good agreement with the observation. The RCM 42 has shown distinctive overestimation throughout the year and it was more evident during late spring and summer. The RCM 41 agreed well with observation for the seasonal variability of precipitation, however, this model has generally shown a tendency of underestimation in precipitation. Mean bias error values show that three models (11, 12 and 14) originated from GCM, EC-EARTH underestimate precipitation while the model 14 slightly overestimates. The positive mean bias error values for all three RCMs originated from GCM, CNRM-CM5 show significant overestimation. Similarly, RCMs 32 and 41 have the negative mean bias while RCMs 31, 32 and 42 takes the positive mean bias. As it is seen in Figure 4.2 and Table 4-2, RCMs 41 and 14 have shown the highest overestimation and highest underestimation, respectively. RCMs 12, 21, and 42 contained the highest RMSE as well as MAE values. Based on the average rank values, RCM 32 (HadGEM2-ES-RACMO22E) was found to be the best model for the Aegean region of Turkey. Similarly, the averaged rank values show that RCM 21 (CNRM-CM5-ALADIN53) was the worst model among these ensembles.

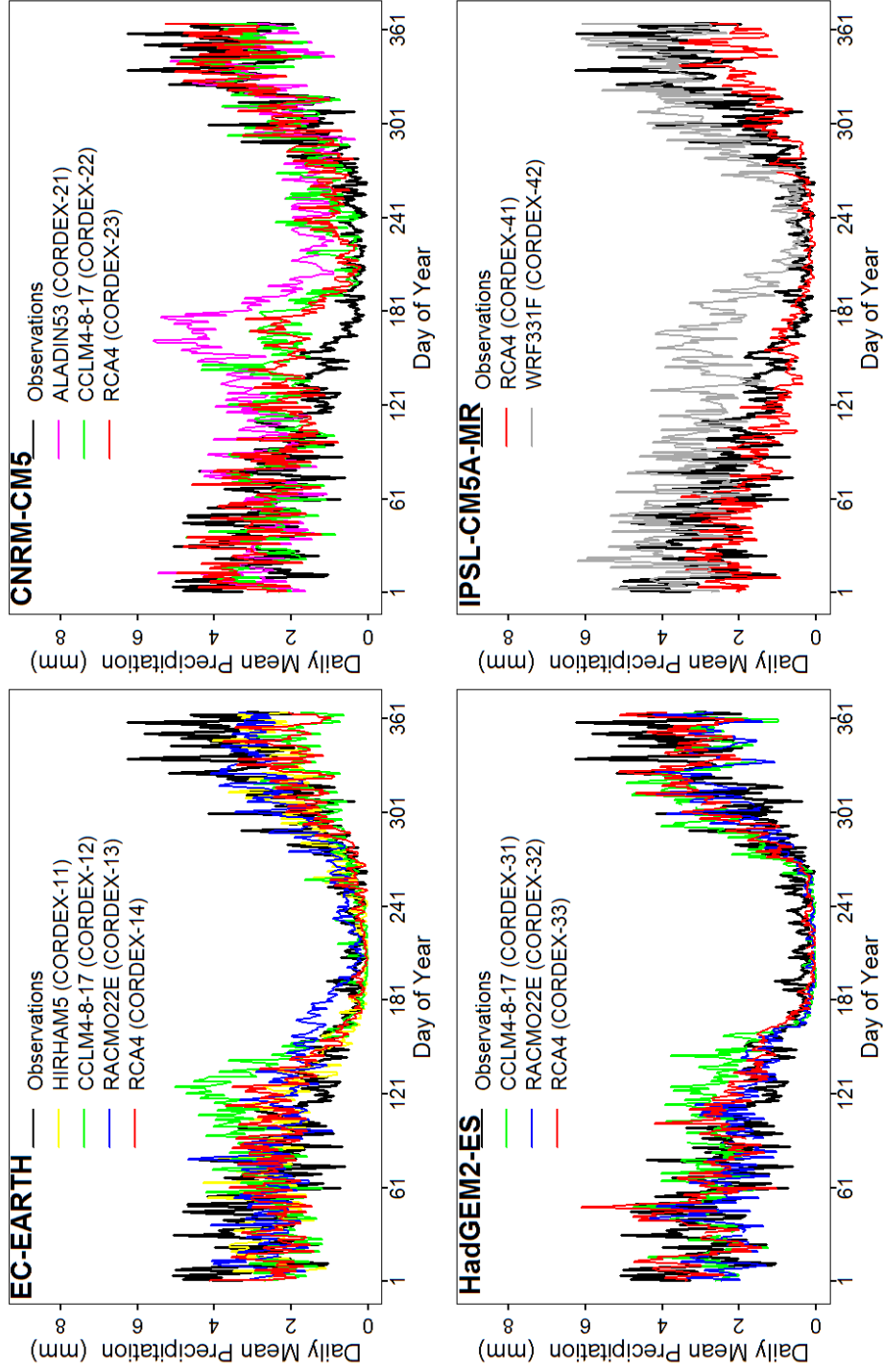


Figure 4.2 Comparison of regionally averaged mean daily observed and RCM precipitation for the Aegean region of Turkey.

Table 4-2 Performance statistics summary of precipitation for the Aegean region

CORDEX ID	Mean Daily Precipitation				Successive Monthly Total Precipitation				Average Rank
	RMSE (mm)	MAE (mm)	MBE (mm)	CORR	RMSE (mm)	MAE (mm)	MBE (mm)	CORR	
1 1	1.04	0.74	-0.17	0.68	49.29	34.50	-5.44	0.43	4.4
1 2	1.41	0.99	-0.15	0.44	55.24	37.46	-4.78	0.34	9.6
1 3	1.00	0.77	0.11	0.70	50.48	35.38	3.39	0.41	4.8
1 4	1.15	0.79	-0.30	0.61	47.34	30.41	-9.39	0.47	5
2 1	1.78	1.42	0.73	0.15	66.91	53.11	22.27	0.09	<b>11.8</b>
2 2	1.21	0.94	0.30	0.56	55.50	41.31	9.16	0.30	9.6
2 3	1.12	0.89	0.38	0.67	53.94	39.72	11.65	0.41	7.2
3 1	1.17	0.86	0.15	0.63	49.45	34.55	3.18	0.49	7
3 2	0.99	0.70	-0.24	0.73	44.36	29.68	-8.28	0.55	<b>1.4</b>
3 3	0.99	0.68	0.14	0.75	48.93	33.37	3.22	0.54	2.4
4 1	1.15	0.79	-0.57	0.69	48.04	32.58	-17.37	0.48	4.4
4 2	1.51	1.21	1.00	0.67	68.17	50.70	30.93	0.34	10.4

### 3) Mediterranean Region

Area-averaged mean daily precipitation from individual RCM gridded stations is plotted against observed mean daily precipitation for the Mediterranean region as shown in Figure 4.3. Model performance statistics are given in Table 4-3. Plots given in Figure 4.3 show that RCMs originated from GCMs, EC-EARTH and HadGEM2-ES were able to reproduce the seasonal variability of precipitation better than the RCMs originated from other two GCMs, CNRM-CM5 and IPSL-CM5A-MR. This emulating of seasonal variability of precipitation is also evident from their higher correlation values. However clear overestimation was observed in Figure 4.3 for RCMs 11, 22, 14, and 33 particularly during the winter season. The mean bias errors which are given in Table 4-3, also explain these features. Visual inspection of Figure 4.3 also shows that all the RCMs originated from GCM, CNRM-CM5 have shown overestimation obviously during the late spring and early summer seasons. However, all three RCMs were found to be in fair agreement with observation during other seasons. Both RCMs (41 and 42) originated from GCM of IPSL-CM5A-MR have also shown fair match with observations however in case of RCM 41, a slight overestimation and underestimation were found during summer and winter, respectively. RCMs 11, 22 and 33 have shown more RMSE and MAE values. Based on mean bias error values for daily mean precipitation and successive monthly precipitation, RCMs 11, 13, 22 and 33 have shown significant overestimation overall. Similarly, the negative sign of mean bias error (dry bias) with higher magnitude for RCM 12 and 31 suggests that these models have tendencies to underestimate overall precipitation. Based on the average rank values given in Table 4-3, RCM 32 (HadGEM2-ES-*RACMO22E*) was found to be the best model for the Mediterranean region of Turkey. Similarly, RCM 22 (CNRM-CM5-*CCLM4-8-17*) was the worst model among ensemble members.

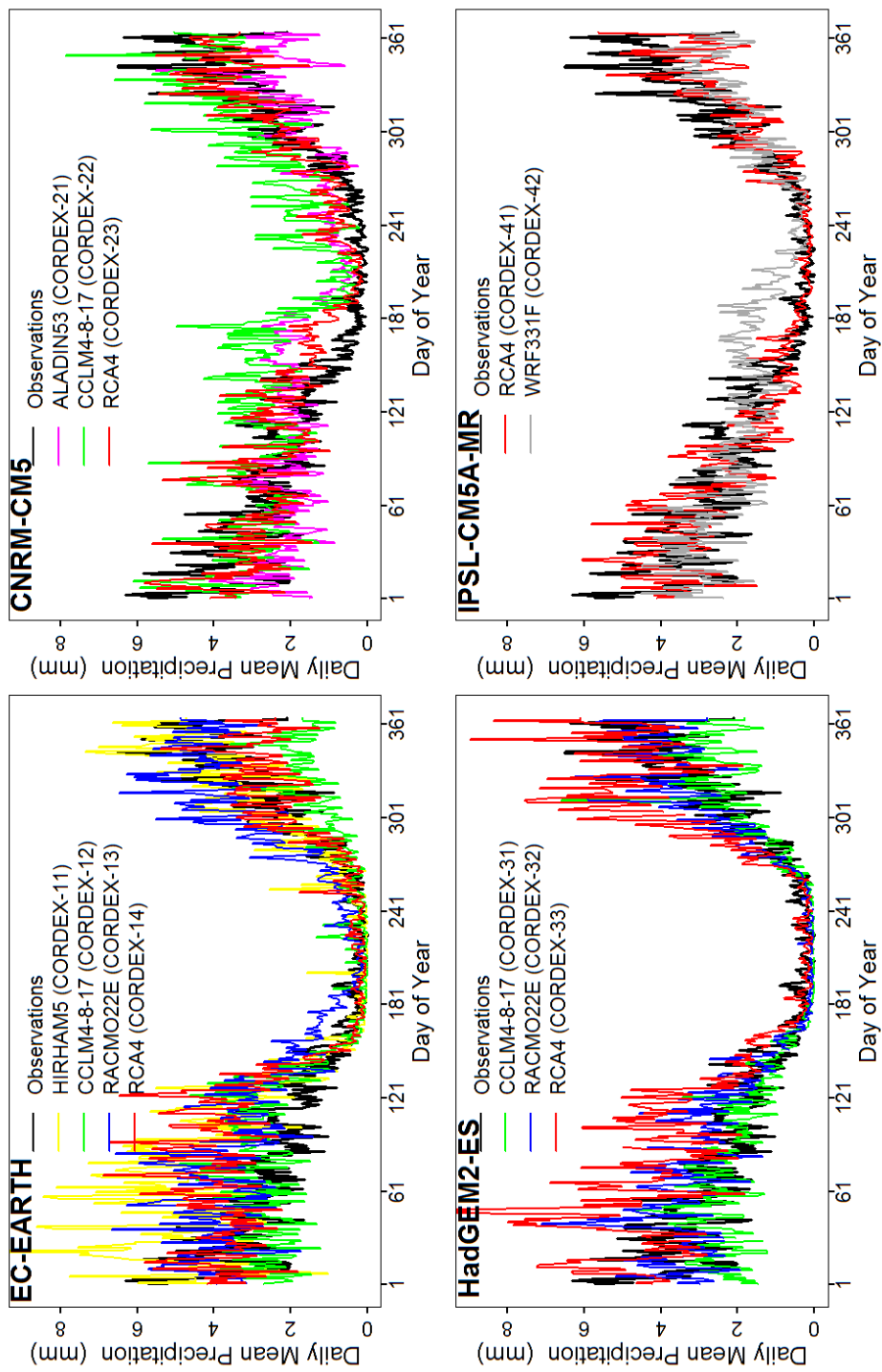


Figure 4.3 Comparison of regionally averaged mean daily observed and RCM precipitation for the Mediterranean region of Turkey.

Table 4-3 Performance statistics summary of precipitation for the Mediterranean region

CORDEX ID	Mean Daily Precipitation				Successive Monthly Total Precipitation				Average Rank
	RMSE (mm)	MAE (mm)	MBE (mm)	CORR	RMSE (mm)	MAE (mm)	MBE (mm)	CORR	
1 1	1.77	1.22	0.84	0.76	79.33	52.14	25.85	0.54	9.2
1 2	1.36	0.95	-0.42	0.60	58.12	38.58	-13.25	0.44	6.6
1 3	1.39	1.04	0.74	0.74	69.27	47.02	22.52	0.49	7.4
1 4	1.40	0.98	0.29	0.66	65.25	43.41	8.56	0.47	8.2
2 1	1.37	1.04	-0.19	0.50	56.74	41.91	-6.10	0.36	8.2
2 2	1.59	1.29	0.81	0.55	70.92	53.26	24.69	0.35	11
2 3	1.10	0.82	0.21	0.73	55.67	39.53	6.46	0.51	4.2
3 1	1.15	0.75	-0.45	0.74	51.61	33.58	-15.80	0.56	2.8
3 2	1.09	0.74	0.22	0.79	54.68	36.87	4.24	0.58	1.4
3 3	1.86	1.27	1.01	0.73	76.30	50.04	27.94	0.56	10.2
4 1	1.12	0.79	-0.18	0.74	56.01	37.46	-5.97	0.54	3.6
4 2	1.13	0.87	-0.10	0.70	55.79	38.83	-3.51	0.43	5.2

#### 4) Central Anatolia

Regionally averaged mean daily precipitation from individual RCM gridded stations is plotted against observed mean daily precipitation for Central Anatolia region in Figure 4.4. Model performance statistics are given in Table 4-4. Visual inspection of plots given in Figure 4.4 suggests that RCMs originated from GCMs, EC-EARTH and HadGEM2-ES were able to reproduce the seasonal variability of precipitation better than the RCMs originated from other two GCMs, CNRM-CM5 and IPSL-CM5A-MR. This ability is also evident from the comparatively higher correlation values in Table 4-4. Plots also show that the two RCMs originated from GCM of CNRM-CM5 have shown overestimation during the late spring and early summer, however, these models were able to fairly mimic the daily mean precipitation during other seasons. In addition, the RCM 23 originated from the same GCM were able to explain the seasonal variation throughout the year quite well. In case of RCMs originated from GCM of IPSL-CM51-MR the RCM 41 has shown significant overestimation during winter season while RCM 42 clearly overestimated precipitation during the late spring and early summer. Positive values of mean bias errors for daily mean precipitation and successive monthly total precipitation suggest that all the RCMs have a tendency to overestimate mean daily and monthly total precipitation. Furthermore, RCMs 11, 13, 21 and 31 contain relatively higher RMSE values. Based on the average rank values provided in Table 4-4, RCM 12 (EC-EARTH-CCLM4-8-17) was found to be the best model for the Central Anatolia region of Turkey. Similarly, the averaged rank values show that RCM 21 (CNRM-CM5-ALADIN53) was found to be the worst model out of this ensemble.

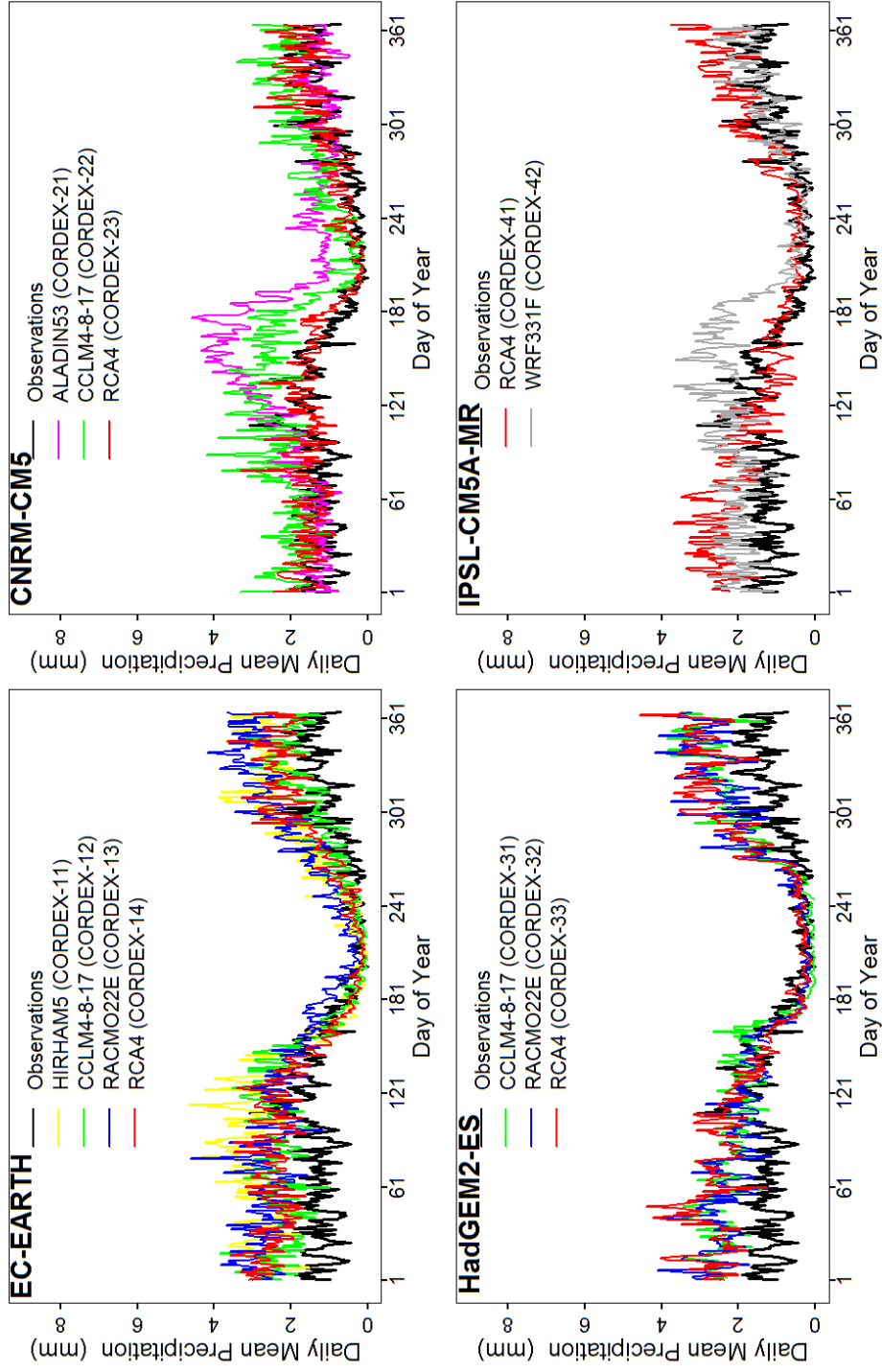


Figure 4.4 Comparison of regionally averaged mean daily observed and RCM precipitation for the Central Anatolia region of Turkey.

Table 4-4 Performance statistics summary of precipitation for the Central Anatolia region

CORDEX ID	Mean Daily Precipitation				Successive Monthly Total Precipitation				Average Rank
	RMSE (mm)	MAE (mm)	MBE (mm)	CORR	RMSE (mm)	MAE (mm)	MBE (mm)	CORR	
1 1	1.32	1.06	0.96	0.64	47.03	35.75	29.54	0.48	10.2
1 2	0.85	0.66	0.52	0.70	34.00	25.02	16.29	0.52	2
1 3	1.24	1.01	0.98	0.60	46.26	35.02	30.26	0.37	9.8
1 4	0.98	0.76	0.63	0.64	35.27	27.02	19.60	0.50	4
2 1	1.24	0.94	0.73	0.24	42.81	32.88	22.52	0.14	10.2
2 2	1.07	0.87	0.82	0.59	40.21	31.24	25.56	0.39	7.4
2 3	0.60	0.45	0.21	0.58	25.89	19.48	6.99	0.39	2.2
3 1	1.06	0.82	0.64	0.61	38.01	28.35	19.37	0.46	6
3 2	1.07	0.79	0.63	0.54	38.47	28.27	19.19	0.42	7.4
3 3	1.22	0.93	0.79	0.56	43.57	32.20	24.00	0.40	9
4 1	0.95	0.73	0.53	0.49	36.36	27.25	16.50	0.31	5.8
4 2	0.91	0.70	0.56	0.55	33.55	26.21	17.40	0.39	4

## 5) Black Sea Region

Regionally averaged mean daily precipitation from individual RCM gridded stations is plotted against observed mean daily precipitation in Figure 4.5 for Black sea region. Model performance statistics are given in Table 4-5. Visual inspection of plots given in Figure 4.5 shows that RCMs originated from GCMs, EC-EARTH and HadGEM2-ES were able to reproduce the seasonal variability of precipitation better than those RCMs originated from other two GCMs, CNRM-CM5 and IPSL-CM5A-MR. This emulation of seasonal variability of precipitation is also clear from the comparatively higher correlation between daily mean precipitation of these RCMs and observations as given in Table 4-5. However, all these seven RCMs have shown the tendency of underestimation during the summer season as can be seen in plots. Also, it is evident from the plots that all three RCMs originated from GCM of HadGEM2-ES slightly overestimated the winter precipitation. Two RCMs (21, 22) overestimated the spring and early summer precipitation while the third RCM (23) underestimated it during same seasons. In the case of RCM 41, there was slight underestimation observed, however, the RCM was able to explain the seasonal variability at a fair level. RCM 42 also overestimated the spring and early summer precipitation. The negative bias errors of all RCMs originated from GCM EC-EARTH are evidence of their tendencies of underestimation for daily mean and monthly total precipitations overall. RCMs 22, 31 and 42 contain higher RMSE and MAE values for both daily mean and successive monthly precipitation. It is also worth mentioning that all the RCA models have shown negative bias errors which indicated their aptness of underestimation in the Black Sea region. Based on the average rank values provided in Table 4-5, RCM 11 (EC-EARTH-*HIRHAM5*) was found to be the best model for the Black Sea region of Turkey. Similarly, the averaged rank values show that RCM 42 (CNRM-CM5-*WRF331F*) was found to be the worst model out of this ensemble.

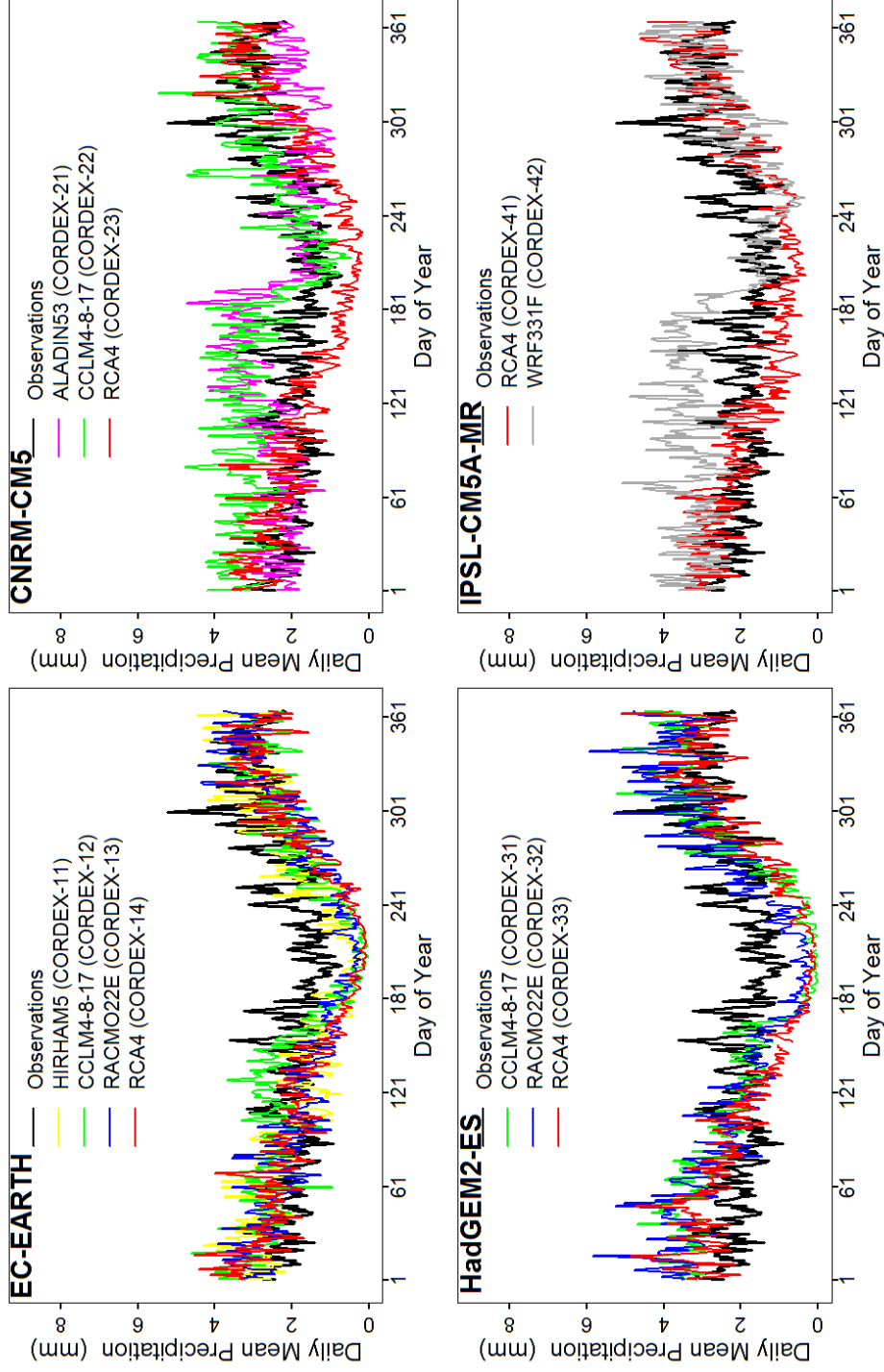


Figure 4.5 Comparison of regionally averaged mean daily observed and RCM precipitation for the Black Sea region of Turkey

Table 4-5 Performance statistics summary of precipitation for the Black Sea region

CORDEX ID	Mean Daily Precipitation				Successive Monthly Total Precipitation				Average Rank
	RMSE (mm)	MAE (mm)	MBE (mm)	CORR	RMSE (mm)	MAE (mm)	MBE (mm)	CORR	
1 1	0.95	0.79	-0.17	0.50	39.72	30.96	-2.90	0.30	 <b><u>1.40</u></b>
1 2	0.99	0.82	-0.11	0.45	40.54	32.78	-0.94	0.30	 5.20
1 3	1.00	0.82	-0.35	0.49	40.44	31.55	-8.27	0.30	 3.40
1 4	1.05	0.87	-0.43	0.48	40.15	32.28	-10.53	0.32	 5.00
2 1	1.13	0.90	0.06	-0.16	44.55	35.50	4.34	-0.12	 8.80
2 2	1.20	0.97	0.73	0.34	49.20	38.55	24.67	0.17	 <b>10.60</b>
2 3	1.04	0.85	-0.42	0.48	42.26	33.36	-10.26	0.28	 5.80
3 1	1.19	1.00	0.02	0.51	45.69	36.20	2.41	0.34	 8.60
3 2	1.15	0.95	0.19	0.53	45.40	35.50	7.41	0.35	 7.20
3 3	1.11	0.94	-0.33	0.48	42.63	34.40	-8.32	0.30	 6.80
4 1	0.98	0.81	-0.32	0.48	39.88	31.98	-7.36	0.30	 3.40
4 2	1.32	1.08	0.50	0.09	50.47	40.20	17.82	0.09	 <b><u>11.80</u></b>

## 6) Eastern Anatolia Region

Plots of regionally averaged mean daily precipitation from individual RCM gridded stations against observed mean daily precipitation is plotted as given in Figure 4.6 for Black sea region. Model performance statistics are given in Table 4-6. Plots given in Figure 4.6 show that most of the RCMs originated from GCMs, EC-EARTH and HadGEM2-ES were able to reproduce the seasonal variability of precipitation better than those RCMs originated from other two GCMs, CNRM-CM5 and IPSL-CM5A-MR. This proclivity of reproducing the seasonal variability of precipitation is also obvious from the comparatively higher correlation values given in Table 4-6. However, RCMs 11, 13, 14 (all originated from GCM EC-EARTH) apparently have slight underestimation during the spring season (see the relevant panel in Figure 4.6). Similarly, RCMs 31 and 32 originated from GCM of HadGEM2-ES have overestimation during the autumn season. RCM 2-1 underestimated the mean daily precipitation during winter and overestimated it during late spring and early summer. RCMs 21 and 22 show fair agreement with observed mean daily precipitation however in case of RCM 22, overestimation was observed during the spring season. RCM 41 was found to be overestimating precipitation during winter, spring and autumn seasons while RCM 42 underestimated it during spring and autumn seasons. Furthermore, negative mean bias error value for successive monthly total precipitation show that three RCMs (11, 13, and 14) originated from GCM EC-EARTH have inclinations towards overestimation overall. Similarly, all the RCMs originated from GCM of CNRM-CM5 contain positive biases (wet biases). Mean bias error values which are given in Table 4-6, also suggest that the RCM 42 and 41 were found to be the model with the highest amount of overestimation and underestimation, respectively. RCMs 22, 23 and 42 contain relatively higher RMSE and MAE for both daily mean and successive monthly precipitation. Based on the average rank values provided in Table 4-6, RCM 12 (EC-EARTH-CCLM4-8-17) and RCM 42 (CNRM-CM5

*WRF331F*) were found to be the best and the worst RCMs for Eastern Anatolia region of Turkey.

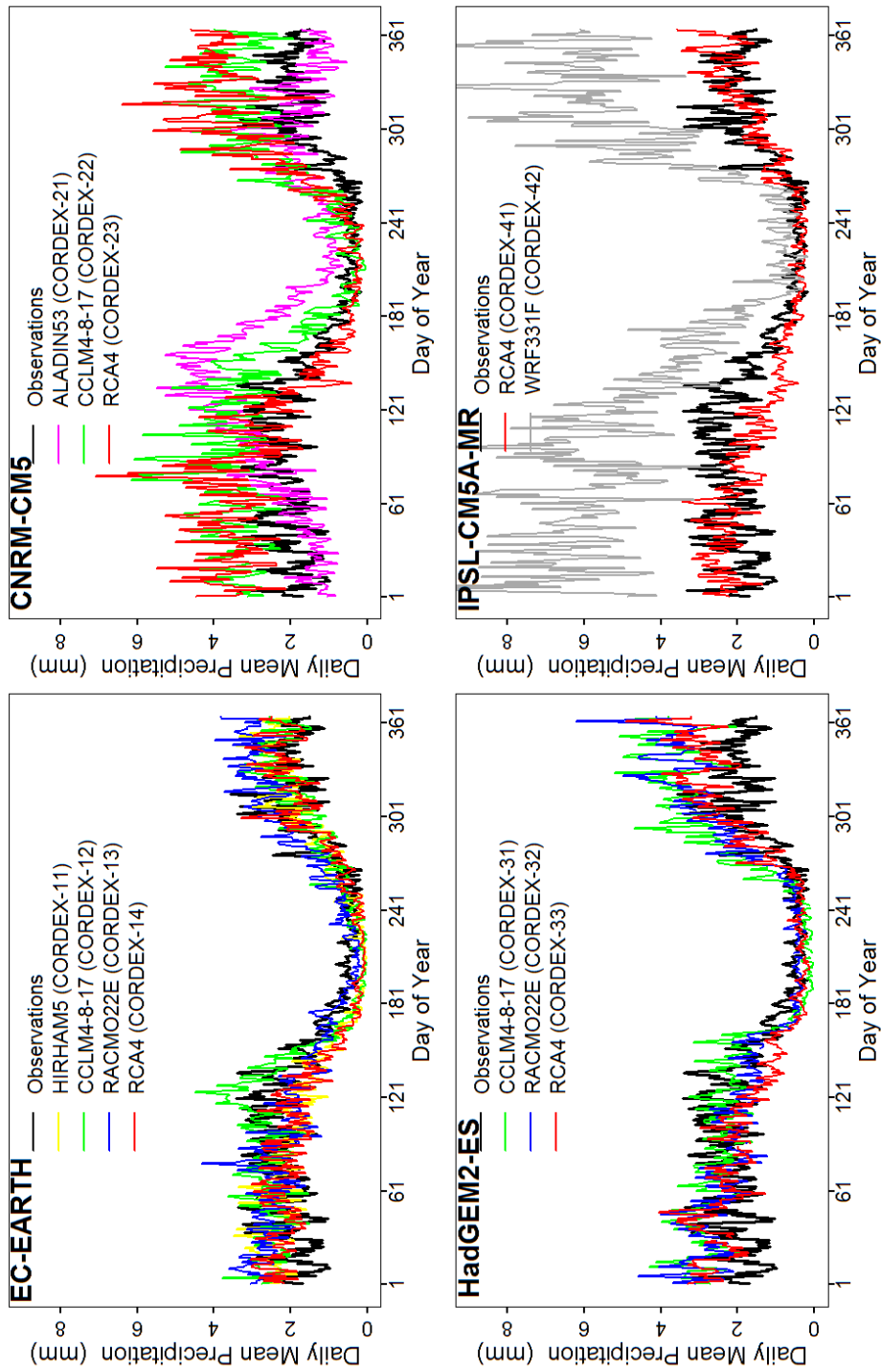


Figure 4.6 Comparison of regionally averaged mean daily observed and RCM precipitation for the Eastern Anatolia region of Turkey.

Table 4-6 Performance statistics summary of precipitation for the Eastern Anatolia region

CORDEX ID	Mean Daily Precipitation				Successive Monthly Total Precipitation				Average Rank
	RMSE (mm)	MAE (mm)	MBE (mm)	CORR	RMSE (mm)	MAE (mm)	MBE (mm)	CORR	
11	0.75	0.59	-0.08	0.66	42.00	31.17	-23.48	0.47	4.6
12	0.72	0.57	0.15	0.77	38.56	28.43	0.51	0.54	<b>1.8</b>
13	0.87	0.68	0.29	0.62	38.47	27.74	-13.91	0.44	4.4
14	0.70	0.56	-0.15	0.71	38.97	28.69	-20.69	0.55	2.4
21	1.33	1.06	0.58	0.32	53.27	41.67	12.44	0.19	9.8
22	1.52	1.22	1.13	0.71	57.81	42.14	29.29	0.48	9.2
23	1.54	1.15	0.87	0.63	53.60	37.37	10.75	0.42	9.4
31	1.14	0.86	0.57	0.67	48.22	34.84	13.67	0.47	7.2
32	1.06	0.77	0.40	0.60	39.88	28.97	-4.68	0.47	6.8
33	0.89	0.67	0.11	0.62	38.73	28.64	-18.68	0.52	5
41	0.82	0.61	-0.17	0.58	44.30	32.84	-26.24	0.43	6.6
42	3.46	2.81	2.79	0.66	94.12	66.04	58.10	0.45	<b>10.8</b>

## 7) South-Eastern Anatolia Region

Plots of regionally averaged mean daily precipitation from individual RCM gridded stations against observed mean daily precipitation is given in Figure 4.7 for South-Eastern Anatolia region. Model performance statistics are given in Table 4-7. As long as seasonal variability is concerned, the visual inspection of plots and the correlation values given in Table 4-7, suggest that all the RCMs (except RCM 21) were able to describe it at an equally fair level (similar correlation values are found for most of the RCMs). However, it can also be observed that RCM 11 overestimated the winter and autumn precipitation. Similarly, RCM 12 slightly underestimated precipitation during autumn and winter season. RCM 21 have a tendency to underestimate the winter precipitation and slightly overestimate the late spring and early summer precipitation. Small overestimations are visible during autumn season in case of RCM 22 and 23. All the RCMs originated from GCM HadGEM2-ES found evidence of overestimation during the autumn season. RCM 42 has significantly shown overestimation throughout the year while the RCM 41 from the same GCM has underestimation during winter, spring and autumn seasons. Most of the RCMs (except RCM 12, 14 and 41) showed positive mean bias error values for daily mean as well as successive monthly total precipitation which suggest a wet bias for monthly total precipitation. RCM 42 and RCM 41 showed the highest positive and negative value of mean bias, respectively. RCMs 11, 21 and 42 contain relatively higher values of RMSE and MAE for daily mean and successive monthly total precipitation. Based on the average rank values provided in Table 4-7, RCM 11 (*EC-EARTH-RCA4*) was found to be the best model for South-Eastern Anatolia region of Turkey. Similarly, the averaged rank values also show that RCM 42 (*CNRM-CM5-WRF331F*) was found to be the worst model out of this ensemble.

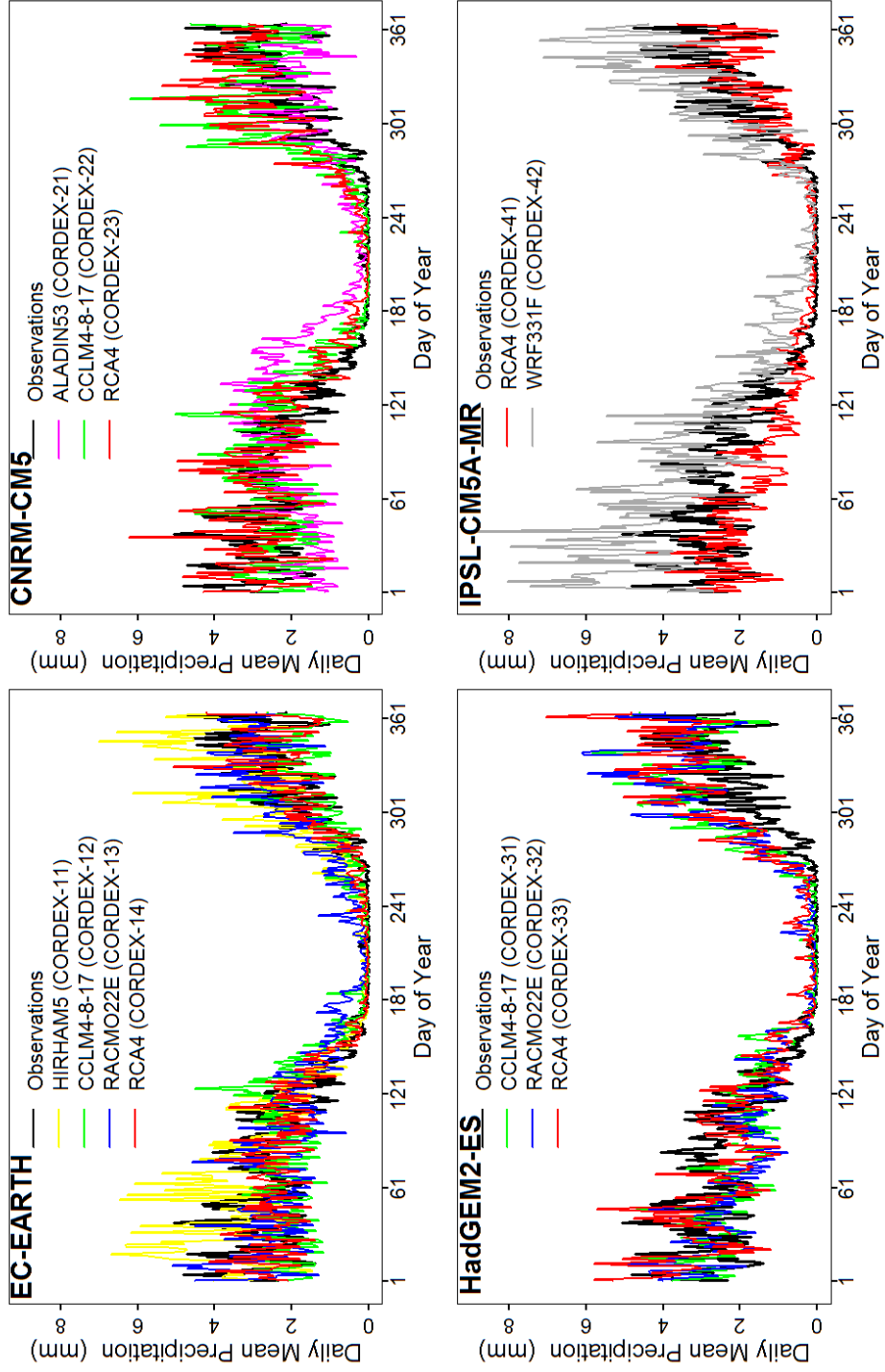


Figure 4.7 Comparison of regionally averaged mean daily observed and RCM precipitation for South-Eastern Anatolia region of Turkey.

Table 4-7 Performance statistics summary of precipitation for South-Eastern Anatolia

CORDEX ID	Mean Daily Precipitation				Successive Monthly Total Precipitation				Average Rank
	RMSE (mm)	MAE (mm)	MBE (mm)	CORR	RMSE (mm)	MAE (mm)	MBE (mm)	CORR	
11	1.26	0.86	0.59	0.78	54.68	36.36	18.80	0.59	7.8
12	0.97	0.68	-0.19	0.70	44.56	29.95	-5.41	0.50	3
13	1.00	0.76	0.19	0.70	46.20	32.02	6.80	0.52	4.6
14	0.83	0.56	-0.08	0.79	42.90	29.05	-1.65	0.56	1
21	1.29	0.99	0.03	0.41	51.79	38.45	1.17	0.28	10.4
22	1.17	0.80	0.25	0.64	54.88	36.29	8.33	0.43	9
23	1.08	0.77	0.40	0.74	55.16	36.49	13.10	0.51	7
31	1.06	0.76	0.21	0.70	49.38	34.23	5.14	0.48	5.6
32	1.11	0.79	0.22	0.69	49.84	33.67	5.48	0.49	6.8
33	1.13	0.81	0.41	0.73	53.48	37.03	11.36	0.51	7.8
41	1.01	0.71	-0.39	0.72	45.02	29.79	-11.76	0.50	3.4
42	1.66	1.20	1.04	0.69	77.16	51.83	33.39	0.50	11.6

## **Precipitation Evaluation Summary**

A summary of performance evaluation of ensemble members is presented in Figure 4.8a and Figure 4.8b.

A summary of performance evaluation of ensemble members is presented in Figure 4.8a and Figure 4.8b. Figure 4.8a provides the regional comparison of performance for individual ensemble members while Figure 4.8b provides the intra-model performance comparison of ensemble members in each region in terms of bar plots of averaged rank values.

The plots suggest that for temperature, the performance of some individual ensemble members remains more or less consistent (good or poor) for different regions. For example, visual inspection of Figure 4.8a suggests that precipitation models 21, 22 and 42 were consistently poor for majority of the regions while models 13, and 14 and 41 shown better performance in most of the regions. However, few models shown higher region to region performance variability as well. For example, in case of model 11, 12 and 32, at some regions performance was better but for other regions, the same models provided poor performance.

Visual inspection of Figure 4.8b suggests that there is much intra-model variability present within regions. Within a region, models tend to reproduce historical precipitation differently. Somewhat similar performance pattern of ensemble members at neighboring regions is also observable. For example, a performance variability pattern can be seen in Marmara and its neighboring Aegean region. Similar pattern can be seen for Eastern Anatolia and its neighboring South-Eastern Anatolia region.

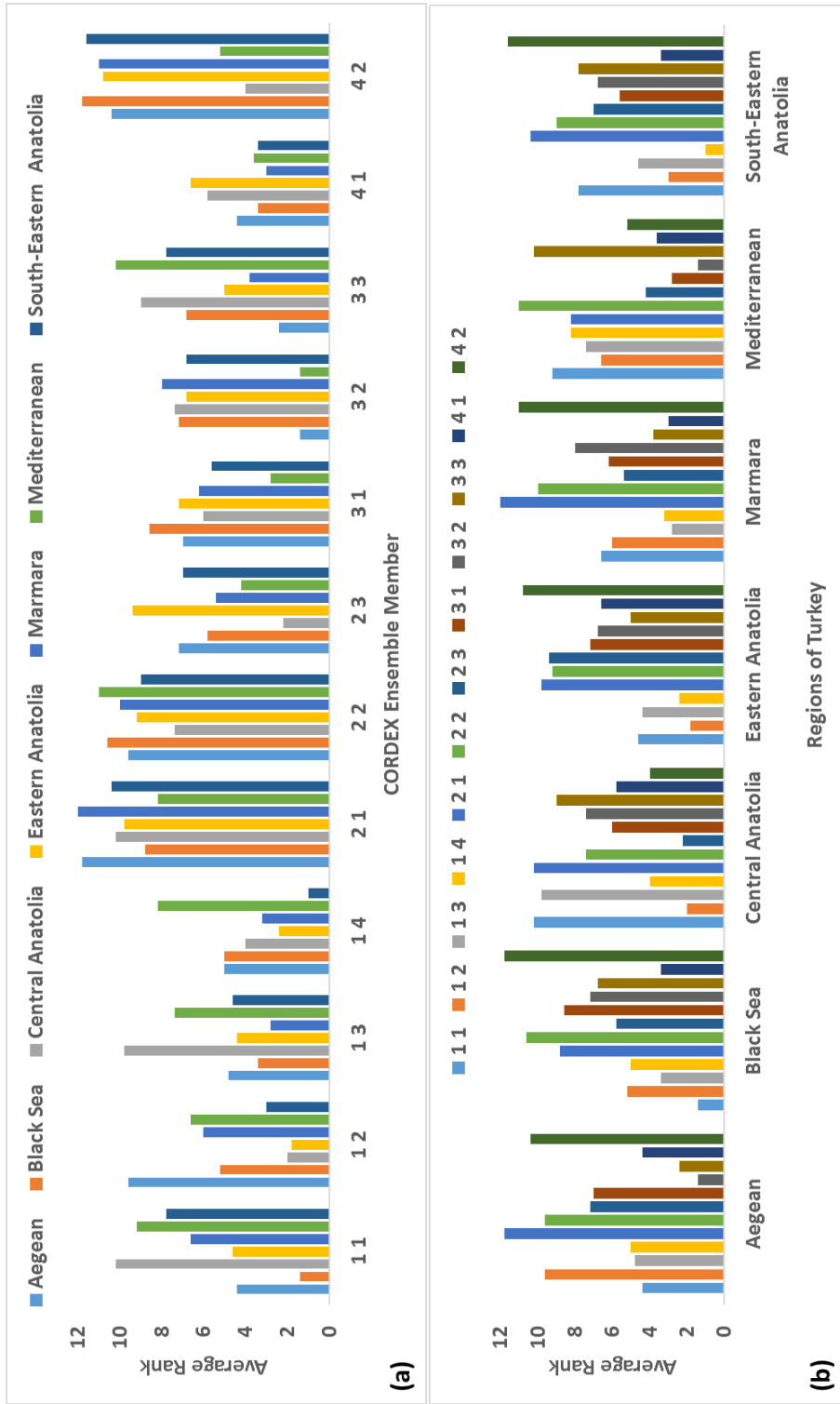


Figure 4.8 Summary of regional evaluation of CORDEX RCMs for precipitation.

#### **4.1.2. Temperature Evaluation**

##### **1) Marmara Region**

Regionally averaged mean daily temperature from individual RCM gridded stations against observed mean daily temperature is plotted for Marmara region in Figure 4.9. Model performance statistics are given in Table 4-8. The visual inspection of plots given in Figure 4.9 shows that all the RCMs were able to detect the seasonal variations of temperature fairly well. High correlation values provided in Table 4-8 also depict good agreement between seasonal variability of observed and RCM simulated mean daily temperature. But most of the RCMs underestimated temperature as can be seen in plots and the negative signs of mean bias error values given in Table 4-8. Amongst all, the RCMs originated from GCM EC-EARTH have shown larger underestimation which is clear from plots and mean bias values. RCMs 33, 41 and 42 have shown relatively better performance in terms of RMSE and MAE. Highest mean bias error was found in RCM 31. Based on the average rank values, RCM 33 (HadGEM2-ES-RCA4) was found to be the best model for the Marmara region of Turkey. Similarly, the averaged rank values also show that RCM 13 (EC-EARTH-RACMO22E) and RCM 21 (CNRM-CM5-ALADIN53) were found to be the worst model among ensemble members.

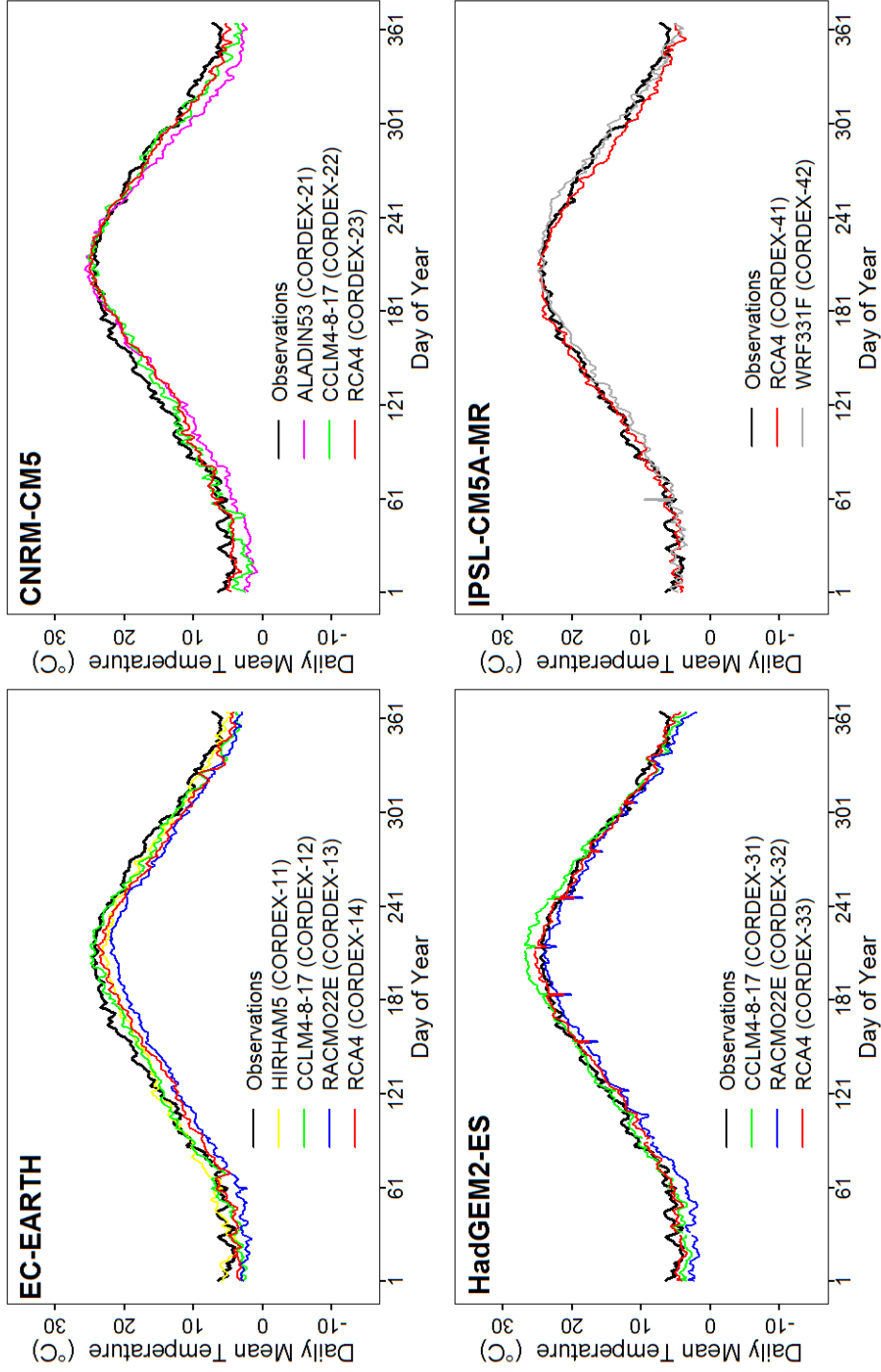


Figure 4.9 Comparison of regionally averaged mean daily observed and RCM temperature for the Marmara region of Turkey.

Table 4-8 Performance statistics summary of temperature for the Marmara region

CORDEX ID	Mean Daily Temperature				Successive Monthly Mean Temperature				Average Rank
	RMSE (°C)	MAE (°C)	MBE (°C)	CORR	RMSE (°C)	MAE (°C)	MBE (°C)	CORR	
1 1	1.34	1.16	-0.66	0.99	2.37	1.92	-0.65	0.95	5.6
1 2	1.43	1.15	-0.89	0.99	2.41	1.87	-0.89	0.95	6.4
1 3	2.83	2.72	-2.72	0.99	3.45	2.98	-2.71	0.95	<b>9.8</b>
1 4	1.89	1.70	-1.67	0.99	2.67	2.20	-1.67	0.95	8.8
2 1	2.48	2.19	-1.98	0.99	3.18	2.55	-1.99	0.96	<b>9.8</b>
2 2	1.48	1.19	-0.94	0.99	2.72	2.13	-0.99	0.94	8.4
2 3	1.32	1.07	-0.81	0.99	2.43	1.94	-0.81	0.95	5.8
3 1	1.28	1.05	0.14	0.99	2.48	1.96	0.18	0.95	4.8
3 2	1.84	1.56	-1.54	0.99	2.76	2.13	-1.50	0.95	8.2
3 3	0.94	0.75	-0.39	0.99	2.18	1.73	-0.35	0.95	<b>1.4</b>
4 1	1.19	0.95	-0.49	0.99	2.33	1.79	-0.50	0.95	4
4 2	1.19	0.95	-0.36	0.99	2.47	1.88	-0.37	0.94	5

## 2) Aegean Region

Regionally averaged mean daily temperature from individual RCM gridded stations against observed mean daily temperature is plotted for the Aegean Sea region in Figure 4.10. Model performance statistics are given in Table 4-9. The visual inspection of the plots given in Figure 4.10 and correlation values provided in Table 4-9 for daily mean shows that all the RCMs were able to reproduce the seasonal variations of temperature appropriately. Also, it is evident from plots and from the negative sign of mean bias error for daily and successive monthly mean temperature, that all models have a tendency to underestimate the temperature. These underestimations were more obvious during the winter season. RCM 21 has provided the maximum negative value of mean bias error while RCM 31 has shown the minimum. Overall RCMs originated from GCM HadGEM2-ES were found to be in better agreement with observation. Higher RMSE and MAE values were found with RCMs originated from CNRM-CM5 among which the RCM 21 was worst one. . Based on the average rank values, RCM 31 (HadGEM2-ES-CCLM4-8-17) was found to be the best model for the Aegean region of Turkey. Similarly, the averaged rank values also show that RCM 14 (EC-EARTH-RCA4) and RCM 21 (CNRM-CM5-ALADIN53) were found to be the worst model out of this ensemble.

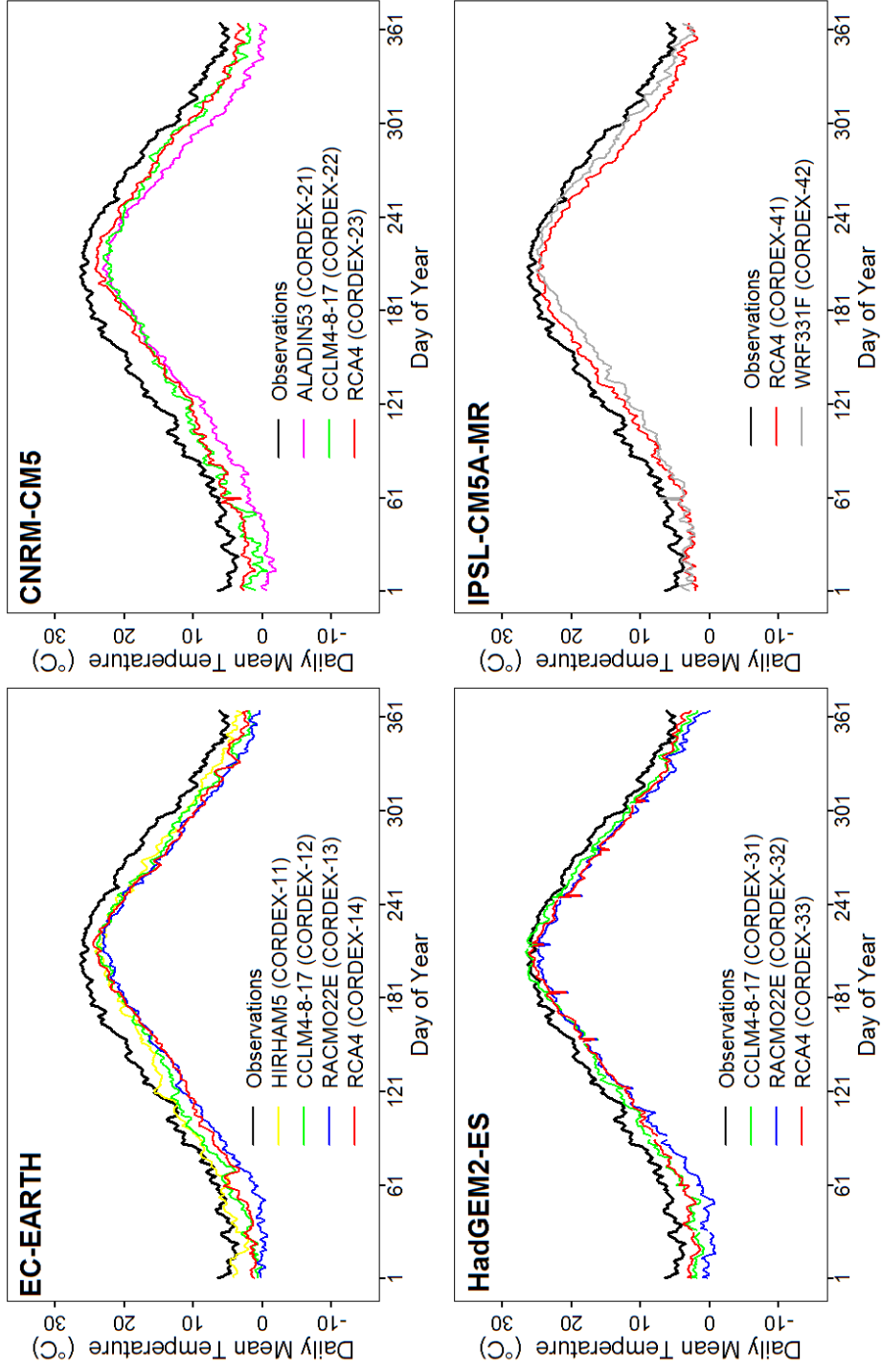


Figure 4.10 Comparison of regionally averaged mean daily observed and RCM temperature for the Aegean region of Turkey.

Table 4-9 Performance statistics summary of temperature for the Aegean region.

CORDEX ID	Mean Daily Temperature				Successive Monthly Mean Temperature				Average Rank
	RMSE (°C)	MAE (°C)	MBE (°C)	CORR	RMSE (°C)	MAE (°C)	MBE (°C)	CORR	
<b>11</b>	2.40	2.11	-2.09	0.99	3.02	2.51	-2.08	0.96	3.4
<b>12</b>	3.26	3.08	-3.08	0.99	3.83	3.26	-3.08	0.95	7.4
<b>13</b>	4.51	4.40	-4.40	0.99	4.94	4.43	-4.40	0.96	9.4
<b>14</b>	3.79	3.62	-3.62	0.99	4.26	3.70	-3.63	0.96	<u>9.8</u>
<b>21</b>	5.36	5.28	-5.28	0.99	5.70	5.30	-5.28	0.96	<u>9.8</u>
<b>22</b>	3.62	3.43	-3.43	0.99	4.27	3.70	-3.48	0.94	9.6
<b>23</b>	3.25	3.05	-3.05	0.99	3.81	3.26	-3.04	0.95	6.8
<b>31</b>	2.13	1.85	-1.79	0.99	2.91	2.29	-1.75	0.96	<u>1.2</u>
<b>32</b>	3.41	3.12	-3.12	0.99	3.97	3.24	-3.08	0.96	6.8
<b>33</b>	2.40	2.20	-2.19	0.99	3.05	2.50	-2.15	0.96	3
<b>41</b>	2.77	2.58	-2.58	0.99	3.40	2.82	-2.58	0.96	4.8
<b>42</b>	2.78	2.41	-2.39	0.98	3.40	2.78	-2.39	0.95	6

### 3) Mediterranean Region

Regionally averaged mean daily temperature from individual RCM gridded stations is plotted against observed mean daily temperature for Mediterranean region in Figure 4.11. Model performance statistics for the Mediterranean region are given in Table 4-10. The visual inspection of plots given in Figure 4.11 and correlation values provided in Table 4-10 for daily mean show that all the RCMs were able to explain the seasonal variations of temperature at a fair level. However, it is also observable from plots as well as from the negative sign of mean bias error for daily and successive monthly mean temperature, that all models have a tendency to underestimate the temperature. These underestimations were found to be more apparent during the winter season. Maximum negative bias error was found in RCM 13 while RCM 31 shown the least. Similarly, RCMs 13, 14 and 32 contained distinctively higher RMSE and MAE. Based on the average rank values, RCM 31 (HadGEM2-ES-CCLM4-8-17) was found to be the best model for the Mediterranean region of Turkey. Similarly, the averaged rank values also show that RCM 13 (EC-EARTH-RACMO22E) were found to be the worst model out of this ensemble.

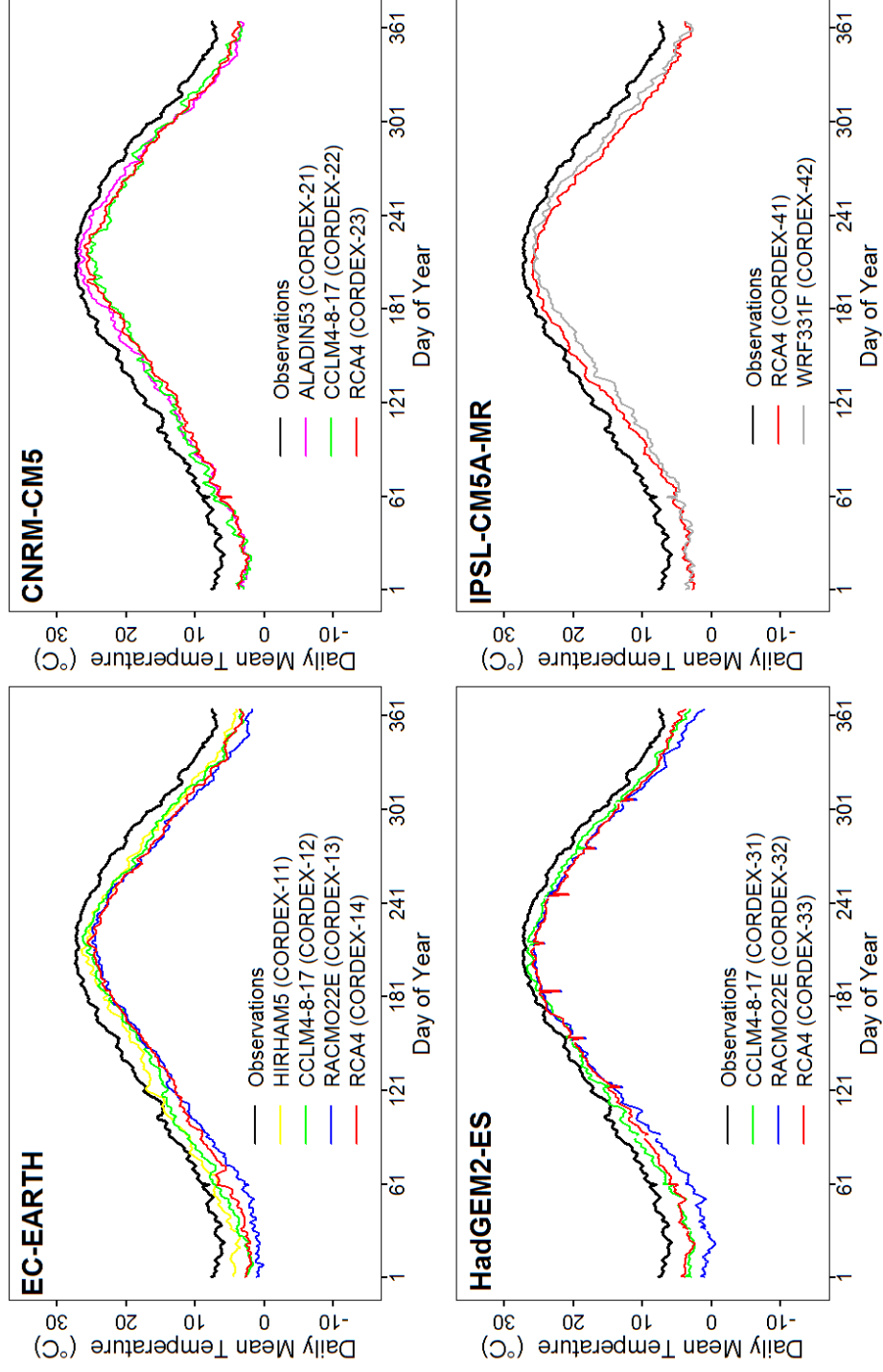


Figure 4.11 Comparison of regionally averaged mean daily observed and RCM temperature for the Mediterranean region of Turkey.

Table 4-10 Performance statistics summary of temperature for the Mediterranean region

CORDEX ID	Mean Daily Temperature				Successive Monthly Mean Temperature				Average Rank
	RMSE (°C)	MAE (°C)	MBE (°C)	CORR	RMSE (°C)	MAE (°C)	MBE (°C)	CORR	
1 1	2.34	2.20	-2.20	0.99	2.82	2.37	-2.21	0.97	2.2
1 2	3.03	2.88	-2.88	0.99	3.52	3.00	-2.88	0.96	5.2
1 3	4.58	4.45	-4.45	0.99	4.93	4.46	-4.45	0.97	11
1 4	3.86	3.78	-3.78	0.99	4.22	3.81	-3.79	0.97	10
2 1	2.96	2.75	-2.75	0.99	3.41	2.89	-2.76	0.97	4.6
2 2	3.20	3.07	-3.07	0.99	3.80	3.29	-3.14	0.96	7
2 3	3.33	3.24	-3.24	0.99	3.78	3.32	-3.25	0.97	8.2
3 1	2.23	2.00	-2.00	0.99	2.79	2.23	-1.96	0.97	2.2
3 2	3.86	3.47	-3.47	0.99	4.24	3.49	-3.43	0.97	8.4
3 3	2.63	2.50	-2.50	0.99	3.08	2.58	-2.46	0.97	3.8
4 1	3.15	2.96	-2.96	0.99	3.59	3.04	-2.97	0.97	5.2
4 2	3.33	3.14	-3.14	0.99	3.73	3.21	-3.14	0.97	7.2

#### 4) Central Anatolia

Regionally averaged mean daily temperature from individual RCM gridded stations against observed mean daily temperature is plotted for Central Anatolia region in Figure 4.12. Model performance statistics for Central Anatolia region are given in Table 4-11. These plots and mean bias values provided in Table 4-11 show that all the RCMs underestimated the temperatures. These underestimations were more apparent during the winter season. Generally, RCMs were in better agreement during the summer season as compared to other seasons. Highest and lowest negative (dry) biases were found in RCM 13 and RCM 31, respectively. RCMs originated from GCM IPSL-CM5A-MR have shown better agreement with observation during the winter season as compared to other GCMs. RCM 13 gave maximum values of RMSE and MAE for both mean daily and successive monthly mean temperatures. According to the average rank values, RCM 31 (HadGEM2-ES-CCLM4-8-17) was found to be the best model for Central Anatolia of Turkey. Similarly, the averaged rank values also show that RCM 13 (EC-EARTH-RACMO22E) were found to be the worst model out of this ensemble.

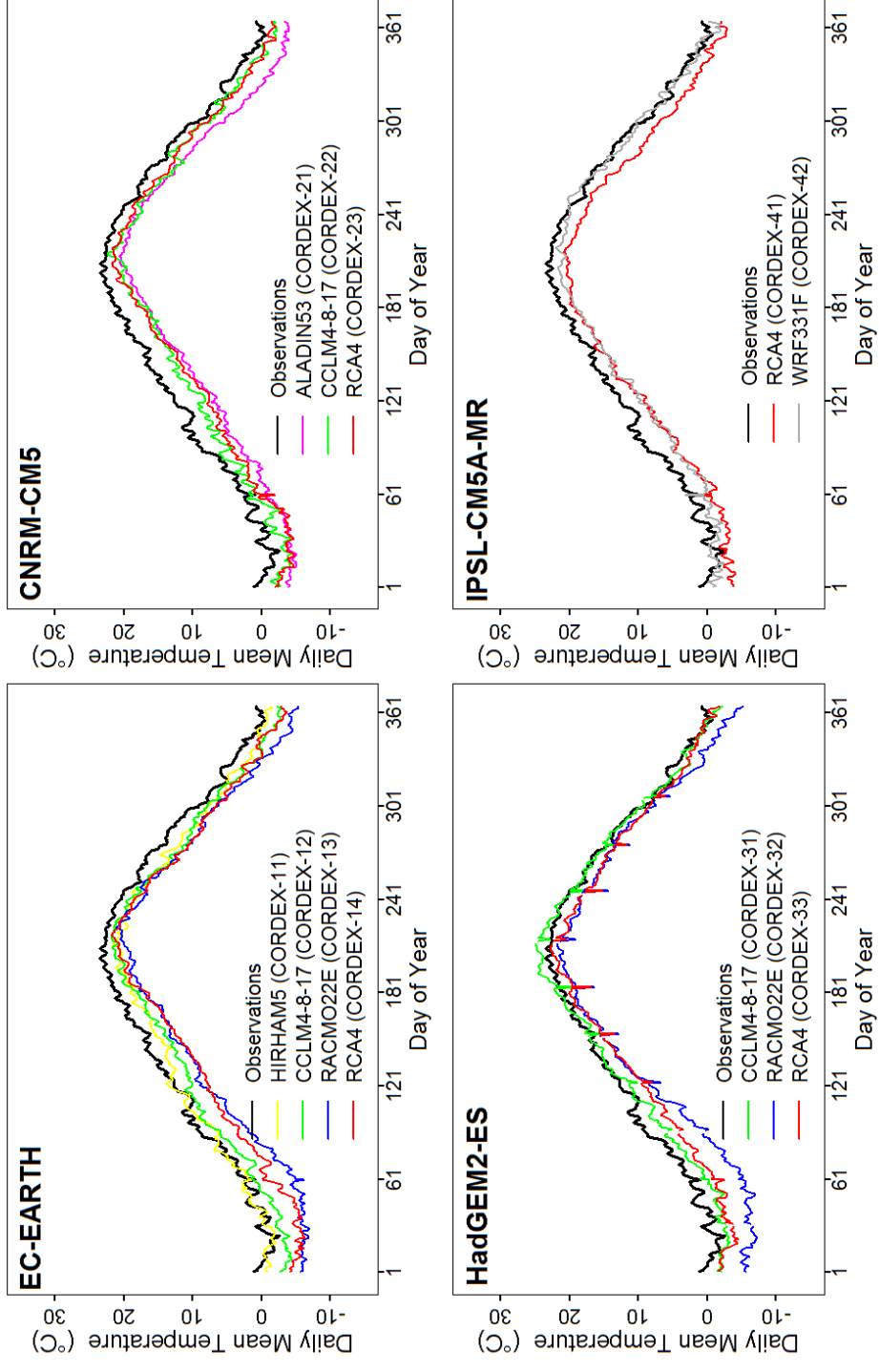


Figure 4.12 Comparison of regionally averaged mean daily observed and RCM temperature for the Central Anatolia region of Turkey.

Table 4-11 Performance statistics summary of temperature for the Central Anatolia region.

CORDEX ID	Mean Daily Temperature				Successive Monthly Mean Temperature				Average Rank
	RMSE (°C)	MAE (°C)	MBE (°C)	CORR	RMSE (°C)	MAE (°C)	MBE (°C)	CORR	
<b>11</b>	1.85	1.60	-1.36	0.99	2.92	2.39	-1.34	0.95	2.6
<b>12</b>	2.52	2.33	-2.33	0.99	3.45	2.81	-2.32	0.95	4
<b>13</b>	4.82	4.57	-4.57	0.99	5.44	4.70	-4.56	0.95	<b>11</b>
<b>14</b>	4.01	3.77	-3.77	0.99	4.82	4.05	-3.77	0.94	9.6
<b>21</b>	4.22	4.07	-4.07	0.99	4.81	4.24	-4.06	0.95	9
<b>22</b>	2.69	2.43	-2.43	0.99	3.72	3.10	-2.45	0.94	6
<b>23</b>	3.07	2.77	-2.77	0.99	4.07	3.36	-2.77	0.94	8.4
<b>31</b>	1.52	1.20	-0.63	0.99	2.83	2.19	-0.57	0.95	<b>1.4</b>
<b>32</b>	4.30	3.64	-3.63	0.98	4.92	3.85	-3.58	0.94	10.4
<b>33</b>	2.49	2.15	-2.12	0.99	3.55	2.80	-2.06	0.94	5
<b>41</b>	2.91	2.74	-2.73	0.99	3.86	3.15	-2.73	0.95	6
<b>42</b>	2.03	1.68	-1.37	0.98	3.17	2.52	-1.36	0.94	4.6

## 5) Black Sea Region

Regionally averaged mean daily temperature from individual RCM gridded stations against observed mean daily temperature is plotted for Central Anatolia region in Figure 4.13. Model performance statistics for Central Anatolia region are given in Table 4-12. The visual inspection of plots and the higher values of correlation provided in Table-4-12 suggest that all RCMs were able to fairly emulate the seasonal variation of temperature. However, the plots and negative signs of mean bias errors also suggest that RCMs contains the tendency of underestimation of temperatures in this region as well. Like in other regions, these underestimations were more obvious during the winter season. The highest amount of negative mean bias error was found in RCM 13 for mean daily temperature as well as successive monthly mean temperature. Similarly, RCM 31 has shown the lowest amount of mean bias. RCMs 13, 14 and 21 gave a distinctively higher RMSE and MAE. According to the average rank values, RCM 31 (HadGEM2-ES-CCLM4-8-17) was found to be the best model for Black Sea of Turkey. Similarly, the averaged rank values also show that RCM 13 (EC-EARTH-RACMO22E) were found to be the worst model out of this ensemble.

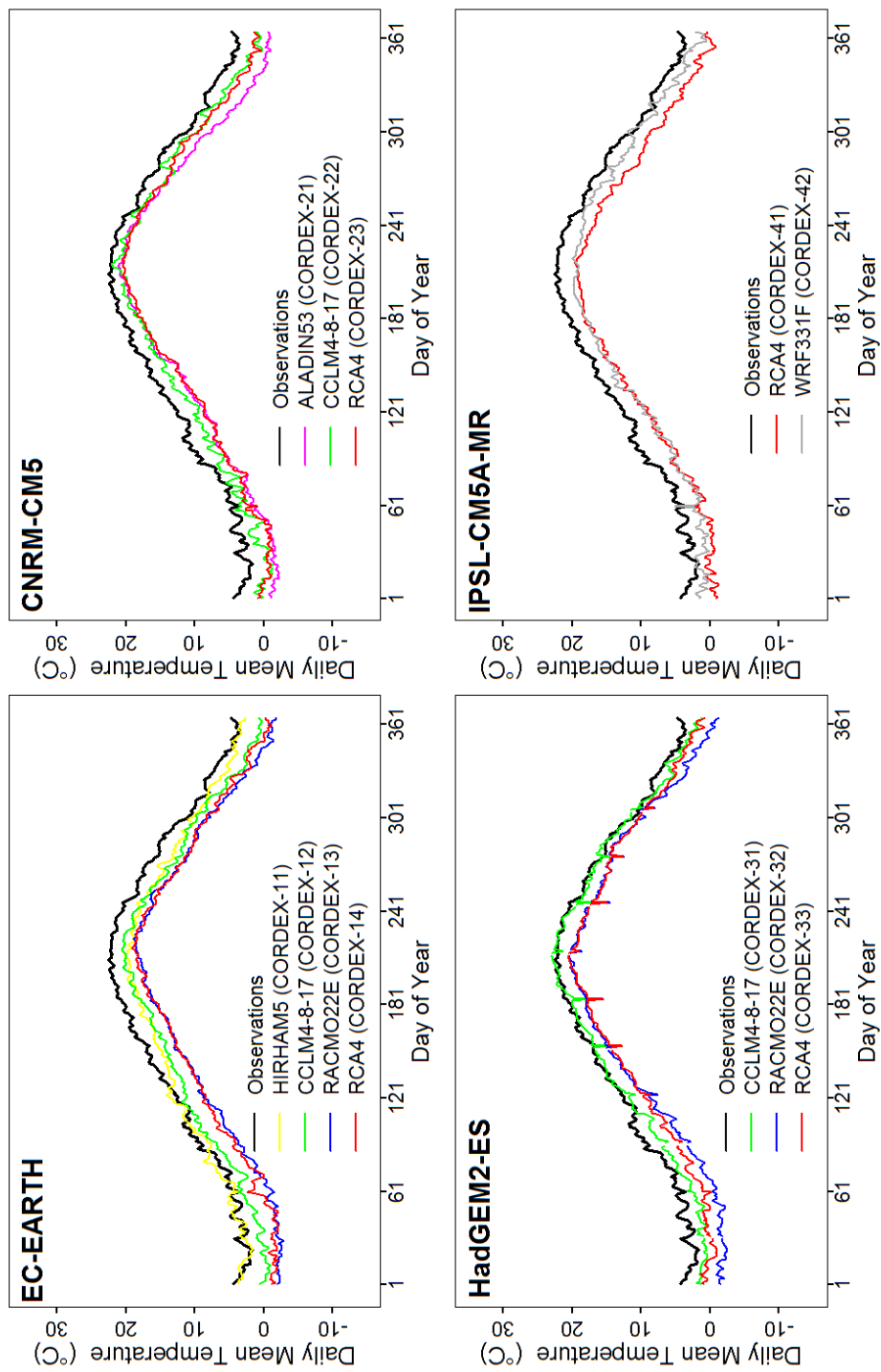


Figure 4.13 Comparison of regionally averaged mean daily observed and RCM temperature for the Black Sea region of Turkey.

Table 4-12 Performance statistics summary of temperature for the Black Sea region

CORDEX ID	Mean Daily Temperature					Successive Monthly Mean Temperature					Average Rank
	RMSE (°C)	MAE (°C)	MBE (°C)	CORR		RMSE (°C)	MAE (°C)	MBE (°C)	CORR		
<b>11</b>	1.83	1.56	-1.25	0.99		2.70	2.26	-1.22	0.94	▼	3.6
<b>12</b>	2.63	2.49	-2.48	0.99		3.23	2.71	-2.48	0.95	▼	5.4
<b>13</b>	4.74	4.67	-4.67	0.99		5.15	4.68	-4.66	0.95	▼	<b>10</b>
<b>14</b>	4.33	4.25	-4.25	0.99		4.79	4.29	-4.25	0.95	▼	9.6
<b>21</b>	3.72	3.52	-3.52	0.99		4.19	3.60	-3.52	0.96	▼	8.2
<b>22</b>	2.32	2.13	-2.13	0.99		3.15	2.56	-2.15	0.95	▼	3.6
<b>23</b>	3.06	2.91	-2.91	0.99		3.76	3.13	-2.91	0.94		7
<b>31</b>	1.39	1.07	-0.90	0.99		2.46	1.91	-0.86	0.95	▼	<b>14</b>
<b>32</b>	3.68	3.39	-3.39	0.99		4.16	3.47	-3.35	0.95	▼	9
<b>33</b>	2.86	2.68	-2.68	0.99		3.49	2.91	-2.64	0.95		6.6
<b>41</b>	3.49	3.40	-3.40	0.99		4.05	3.48	-3.39	0.95		7.8
<b>42</b>	2.51	2.29	-2.26	0.99		3.26	2.67	-2.26	0.94		5.8

## 6) Eastern Anatolia Region

Regionally averaged mean daily temperature from individual RCM gridded stations against observed mean daily temperature is plotted for Central Anatolia region in Figure 4.14. Model performance statistics for Central Anatolia region are given in Table 4-13. Plots and high values of correlation given in Table 4-12 suggest a good representation of seasonal variability of temperature from all RCMs. However, plots and mean bias error values suggest significant underestimations. In this region, RCMs have shown more tendencies of underestimation than any other region of Turkey. Both RCMs originated from IPSL-CM5A-MR have shown the most underestimations and RCM 42 gave the highest negative mean bias error. Furthermore, RCMs 14, 41 and 42 contains the highest amount of RMSE and MAE for both daily mean and successive monthly mean temperature. Based on the average rank values, RCM 31(HadGEM2-ES-CCLM4-8-17) was found to be the best model for the Mediterranean region of Turkey. Similarly, the averaged rank values also show that RCM 42 (IPSL-CM5A-MR-WRF331f) were found to be the worst model out of this ensemble.

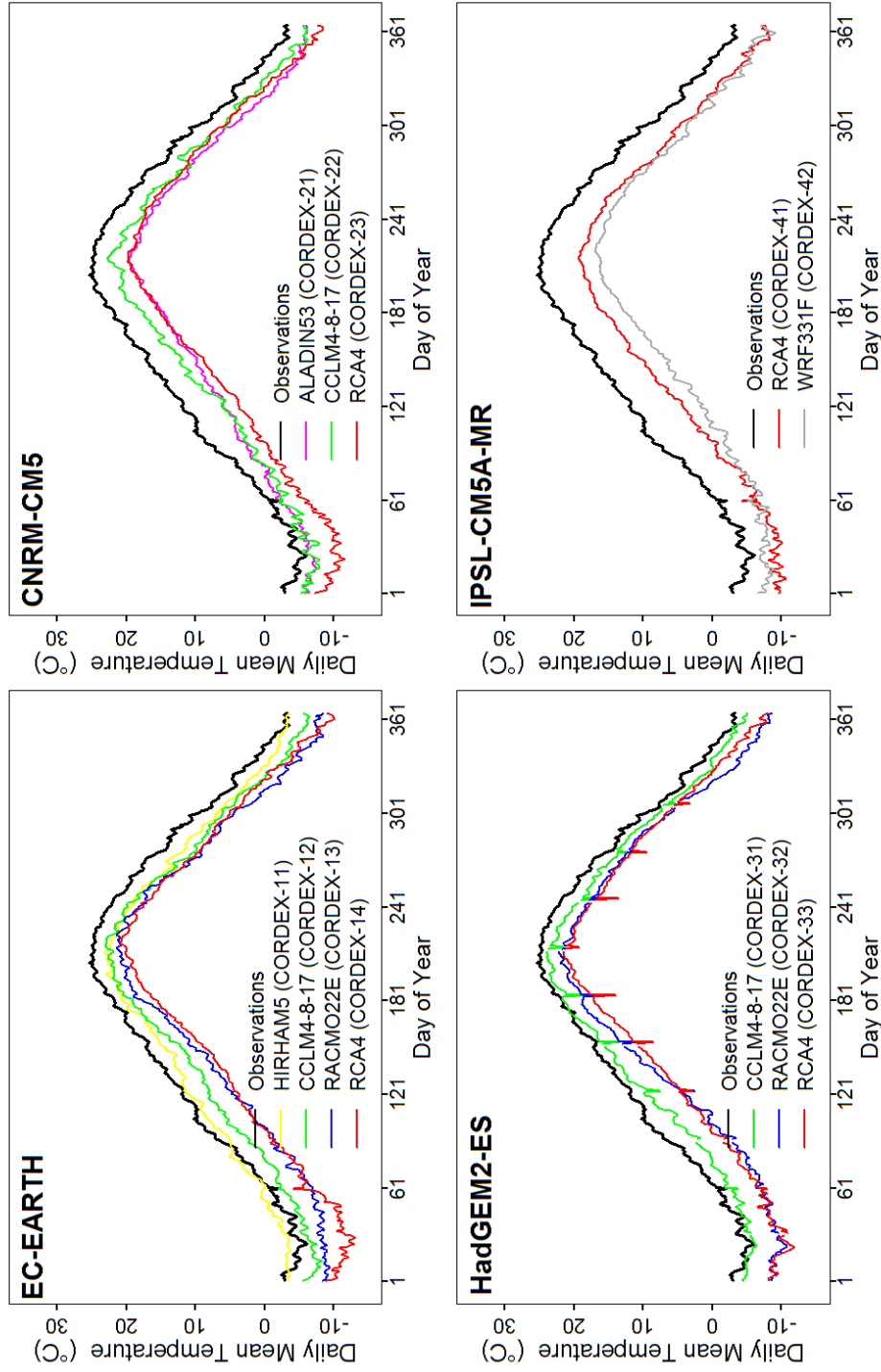


Figure 4.14 Comparison of regionally averaged mean daily observed and RCM temperature for the Eastern Anatolia region of Turkey.

Table 4-13 Performance statistics summary of temperature for the Eastern Anatolia region.

CORDEX ID	Mean Daily Precipitation					Successive Monthly Total Precipitation					Average Rank
	RMSE	MAE	MBE	CORR		RMSE	MAE	MBE	CORR		
1-1	2.22	2.00	-1.42	0.99		3.14	2.63	-1.41	0.97		2.8
1-2	3.46	3.29	-3.29	0.99		4.11	3.54	-3.29	0.97		2.6
1-3	5.78	5.59	-5.59	0.99		6.33	5.67	-5.59	0.96		8
1-4	6.36	6.19	-6.19	0.99		6.81	6.22	-6.20	0.96		10.2
2-1	5.07	4.76	-4.76	0.99		5.53	5.00	-4.75	0.97		4.8
2-2	3.82	3.58	-3.58	0.99		4.52	3.93	-3.61	0.96		4.2
2-3	5.91	5.68	-5.68	0.99		6.40	5.75	-5.68	0.96		9
3-1	2.14	1.86	-1.85	0.99		3.11	2.49	-1.79	0.97		1.2
3-2	5.40	5.06	-5.06	0.99		5.86	5.07	-5.00	0.96		7.2
3-3	5.40	5.12	-5.12	0.99		5.86	5.19	-5.06	0.96		7.4
4-1	5.97	5.86	-5.86	0.99		6.49	5.90	-5.85	0.96		8.6
4-2	7.54	7.15	-7.15	0.98		7.86	7.20	-7.13	0.95		12

## 7) South-Eastern Anatolia Region

Regionally averaged mean daily temperature from individual RCM gridded stations is plotted against observed mean daily temperature in Figure 4.15 for South-Eastern Anatolia region. Model performance statistics for South-Eastern Anatolia region are given in Table 4-14. The visual inspection of plots and high values of correlation provided in Table 4-14 suggest a good representation of seasonal variability of temperature from all RCMs. However, like most of the other regions of Turkey, plots and the mean bias error values suggest an overall underestimation of all RCMs. RCMs 13 and 42 contain distinctively much higher negative mean bias errors values as compared to other regions. RCMs originated from GCM HadGEM2-ES show better agreement with observation during summer as compared to other seasons. Similarly, RCMs 13 and 42 also provided the highest RMSE and MAE for mean daily and successive monthly mean temperatures. According to the average rank values, RCM 31 (HadGEM2-ES-CCLM4-8-17) was found to be the best model for Black Sea of Turkey. Similarly, the averaged rank values also show that RCM 13 (EC-EARTH-RACMO22E) were found to be the worst model out of this ensemble.

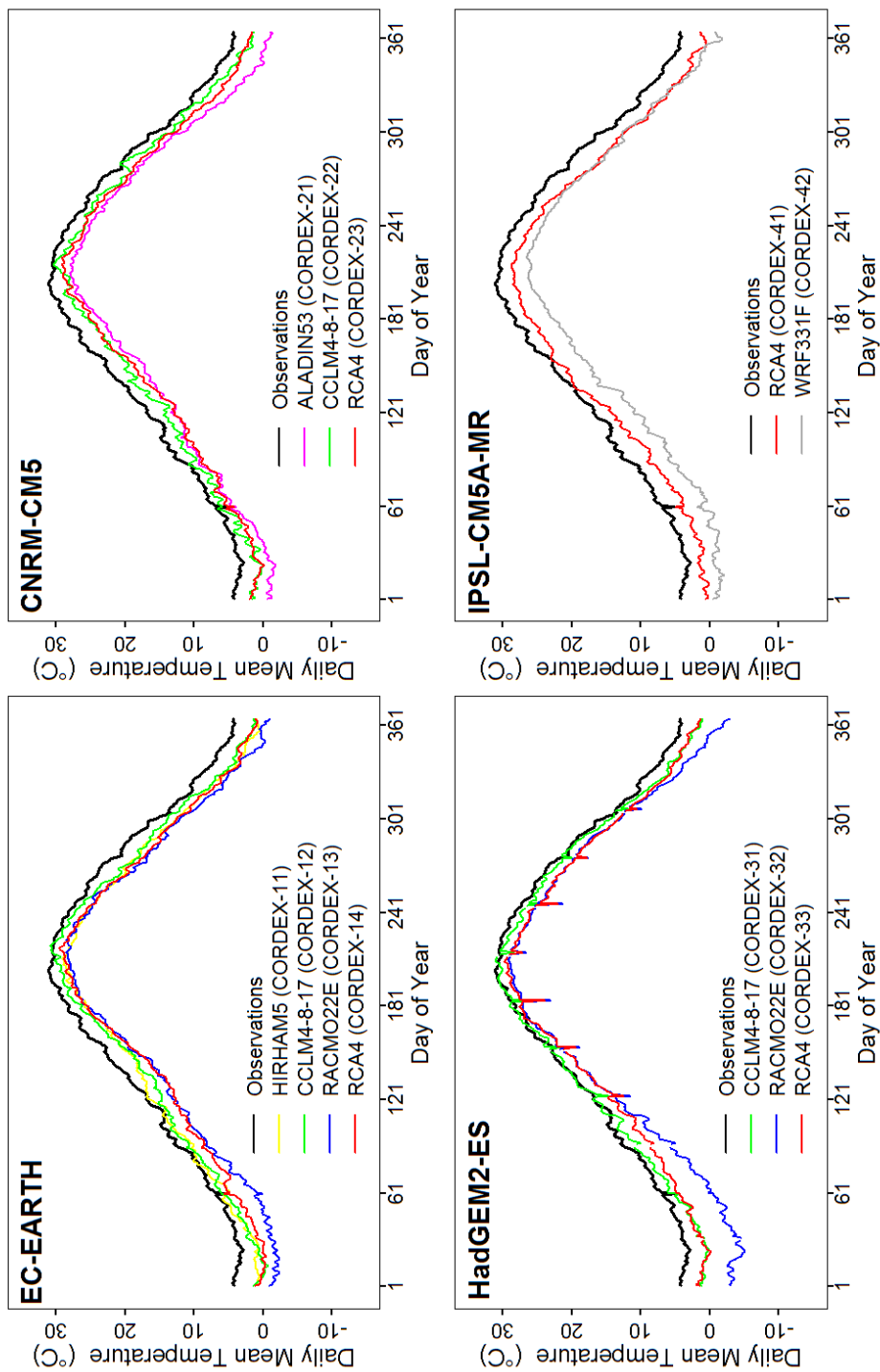


Figure 4.15 Comparison of regionally averaged mean daily observed and RCM temperature for the South-Eastern Anatolia region of Turkey.

Table 4-14 Performance statistics summary of temperature for the South-Eastern Anatolia region.

CORDEX ID	Mean Daily Temperature				Successive Monthly Mean Temperature				Average Rank
	RMSE (°C)	MAE (°C)	MBE (°C)	CORR	RMSE (°C)	MAE (°C)	MBE (°C)	CORR	
1 1	2.64	2.43	-2.42	0.99	3.26	2.75	-2.42	0.97	4.6
1 2	2.28	2.05	-2.04	0.99	3.05	2.45	-2.04	0.97	2.6
1 3	4.27	4.12	-4.12	0.99	4.77	4.17	-4.11	0.97	9.6
1 4	3.37	3.24	-3.24	0.99	3.91	3.36	-3.24	0.97	7.6
2 1	4.06	3.93	-3.93	0.99	4.51	4.00	-3.93	0.97	7.6
2 2	2.21	2.03	-2.02	0.99	3.13	2.56	-2.07	0.97	3.6
2 3	2.91	2.80	-2.80	0.99	3.57	3.02	-2.79	0.97	6.6
3 1	1.61	1.31	-1.17	0.99	2.49	1.90	-1.11	0.98	2
3 2	4.53	3.94	-3.94	0.99	4.95	3.97	-3.87	0.97	9
3 3	2.46	2.35	-2.34	0.99	3.04	2.53	-2.28	0.98	3.8
4 1	2.92	2.78	-2.77	0.99	3.56	2.96	-2.77	0.97	6.2
4 2	5.06	4.92	-4.92	0.99	5.44	4.93	-4.91	0.97	10.6

## Temperature Evaluation Summary

A summary of performance evaluation of ensemble members is presented in Figure 4.16a and Figure 4.16b. Figure 4.16a provides the regional comparison of performance for individual ensemble members while Figure 4.16b provides the intra-model performance comparison of ensemble members in each region in terms of bar plots of averaged rank values.

The plots also suggest that for temperature, the performance of some individual ensemble members remains more or less consistent (good or poor) for different regions. For example, visual inspection of Figure 4.16a suggests that temperature model 13, 14 and 32 were consistently poor for all the regions while models 31, 11 and 12 and 33 shown better performance in most of the regions. The bar plots also show that model 31 is consistently the best model at six out of seven regions for representation of temperature. However, few models shown higher region to region performance variability as well. For example, in case of model 21, 22 and 42, at some regions performance was better but for other regions, the same models provided poor performance.

Visual inspection of Figure 4.16b suggests that there is much intra-model variability present within regions. Within a region, few models were able to reproduce historical temperatures differently. Somewhat similar performance pattern of ensemble members at neighboring regions is also observable. For example, a performance variability pattern can be seen in Marmara and its neighboring Aegean region. Similar pattern can be seen for Eastern Anatolia and its neighboring South-Eastern Anatolia region.

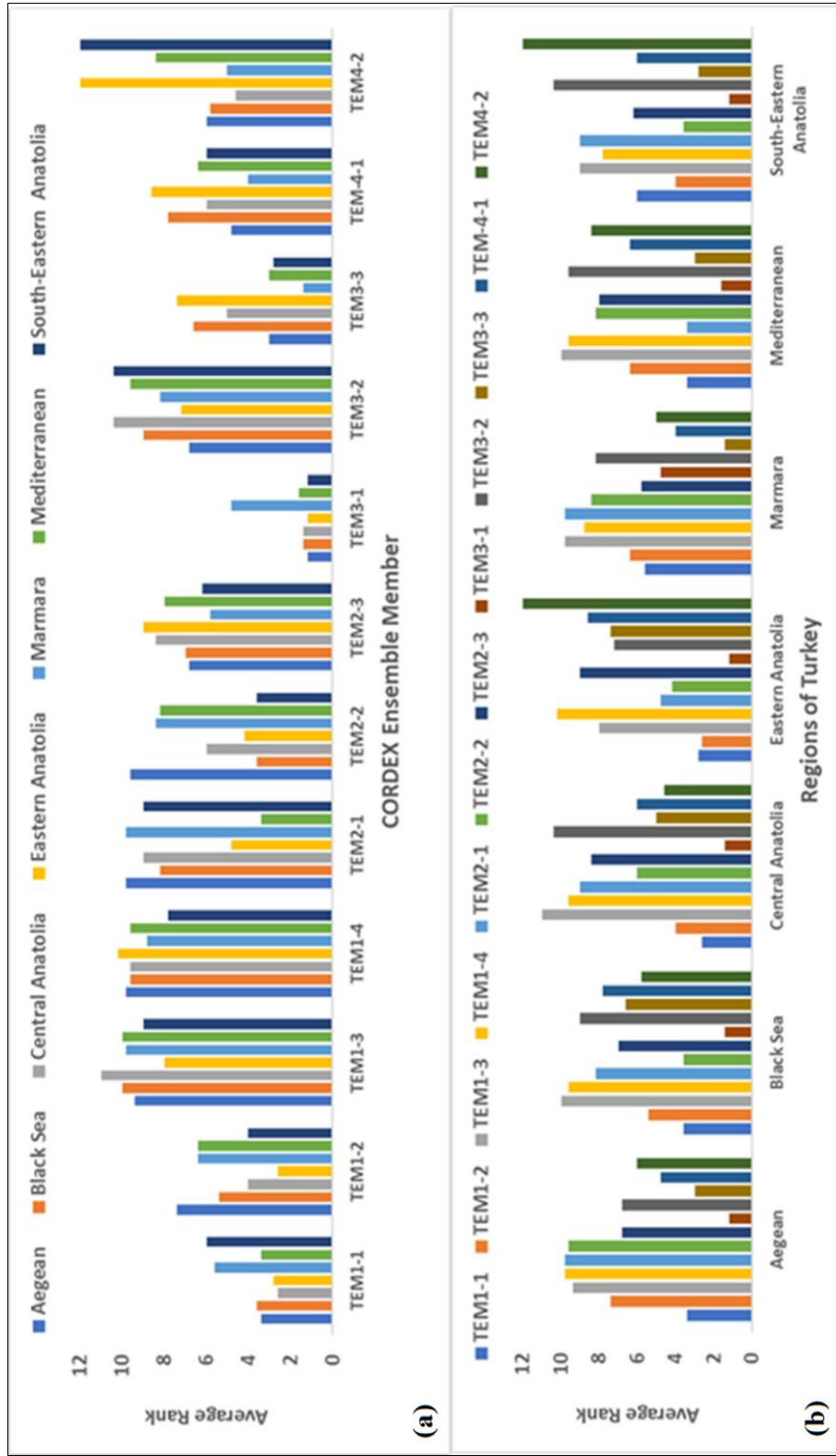


Figure 4.16 Summary of regional evaluation of CORDEX RCMs for temperature

## 4.2. Discussion

The performance evaluation for each of the individual CORDEX ensemble member was evaluated using four performance evaluation indicators. The correlation coefficient (especially for mean daily precipitation and temperature) shed light on the ability to explain the seasonal variability of the variable. Mean bias error is used to understand the tendency of a model to underestimate or overestimate the variable values. Mean absolute values are used to estimate the mean departures of model data from the reference or observation data. Similarly, root mean square errors are used to incorporate the effects of large deviations of model data from the reference or observation data. The variation of performance indicator values of different RCMs coupled with the same GCM explains the performance variability of RCMs. Similarly, the same RCM coupled with different GCMs explained the GCM related performance variability.

Visual inspection of plots (provided for each region), as well as the correlation values (provided in performance evaluation tables), have suggested that most of the regions in Turkey, generally RCMs originated from GCMs EC-EARTH and HadGEM2-ES were able to emulate the seasonal variability of precipitation better than GCMs CNRM-CM5 and IPSL-CM5A-MR. Also, correlation values of RCMs from these two GCMs were apparently higher than the other two GCMs in most of the regions. Visual inspection of plots also suggests that for most of the regions in Turkey, the RCMs originated from GCM CNRM-CM5 unrealistically simulated higher precipitation during the late spring and early summer days. Thus, this model was distorting the precipitation seasonality curve. These findings suggest that GCM has more impact on simulation of seasonal variability and can be concluded that at the regional scale, the ability of any RCM in reproducing the true seasonality in precipitations is mainly dependent on the driving GCM. The results also suggest that these GCM-RCM combinations perform differently for different regions however based on averaged ranks, most of the RCMs originated from GCMs, EC-EARTH

and HadGEM2-ES performed better as compared to the RCMs originated from GCMs, CNRM-CM5, and IPSL-CM5A-MR. However, both RCMs coupled with GCM of IPSL-CM5A-MR performed at a fair level in the Mediterranean region. In almost all the regions, the RCMs coupled with GCMs, EC-EARTH, and HadGEM2-ES were found to be standing at top two ranks. Similarly, RCMs originated from GCM GCMs CNRM-CM5 and RCM WRF331F coupled with IPSL-CM5A-MR were found to be the worst models in most of the regions in Turkey for precipitation.

In case of temperature, better performance was observed when RCM CCLM4-8-17 is coupled with any GCM (IC-EARTH, CNRM-CM5, and HadGEM2-ES) as compared to other RCMs coupled with same GCMs. In most regions, RCM CCLM4-8-17 coupled with GCM HadGEM2-ES provided the highest value for averaged rank, so it is considered as the best model for most of the regions in Turkey. RCMs RACMOO22E and RCA4 coupled with GCM IC-EARTH and RCMs ALADIN53 and CCLM4-8-17 coupled with GCM CNRM-CM5 were consistently worse for most of the regions in Turkey. The negative signs of mean bias error show that most of the models underestimated temperatures in many regions.



## CHAPTER 5

### NONSTATIONARITY ANALYSES OF PRECIPITATION

#### 5.1. Results

##### 5.1.1. Distribution Fitting Under Stationary and Nonstationary Conditions

Four distributions (GEV, Gumbel, Normal and Log-normal) are used for five precipitation indices annual maximum precipitation during whole year as well as annual maximum precipitation during each season (Yearly AMPs and seasonal AMPs) obtained from observed precipitation data to evaluate the impacts of nonstationarities. The parameters of each distribution were estimated by minimizing the Negative Log-Likelihood value (NLLH). The distribution with a lower value of NLLH is considered to be the better one. The Negative Log-Likelihood values of each distribution for stationary and nonstationary cases are presented here as boxplots for each of the precipitation indices (Yearly AMPs and seasonal AMPs) in Figure 5.1 and Figure 5.2. Each boxplot contains 77 values of NLLH corresponding to 77 stations used in this study.

It is observable from Figure 5.1 and Figure 5.2 that generally, boxplots representing NLLH values of each of the distribution for nonstationary cases are a bit lower than the ones for stationary case. This indicates that each distribution has shown slightly

better fit when covariate of time was introduced. This shows that the fit of distributions was slightly improved with the assumption of nonstationarity. It is also evident from these figures that NLLH values for Normal distributions were found to be higher than the NLLH values of other three distributions for both stationary and nonstationary cases. In most of the precipitation indices, NLLH values of GEV distribution were lower than all other distributions for both stationary and nonstationary cases as can be seen from boxplots in almost every figure. Among the distributions with two parameters (Gumbel, Normal and Log-normal), Gumbel distribution has shown comparatively lower NLLH values as compared to the other two distributions in both stationary and nonstationary cases for most of the precipitation indices. The figures also suggest that the NLLH values of Log-Normal distributions were not much higher than Gumbel and GEV distributions. Considering the lowest values of NLLH and historically more frequent usage of GEV in literature to perform frequency analysis of extremes because of its ability to show better fit for tails, only GEV distribution will be used for future projected data.

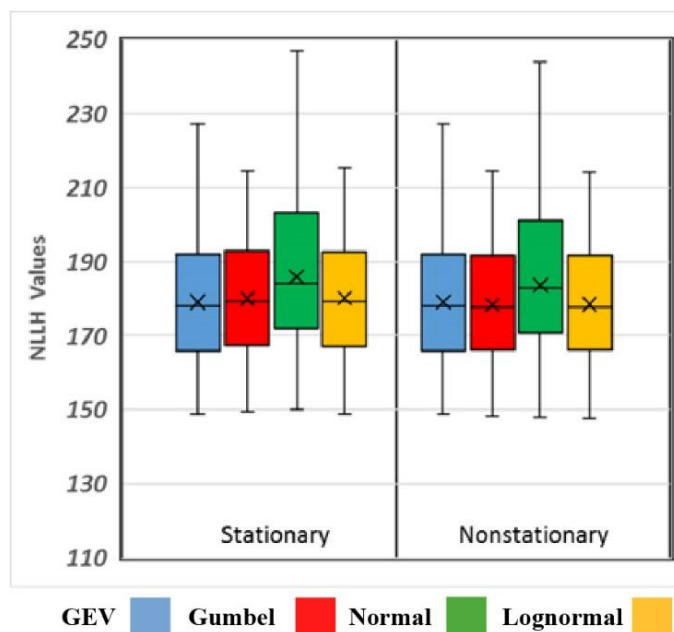


Figure 5.1 Comparison of Negative Log-Likelihood of distributions for Yearly AMPs of observed data

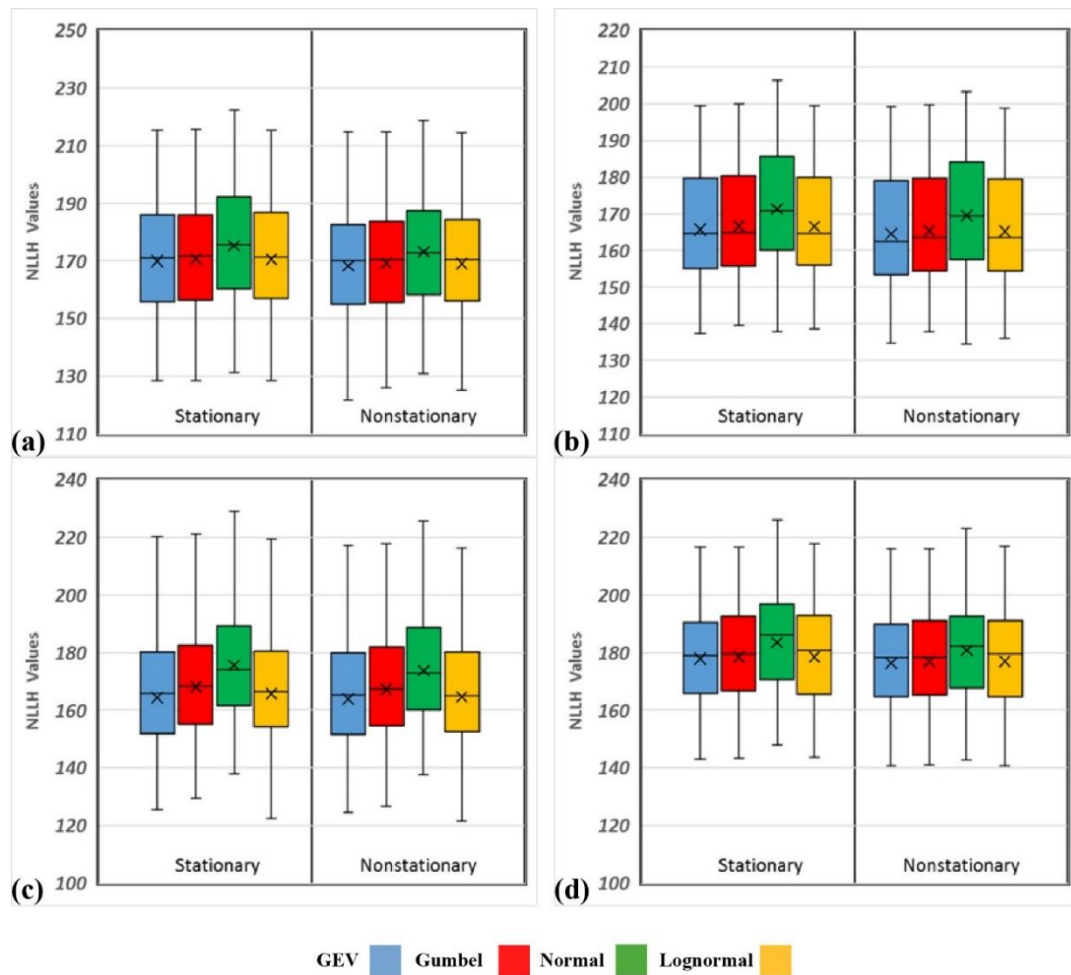


Figure 5.2 Comparison of Negative Log-Likelihood of stationary and nonstationary distributions for (a) Winter (b) Spring (c) Summer and (d) Autumn AMPs of observed data

Further, for an example, the probability density function, cumulative probability density functions and QQ-plots of this four distribution are plotted for yearly maximum precipitation of Ankara station as given in Figure 5.3, 5.4, and 5.5 respectively. From these plots, the variability in fitting the distribution can be observed. All three plots clearly show that GEV and Lognormal distributions provided better fit as compared to Gumbel and Normal distributions for annual maximum precipitation of Ankara. Visual inspection of all three figures also

suggests that amongst two-parameter distributions, Lognormal distribution better fitted the observation.

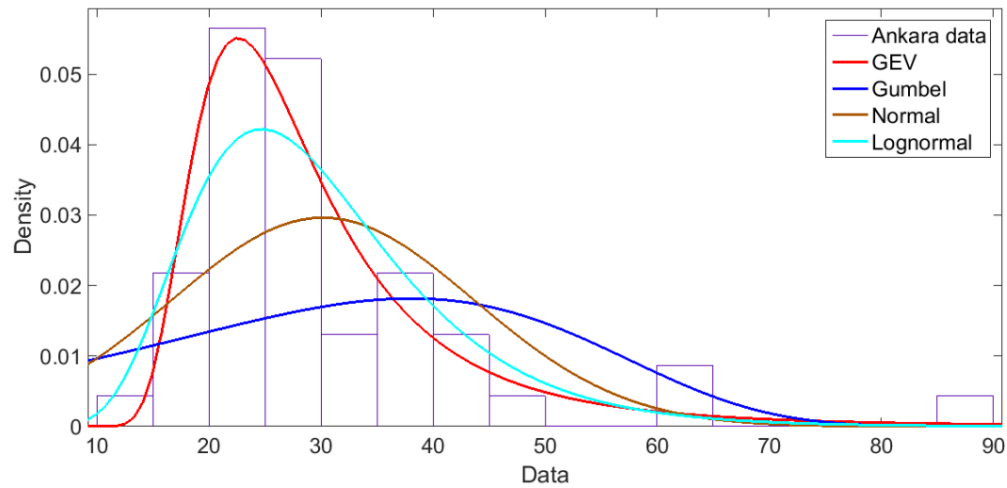


Figure 5.3 Comparative plots of probability density functions of GEV, Gumbel, Normal, and Lognormal distributions for annual maximum precipitation of Ankara.

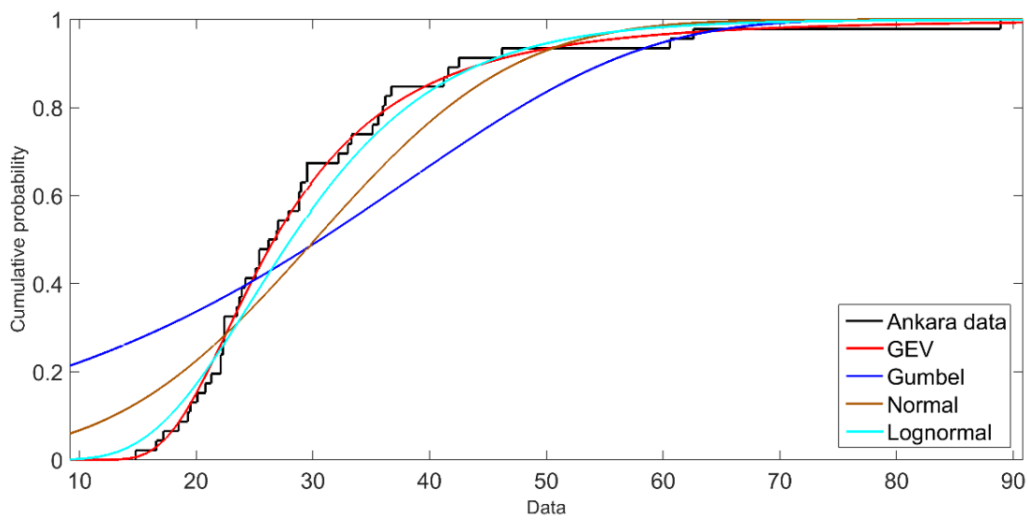


Figure 5.4 Comparative plots of cumulative probability density functions of GEV, Gumbel, Normal, and Lognormal distributions for annual maximum precipitation of Ankara.

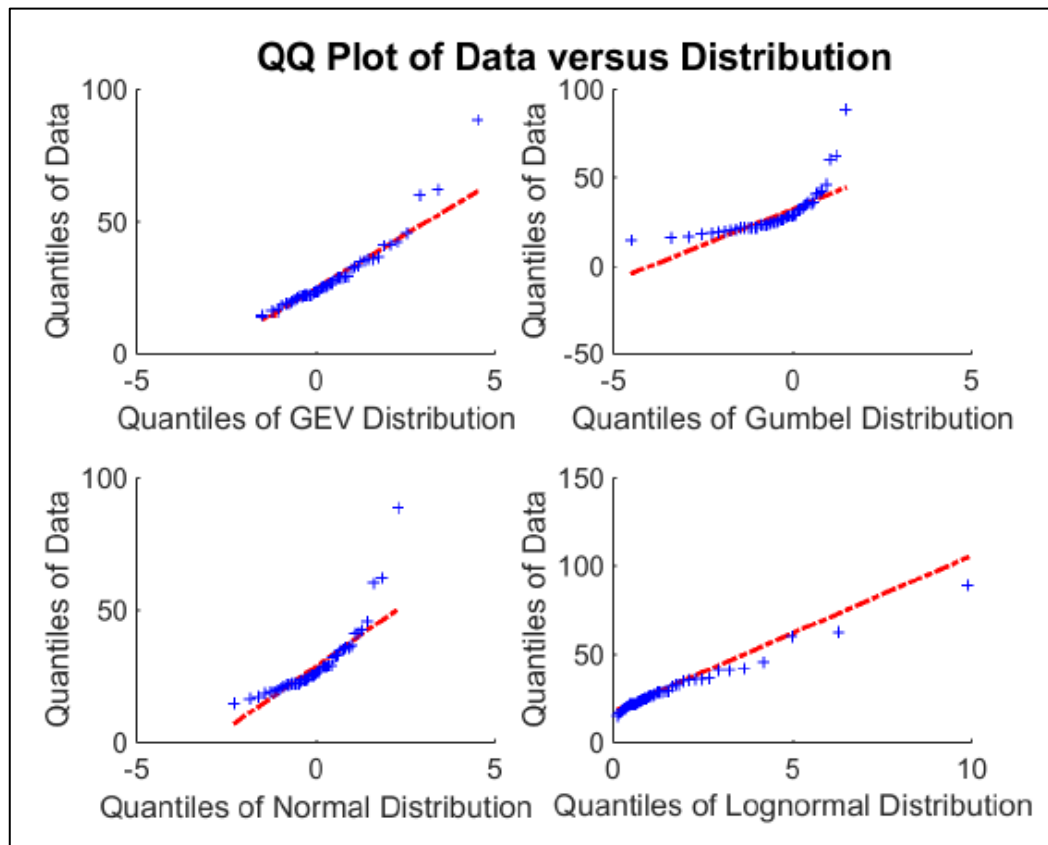


Figure 5.5 QQ-plots of GEV, Gumbel, Normal, and Lognormal distributions for annual maximum precipitation of Ankara.

### 5.1.2. Nonstationarity Impacts During Historical Time Period (1971-2015)

Four distributions namely GEV, Gumbel, Normal and Lognormal distributions were used under stationary and nonstationary assumptions for yearly and seasonal maximum precipitations as 1)- Yearly AMPs 2)- Winter AMPs 3)- Spring AMPs 4)- Summer AMPs and 5)- Autumn AMPs series obtained from observed daily precipitation. Impacts of nonstationarities were quantified as the percentage difference between nonstationary and stationary return levels of 100-year return periods. In this section, the interpolated maps of the percentage difference between

nonstationary and stationary 100-year return levels are presented for each distribution using yearly as well as seasonal AMPs.

### **1) Yearly AMPs**

Maps of difference between 100-year nonstationary and stationary return levels of four distributions for yearly AMPs are shown in Figure 5.6. Visual inspection of maps given in Figure 5.6 shows that overall all three distributions have indicated similar impacts for yearly AMPs with few exceptions. There are some consistent impact results that are supported by all four distributions in varying magnitude throughout the country. Results demonstrated that all four distributions have shown positive impacts for stations located in the Marmara region, Aegean region and most part of the Mediterranean region. In Aegean and western Mediterranean regions, the magnitude of impacts obtained using GEV and Lognormal distributions is found to be more compared to the other two distributions. Most of the eastern and central coastline of Black Sea region exhibits positive impacts using GEV and Gumbel distributions while Normal and Lognormal distribution show negative impacts at few locations of central Black Sea region. Impacts of nonstationarities were found to be negative at most western part of Black Sea region as shown in maps of all distribution. Relatively mix kind of impacts was estimated at the Central Anatolian region. Estimated impacts from all four distributions were negative at the northern part of Central Anatolia and the areas extended to Black Sea region. Similar impacts are obtained in an eastern part of Central Anatolia. The border side and towards the north of the South-Eastern Anatolian region exhibits negative impacts as explained by dark green colored region in all four distribution while in the same region (Hakkari province) there is also strong positive impact. It is noted that nonstationary impact analysis suggests variable impacts in the Eastern Anatolian region where impacts were positive at some locations and negative for other locations.

Percentage Difference Between 100-year Stationary and Nonstationary Return Levels (Yearly-AMP)

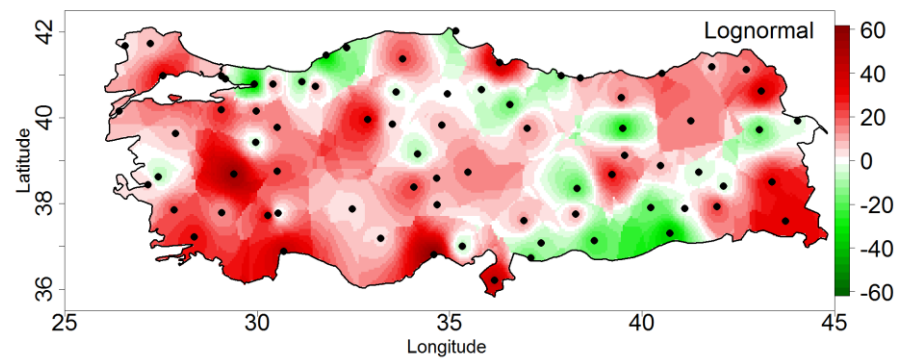
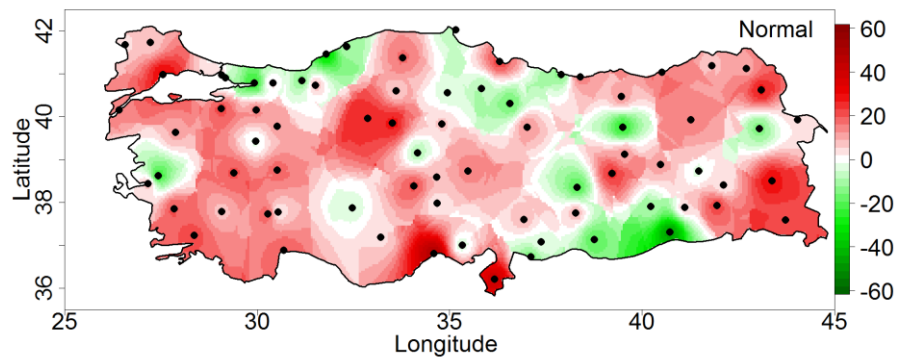
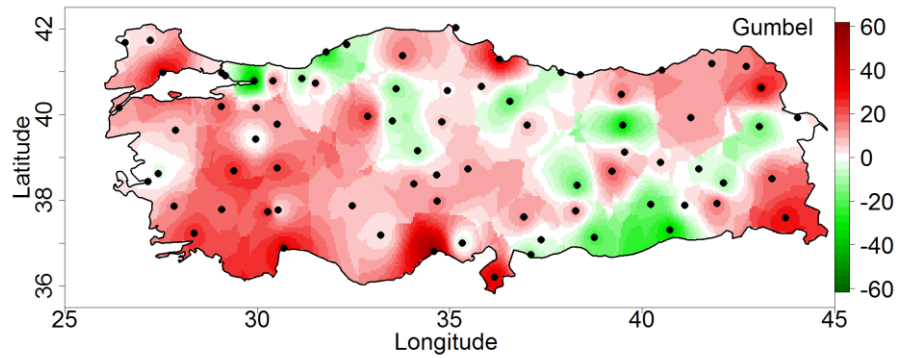
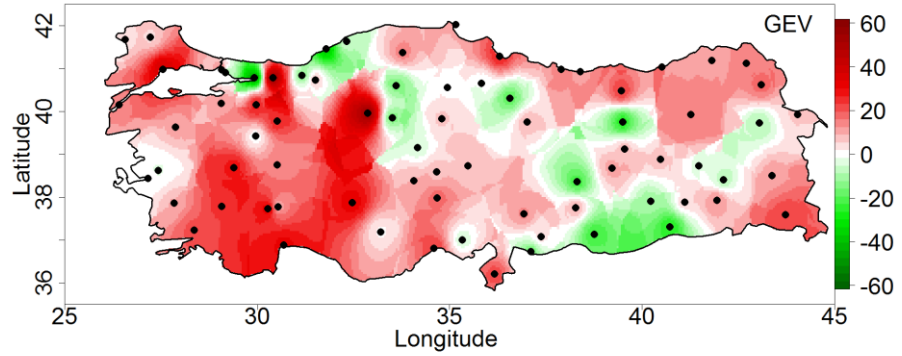


Figure 5.6 Percentage Difference between 100-year stationary and nonstationary return levels for annual precipitation maxima using GEV, gumbel, normal and lognormal distributions.

## 2) Winter AMPs

Maps of difference between 100-year nonstationary and stationary return levels obtained from four distributions for winter AMPs are shown in Figure 5.7. Overall inspection at the results for winter AMPs suggests that all four distributions have shown more or less similar impacts of nonstationarities during the winter season. The results demonstrate that most parts of the Mediterranean region have shown the tendency of positive impacts excepts some locations at the central part of the Mediterranean region adjacent to Central Anatolia. Aegean region exhibits a mixed kind of impacts as at some location the impacts were negative while at some other areas were positive. Unlike the other distributions, the Lognormal distribution shows high positive impacts along with the coastal line of the region. At most of the Marmara region, impacts were positive. The results show that mixed impacts are present for the Black Sea region where the western coast of the Black Sea region has positive impacts while central and eastern Black Sea region has shown negative impacts. Central Anatolia region and South-Eastern Anatolia regions demonstrate consistently negative impacts (up to 60 %) according to all four distributions. Evidence of mixed kind of impacts was found in the Eastern Anatolian region as the interpolated map shows green as well as red areas. The positive impacts are more significant (up to 60 %) particularly with GEV distribution over the Eastern Anatolia region.

Percentage Difference Between 100-year Stationary and Nonstationary Return Levels (Winter-AMP)

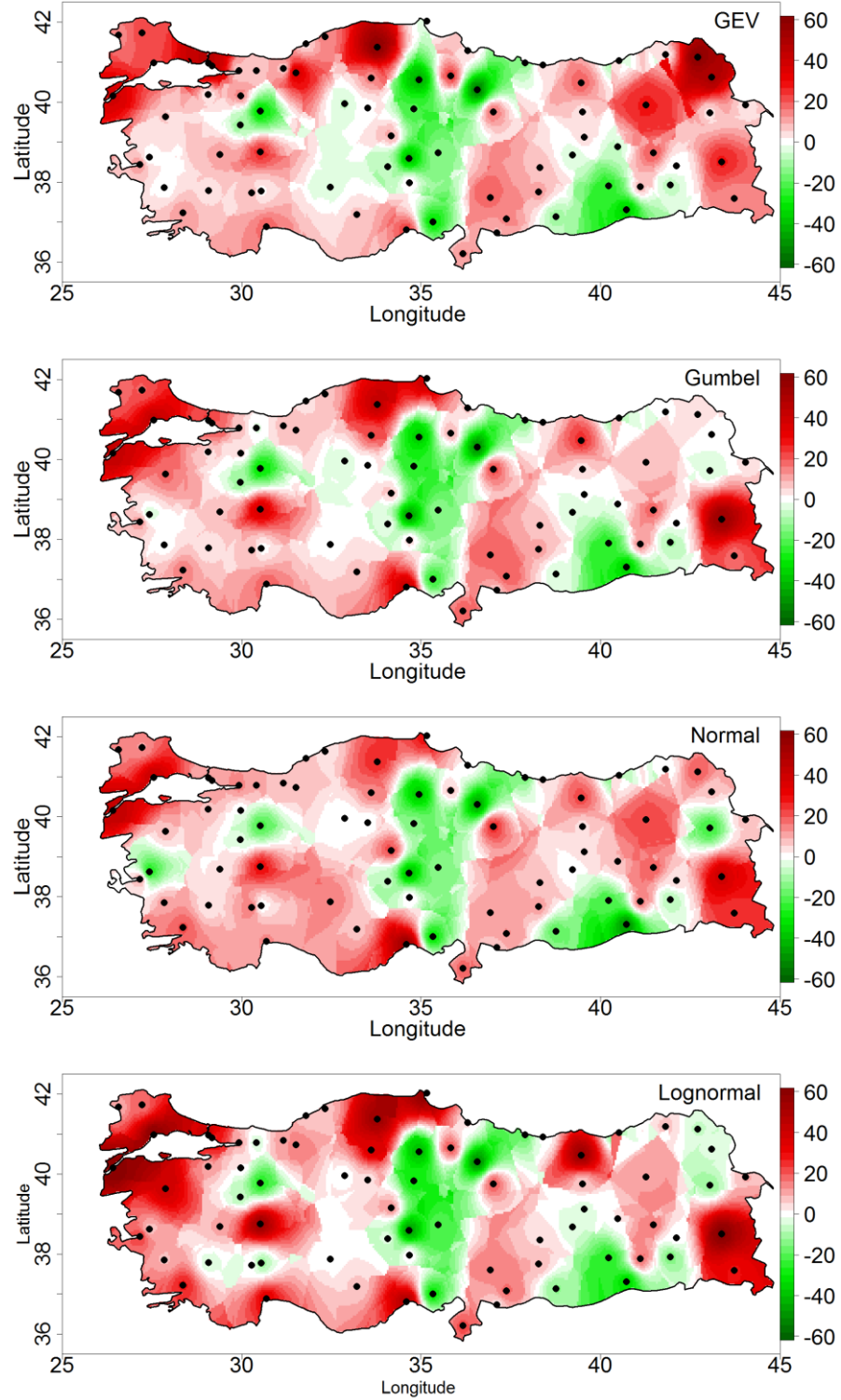


Figure 5.7 Percentage Difference between 100-year stationary and nonstationary return levels for annual precipitation maxima during winter using GEV, gumbel, normal and lognormal distributions.

### 3) Spring AMPs

Maps of difference between 100-year nonstationary and stationary return levels obtained from four distributions for spring AMPs is given in Figure 5.8. Results demonstrate that all four distributions were able to find similar impacts during spring. There are some persistent patterns of impact types over several regions throughout Turkey. The results are evident with negative impacts over the most of the eastern and central Mediterranean region. However, the western part of the Mediterranean region and the adjacent eastern part of the Aegean region showed positive impacts. Asian and European part of Marmara region exhibits negative and positive impacts respectively. Results have shown the mixed type of impacts throughout the Black Sea region and generally, the magnitudes of these impacts (up to 20 %) were less as compared to other geographical regions of Turkey. Similarly, the positive and negative impacts were evident for the eastern and western part of Central Anatolia respectively. All four distribution have shown the negative tendency of impacts at Eastern Anatolia and South-Eastern Anatolia.

Percentage Difference Between 100-year Stationary and Nonstationary Return Levels (Spring-AMP)

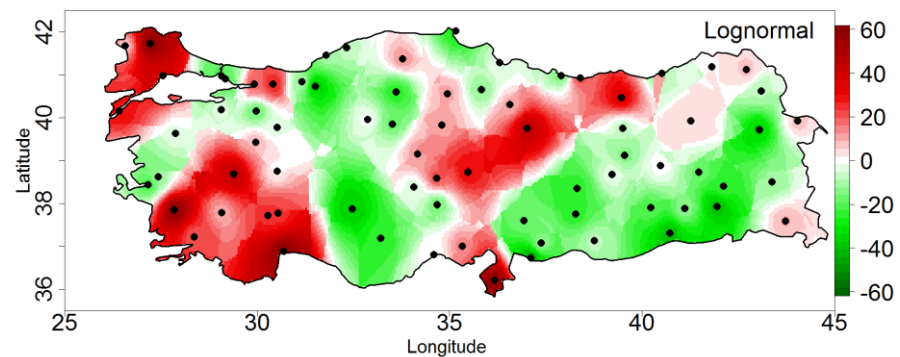
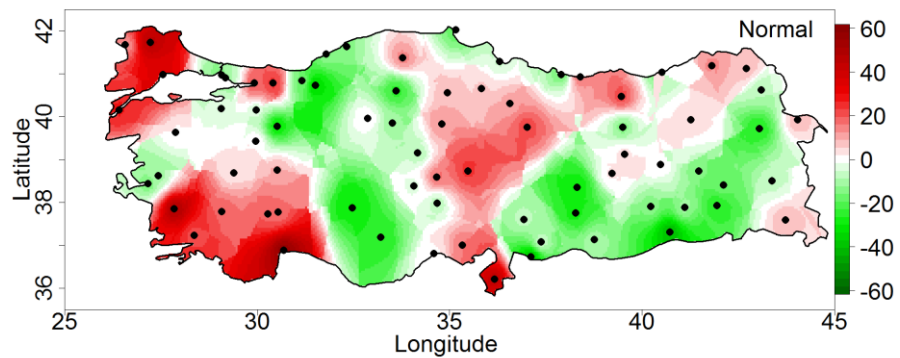
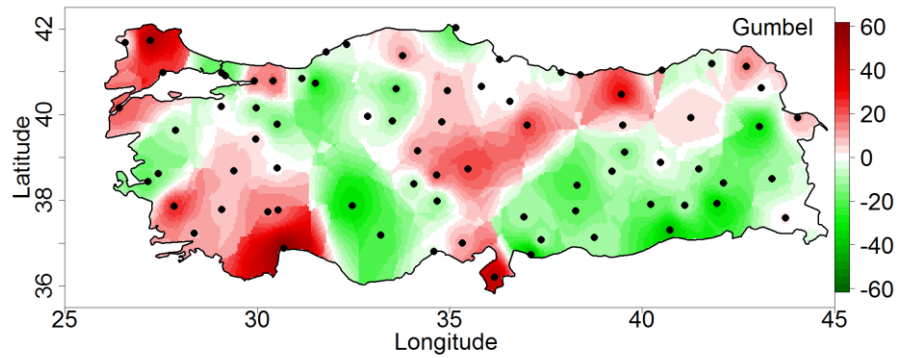
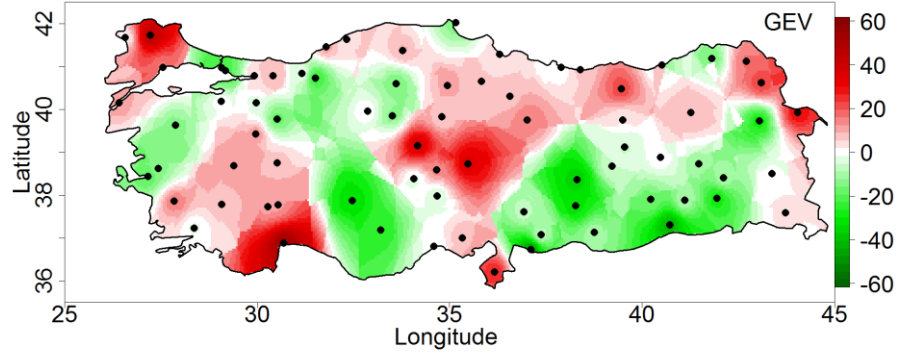


Figure 5.8 Percentage Difference between 100-year stationary and nonstationary return levels for annual precipitation maxima during spring using GEV, gumbel, normal and lognormal distributions

#### 4) Summer AMPs

Maps of difference between 100-year nonstationary and stationary return levels obtained from four distributions for summer AMPs is given in Figure 5.9. The results of nonstationary impact analysis during summer demonstrates that overall relatively more spatial variability is present for the type of impacts throughout Turkey. Most of the geographical regions contained both positive and negative impacts. For example, the results highlight the. Also, it is evident that at some location one distribution has shown positive impacts while another negative. For example, GEV shows negative impact at western Mediterranean region while others show a very strong positive impact. Similarly, results of Lognormal distribution in some areas located at the south-east of Turkey have shown negative impact while other three distributions have shown positive impacts. Asian Marmara and adjacent areas of Black Sea region have the negative impacts while all four distribution suggest positive impacts at European Marmara. Results also hint about diverse impacts for Central Anatolia between GEV and other three distributions. Most of the distribution have shown positive impacts at South Eastern Anatolia. GEV, Gumbel and Normal release very strong positive impact at the southeast part of the Eastern Anatolia. In addition, GEV, Gumbel, and Lognormal show strong positive impact at eastern Black Sea region. In spite of some diverse impacts from distributions at some locations, the spatial pattern of nonstationarity effect across the country is more or less the similar from all four distributions during summer.

Percentage Difference Between 100-year Stationary and Nonstationary Return Levels (Summer-AMP)

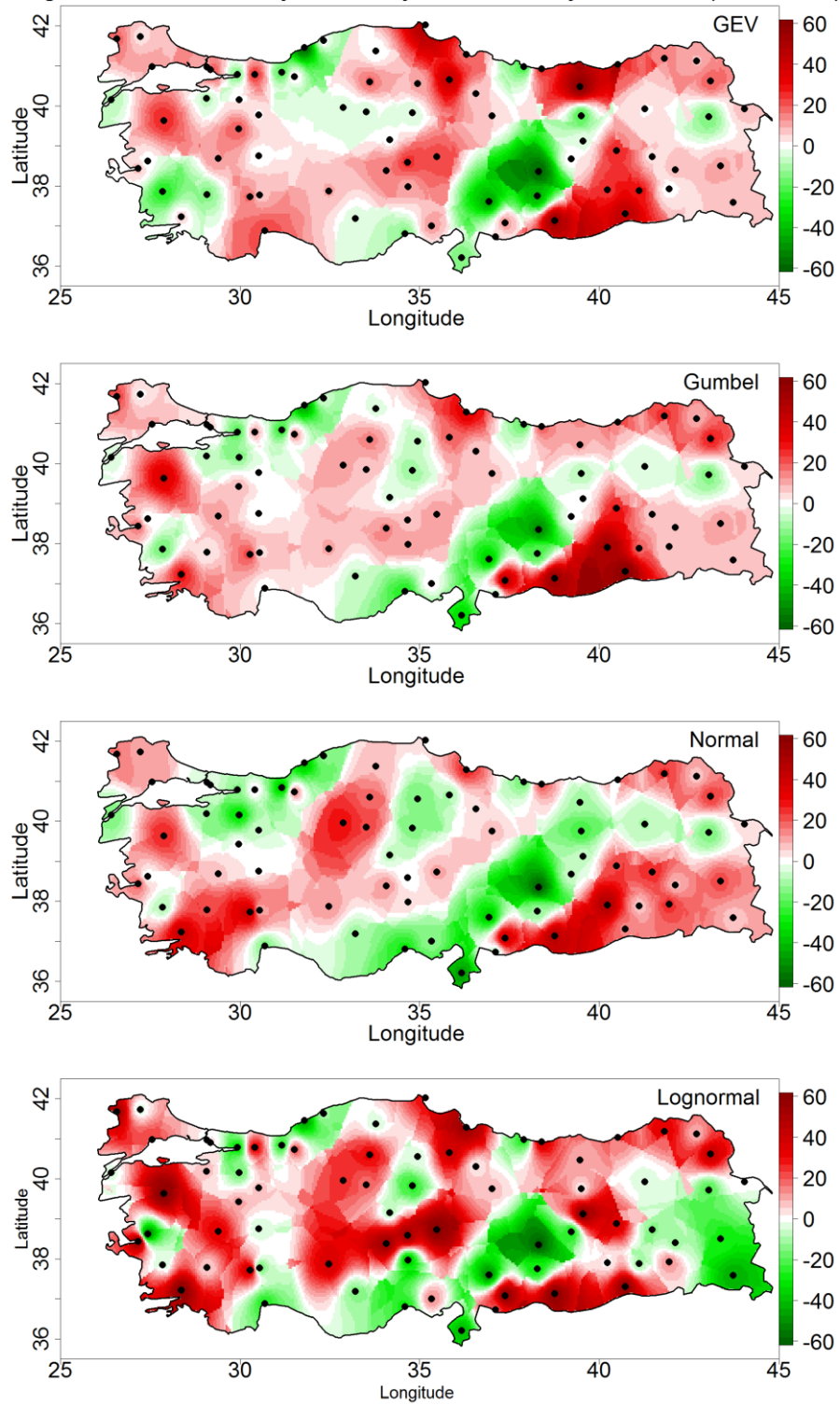


Figure 5.9 Difference between 100-year stationary and nonstationary return levels for annual precipitation maxima during summer using GEV, gumbel, normal and lognormal distributions.

## 5) Autumn AMPs

Maps of difference between 100-year nonstationary and stationary return levels obtained from four distributions for autumn AMPs is given in Figure 5.10. The results of nonstationary impacts analysis from all distributions found evidence that most of Turkey experienced positive impacts during the autumn season. Especially, GEV pronounced this feature more. However, there were some areas with small extent where nonstationary 100-year return values were found to be less than the stationary ones. For example, a few greener spots in Marmara regions hints towards the negative impacts. Similarly, some part of Central Anatolia also exhibits negative impacts as can be seen from maps obtained using Gumbel, Normal and Lognormal distributions. This is also more pronounced with Lognormal distribution. Almost all distributions have shown positive impacts over most part of Black Sea region. Similar were the findings for Aegean region, Mediterranean Region and South Eastern Anatolian region. Few greener spots in Eastern Anatolia suggests that impacts of nonstationarities were negative at some locations. In terms of magnitude, lognormal distribution has given higher impacts as compared to other distributions across all regions.

Percentage Difference Between 100-year Stationary and Nonstationary Return Levels (Autumn-AMP)

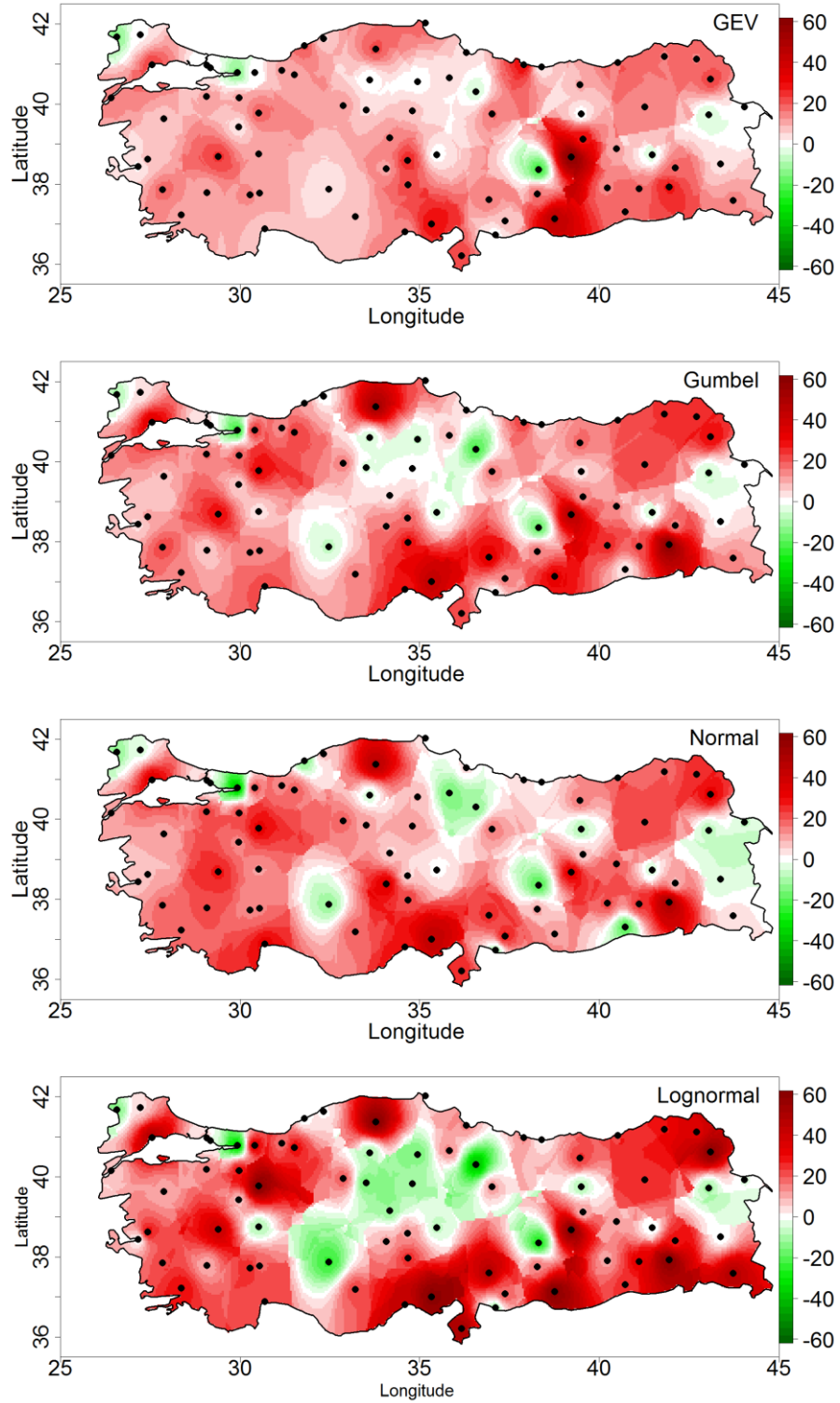


Figure 5.10 Percentage Difference between 100-year stationary and nonstationary return levels for annual precipitation maxima during autumn using GEV, gumbel, normal and lognormal distributions.

### **5.1.3. Nonstationarity Impacts During Projection Time Period (2050-2100)**

Stationary and nonstationary GEV distribution was used to assess the impacts of nonstationarities on projected precipitation extremes. The only GEV distribution is used in future projection because it is the most preferable model in extreme frequency analyses. Nonstationarity impacts were estimated for yearly as well as seasonal precipitation extremes. Impacts of nonstationarities were estimated in terms of the percentage difference between 100-year stationary and nonstationary return values(levels). The 12 ensemble members of CORDEX RCMs were used. The results are presented using the ensemble mean and ensemble median throughout Turkey falling within the CORDEX EURO domain. Boxplots of seven regionally categorized individual gridded stations are also presented in figures. Each box contains 12 nonstationarity impact values corresponding to each of individual CORDEX ensemble member. The size of boxplot explains the variability of results as obtained from each of individual ensemble member.

#### **1) Projected Yearly AMPs**

Maps of ensemble mean (left panel) and ensemble median (right panel) of the difference between 100-year nonstationary and stationary return levels obtained from GEV distribution for yearly AMPs are given in Figure 5.11. From Visual inspection of these maps it is evident that ensemble mean, as well as ensemble median, have shown similar impacts of nonstationarities. The nonstationarity effect is almost the same for at least half of the ensemble members. The overall red color of the map throughout Turkey explains that yearly precipitation extremes are increasing. There were a few gridded stations in Marmara (around Istanbul province) and western Mediterranean region where estimated impacts were found to be negative. The results presented in boxplots in Figure 5.12 also explain that most of the stations throughout Turkey exhibits positive impacts as both ensembles mean

and ensemble median values fall above the zero reference line. Each box has 12 members and the greater the box size the more variability among the models for showing the impact type and its magnitude. For example, as the box size gets larger the mean and median apart from each other and the mean value shows a tendency towards higher values either in a positive or negative impact direction. There have been few gridded stations (17238 and 17240 in Mediterranean region, 17848 in Eastern Anatolia, and 17062 in Marmara where both indicators (ensemble mean and ensemble median) have shown negative impacts. The mean and median values of all stations in the Mediterranean region are close to each other and not much deviated from zero line. However, in all other regions, such statistical values show high variability among stations and high deviations from zero line toward positive values. Also, there is more tendency to diverge between mean and median values at most of the stations in regions except the Mediterranean. The highest positive impact is obtained at 17220 in Aegean region where almost all ensemble members in each box are above zero line.

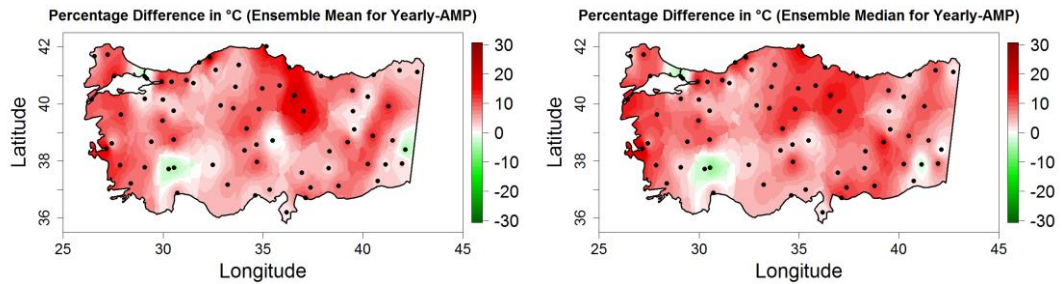


Figure 5.11 Ensemble mean and ensemble median of the percentage difference between 100-year stationary and nonstationary return levels for yearly AMPs of projected precipitation.

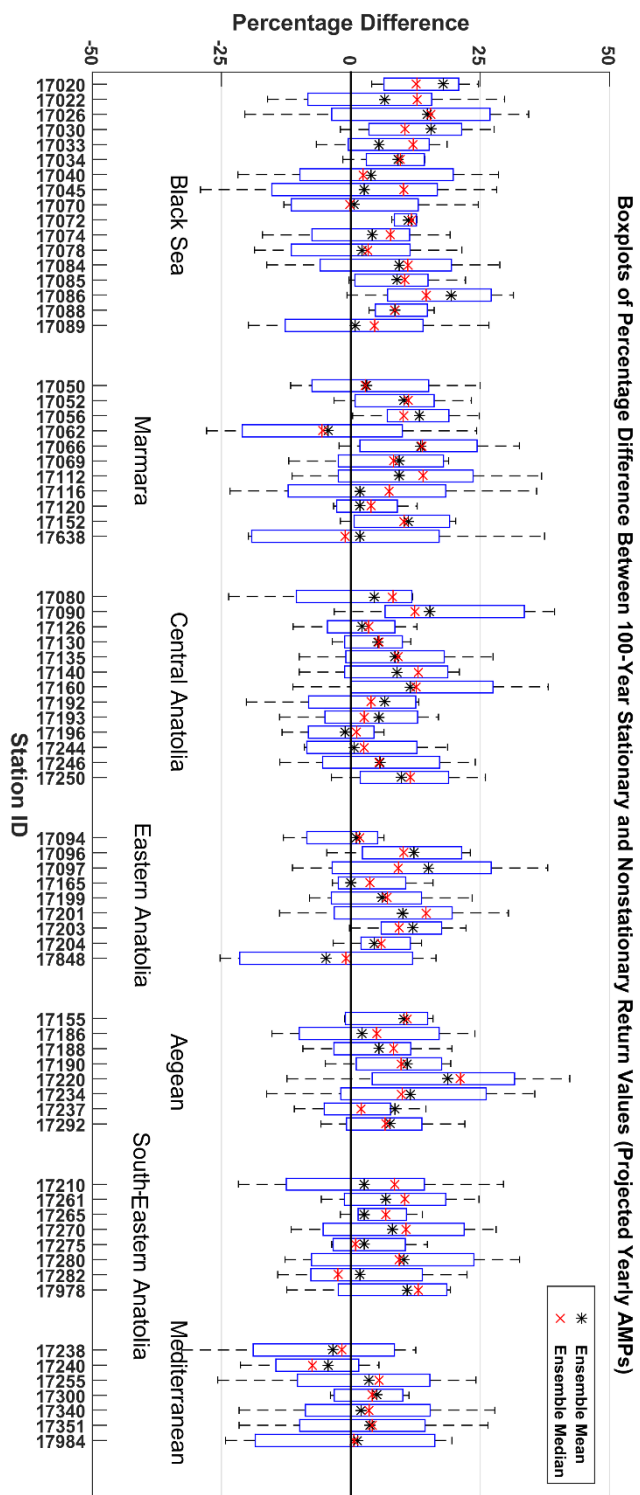


Figure 5.12 Boxplots containing nonstationary impact values of 12 individual CORDEX ensemble members at gridded stations for yearly AMPs. Ensemble mean pointer (black asterisk) and ensemble median pointer (red asterisk) are also given

## 2) Projected Winter AMPs

Maps of ensemble mean (left panel) and ensemble median (right panel) of the difference between 100-year nonstationary and stationary return levels obtained from GEV distribution for winter AMPs are given in Figure 5.13. The results explain that for winter AMPs in all seven regions of Turkey, positive nonstationarity impacts (median map) were found. The ensemble means map differs from the median map at the mid-part of the Mediterranean region (Antalya Province) where negative impact up to 20% appears. However, at least 50% of the models at this location shows no significant impact from nonstationarity in the median map. Both ensemble indicators have shown similar impacts overall. The 12-member ensemble results of each station are presented in form of boxplots in Figure 5.14. These boxplots also verify the findings of interpolated maps as ensemble mean and medians of most of the gridded stations fall above the zero reference line. There were a couple of gridded stations (17240 in Mediterranean region and 17848 in Eastern Anatolia) where ensemble mean has shown negative results as opposed to the ensemble median where impacts were found to be negative. Also, the variability among stations and among ensemble members in all regions is less in winter AMPs. Both statistical measures are close to each other except a few stations in the Mediterranean and Black Sea regions and thus, both are a good representative for model results.

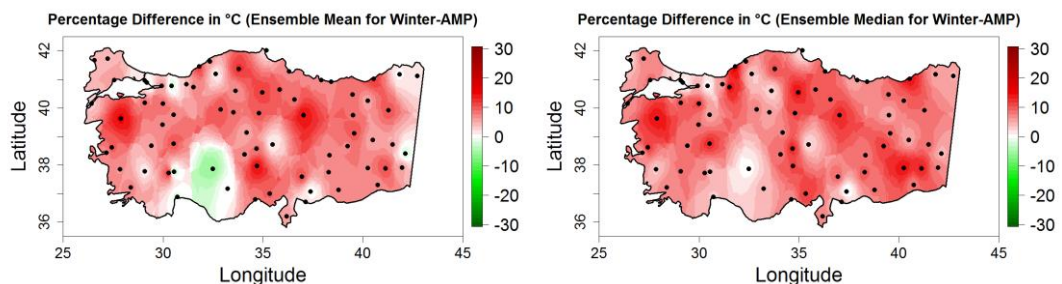


Figure 5.13 Ensemble mean and ensemble median of the percentage difference between 100-year stationary and nonstationary return levels for winter AMPs of projected precipitation.

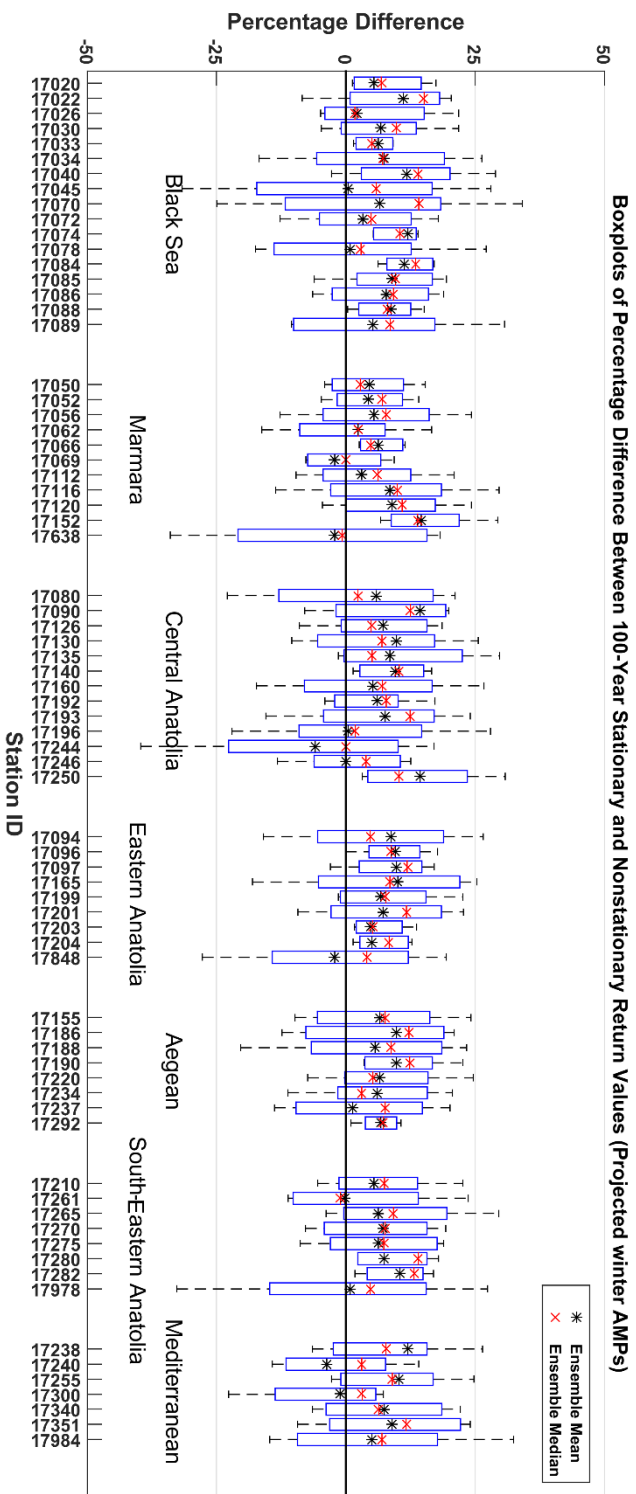


Figure 5.14 Boxplots containing nonstationary impact values of 12 individual CORDEX ensemble members at gridded stations for winter AMPs. Ensemble mean pointer (black asterisk) and ensemble median pointer (red asterisk) are also given

### 3) Projected Spring AMPs

Ensemble mean (left panel) and ensemble median (right panel) of the difference between 100-year nonstationary and stationary return levels obtained for spring AMPs are mapped over the whole Turkey falling within the Euro-11 domain and is given in Figure 5.15. Plotted ensemble mean and median shows that the most of Turkey is under positive impacts and the magnitudes of these impacts were higher in the Black Sea region, Marmara, Eastern, and South-Eastern Anatolia. Central Anatolia, Istanbul province, and eastern Mediterranean regions show negative impacts and they are more highlighted with the median map. The same can be viewed in regionally categorized boxplots of individual gridded stations boxplots given in the Figure 5.16. It is also evident that there were very few gridded stations especially in Marmara and Mediterranean regions where at least one ensemble analysis indicator have shown negative impacts as well. The greater variability among ensemble members (larger box size that is more than plus and minus %25) for impact type and its magnitude at each station throughout regions is available in Spring. Higher deviations between mean and median of boxes at some stations also exist in this figure.

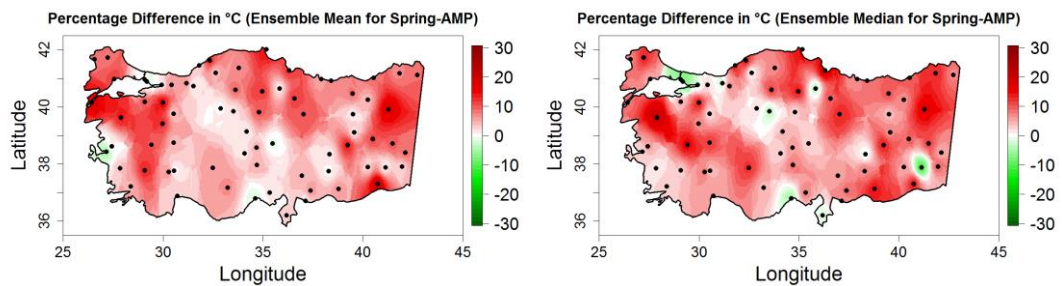


Figure 5.15 Ensemble mean and ensemble median of the percentage difference between 100-year stationary and nonstationary return levels for spring AMPs of projected precipitation.

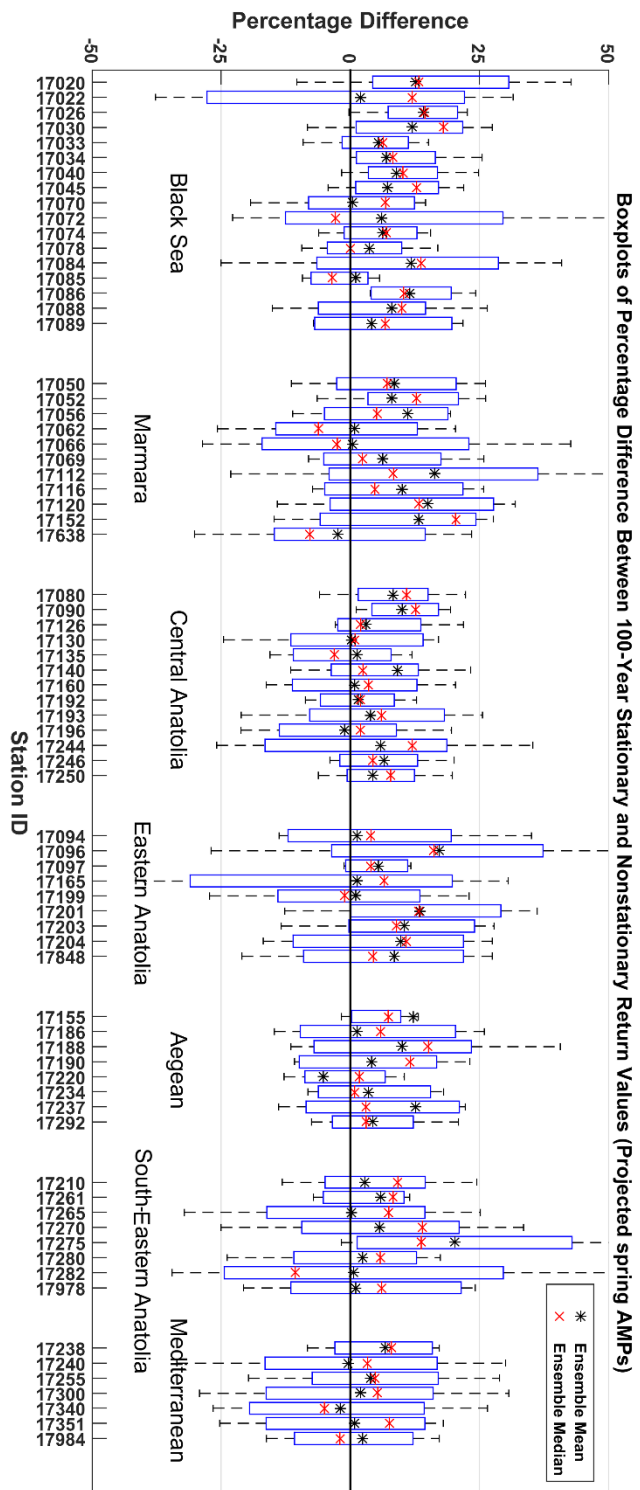


Figure 5.16 Boxplots containing nonstationary impact values of 12 individual CORDEX ensemble members at gridded stations for spring AMPs. Ensemble mean pointer (black asterisk) and ensemble median pointer (red asterisk) are also given.

#### 4) Projected Summer AMPs

Nonstationarities impact results are presented as maps of ensemble mean (left panel) and ensemble median (right panel) in Figure 5.17 and boxplots of individual gridded stations in Figure 5.18. The results presented in Figure 5.17 and Figure 5.18 suggest that during the summer season, mixed types of impacts are present in Turkey. For example, at least half of the ensemble members (median map) have shown negative impacts in the eastern part and Black sea region, South-Eastern Anatolia, and eastern part of the Mediterranean regions. Over these regions, the mean map increased the strength of negative impact. With mean map a few models show the high magnitude and thus, they have a greater influence on the mean value. In this case, the median map can be a better representative for the consistency of the signal. For the western part of the Black Sea region and the adjacent Marmara regions have mostly positive impacts (median map). Similarly, the western part of Central Anatolia and the adjacent Aegean region have mostly positive impacts but there were few gridded stations where at least one of the ensemble analysis indicator have shown negative impacts as can be observed from boxplots. It is also worth mentioning that during summer, more areas were found to be under the influence of negative impacts as compared to other seasons. In addition, the largest variability among ensemble members at all regions is seen in the summer season.

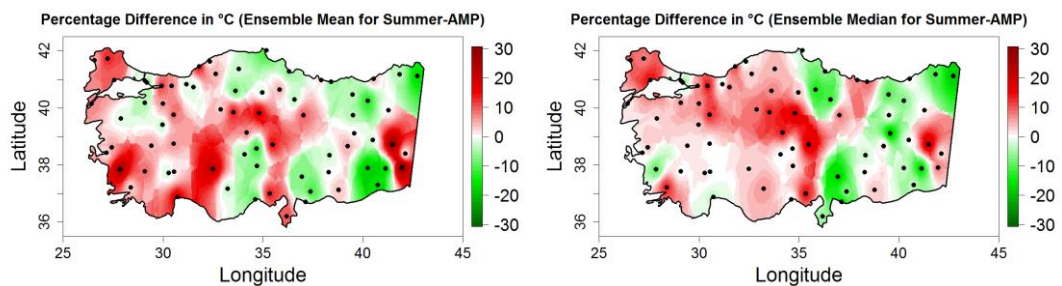


Figure 5.17 Ensemble mean and ensemble median of the difference between 100-year stationary and nonstationary return levels for summer AMPs of projected precipitation.

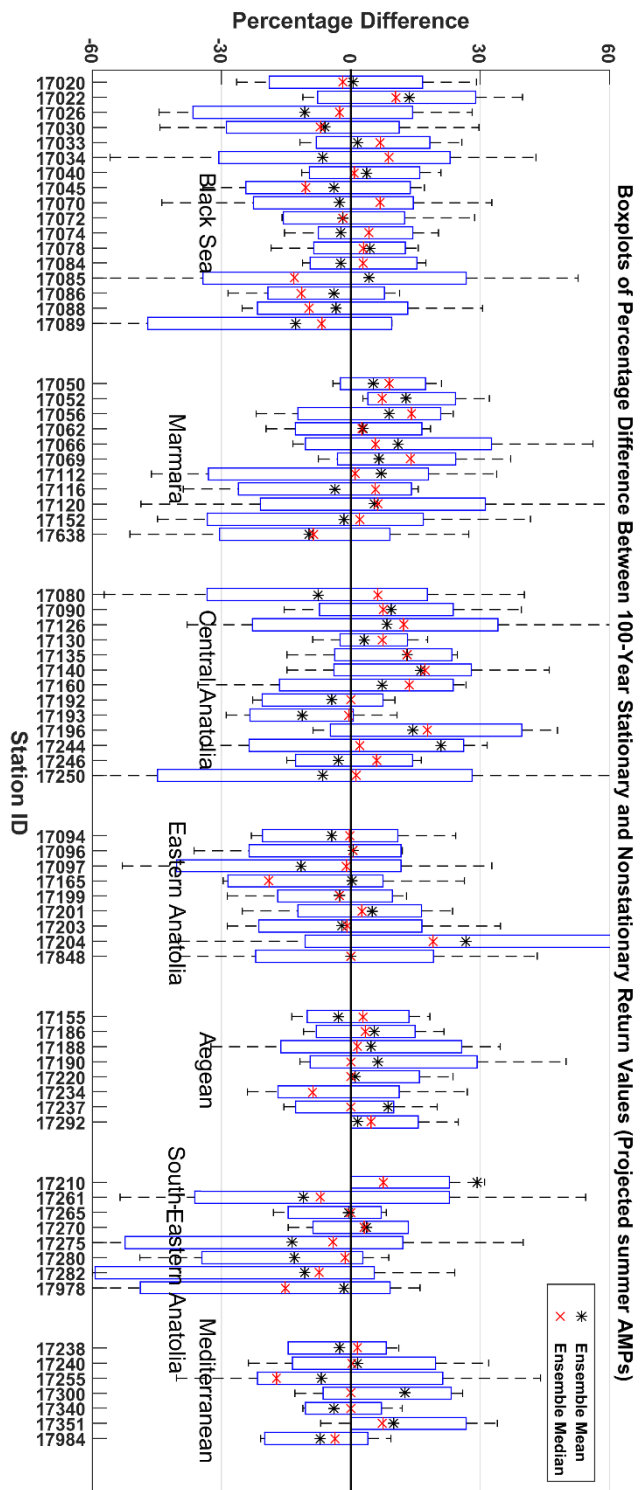


Figure 5.18 Boxplots containing nonstationary impact values of 12 individual CORDEX ensemble members at gridded stations for summer AMPs. Ensemble mean pointer (black asterisk) and ensemble median pointer (red asterisk) are also given.

## 5) Projected Autumn AMPs

Nonstationarities impact results are presented as maps of ensemble mean (left panel) and ensemble median (right panel) in Figure 5.19 and boxplots of individual gridded stations in Figure 5.20. These ensemble analysis results suggest positive impacts in most of the Black Sea region, European part of Marmara region, Aegean region and Eastern as well as Southeastern Anatolia. Eastern Marmara and mid part of Mediterranean regions show negative impacts in both mean and median maps. Negative impacts over these regions are more dispersed in the mean map as the magnitude of the impact is more dominant from a few models. Other regions from both maps show similar impact pattern. Most of the gridded stations in the Asian part of Marmara as well as adjacent stations of Central Anatolia exhibits negative impacts as the at least one of the ensemble indicator value fall below the zero reference line. Ensemble analysis shows that few gridded stations of the western Mediterranean region are also under the influence of negative impacts. In the case of Autumn AMPs, many variations can be seen between the results of ensemble mean and ensemble median. The variability among stations and ensemble members is significantly high and this results in increasing the uncertainty in model signal for a location and providing non-homogenous nonstationarity impact across the regions.

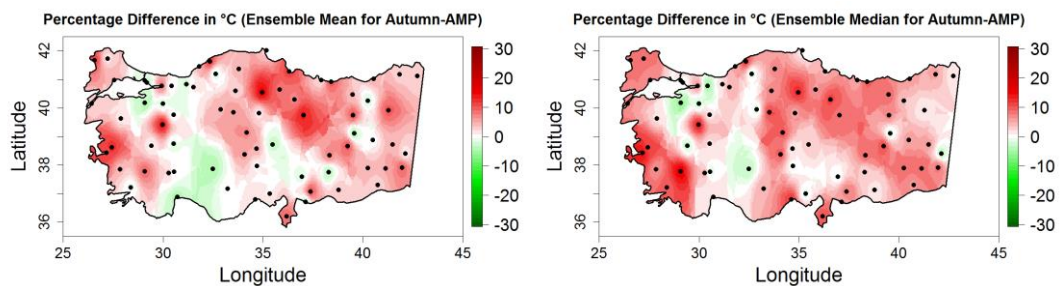


Figure 5.19 Ensemble mean and ensemble median of the percentage difference between 100-year stationary and nonstationary return levels for autumn AMPs of projected precipitation.

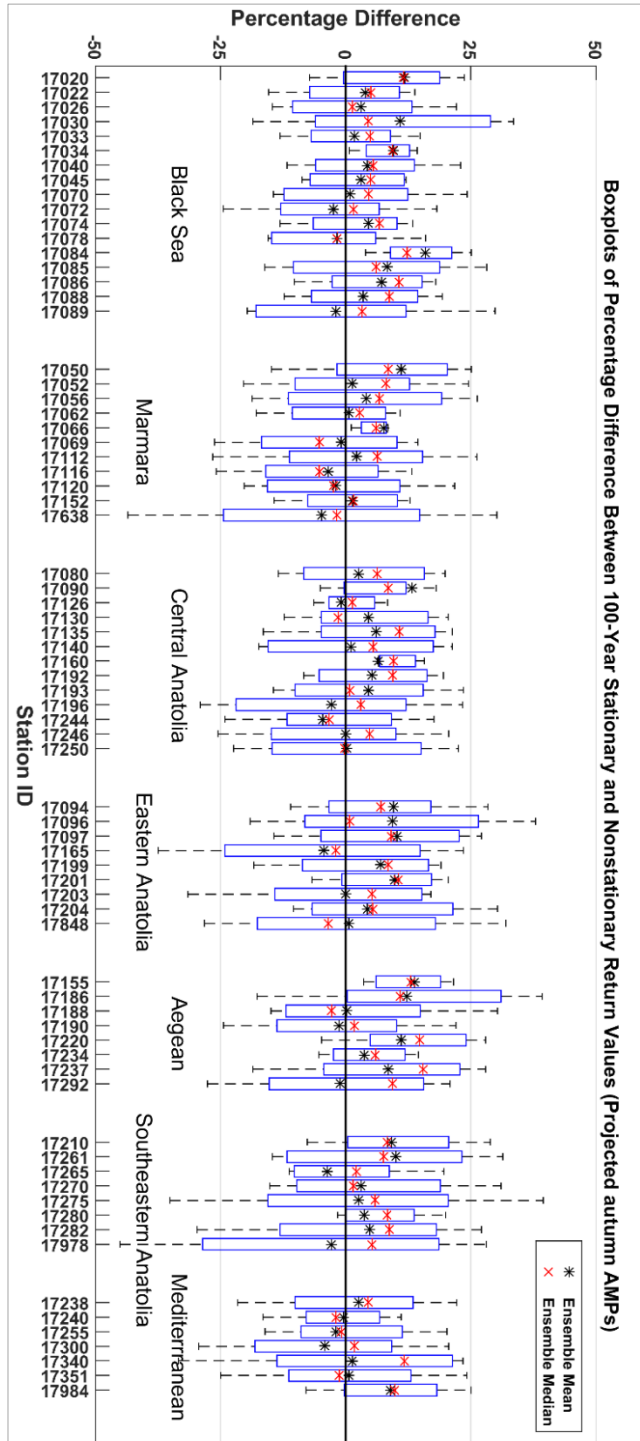


Figure 5.20 Boxplots containing nonstationary impact values of 12 individual CORDEX ensemble members at gridded stations for autumn AMPs. Ensemble mean pointer (black asterisk) and ensemble median pointer (red asterisk) are also given.

### **Intra-model Variability of Nonstationary Impacts**

Nonstationarity impact values at each gridded station estimated from individual ensemble members are plotted as box plots for each region separately to present the variability of nonstationarity impacts amongst ensemble members in Figure 5.21. The size of individual box plots explains the variability of nonstationarity impact values at gridded stations within the respective region. Regional mean and median values are also provided in the Figure 5.21. So, larger the box size, more is the variability of nonstationarity impacts within the region. The larger portion of the box with regional median values above zero indicates that most of the stations in that region exhibited positive impacts. Similarly, if a larger portion of the box and regional median value fall below zero, it indicates that most of the gridded stations in that region experience the negative impacts. Boxes of individual RCMs explains that there is much variability present amongst RCMs in South-Eastern Anatolia, Mediterranean region and Central Anatolia region. However, in the Black Sea region, Marmara region, and Aegean region, smaller variability is observed between the ensemble members as most of the RCMs predicted similar impacts of nonstationarities.

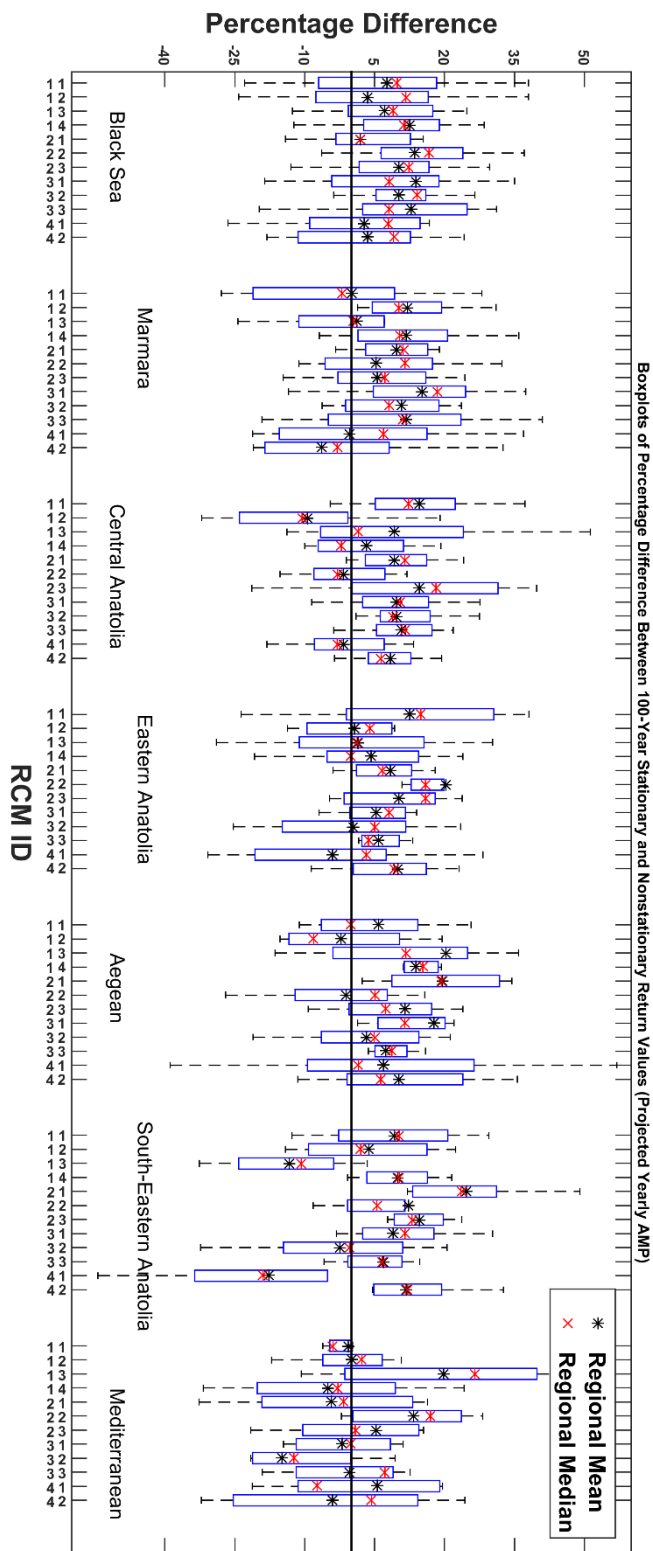


Figure 5.21 Boxplots describing the intra-model variability of nonstationarity impact prediction

## 5.2. Discussion

As temperature increases, the planet becomes warmer and water holding capacity of air increases which results into increases in heavy precipitation events (Trenberth et al., 2003; Karl and Trenberth, 2003; Emori and Brown, 2005; Willett et al., 2007, WEB4). Each degree of temperature rise can increase around 7 percent of water vapors (WEB4). The results presented in chapter 6 show that generally in Turkey, magnitudes of 100-year annual maximum temperatures increased in the case of time-variant nonstationary distributions, so does the 100-year and other return periods annual maximum precipitation magnitudes. Therefore, the findings of this study are consistent with the above-mentioned studies and contribute to this area. At the same time, increases in the magnitude of precipitation extremes may not always hint towards an increase in total precipitation during a season or year. Some climate simulations have shown decreases in average precipitation while increases in magnitudes of precipitation extremes or sometimes increases in dry period lengths were found (WEB4). This phenomenon was observed in this study in a few regions. For example, Sensoy (2013) shows that annual total precipitation decreased at some parts of Central Anatolia, the Mediterranean as well as the Aegean region. On the other hand, over these regions, we could see the higher 100-year return values with the impacts of nonstationary for annual maximum precipitations. For winter precipitation extremes impacts of nonstationary was mostly positive at Black Sea regions while Turgay and Kahya (2005) found decreases in total precipitation during winter months. These kinds of tendencies generally lead to the situations where the tails of extremes widen at both ends and on one side of the distributions. Consequently, we experience the severity of extremes in the form of intense precipitation, while on the other hand, we may encounter less number of rainy days and overall decreases in lower quantiles. Increased or decreased magnitudes (using nonstationary distributions) of return levels of extreme precipitation events can have very adverse implications. The adversity of these implications becomes more complicated at a seasonal scale because of different temperature, soil moisture conditions, land-cover patterns, and other seasonal variations. The results from this

study show more intense precipitation extremes during winter (because of positive nonstationarities impacts) in the eastern part of Central Anatolia, most of the Mediterranean, Aegean and Marmara region as well as some parts of the Eastern Anatolian region. These increases in the magnitude of precipitation extremes in winter, particularly in Eastern Anatolia and Eastern part of Central Anatolia together with winter temperatures normally falling below freezing level may indicate hints about more precipitation in form of snowfall. However, with an increase in temperature, (which are obvious from the studies (Yucel et al., 2014; Önoel and Semazzi, 2009; Önoel et al., 2014) as well as chapter 6 of this thesis) the precipitation patterns might become complicated. Yucel et al. (2014) also indicated a decreasing trend in the snowy days for the historical period. This also supports more extreme snowfall (the case with nonstationarity) when it occurs in these regions. Usually increases in winter precipitation intensities (especially in mountainous regions of Turkey) might not directly lead towards high flood situations but increase snowmelt discharge because of gradual snowmelt during the later months. But increased magnitudes of precipitation extremes for some given return period may hint towards observing more intense snow or winter storms over these regions. The increased thickness of snow cover due to more intense winter storms can have effects on winter crops, public mobilization, property damages and even loss of human lives. During the spring season, impacts of nonstationary were positive in the Aegean region, and some parts of Marmara, Black Sea region as well as Central Anatolia region. These results suggest more intense spring precipitation events are expected during the spring season. Any increase in the magnitude of spring precipitation extremes has a more directed influence towards streamflow extremes as most of the time streamflow extreme events fall in spring (Small et al., 2006). Similarly, any decreases in precipitation extremes during spring season might cause reducing the streamflow extremes as well. Most of Turkey have positive impacts of nonstationarities on precipitation extremes during the autumn season with few exceptions in Central Anatolia. Unlike spring, the increased magnitudes of extreme precipitation in fall season usually doesn't imply the higher streamflow. Small et al. (2006) claimed that one of the major reason for this phenomenon is that during fall

season most of the precipitation is contributed towards baseflow rather than inducing floods. So, these positive impacts on precipitation extremes during the autumn season may increase the magnitudes of lower quantiles of flow rather than flow extremes.

Inferences about climate nonstationarities based on historical record shed light on the status that time-variant precipitation extremes and its implications are expected in near future and the current status of nonstationarities might change over a long duration in the future. So, decisions based on historical record are usually short termed. Regional climate model projections are used to evaluate the long-term status of climate change, the status of nonstationarities and its implications in different sectors of human life. The nonstationarity impact results of this study from ensemble regional climate models during projection period (2051-2100) are found to be different than the results obtained during the historical period (1971-2016) in many regions of Turkey. During projection period, for yearly AMPs, there were more widespread positive impacts in Eastern Anatolia, Southeastern Anatolia and eastern part of Central Anatolia than those in the historical period over these same regions. But the results also found evidence that most of the Marmara and Aegean have shown positive impacts during historical as well as projection periods. One of the reasons for this widespread impact in a positive direction might be related to increased temperature because of the global warming. Similar was the situation during the winter season. The regions of Central Anatolia, Eastern Anatolia and Southeastern Anatolia have shown positive impacts in projection period while mixed (positive and negative) impacts were found in the historical period over these regions. The nonstationarity impact results were similar for most of the Marmara, Aegean and western part of the Black Sea region. With the seasonality, more inconsistencies of nonstationarity impacts between historical and projections periods were observed throughout Turkey. These inconsistencies were more notable in South-Eastern Anatolia, Eastern Anatolia and western part of Central Anatolia where impacts estimated during the historical period were found to be opposite to those

obtained during the projection period. Similarly, clear differences were found during the summer season in Black sea region, Eastern Anatolia as well as South-Eastern Anatolia. During Autumn, more inconsistencies were found between results during historical period and projection period in the Mediterranean region and the western part of Central Anatolia where impacts were positive during the historical period and negative during the projection period. Results show similar (positive) impacts at Marmara, Black Sea, East and Southeastern Anatolian region during historical as well as projection period. These variations in results of observed and projected nonstationarities impacts on yearly as well as seasonal precipitation extremes explained the complexity of climate system and the genre of nonstationarities. It is also envisaged that the current trends in time-dependent variations (increase or decrease due to nonstationarities) in return level corresponding to a given return period might not continue over a longer time period into future. In result, the overall impacts of nonstationarities at the end of the century might be more severe (in case nonstationary impacts follow the same direction during historical or projection period) or reversed (in case nonstationary impacts direction during historical or projection period are estimated to be opposite in direction) or moderate. Any risk and reliability analysis based on historical impacts might only be useful for short-term planning and decision making while for long-term, analysis based on historical as well as projected data might be more appropriate. Analysis of intra-model variability explains the importance of ensemble analysis approach. Regions (e.g., Black Sea region, Marmara region and Aegean region) where most of the ensemble members provide homogenous impact, smaller ensemble size or even single model might be enough for impact studies. However, the regions (e.g., Central Anatolia region, South-Eastern Anatolia, and Mediterranean region) where more intra-model variability is observed, the use of ensemble analysis approach even with more members become critically important.

## CHAPTER 6

### NONSTATIONARITY ANALYSES OF TEMPERATURE

#### 6.1. Results

##### 6.1.1. Distribution Fitting Under Stationary and Nonstationary Conditions

Three distributions (GEV, Gumbel and Normal) are used for five maximum temperature indices (Yearly AMTmax and Seasonal AMTmax) and five minimum temperature indices (Yearly AMTmin and Seasonal AMTmin) obtained from observed daily maximum and daily minimum temperature data to evaluate the impacts of nonstationarities. The parameters of each distribution were estimated by minimizing the Negative Log-Likelihood value (NLLH). The distribution with a lower value of NLLH is considered to be the better one. The boxplots of Negative Log-Likelihood values of GEV, Gumbel and Normal for stationary and nonstationary cases are shown for each of the precipitation indices (Yearly AMTmax, AMTmin, and seasonal AMTmax, AMTmin) in Figure 6.1 and Figure 6.2, respectively. Each boxplot contains 77 values of NLLH corresponding to 77 stations used in this study.

It is observable from most of these figures, that generally, boxplots representing NLLH values of each of the distribution for nonstationary cases are slightly lower

than the ones for stationary case. This indicates that each distribution has shown slightly better fit when covariate of time was introduced. It is also clear from all the figures that NLLH values for Gumbel distributions were found to be higher than the NLLH values of other two distributions for both stationary and nonstationary cases. The boxplots of GEV distributions in almost every subplot shows that NLLH values of GEV distribution were lower than the other two (Gumbel and Normal) distributions for both stationary and nonstationary cases. It is also clear that among the distributions with two parameters (Gumbel and Normal), Normal distribution has shown comparatively lower NLLH values as compared to the other two distributions in both stationary and nonstationary cases for most of the temperature indices. However, these comparatively higher values in case of Gumbel distribution was more significant in case of Yearly and Seasonal AMTmax indices than in case of Yearly and Seasonal AMTmin indices. However, NLLH values of Normal distribution for summer and spring AMTmins were slightly higher than the Gumbel distribution as can be seen from the respective figures.

Considering the lowest values of NLLH and historically more frequent usage of GEV in literature to perform frequency analysis of extremes because of its ability to show better fit for tails, only GEV distribution will be used for future projected data.

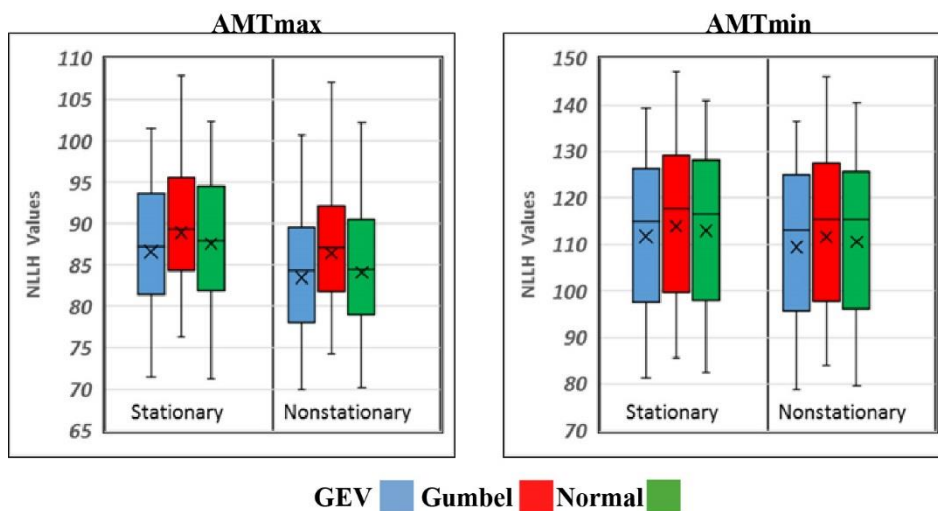


Figure 6.1 Comparison of Negative Log-Likelihood of distributions for Yearly AMTmax and AMTmin of observed data.

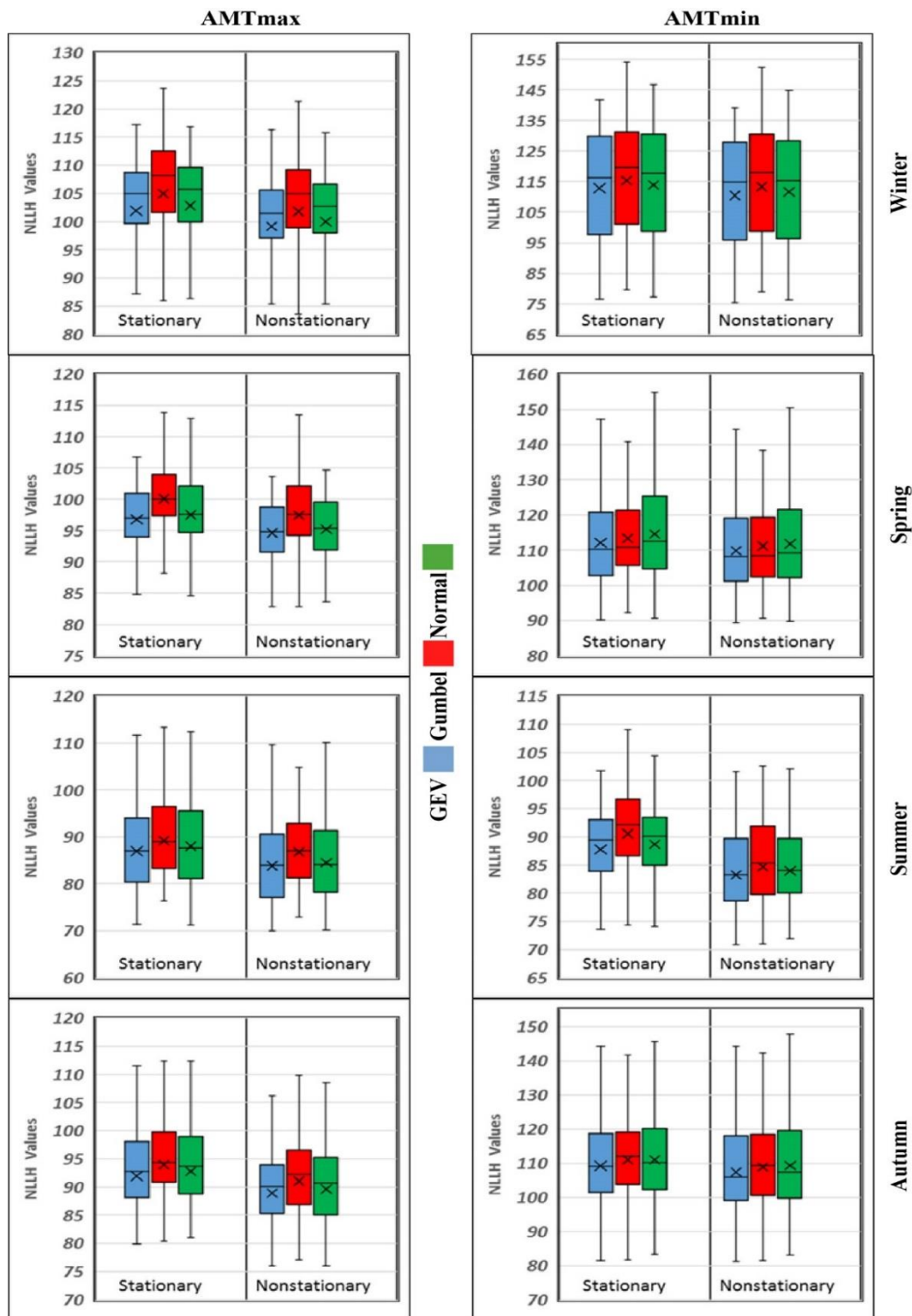


Figure 6.2 Comparison of Negative Log-Likelihood of stationary and nonstationary distributions for (a) Winter (b) Spring (c) Summer and (d) Autumn AMTmax and AMTmin of observed data

Further, for an example, the probability density function, cumulative probability density functions and QQ-plots of these four distributions are plotted for the yearly maximum temperature of Ankara station as given in Figure 6.3, 6.4, and 6.5 respectively. From these plots, the variability in fitting the distributions to observation is observable. All three plots clearly show that GEV provided better fit as compared to Gumbel and Normal distributions for the annual maximum temperature of Ankara. Visual inspection of all three Figures also suggests that amongst two-parameter distributions, Normal distribution better fitted the observation.

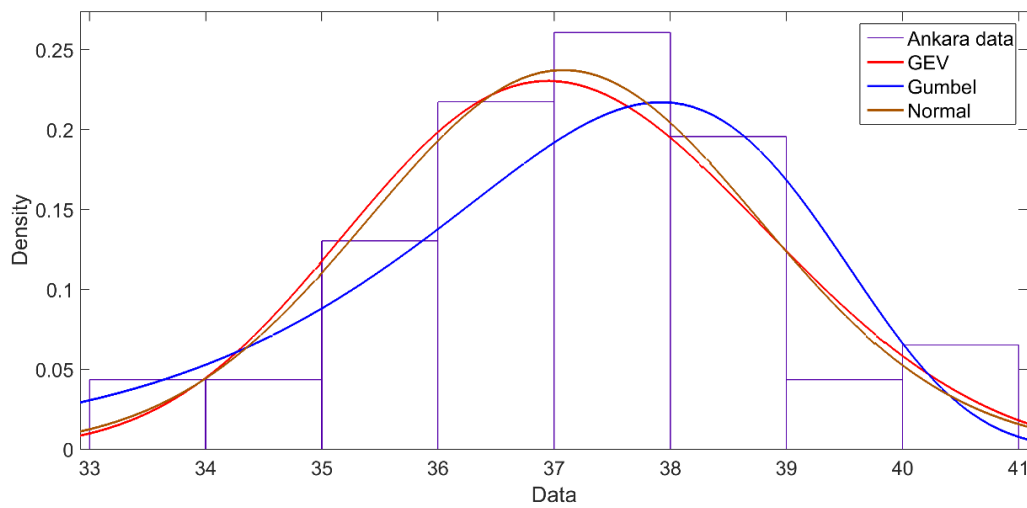


Figure 6.3 Comparative plots of probability density functions of GEV, Gumbel, Normal and Lognormal distributions

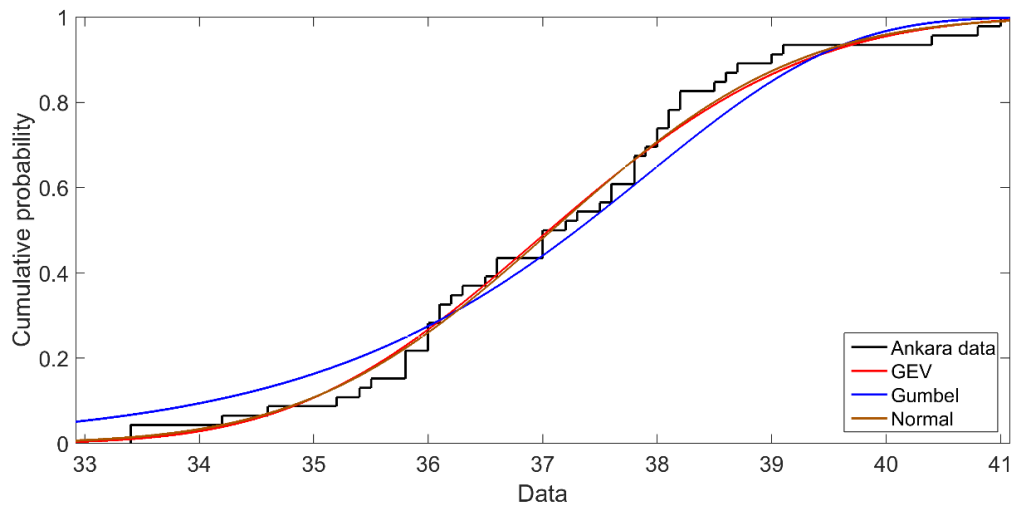


Figure 6.4 Comparative plots of cumulative probability density functions of GEV, Gumbel, Normal and Lognormal distributions

QQ Plot of Sample Data versus Distribution

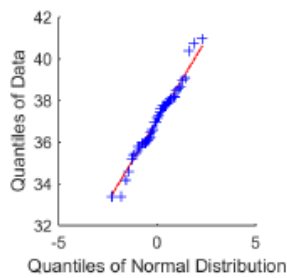
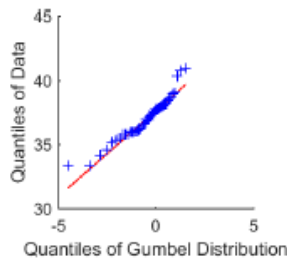
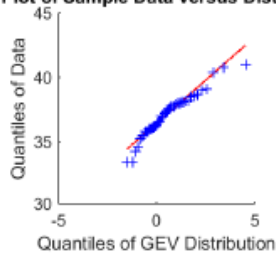


Figure 6.5 QQ-plots of GEV, Gumbel, Normal and Lognormal distributions

### **6.1.2. Nonstationarity Impacts During Historical Time Period (1971-2015)**

Three distributions namely GEV, Gumbel, and Normal distribution were used under stationary and nonstationary assumptions for yearly and seasonal maximum temperature series as 1)- Yearly AMTmax 2)- Winter AMTmax 3)- Spring AMTmax 4)- Summer AMTmax and 5)- Autumn AMTmax series obtained from observed daily maximum temperature at each station. Similarly, the impact analyses were done for yearly and seasonal minimum temperature series named as 1)- Yearly AMTmin 2)- Winter AMTmin 3)- Spring AMTmin 4)- Summer AMTmin and 5)- Autumn AMTmin series

Impacts of nonstationarities were quantified as the difference between nonstationary and stationary return levels of 100-year return periods. In this section, the interpolated maps of the percentage difference between nonstationary and stationary 100-year return levels are presented for each distribution for yearly and seasonal AMTmax and AMTmin.

#### **1) Observed Yearly AMTmax and AMTmin**

Maps of difference between 100-year nonstationary and stationary return levels using distributions for yearly AMTmax are given in Figure 6.6. Visual inspection of maps given in figure suggests that GEV and Normal distribution have shown similar impacts in most of the region while Gumbel distribution has shown more intense impacts and at some locations (for example in Aegean region and Marmara region) even direction of impacts was found to be opposite. Impacts of nonstationarities were found to be positive in most part of the Aegean region using GEV and Normal distributions. Similarly, all three distributions have shown mixed types of impacts in the Black Sea region as at some station there were positive impacts while other

locations have negative impacts. Results (particularly from GEV and Normal distributions) shows positive impacts throughout Central Anatolia, Mediterranean, East Anatolia, and South-eastern Anatolia regions of Turkey. However, at few locations (particularly using Gumbel distribution) impacts of nonstationarities were found to be negative in these regions.

Maps of difference between 100-year nonstationary and stationary return levels of using three distributions for yearly AMT<sub>min</sub> are given in Figure 6.7. Visual inspection of maps given in figure suggests that all three distribution has shown more are less similar impacts. The results show that most of the eastern part (eastern part of Black Sea region, the eastern part of Central Anatolia, all most all of the Eastern and South-Eastern Anatolia) of Turkey are under the influence of positive impacts for yearly minimum temperatures. However, results ( particularly from GEV and Gumbel distributions) have shown negative impacts at few stations in the central part of the Black Sea and Central Anatolia regions. All three distributions have positive impacts in Marmara region, the adjacent locations of the Black Sea region and Aegean region. However, results suggest that magnitudes of these impacts were less as compared to the magnitudes of impacts in the eastern part of Turkey. Furthermore, results from most of the distributions suggest negative impacts at few locations in the western part of the Mediterranean region. It is also noteworthy from the map scales that magnitudes of positive impacts were more significant for Minimum temperature as compared to maximum temperature.

Difference (°C) Between 100-year Stationary and Nonstationary Return Levels (Yearly-AMTmax)

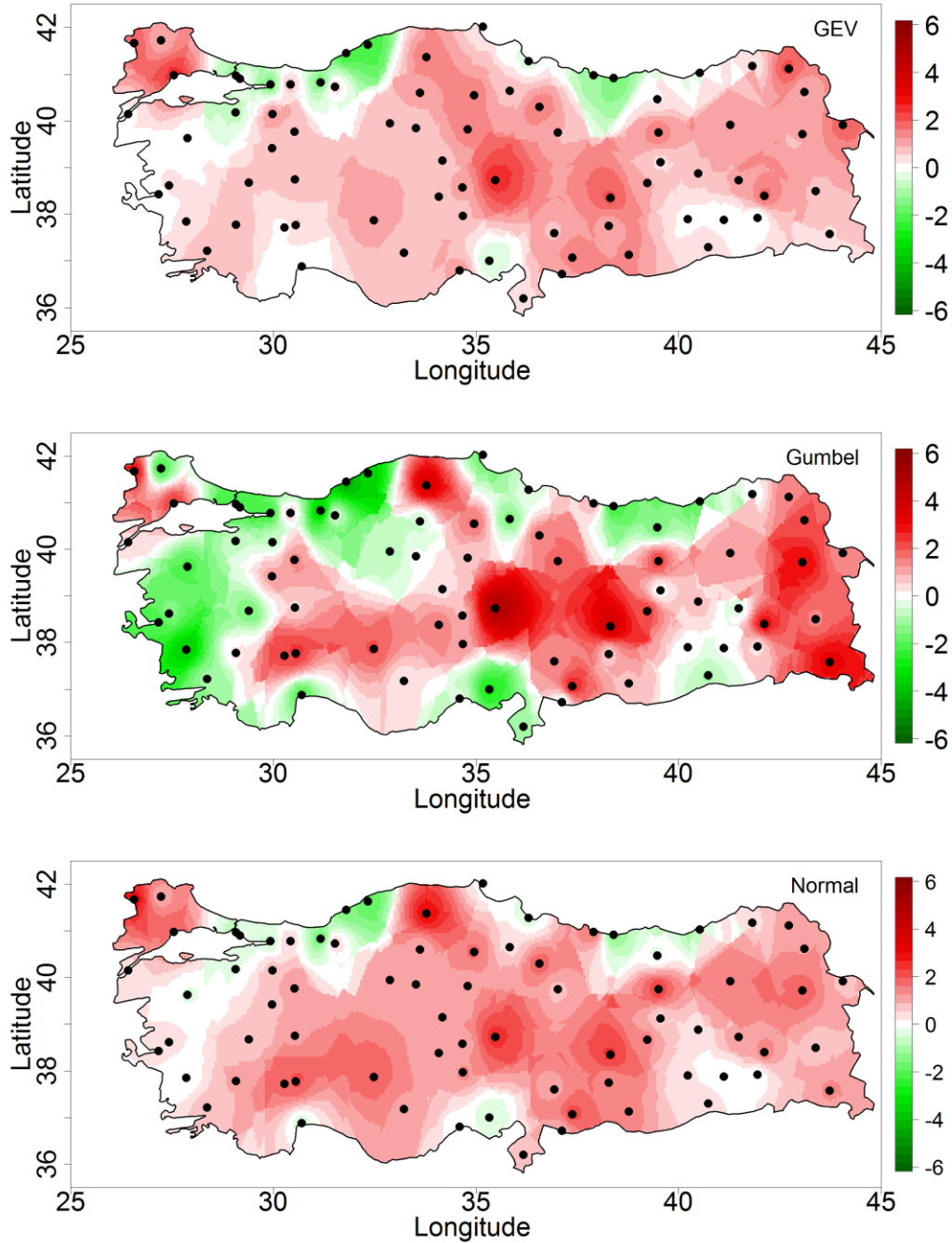


Figure 6.6 Difference (°C) between 100-year stationary and nonstationary return levels for annual temperature maxima using GEV, gumbel and normal distributions.

Difference (°C) Between 100-year Stationary and Nonstationary Return Levels (Yearly-AMTmin)

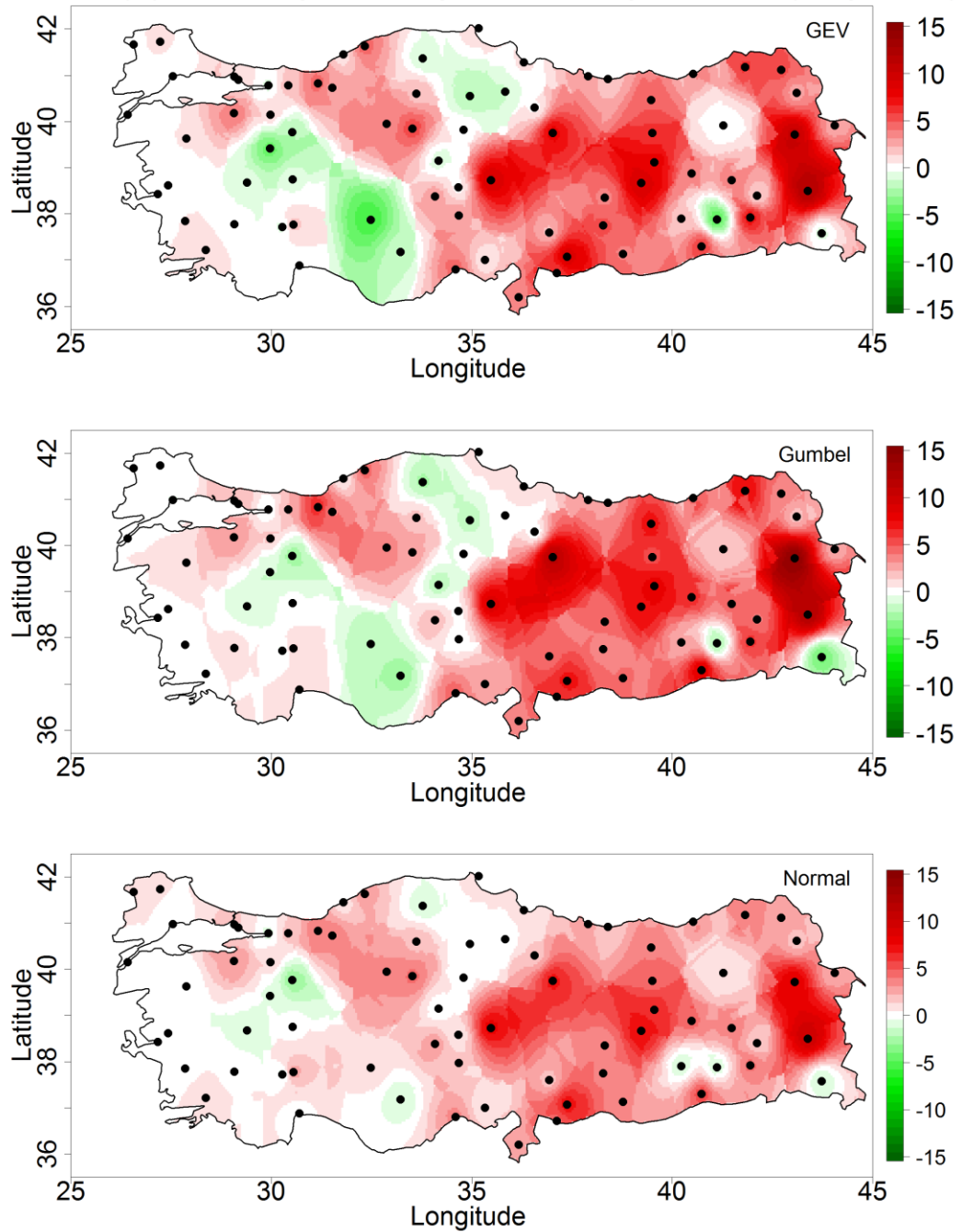


Figure 6.7 Difference (°C) between 100-year stationary and nonstationary return levels for annual temperature minima using GEV, gumbel and normal distributions.

## 2) Observed Winter AMTmax and AMTmin

Maps of difference between 100-year nonstationary and stationary return levels using distributions for winter AMTmax are given in Figure 6.8. The results given in maps show the variability of impacts estimated from three distributions. This inter-distribution variability is more apparent in case of gumbel distribution which has shown opposite direction of impacts in most of Aegean region, Black Sea region, Central Anatolia and South-eastern Anatolia. However, in the case of GEV and Normal distributions, most of the variability can be seen in magnitude rather than the direction of nonstationarity. GEV and normal distribution exhibited positive impacts in most of the Marmara region, Aegean region, Mediterranean region, Eastern and South-Eastern Anatolia. Also, most of the eastern part of Central Anatolia exhibited positive impacts by GEV and Normal distributions while at few stations in western part of Central Anatolia, impacts of nonstationarities were found to be negative. GEV and Normal distribution suggest slightly negative and positive impacts in the eastern and western part of the Black Sea region, respectively.

Maps of difference between 100-year nonstationary and stationary return levels using distributions for winter AMTmin are given in Figure 6.9. Unlike annual maxima in winter, impacts for annual minima of winter from all three distributions have shown less inter-distribution variability in direction and magnitudes in most of Turkey. Most of Turkey was found to be under the influence of positive impacts of nonstationarities in yearly winter minima. , The magnitudes of these positive impacts were higher in the eastern part of Turkey as compared to the western part of Turkey. However, very few stations in different stations have shown negative impacts as well. It is also noteworthy from the map scales that magnitudes of positive impacts were more significant for Minimum temperature as compared to maximum temperature during the winter season.

Difference (°C) Between 100-year Stationary and Nonstationary Return Levels (Winter-AMTmax)

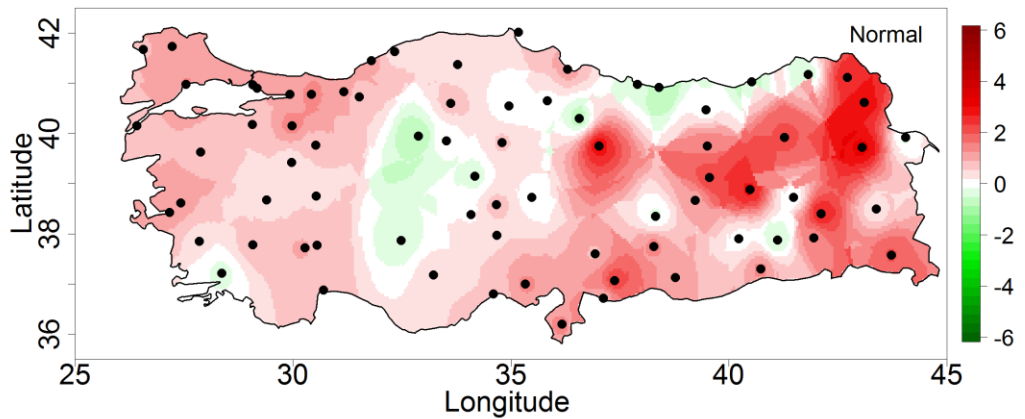
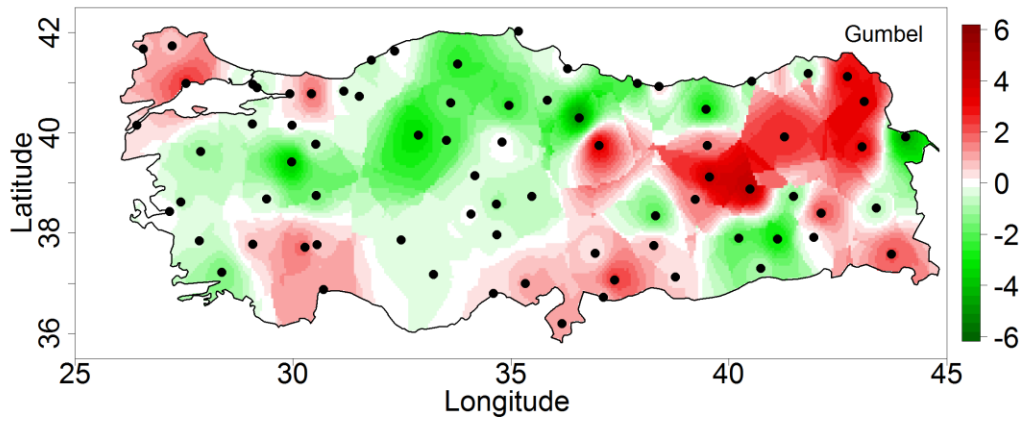
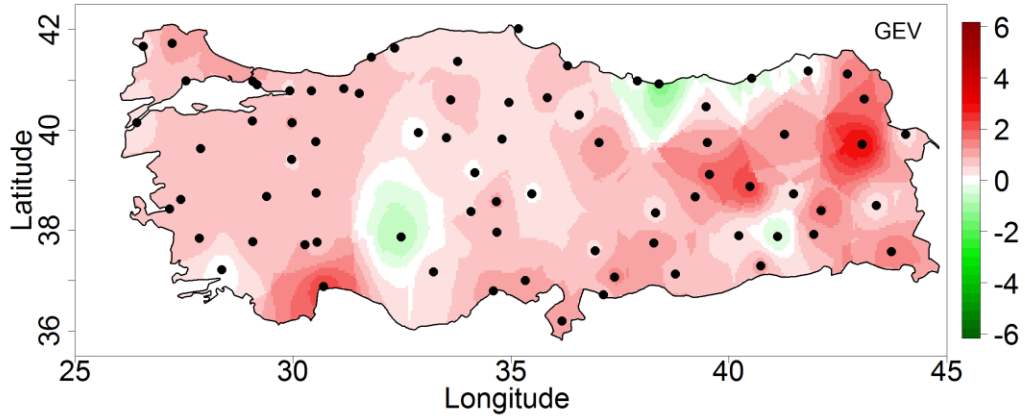


Figure 6.8 Difference (°C) between 100-year stationary and nonstationary return levels for annual temperature maxima during winter using GEV, gumbel and normal distributions.

Difference (°C) Between 100-year Stationary and Nonstationary Return Levels (Winter-AMTmin)

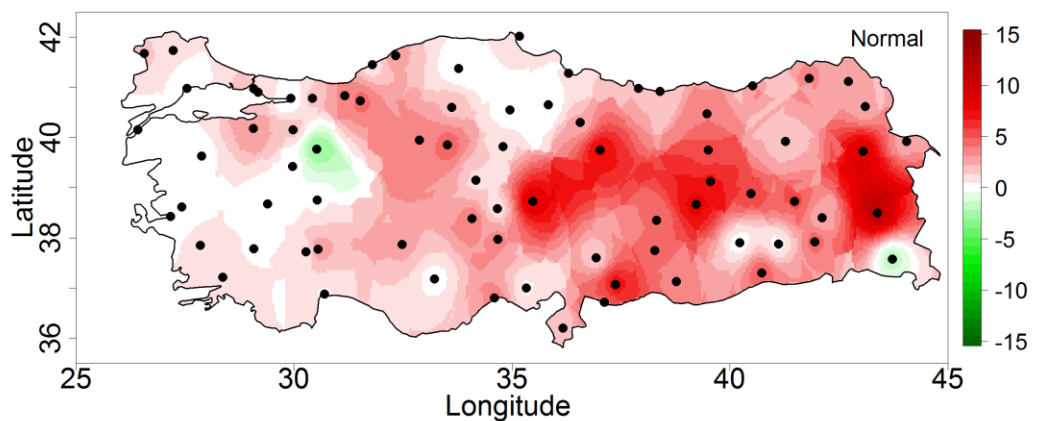
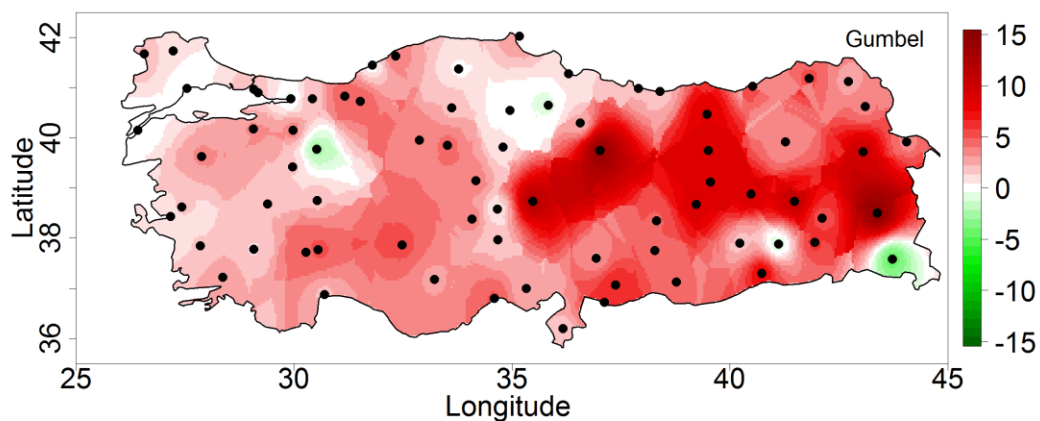
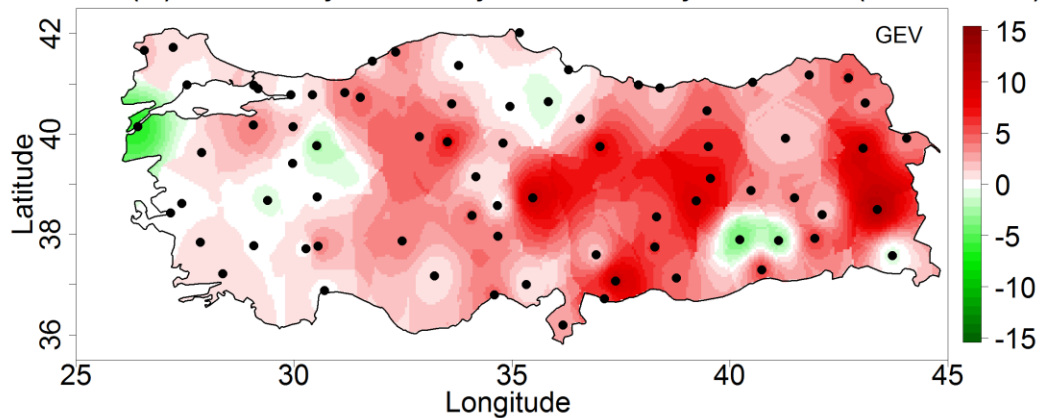


Figure 6.9 Difference (°C) between 100-year stationary and nonstationary return levels for annual temperature minima during winter using GEV, gumbel and normal distributions.

### 3) Observed Spring AMTmax and AMTmin

Maps of difference between 100-year nonstationary and stationary return levels using three distributions for spring AMTmax are given in Figure 6.10. The results given in maps shows the variability of impacts estimated from three distributions. This inter-distribution variability is more obvious in the case of gumbel distribution which has shown higher magnitudes of positive impacts in central Turkey. Similarly, the results obtained from gumbel distribution suggests negative impacts in eastern as well western part of Turkey and magnitudes of these negative impacts were higher than the magnitudes of GEV and Normal distributions. Furthermore, directions of nonstationarity impacts were also opposite in case of gumbel distribution at some locations. However, in the case of GEV and Normal distributions, most of the variability can be seen in magnitude rather than the direction of nonstationarity. Results of GEV and Normal distributions suggest positive impacts in most of the Marmara Region. Results of these distributions also found evidence of negative impacts in the Aegean sea. The Mediterranean region, Central Anatolia and most of the Black Sea region, Eastern and South-eastern Anatolia showed positive impacts using GEV and normal distributions. However, there were also very few stations in these regions which were apparently under the influence of negative impacts in case of annual maximum temperature during the spring season.

Nonstationarity impact maps for spring AMTmin given in Figure 6.11 suggest that there was less inter-distribution variability in case of spring annual minima of temperature. So, unlike the results of spring annual maxima of temperature, directions of nonstationarity impacts obtained from these distributions were consistent with each other. Overall, the results suggest that most of Turkey was under the influence of positive impacts in case of minimum temperature. Again, these positive impacts were apparently higher in the eastern part of Turkey and Central Anatolia. However, there were very few stations in the Aegean region and western part of Central Anatolia which exhibits apparently negative impacts in case of annual minimum temperature during the spring season.

Difference (°C) Between 100-year Stationary and Nonstationary Return Levels (Spring-AMTmax)

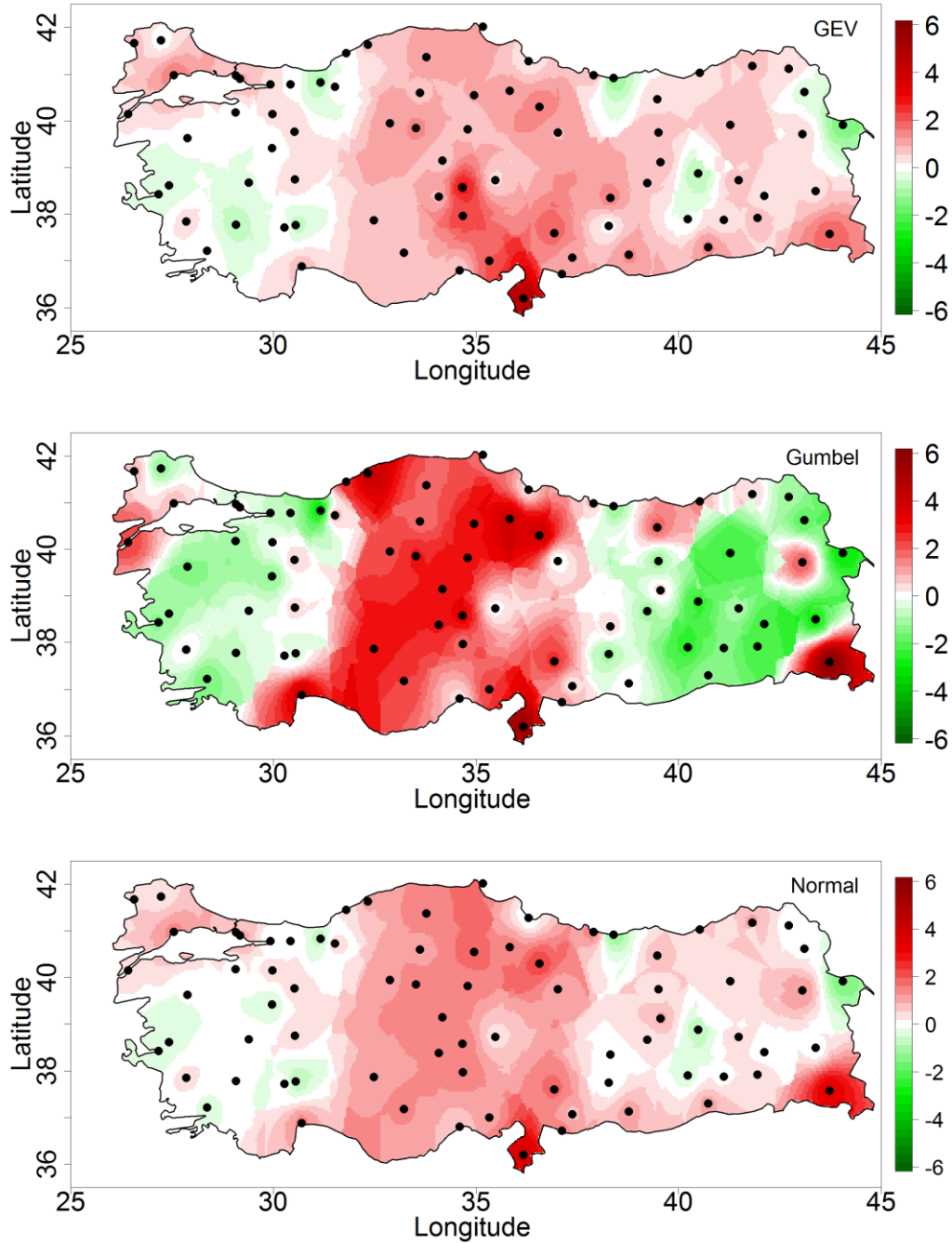


Figure 6.10 Difference (°C) between 100-year stationary and nonstationary return levels for annual temperature maxima during spring using GEV, gumbel and normal distributions.

Difference (°C) Between 100-year Stationary and Nonstationary Return Levels (Spring-AMTmin)

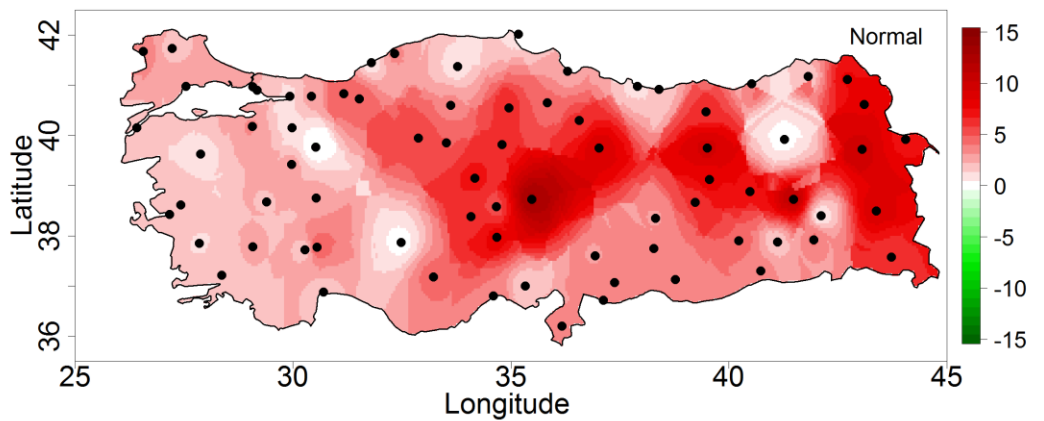
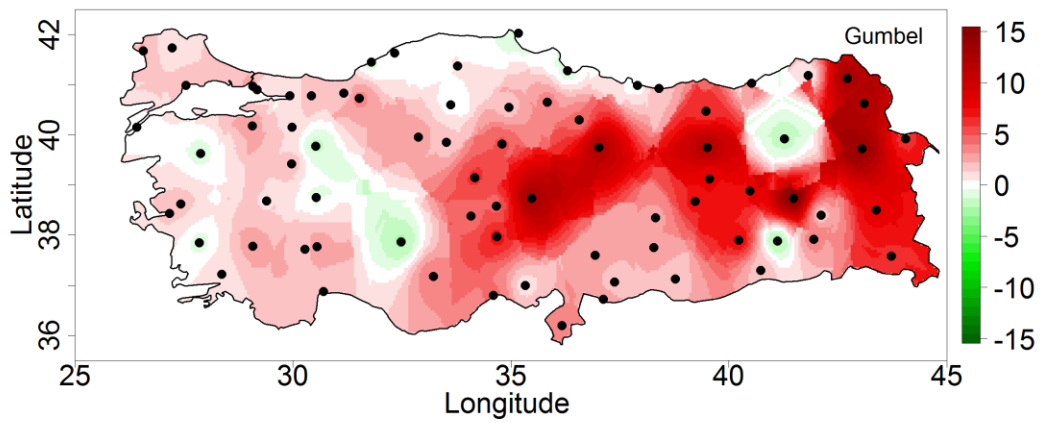
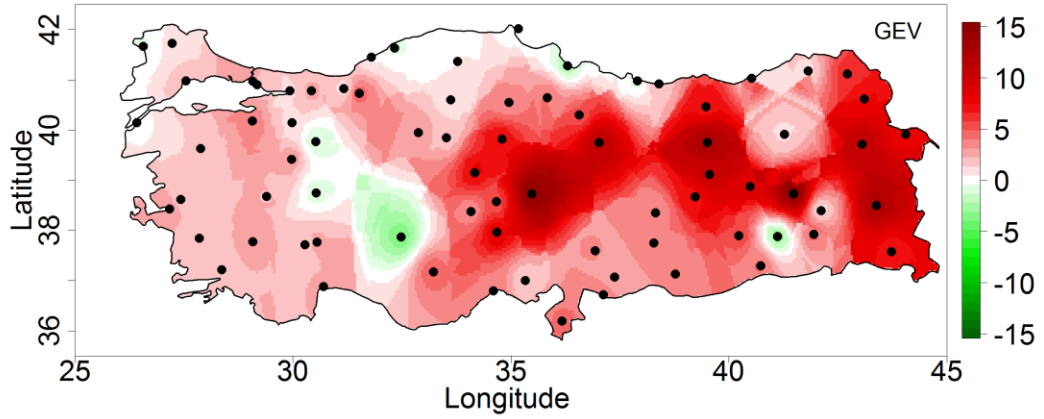


Figure 6.11 Difference (°C) between 100-year stationary and nonstationary return levels for annual temperature minima during spring using GEV, gumbel and normal distributions.

#### 4) Observed Summer AMT<sub>max</sub> and AMT<sub>min</sub>

Maps of difference between 100-year nonstationary and stationary return levels using three distributions for summer AMT<sub>max</sub> are given in Figure 6.12. The results given in maps show the presence of variability of impacts estimated from three distributions. For summer as well, this inter-distribution variability is more obvious in case of gumbel distribution which has shown higher magnitudes of impacts as compared to other distributions. In Aegean regions, impacts of nonstationarities were found negative using Gumbel distributions, while GEV and normal distributions mostly show positive impacts. Nonstationarity impacts as estimated from GEV and normal distributions suggest a general influence of positive impacts in most of Turkey. However, in few areas of the Black Sea and Marmara regions, the impacts were found to be negative. Furthermore, the nonstationarity impact results using Gumbel distribution provided few stations of Mediterranean and South-eastern Anatolia under the influence of negative impacts.

Nonstationarity impact maps for summer AMT<sub>min</sub> given in Figure 6.13 suggest that there was less inter-distribution variability in case of spring annual minima of temperatures as well. So, unlike the results of summer annual maxima of temperature, directions of nonstationarity impacts obtained from these distributions were consistent with each other at most of the stations. The results presented in these maps suggest positive impacts in Marmara regions, most of the Mediterranean, South-Eastern Anatolia regions. Although the eastern part of Central Anatolia exhibited positive impacts, the results found evidence of the influence of negative impacts at stations located in the western part of Central Anatolia. Black sea region contained a mixed type of impacts since at few locations in the eastern part, the impacts were either negative or insignificant, while in the western part of the Black Sea region, stations exhibited positive impacts. Similarly, the results also suggest the presence of a mixed type of impacts in Aegean regions in case of annual minimum temperature during the summer season.

Difference (°C) Between 100-year Stationary and Nonstationary Return Levels (Summer-AMTmax)

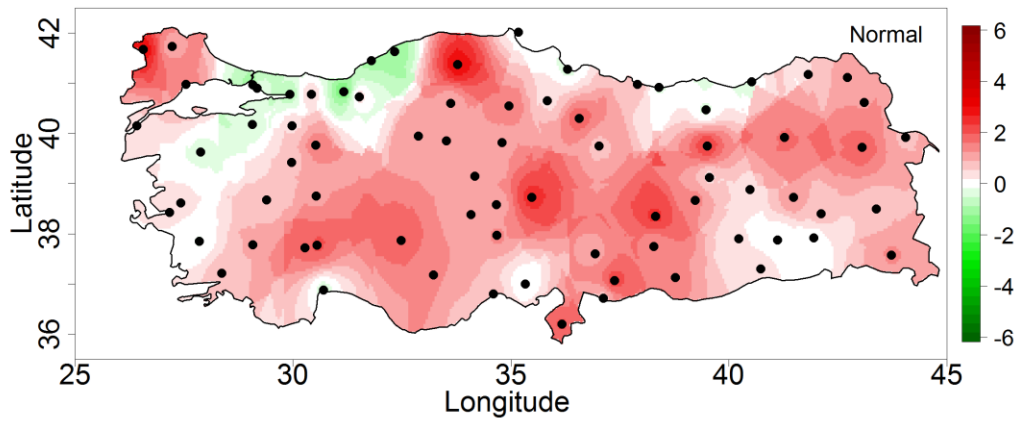
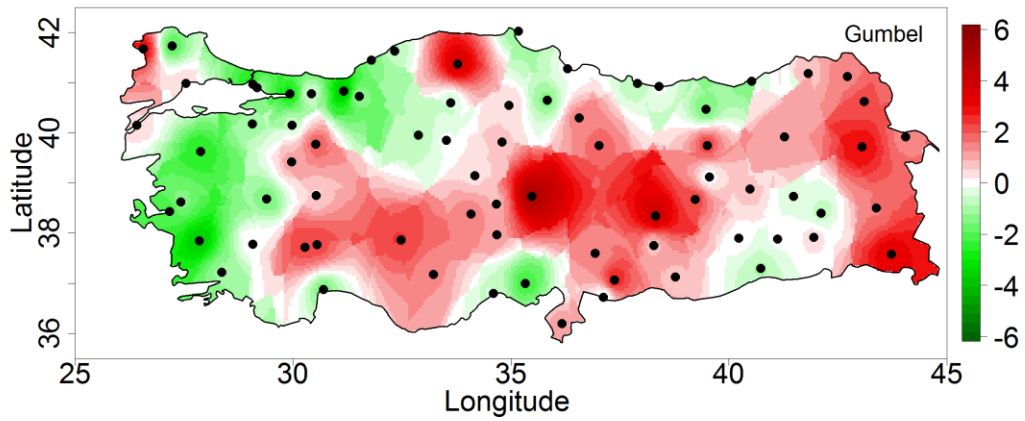
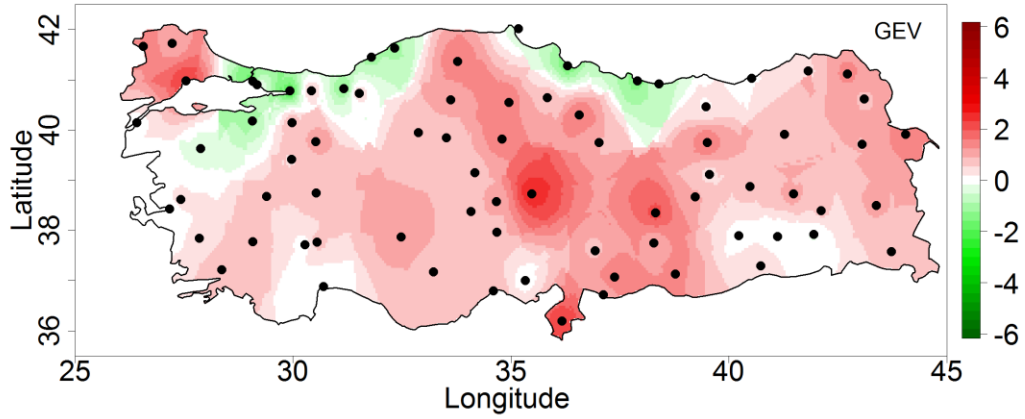


Figure 6.12 Difference (°C) between 100-year stationary and nonstationary return levels for annual temperature maxima during summer using GEV, gumbel and normal distributions.

Difference (°C) Between 100-year Stationary and Nonstationary Return Levels (Summer-AMTmin)

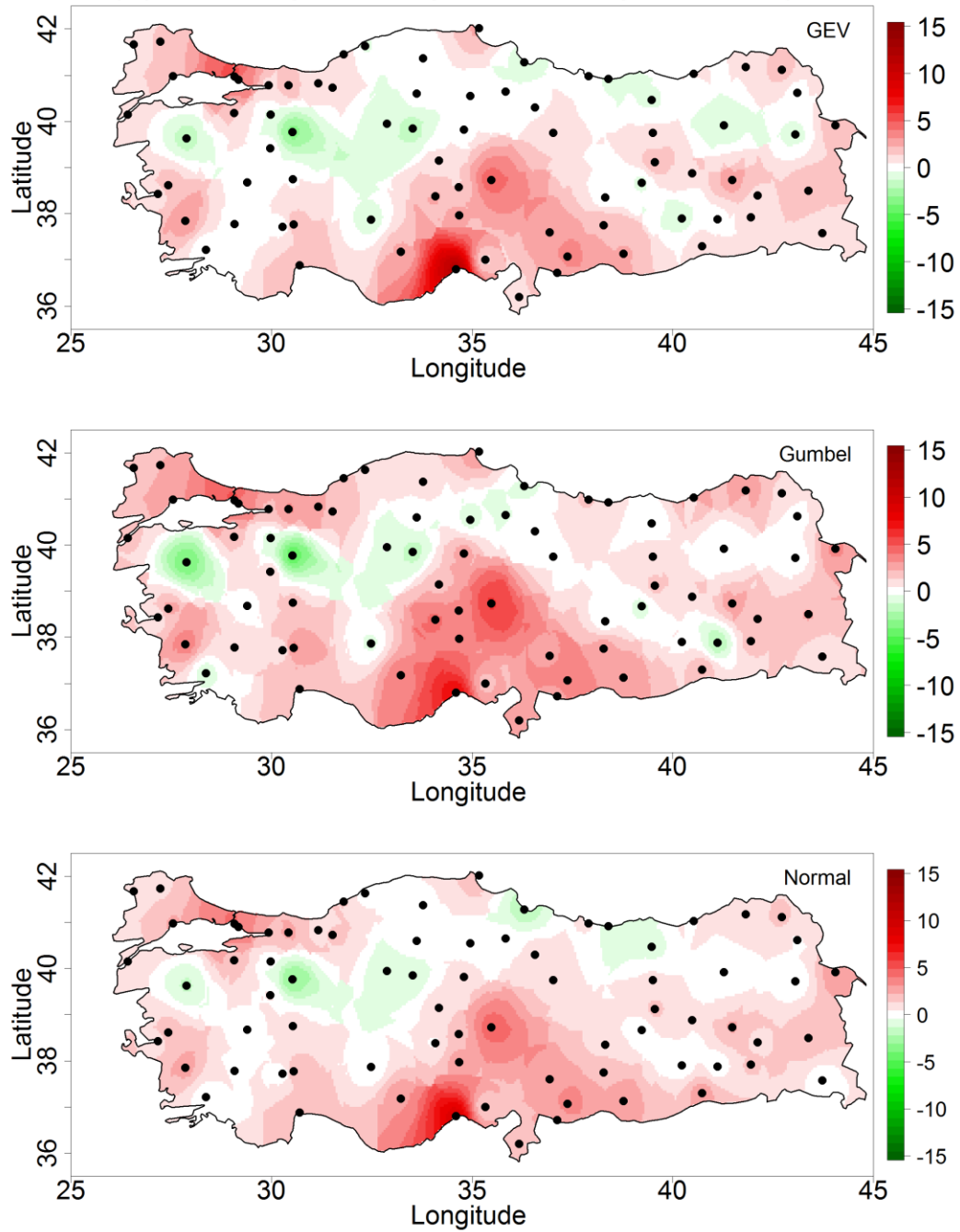


Figure 6.13 Difference (°C) between 100-year stationary and nonstationary return levels for annual temperature minima during summer using GEV, gumbel and normal distributions.

## 5) Observed Autumn AMT<sub>max</sub> and AMT<sub>min</sub>

Maps of difference between 100-year nonstationary and stationary return levels using three distributions for autumn AMT<sub>max</sub> are given in Figure 6.14. The maps of nonstationarity impacts for yearly autumn maxima of temperature suggest that the impacts estimated using GEV and Normal distributions are generally consistent with each other, while impacts estimated using gumbel distribution contained inconsistencies in term of the direction of nonstationarities as well as magnitudes. These inconsistencies were more apparent in the eastern part of Turkey. Results of nonstationarities using GEV and Normal distributions suggest positive impacts in most of Turkey. Results suggest that the Marmara region, Aegean region, Central Anatolia, and most of the Black Sea region and Eastern Anatolia are under the influence of positive impacts. However few stations located in the Black Sea region, Mediterranean, South-eastern, and Eastern Anatolia were found to be under the influence of negative impacts.

Maps of difference between 100-year nonstationary and stationary return levels using three distributions for autumn AMT<sub>min</sub> are given in Figure 6.15. The overall, mixed types of impacts were present in annual minima of temperature in the autumn season. Most of the Marmara, Aegean and Black sea region was found to have negative impacts of nonstationarities. Few stations in Marmara and Aegeans region have shown slightly positive impacts as well. However, most of the Central Anatolia, Mediterranean region, and Eastern Anatolia had positive impacts of nonstationarities. Similarly, most of the South-Eastern Anatolia exhibited negative impacts of nonstationarities for annual minima of temperature during the autumn season.

Difference (°C) Between 100-year Stationary and Nonstationary Return Levels (Autumn-AMTmax)

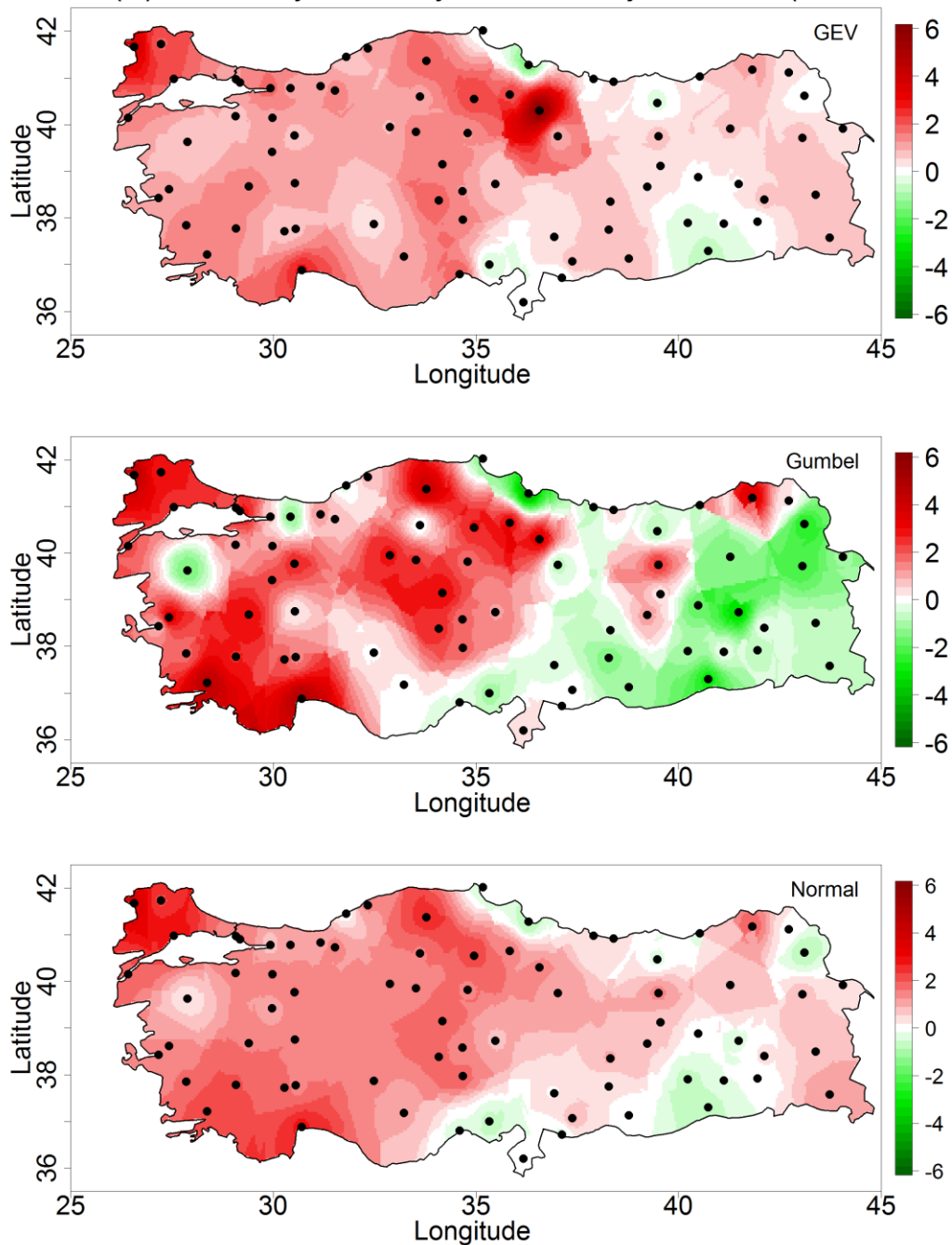


Figure 6.14 Difference (°C) between 100-year stationary and nonstationary return levels for annual temperature maxima during autumn using GEV, gumbel and normal distributions.

Difference (°C) Between 100-year Stationary and Nonstationary Return Levels (Autumn-AMTmin)

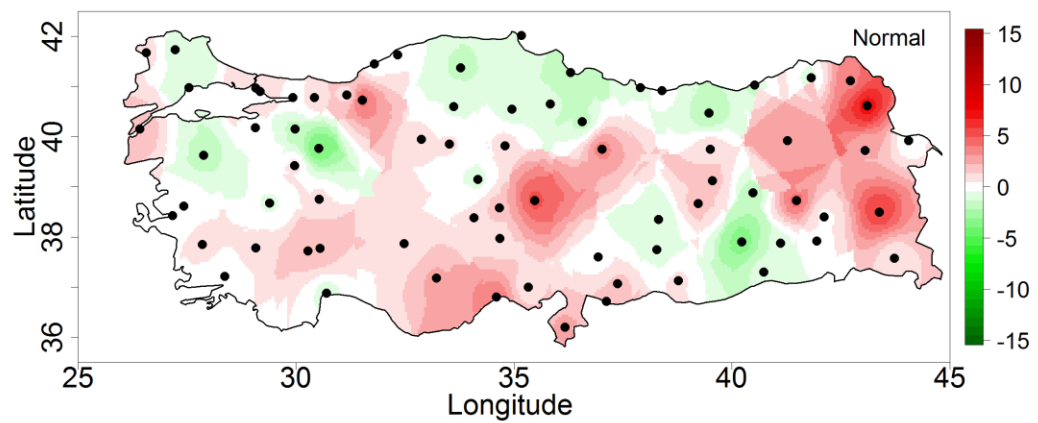
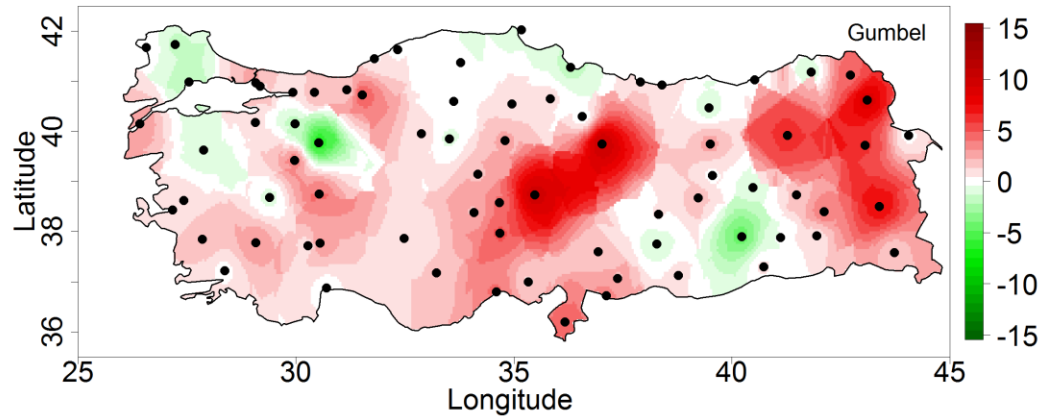
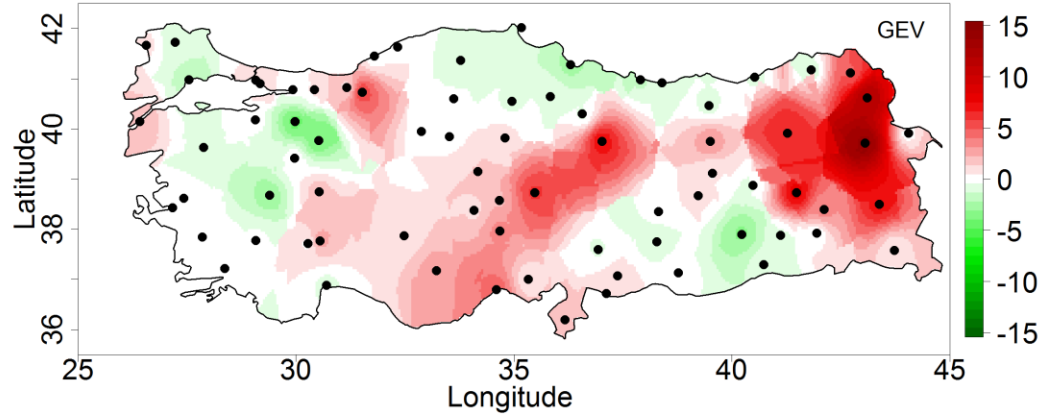


Figure 6.15 Difference (°C) between 100-year stationary and nonstationary return levels for annual temperature minima during autumn using GEV, gumbel and normal distributions.

### **6.1.3. Nonstationarity Impacts During Projection Time Period (2050-2100)**

#### **1) Projected Yearly AMTmax and AMTmin**

Nonstationarities impact results for winter AMTmax and AMTmin are presented here as maps of ensemble mean and ensemble median in Figure 6.16. Boxplots of nonstationary impacts at individual gridded stations in Figure 6.17 and Figure 6.18 are shown for winter AMTmax and AMTmin, respectively. The ensemble mean and ensemble median maps show that impacts of nonstationary are positive throughout Turkey for yearly AMTmax and AMTmin. Maps of ensemble (especially ensemble mean) results, as well as boxplots, show the Northern part of Turkey (Black Sea region and adjacent areas of Central Anatolia) has shown slightly larger magnitudes of impacts on yearly AMTmax as compared to other regions like Marmara, Mediterranean, and Eastern Anatolia. These positive impacts are also evident from boxplots as ensemble mean and median fall above the zero-reference line. Ensemble results for yearly AMTmin (presented in Figure 6.16 and Figure 6.18) suggest higher magnitudes of positive impacts in Eastern and Central Anatolia as well as central part of Black Sea region as compared to other regions of Turkey. The results also show that the impacts of nonstationarities were higher in magnitude for AMTmin than AMTmax.

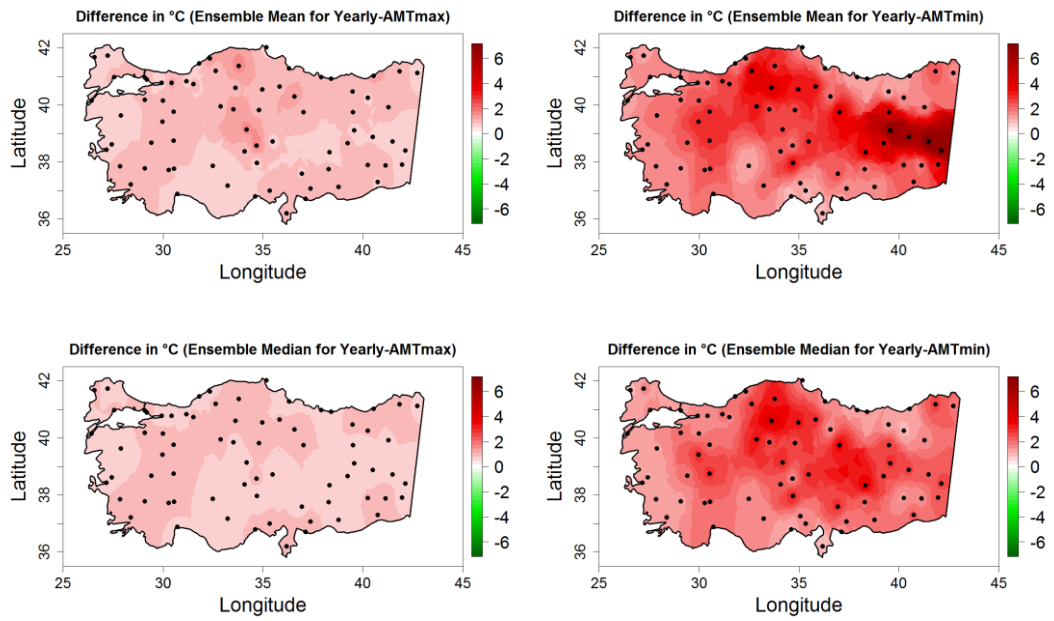


Figure 6.16 Ensemble mean (top) and ensemble median (bottom) of the difference (°C) between 100-year stationary and nonstationary return levels for yearly AMTmax (left) and AMTmin (right).

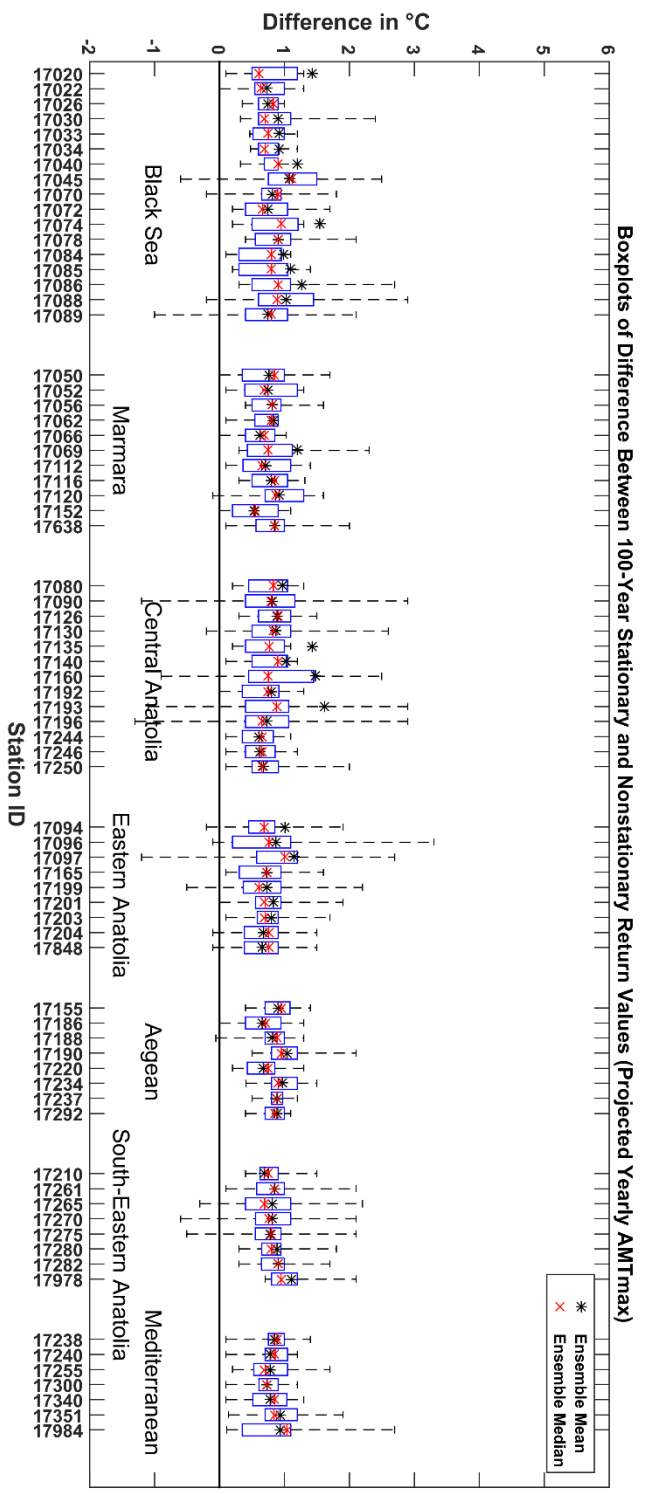


Figure 6.17 Boxplots containing nonstationary impact values of 12 individual CORDEX ensemble members at gridded stations for Yearly AMTmax. Ensemble mean pointer (black asterisk) and ensemble median pointer (red asterisk) are also given.

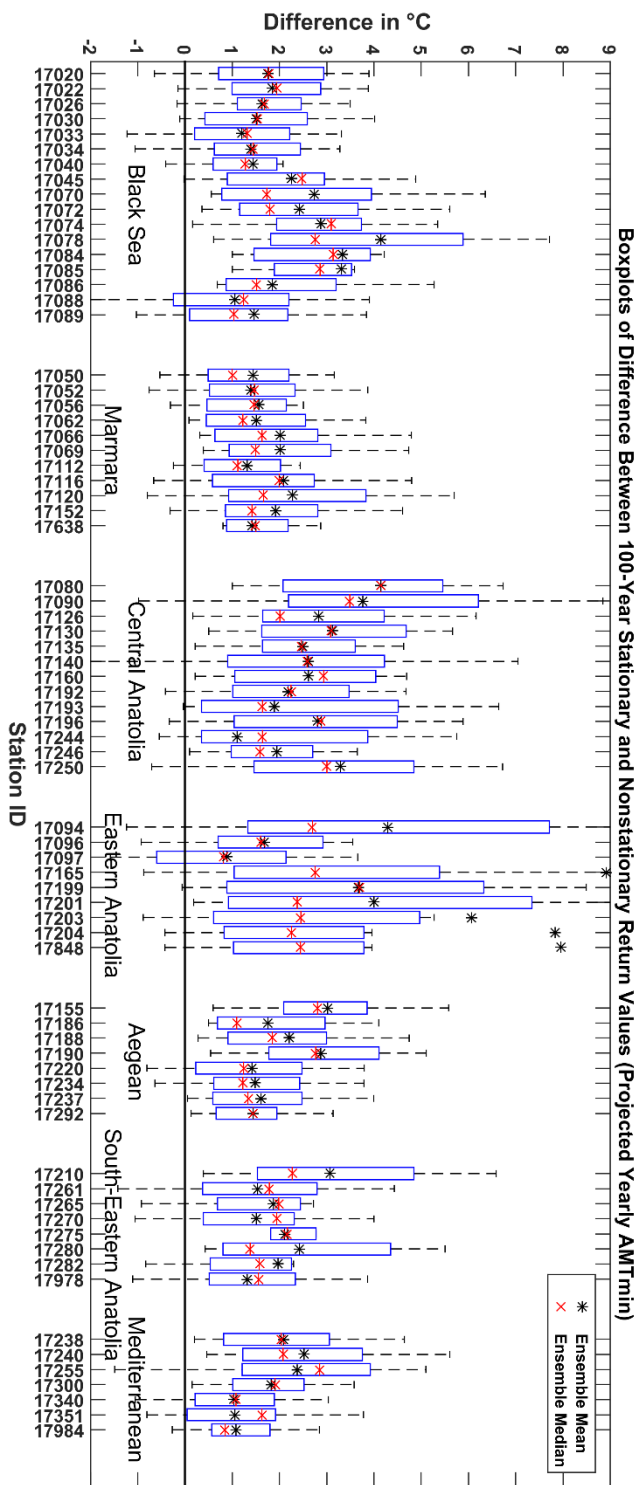


Figure 6.18 Boxplots containing nonstationary impact values of 12 individual CORDEX ensemble members at gridded stations for Yearly AMTmin. Ensemble mean pointer (black asterisk) and ensemble median pointer (red asterisk) are also given

## 2) Projected Winter AMTmax and AMTmin

Nonstationarities impact results for winter AMTmax and AMTmin are presented here as aps of ensemble mean and ensemble median in Figure 6.19. Boxplots of nonstationary impacts at individual gridded stations in Figure 6.20 and Figure 6.21 are shown for winter AMTmax and AMTmin, respectively. The ensemble mean and ensemble median maps show that impacts of nonstationary are positive throughout Turkey for winter AMTmax and AMTmin. Maps of ensemble (especially ensemble mean) results, as well as boxplots, show uniform impacts throughout Turkey except for few gridded stations in east having slight higher magnitudes of impacts on Yearly AMTmax as compared to other regions. The boxplots given in Figure 6.20 also suggest positive impacts throughout Turkey as most of the time ensemble mean and ensemble median fall above the zero-reference line. Ensemble results (presented in Figure 6.19 and Figure 6.21) for winter AMTmin suggest higher magnitudes of positive impacts in Eastern and Central Anatolia as well as central part of Black Sea region as compared to other regions of Turkey. The results also show that the impacts of nonstationarities were higher in magnitude for winter AMTmin as compared to winter AMTmax.

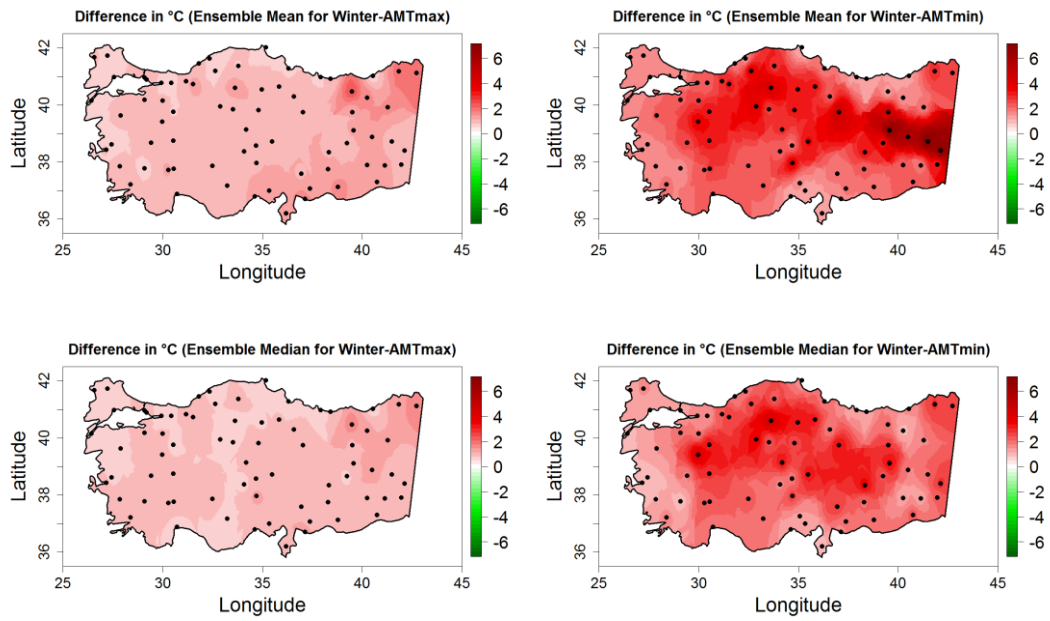


Figure 6.19 Ensemble mean (top) and ensemble median (bottom) of the difference (°C) between 100-year stationary and nonstationary return levels for AMTmax (left) and AMTmin (right) during winter.

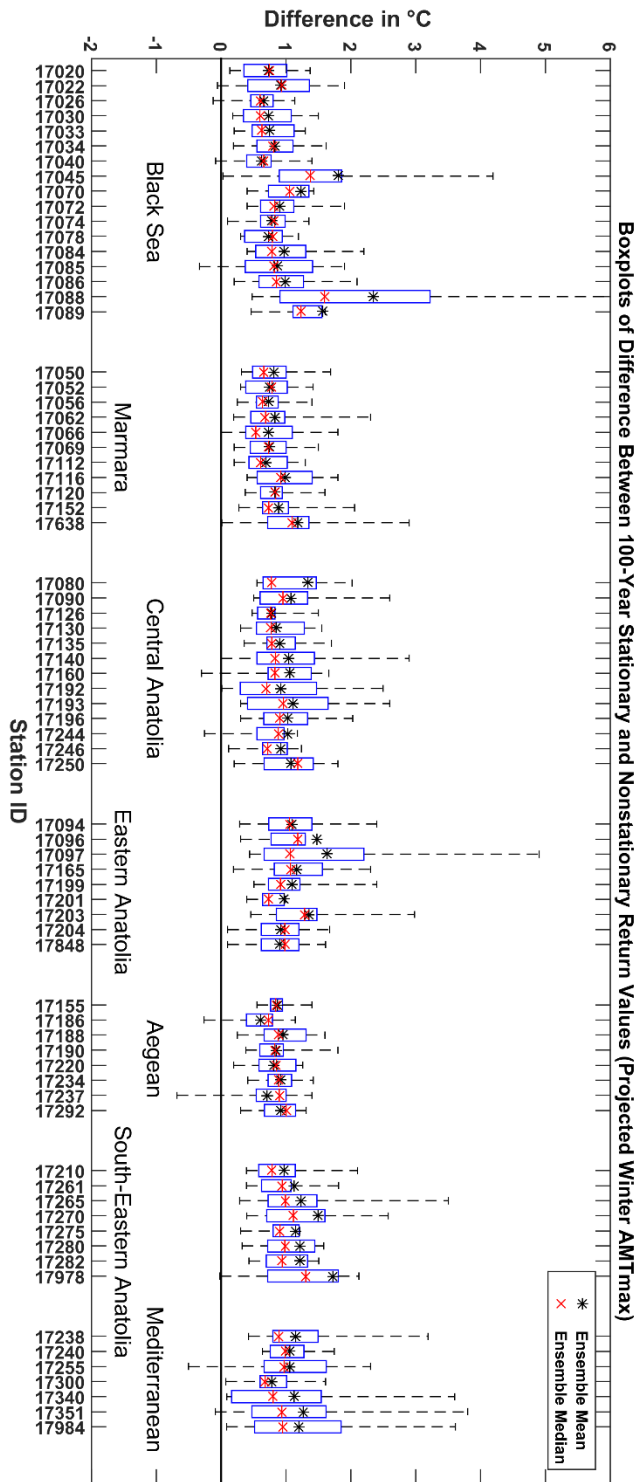


Figure 6.20 Boxplots containing nonstationary impact values of 12 individual CORDEX ensemble members at gridded stations for winter AMTmax. Ensemble mean pointer (black asterisk) and ensemble median pointer (red asterisk) are also given.

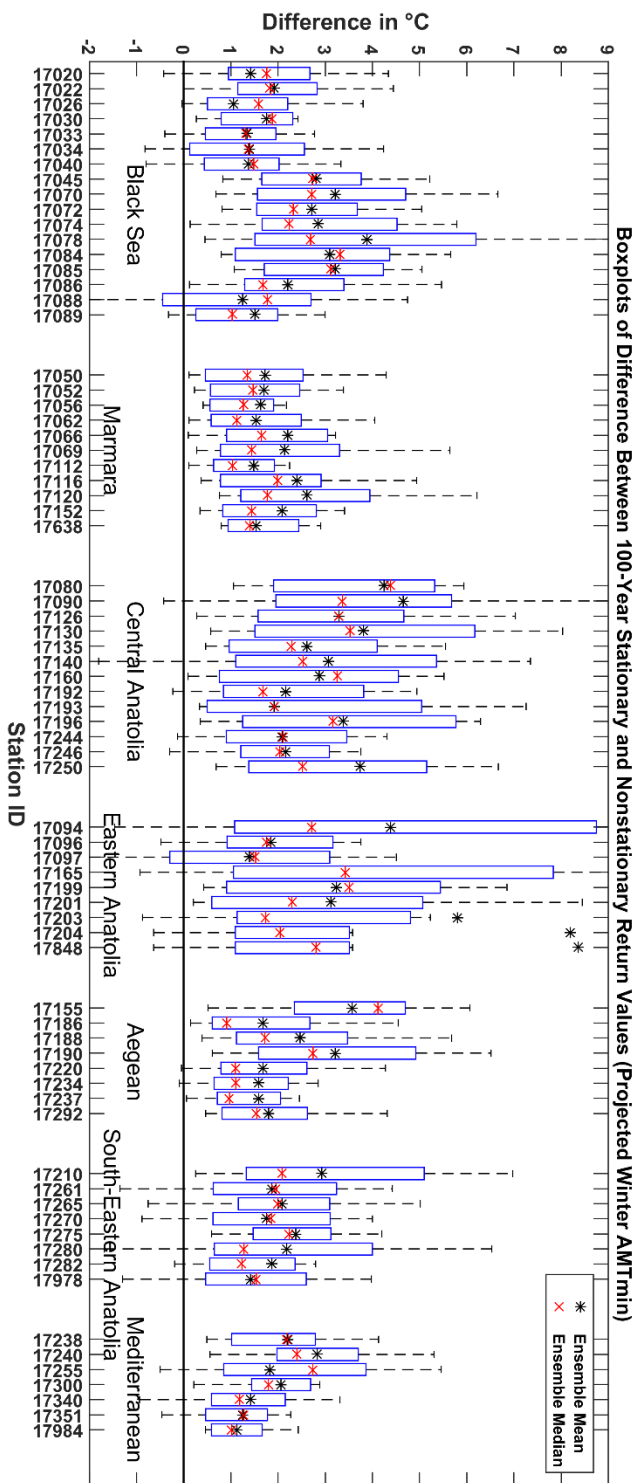


Figure 6.21 Boxplots containing nonstationary impact values of 12 individual CORDEX ensemble members at gridded stations for winter AMTmin. Ensemble mean values (black asterisk) and ensemble median pointer (red asterisk) are also given.

### 3) Projected Spring AMTmax and AMTmin

Nonstationarities impact results for spring AMTmax and AMTmin are presented here as maps of ensemble mean and ensemble median in Figure 6.22. Boxplots of nonstationary impacts at individual gridded stations in Figure 6.23 and Figure 6.24 are shown for spring AMTmax and AMTmin, respectively. The ensemble mean and ensemble median maps show that impacts of nonstationary are positive throughout Turkey for spring AMTmax and AMTmin. Map of ensemble mean suggests slightly lower magnitudes of positive impacts in the central part of Turkey. Similarly, the map of the ensemble median suggested slightly lower magnitudes of positive impacts at some gridded stations of Central Anatolia and Black Sea region as compared to other regions. The boxplots given in Figure 6.23 also suggest positive impacts throughout Turkey as most of the time ensemble mean and ensemble median fall above the zero-reference line. Ensemble results (presented in Figure 6.22 and Figure 6.24) for spring AMTmin suggest higher magnitudes of positive impacts in Eastern and Central Anatolia as well as central part of Black Sea region as compared to other regions of Turkey. The results also show that the impacts of nonstationarities were higher in magnitude for spring AMTmin than spring AMTmax.

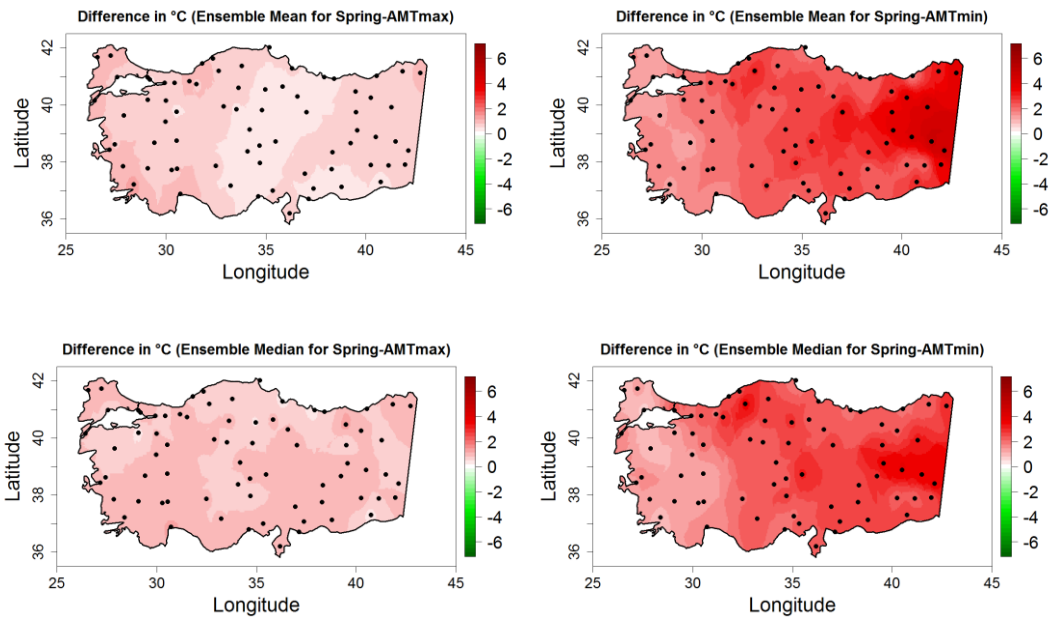


Figure 6.22 Ensemble mean (top) and ensemble median (bottom) of the difference (°C) between 100-year stationary and nonstationary return levels for AMTmax (left) and AMTmin (right) during spring.

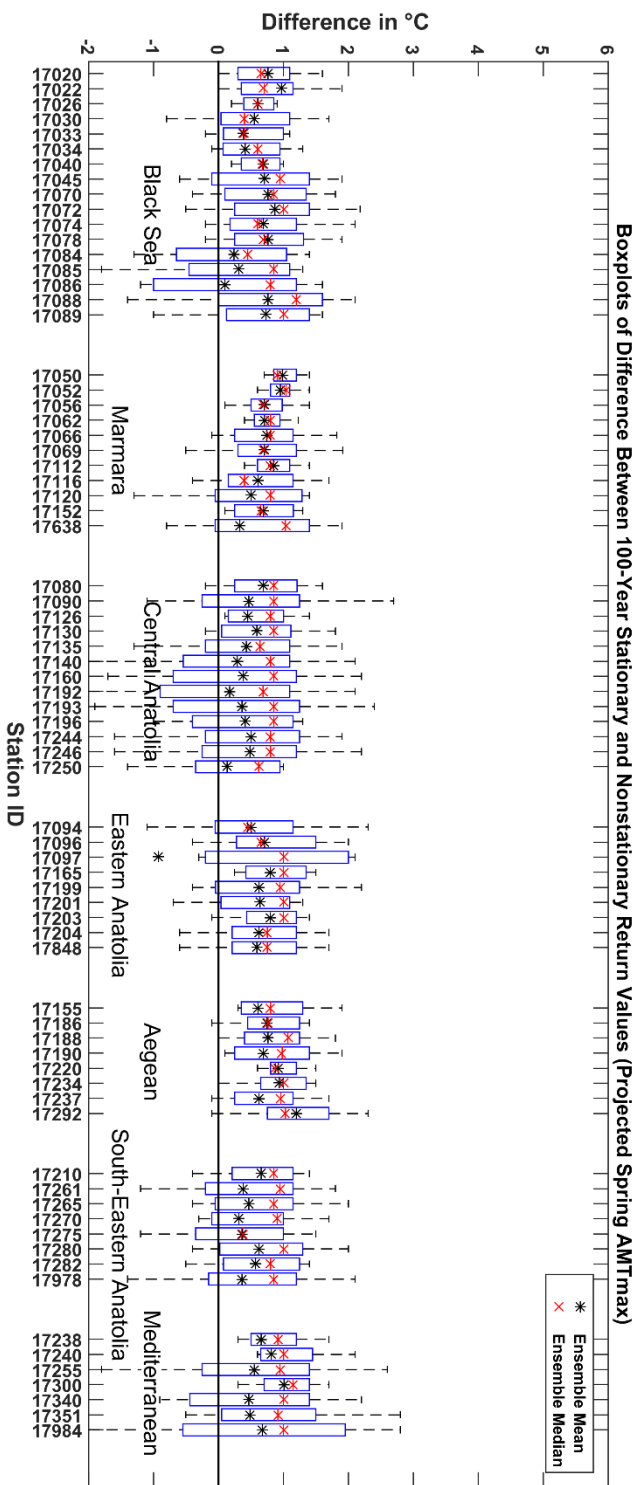


Figure 6.23 Boxplots containing nonstationary impact values of 12 individual CORDEX ensemble members at gridded stations for spring AMTmax. Ensemble mean pointer (black asterisk) and ensemble median pointer (red asterisk) are also given.

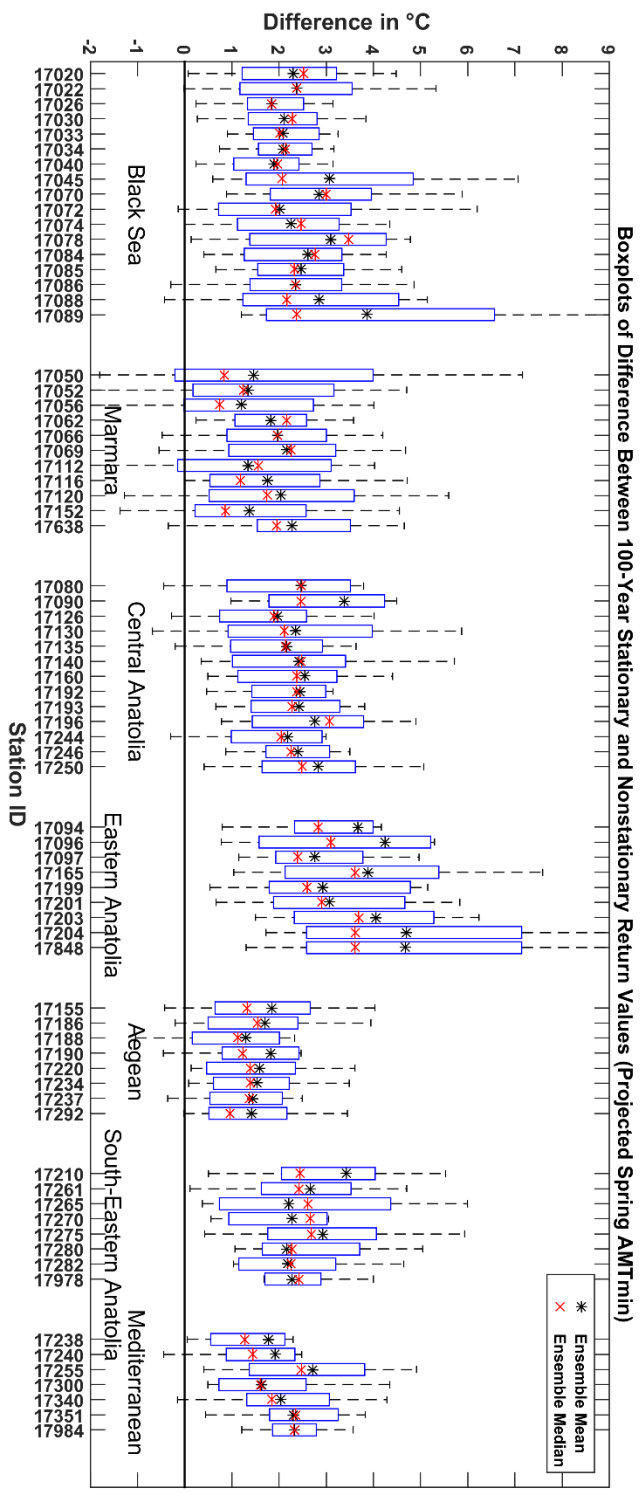


Figure 6.24 Boxplots containing nonstationary impact values of 12 individual CORDEX ensemble members at gridded stations for spring AMTmin. Ensemble mean pointer (black asterisk) and ensemble median pointer (red asterisk) are also given.

#### **4) Projected Summer AMT<sub>max</sub> and AMT<sub>min</sub>**

Nonstationarities impact results for summer AMT<sub>max</sub> and AMT<sub>min</sub> are presented here as maps of ensemble mean and ensemble median in Figure 6.25. Boxplots of nonstationary impacts at individual gridded stations in Figure 6.26 and Figure 6.27 are shown for summer AMT<sub>max</sub> and AMT<sub>min</sub>, respectively. The ensemble mean and ensemble median maps show that the impacts of nonstationary are consistently positive throughout Turkey for summer AMT<sub>max</sub> and AMT<sub>min</sub>. Map of ensemble mean suggests slightly higher magnitudes of positive impacts in the central part of Turkey. Similarly, the map of the ensemble median suggested slightly lower magnitudes of positive impacts at some gridded stations of Black Sea region and adjacent areas of Central Anatolia and as compared to other regions. The boxplots given in Figure 6.26 also suggest positive impacts throughout Turkey as most of the time ensemble mean and ensemble median fall above the zero-reference line for summer AMT<sub>max</sub>. Ensemble results for summer AMT<sub>min</sub> (presented in Figure 6.25 and Figure 6.27) suggest significantly positive impacts throughout Turkey. The results also show that the impacts of nonstationarities were higher in magnitude for summer AMT<sub>min</sub> than summer AMT<sub>max</sub>.

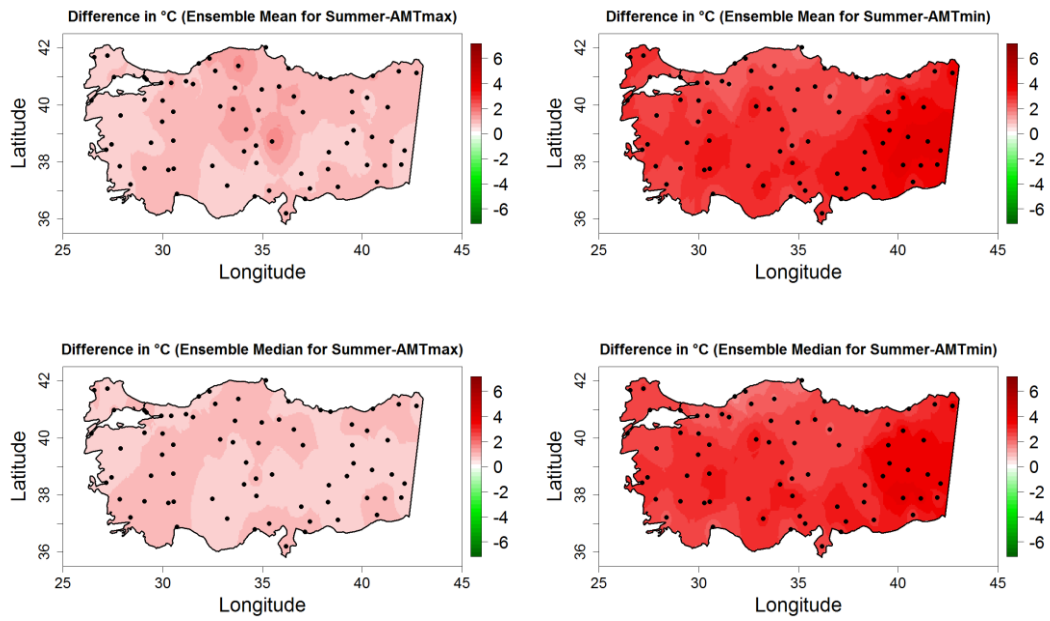


Figure 6.25 Ensemble mean (top) and ensemble median (bottom) of the difference (°C) between 100-year stationary and nonstationary return levels for AMTmax (left) and AMTmin (right) during summer.

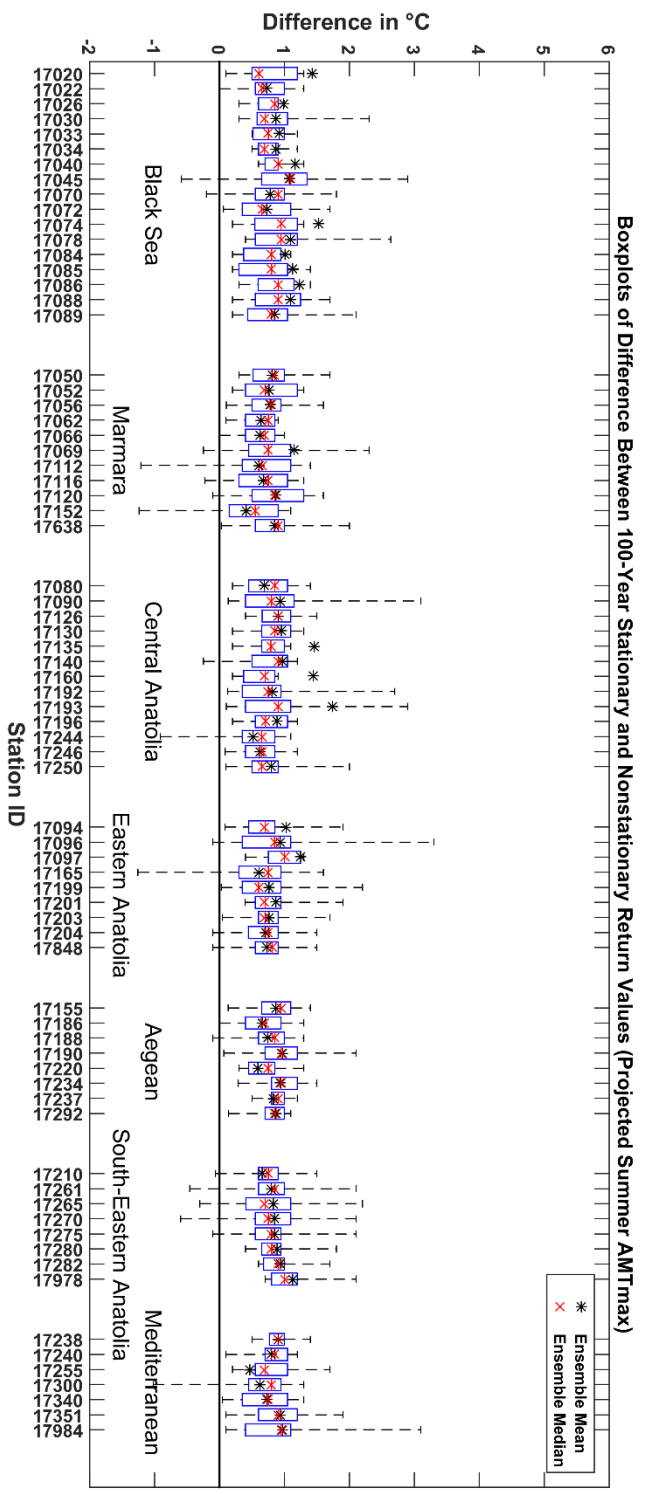


Figure 6.26 Boxplots containing nonstationary impact values of 12 individual CORDEX ensemble members at gridded stations for summer AMTmax. Ensemble mean pointer (black asterisk) and ensemble median pointer (red asterisk) are also given.

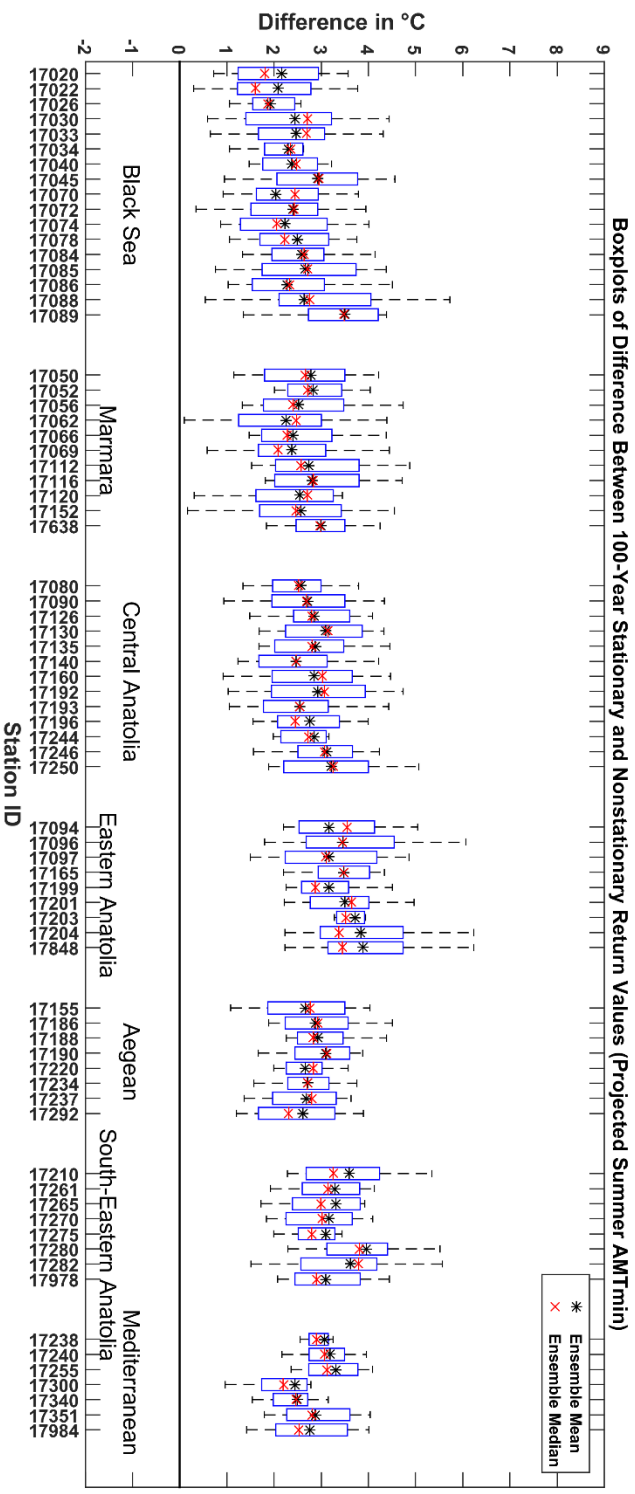


Figure 6.27 Boxplots containing nonstationary impact values of 12 individual CORDEX ensemble members at gridded stations for summer AMTmin. Ensemble mean pointer (black asterisk) and ensemble median pointer (red asterisk) are also given.

## 5) Projected Autumn AMTmax and AMTmin

Nonstationarities impact results for Autumn AMTmax and AMTmin are presented here as maps of ensemble mean and ensemble median in Figure 6.28. Boxplots of nonstationary impacts at individual gridded stations in Figure 6.29 and Figure 6.30 are shown for Autumn AMTmax and AMTmin, respectively. The ensemble mean and ensemble median maps show that the impacts of nonstationary are consistently positive throughout Turkey for autumn AMTmax and AMTmin. Map of ensemble mean suggests slightly higher magnitudes of positive impacts in the central part of Turkey. The boxplots given in Figure 6.29 also suggest positive impacts throughout Turkey as most of the time ensemble mean and ensemble median fall above the zero-reference line. Ensemble results for autumn AMTmin (presented in Figure 6.28 and Figure 6.30) suggest significantly positive impacts throughout Turkey. The magnitudes of positive impacts were slightly higher in the eastern part of Turkey. The results also show that the impacts of nonstationarities were higher in magnitude for autumn AMTmin than winter AMTmax.

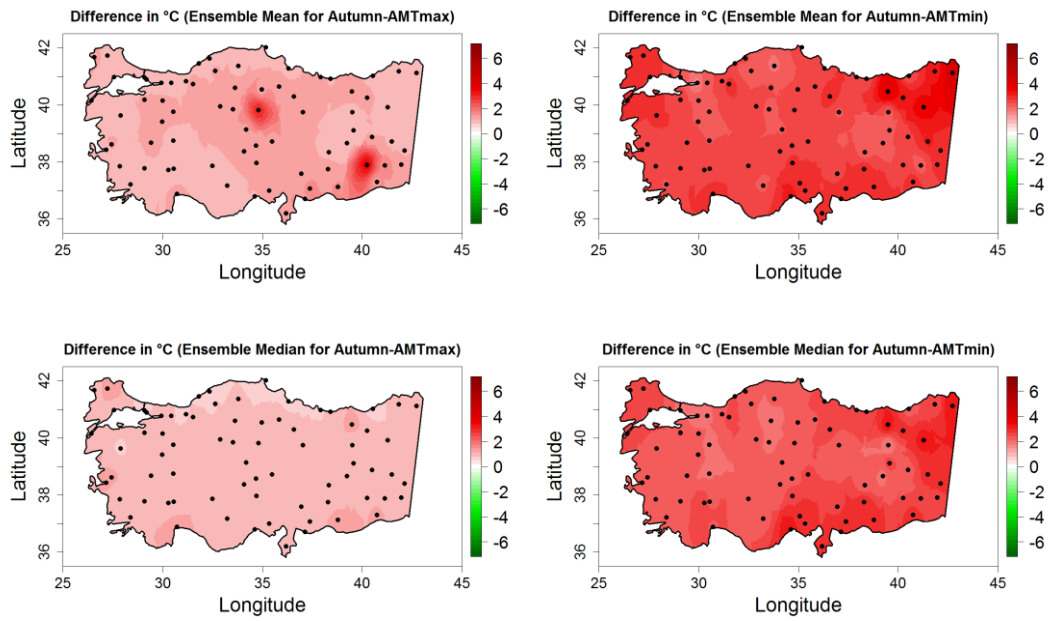


Figure 6.28 Ensemble mean (top) and ensemble median (bottom) of the difference (°C) between 100-year stationary and nonstationary return levels for AMTmax (left) and AMTmin (right) during autumn.

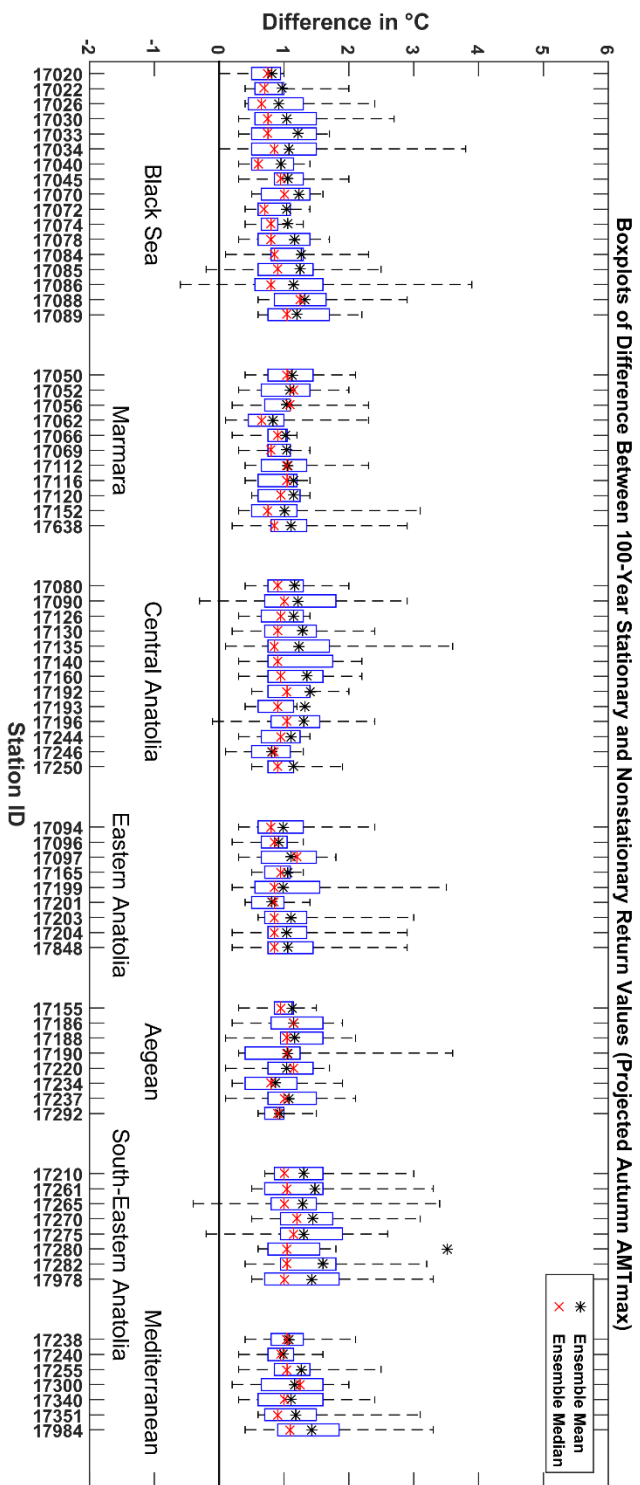


Figure 6.29 Boxplots containing nonstationary impact values of 12 individual CORDEX ensemble members at gridded stations for autumn AMTmax. Ensemble mean pointer (black asterisk) and ensemble median pointer (red asterisk) are also given.

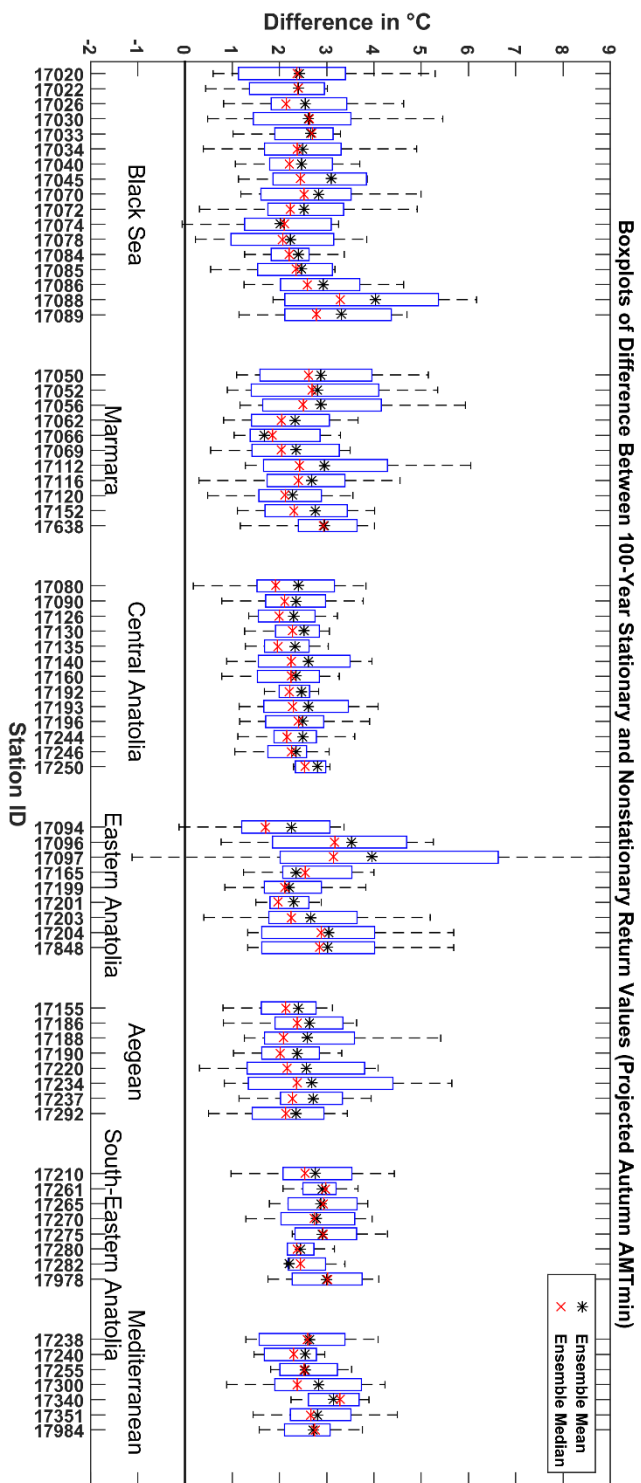


Figure 6.30 Boxplots containing nonstationary impact values of 12 individual CORDEX ensemble members at gridded stations for autumn AMTmin. Ensemble mean pointer (black asterisk) and ensemble median pointer (red asterisk) are also given.

### **Intra-model Variability of Nonstationary Impacts**

Nonstationarity impact values at each gridded station estimated from individual ensemble members are plotted as box plots for each region separately to present the variability of nonstationarity impacts amongst ensemble members for yearly AMTmax and AMTmin in Figure 6.31 and Figure 6.32, respectively.

The boxplots for yearly AMTmax given in Figure 6.31 show that generally, all ensemble members show similar impacts within the region. But still, intra-model variability can be observed. Less intra-model variability was observed in the Mediterranean region, Aegean region, and Marmara region as most of the models predicted more or less similar impacts of nonstationarities. Relatively more intra-model variability was available in South-Eastern Anatolia, Eastern Anatolia, Central Anatolia, and Marmara region for annual maxima of temperature. It is also notable that RCMs 41 and 42 consistently predicted higher values of positive impacts in many regions. Similarly, RCM 13 has shown its tendency to predict the lower value of positive, and even in some cases (Central Anatolia and Eastern Anatolia), the values were negative.

For yearly AMTmin (see Figure 6.32), the intra-model variability was higher as compared to yearly AMTmax. The predicted range of nonstationarity impact values for most of the RCMs was (0.5-4.5) °C in case of yearly AMTmin. Less intra-model variability was observed in the Aegean region and Marmara region as most of the models predicted more or less similar impacts of nonstationarities. Relatively higher intra-model variability was available in Eastern Anatolia, Central Anatolia, and South-Eastern Anatolia in case of annual minima of temperature. Most of the ensemble members predicted positive impacts in most of the regions, however, few members (for example RCM 32 in Eastern Anatolia, RCM 31 in South-Eastern Anatolia) have also shown tendencies to predict negative impacts in few regions as well.

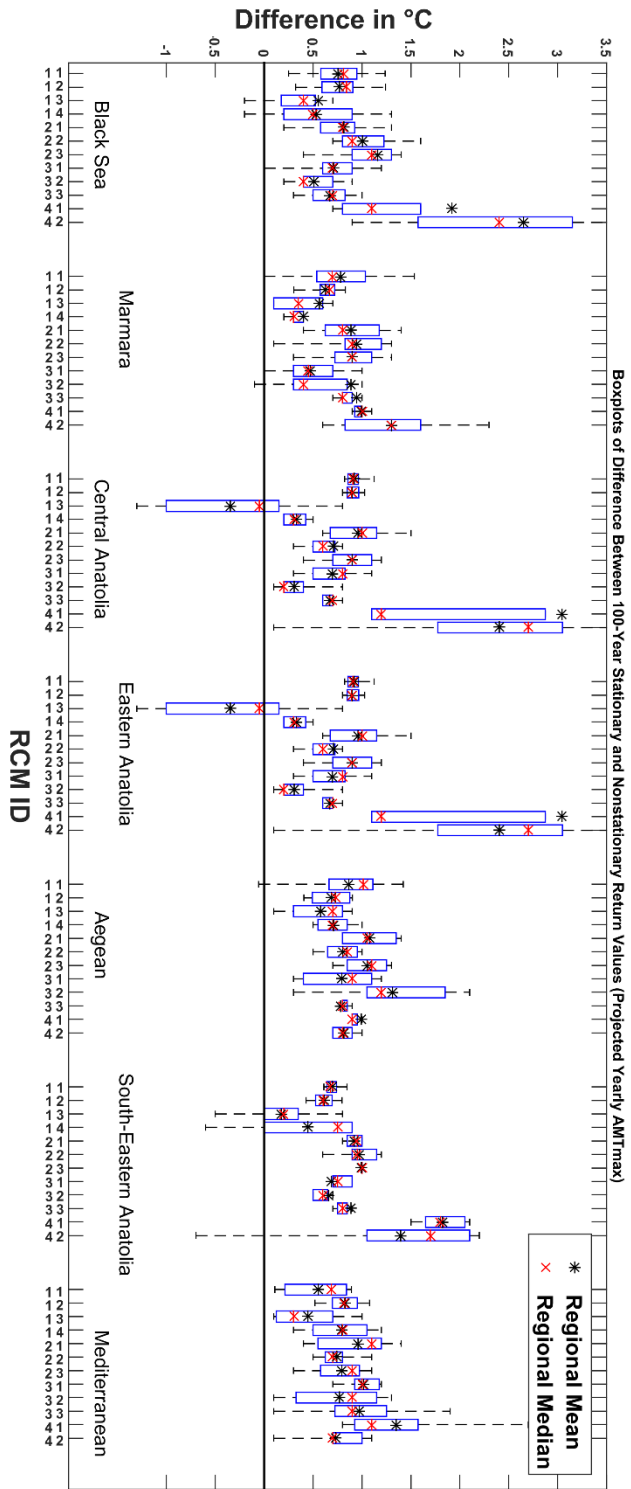


Figure 6.31 Boxplots describing the intra-model variability of nonstationarity impact prediction for yearly AMTmax

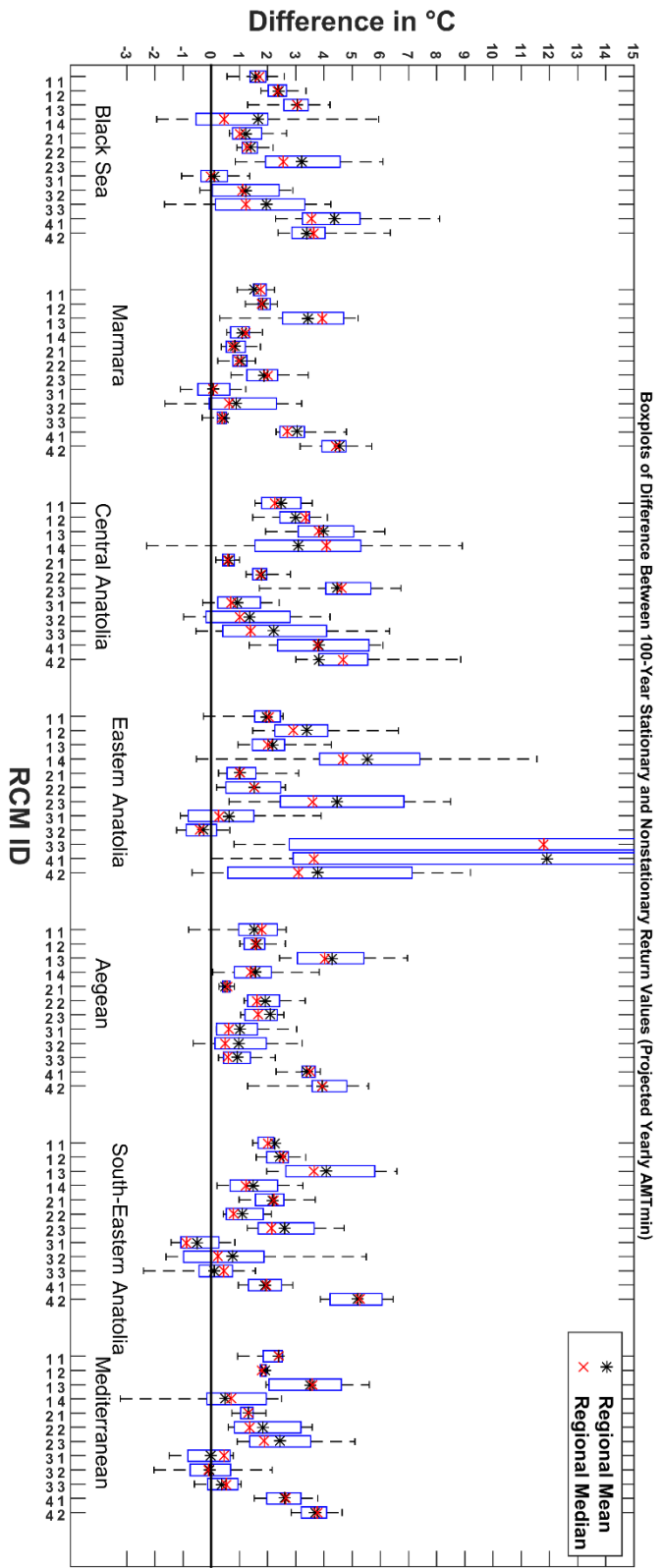


Figure 6.32 Boxplots describing the intra-model variability of nonstationarity impact prediction for yearly AMTmin

## 6.2. Discussion

The parameters of each distribution are estimated by minimizing the value negative log-likelihood function. Smaller the value of the negative log-likelihood function, better the fit. Comparison of negative log-likelihood values shows that GEV can fit temperature extremes better than gumbel and normal distribution. In case of gumbel and normal distribution (each contains two parameters in stationary case), for most of the maximum temperature indices (AMTmax), normal distribution has shown clearly better performance than gumbel as the negative log-likelihood values were smaller. This difference of negative log-likelihood values was small for AMTmin and in some cases (spring and autumn AMTmin) gumbel distribution performed better than the Normal distribution. The results suggest that closer the performance of distribution (in term of negative log-likelihood values), more similar nonstationarity impacts that distribution tends to exhibit.

Nonstationary impacts of the historical period show considerable increases in both extremes of temperature during winter throughout Turkey. However, the eastern part of Turkey shows the highest increases in minimum as well as maximum temperature. Eastern part of Turkey shows the lowest temperature as compared to other regions of Turkey. Because of high elevation and low temperatures, the ratio of precipitation falling as snow is much larger as compared to other parts of Turkey (Yucel et al., 2014; Önoel and Semazzi, 2009; Önoel et al., 2014). These increases in temperature extremes, especially the minimum temperature, hint towards alteration in precipitation type and pattern as some portion of snow might become rain in future. This, in turn, results in a smaller contribution to snowmelt runoff. The increase in temperature over mountainous regions also contributes towards early and accelerated snow-melting process (Yucel et al., 2014; Önoel and Semazzi, 2009; Önoel et al., 2014). Thus, increases in return levels of minimum temperatures might also cause the early snow melting which might alter the peak flow towards the earlier times. Yucel et al. (2014) also stated that the number of dry and wet days below

freezing is reduced due to concurrent warming with the amplification of temperature during the historical period. Together with this the warming in minimum temperatures causes a decrease in snow cover duration. Increases in minimum and maximum temperature also suggest that winter becomes less severe in most of Turkey. However, the negative impacts in few areas of Marmara and Aegean region, suggest relatively bitter and cold winter.

Results suggest increases in maximum temperatures during the summer season in most of Turkey (except few locations in the Black Sea region and Marmara region where summer extremes of maximum temperature are reduced). These increases in 100-year return values indicate that there is more probability of experiencing severe hot summer as time passes. The heatwaves become more frequent and intense with time. These increased intensities and frequencies of heat waves in most of Turkey might have diverse implications. Most of Turkey receives a limited amount of precipitation during the summer season. With limited precipitation and increased evaporation owing to these positive nonstationary impacts might further dwindle the water availability during the summer season. Rising of water temperature during heatwaves contributes to the degradation of water quality as well as the death of many water species (WEB5). Variations in temperature extremes affect plant reproduction as pollination is one of the most sensitive phenological stages to temperature extremes. (Hatfield and Prueger, 2015). There might be significant implications on agriculture, living species and public health sector as well. Increased temperature extremes combined with changing precipitation patterns and shifts in vegetation covers are responsible for modifying the effective range and distribution of many native and agricultural species. Risks of mortality owing to heatwaves (particularly in urban-dwelling elderly and children without access to an air-conditioned environment) might further increase over the years.

In addition to these, changing in magnitudes and frequencies of extremes events have implications on tourism as well. Since the climate has been identified as a key factor for destination selection it can act as the main tourism source and a facilitator to make tourism activities possible (Hu & Ritchie, 1992; Kozak et al., 2008; Gómez Martin, 2005). Tourism activities during summer in Black sea coast and Marmara region (e.g., Istanbul) might increase in near future owing to less severe summer since results have shown decreases in the magnitude of maximum temperatures in summer. A better efficient tourism policy by the government is critical with under changing climate conditions to enhance the tourism activities in the country.

To understand the long-term impacts of nonstationarities and implications, nonstationary analyses were carried out for future projection period (2051-2100) as well. The nonstationary impact results during the projection period suggest consistent increases in 100-year return values for both minimum and maximum temperatures. These increases are spatially more widespread in the case of projection as compared to observation. . It is expected that already observed time shifts in snowmelt runoff peaks will be triggered during the projection period. The ‘number of days below freezing’ and ‘number of wet days below freezing’ are expected to reduce and consequently, the snow cover duration might further shrink during the projection period as well. One of the important findings from the result is that the extent of positive impacts was more for yearly and seasonal minimum temperatures as compared to the extent of positive impacts for yearly and seasonal maximum temperatures. This phenomenon was observed for both observation and the projection period. Analysis of intra-model variability explains the importance of ensemble analysis approach. Regions, where most of the ensemble members provide homogenous impact, smaller ensemble size or even single model, might be enough. However, the regions where higher intra-model variability is observed, the use of ensemble analysis approach becomes more critical for estimation of impacts of nonstationarities.



## CHAPTER 7

### NONSTATIONARITY ANALYSES OF STREAMFLOW

#### 7.1. Results

##### 7.1.1. Hydrological Modelling

###### *Elevation Zones and Land Cover Classification*

The HBV-light is calibrated in a semi-distributed way by dividing the basin area into different elevation and land use classes. Original SRTM 90-meter elevation map was divided into ten equal elevation zones. Similarly, the initially obtained land use map (CONUS) was divided into four major land use classes as 1)-urban area and barren rocks 2)- agricultural area and other small vegetation 3)- forests and 4)-lake and open water bodies as shown in Figure 7.1. Fractional areas of each land use type are used as an input to HBV-light. Hypsometric curves of sub-basin 2133,2164 and 2157 are given in Figure 7.2. Fractional areas of sub-basin 2133,2157 and 2164 of each land use type are provided in Table 7-1, 7-2 and 7-3, respectively.

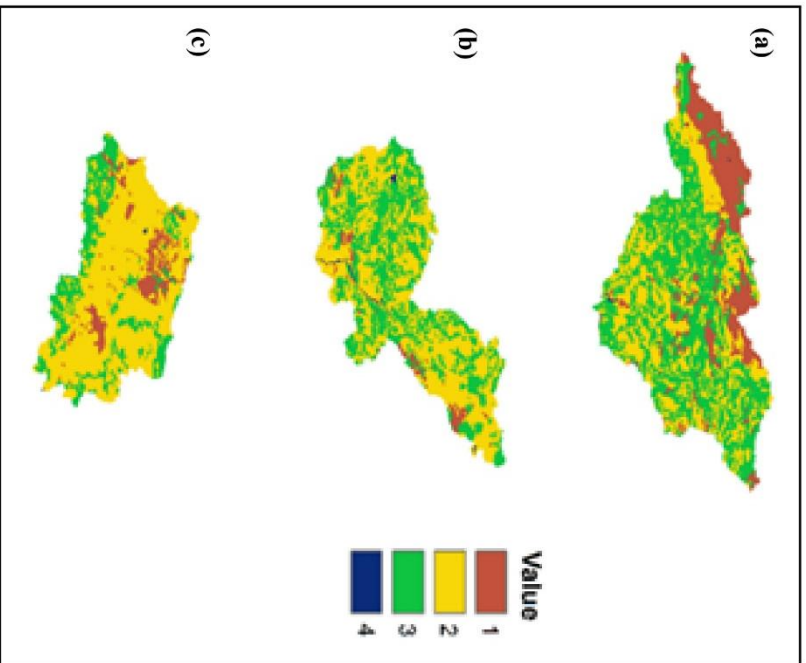
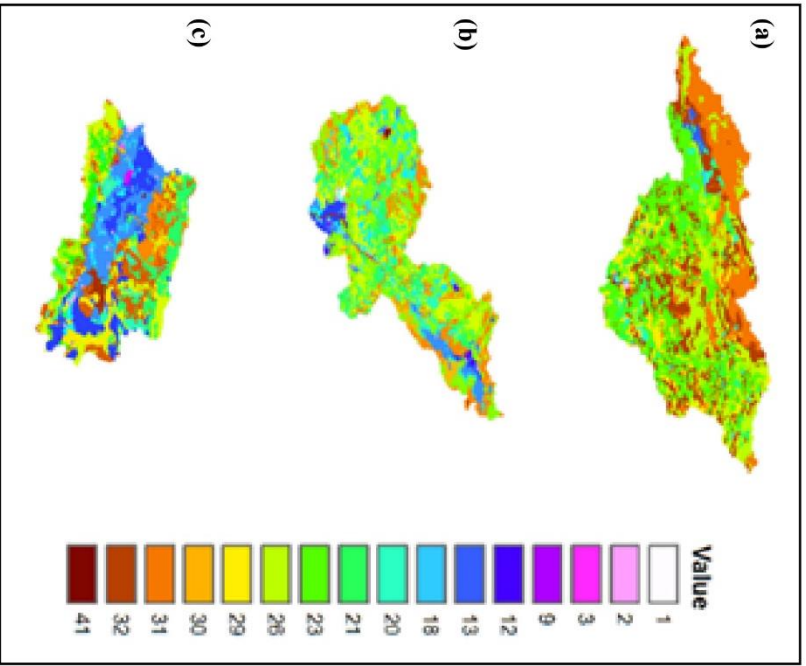


Figure 7.1 CONUS land use Maps of a) sub-basin 2133, b) sub-basin 2164 and c) sub-basin2157 before and after classification.

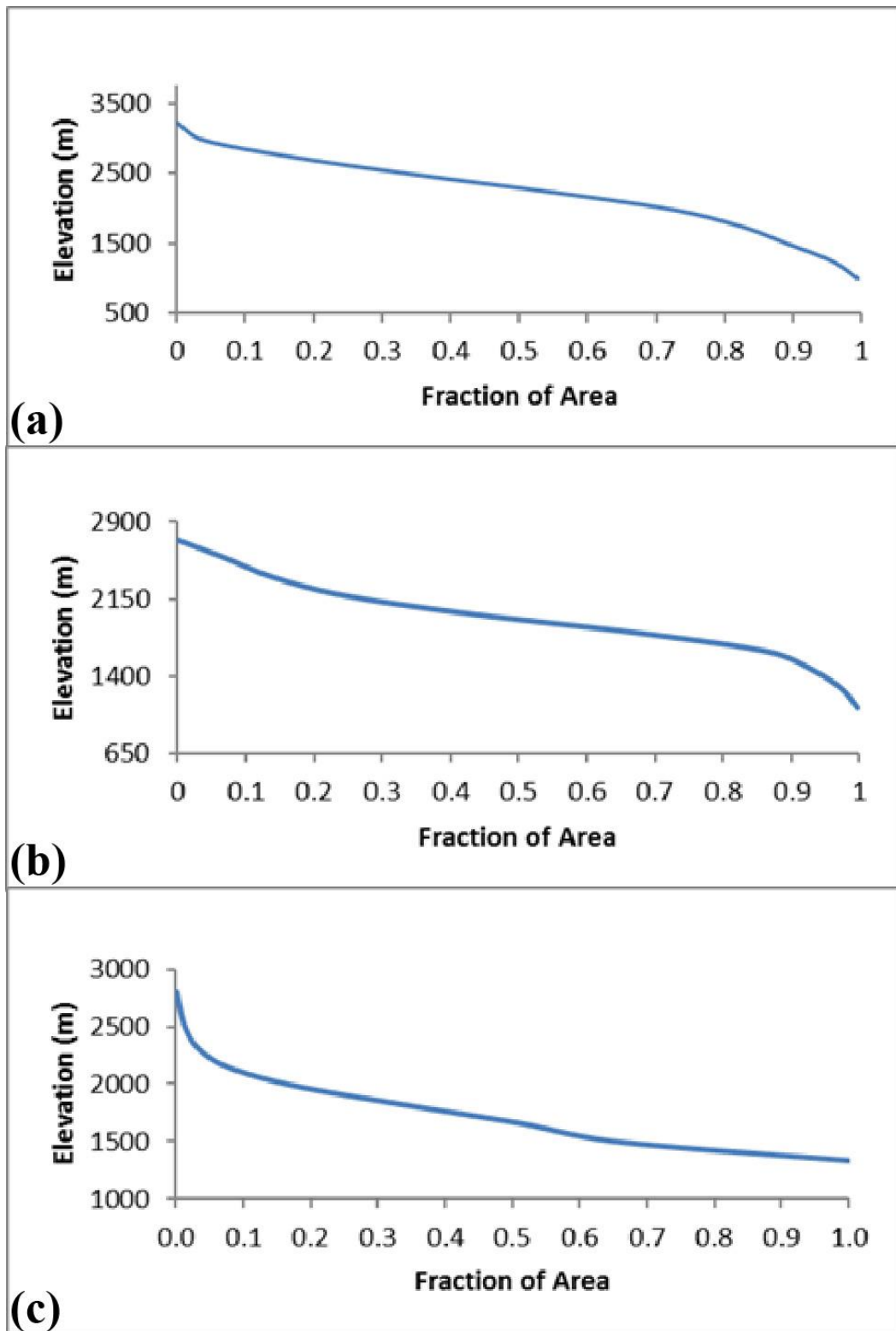


Figure 7.2 Hypsometric curve of sub-basin a) 2133 b) 2164 and c) 2157

Table 7-1 Information about fractional areas of land covers in sub-basin 2133

Elevation (m) zone/ Vegetation class		Bare Rocks Urban Areas	Agriculture Low Vegetation	Forest	Water
1	996.25	0.0018	0.0239	0.0120	0.0009
2	1242.75	0.0028	0.0775	0.0534	0.0000
3	1489.25	0.0108	0.0730	0.0928	0.0000
4	1735.75	0.0200	0.0602	0.1174	0.0000
5	1982.25	0.0226	0.0598	0.0919	0.0000
6	2228.75	0.0228	0.0371	0.0441	0.0001
7	2475.25	0.0260	0.0168	0.0238	0.0000
8	2721.75	0.0414	0.0098	0.0138	0.0000
9	2968.25	0.0332	0.0017	0.0021	0.0000
10	3214.75	0.01	0.00	0.00	0.00

Table 7-2 Information about fractional areas of land covers in sub-basin 2157

Elevation (m) zone/ Vegetation class		Bare Rocks Urban Areas	Agriculture Low Vegetation	Forest	Water
1	1330.5	0.037	0.297	0.007	0.001
2	1493.5	0.017	0.103	0.028	0.000
3	1656.5	0.020	0.109	0.045	0.000
4	1819.5	0.014	0.092	0.054	0.000
5	1982.5	0.007	0.052	0.040	0.000
6	2145.5	0.001	0.021	0.022	0.000
7	2308.5	0.000	0.009	0.008	0.000
8	2471.5	0.000	0.004	0.004	0.000
9	2634.5	0.000	0.004	0.001	0.000
10	2797.5	0.000	0.002	0.000	0.000

Table 7-3 Information about fractional areas of land covers in sub-basin 2165

Elevation (m) zone/ Vegetation class		Bare-Rocks Urban Areas	Agriculture Low Vegetation	Forest	Water
1	1085.5	0.007	0.047	0.014	0.004
2	1268.5	0.001	0.037	0.029	0.000
3	1451.5	0.001	0.065	0.038	0.002
4	1634.5	0.003	0.097	0.091	0.000
5	1817.5	0.010	0.138	0.093	0.000
6	2000.5	0.006	0.097	0.085	0.000
7	2183.5	0.002	0.033	0.031	0.000
8	2366.5	0.002	0.024	0.016	0.000
9	2549.5	0.001	0.013	0.009	0.000
10	2732.5	0.000	0.001	0.002	0.000

### Hydrological Model Calibration

The model parameters were estimated using HBV-light built-in automatic calibration algorithm in two ways. 1)- Using Nash-Sutcliffe (NS) value as the objective function and 2)- Using Log Nash-Sutcliffe (LNS) value as objective function during optimization for low flow analysis. *Genetic Algorithm and Powel* (GAP) method was used for optimization. Optimization was done by using fifty thousand genetic algorithm runs and another set of ten thousand runs were used for Powel's algorithm for fine-tuning of parameters. Daily precipitation, temperature and streamflow data from 1971 to 1992 was used for model calibration and remaining data (1993-2008) was used for validation. Once the HBV-light model is calibrated for three selected watersheds, we used daily precipitation, temperature and estimated monthly potential evapotranspiration from twelve CORDEX GMC-RCM combinations to generate future daily streamflow series from 2051 to 2100. Stationary and nonstationary forms of all three distributions (GEV, gumbel and normal) were used during the observed streamflow data analysis to examine the impacts of nonstationarities as well as to make a comparison between these distributions. For future projected streamflow data, GEV distribution is applied as NLLH of GEV

suggests better fit as compared the normal and gumbel distribution. It is used most commonly in the literature for extreme value analyses. Daily time series of observed and simulated streamflow and observed precipitation during calibration and validation periods for three sub-basins are shown in Figure 7.3. Values of the different goodness of fit indices obtained from model calibration and validation are given in Table 7-4 and Table 7-5 for Nash-Sutcliffe and logged Nash-Sutcliffe objective functions, respectively. Fluctuations in streamflow as a response to precipitation are followed well by the calibrated model at three sub-basins. There are some over- and underestimation for peak flow values at all three basins but NS statistics together with other efficiency measures stay above 70% even during validation period for both calibrations performed for high and low flow analyses (see Table 7-4 and Table 7-5). It is assumed that the calibrated model can simulate rainfall-runoff processes in these basins and it can be applied to a future period using the daily temperature and precipitation obtained from ensemble CORDEX climate projections.

Table 7-4 Values of the goodness of fit indices for observed and simulated daily streamflow obtained from calibrated HBV-light model using Nash-Sutcliffe as the objective function

Basin ID	NS		Coefficient of Determination		Kling-Gupta Efficiency	
	Calibration	Validation	Calibration	Validation	Calibration	Validation
<b>2133</b>	0.827	0.825	0.836	0.828	0.91	0.9
<b>2157</b>	0.809	0.711	0.816	0.79	0.854	0.778
<b>2164</b>	0.761	0.705	0.772	0.721	0.863	0.829

Table 7-5 Values of the goodness of fit indices for observed and simulated daily streamflow obtained from calibrated HBV-light model using log Nash-Sutcliffe as the objective function

Basin ID	LNS		Coefficient of determination		Kling-Gupta Efficiency	
	Calibration	Validation	Calibration	Validation	Calibration	Validation
<b>2133</b>	0.891	0.8645	0.804	0.827	0.891	0.8971
<b>2157</b>	0.802	0.792	0.761	0.749	0.805	0.811
<b>2164</b>	0.8501	0.818	0.761	0.732	0.85	0.818

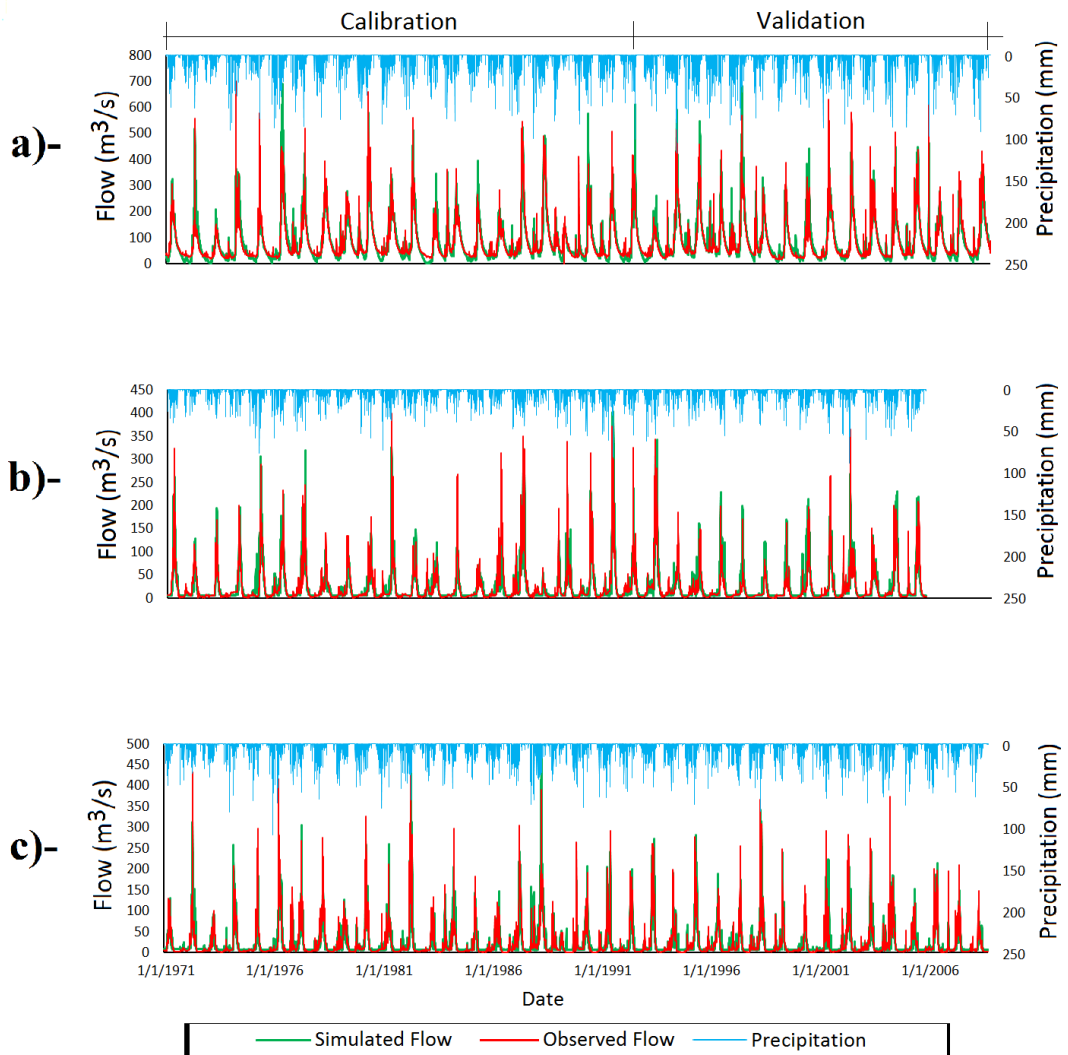


Figure 7.3 Comparison of daily observed and simulated streamflow at the station a)- 2133, b)- 2157 and c)- 2164. Daily total precipitation is also given at the right-hand side y-axis.

### 7.1.2. Impacts of Nonstationarities on Observed Streamflow

Impacts of nonstationarities are estimated using GEV, gumbel and normal distribution for historical data while only GEV is used for projection data. One of the reasons to use GEV in the projection period is that GEV is considered to provide a better fit for streamflows. An example of Murat Nehri is provided here for a

comparison of distribution fit. Probability density functions, cumulative probability density functions and qq-plots for sub-basin Murat Nehri are provided in Figure 7.4, 7.5 and 7.6, respectively. From these plots, the variability of distribution fit can be observed. All three plots clearly show that GEV provided better fit as compared to Gumbel and Normal distributions for annual maximum streamflow of Murat Nehri sub-basin. Visual inspection of all three figures also suggests that amongst two-parameter distributions, Normal distribution better fitted the observation.

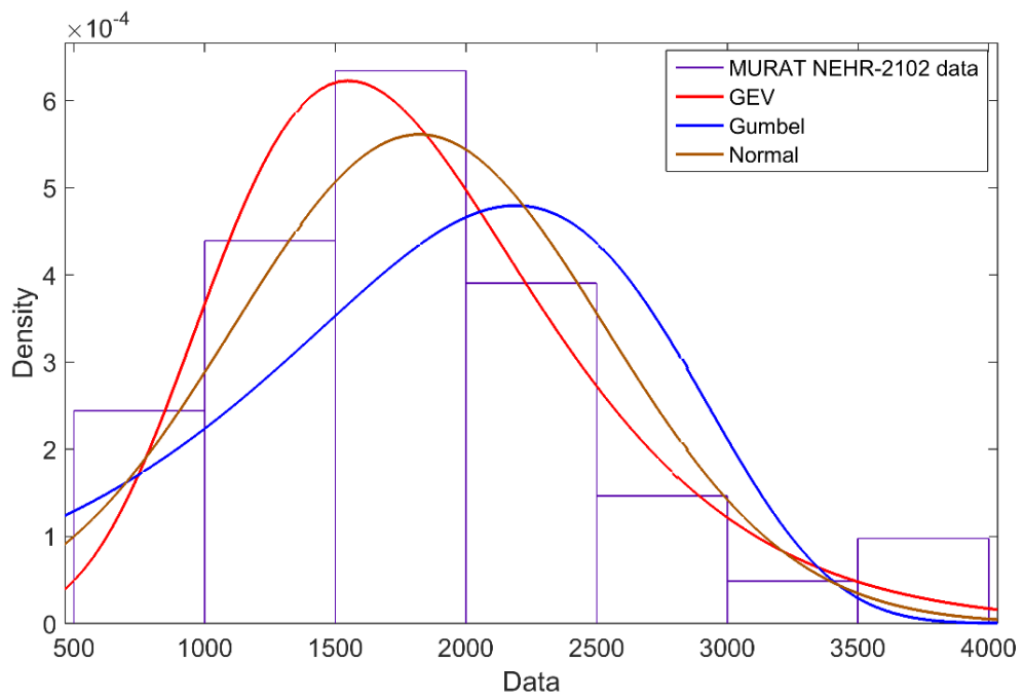


Figure 7.4 Comparative plots of probability density functions of GEV, Gumbel, Normal and Lognormal distributions

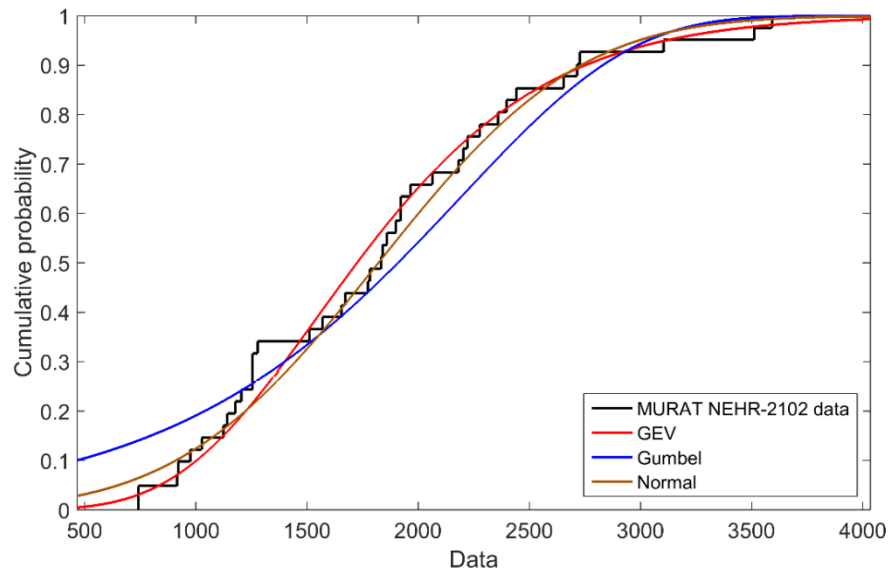


Figure 7.5 Comparative plots of cumulative probability density functions of GEV, Gumbel, Normal and Lognormal distributions

**QQ Plot of Sample Data versus Distribution**

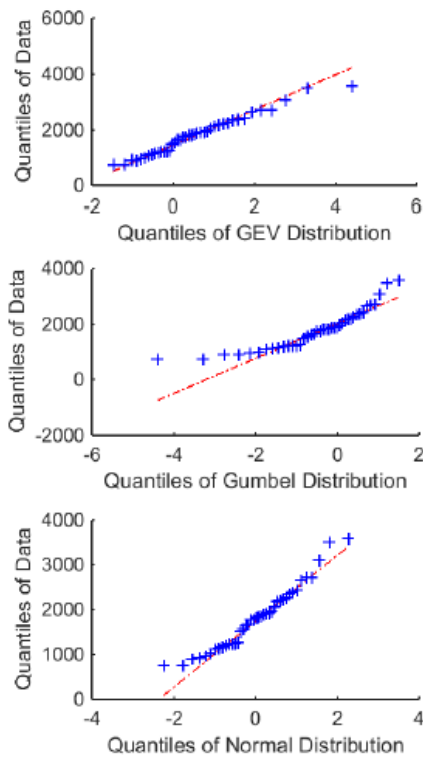


Figure 7.6 QQ-plots of GEV, Gumbel, Normal and Lognormal distributions

## 1) High Flows

Stationary and nonstationary return levels as a function of return period obtained from GEV, Gumbel and Normal distributions with stationary and nonstationary for annual maximum streamflow (yearly AMF) at each gauge station are shown in Figure 7.7. The percentage difference of the 100-year return period (a probability of occurrence of 1% every year) between stationary and nonstationary return levels is shown in Figure 7.8. The results in Figure 7.7 show that four stations (2122,2124,2156 and 2157) out of eight estimated higher nonstationary return levels than stationary values while nonstationary return levels from the other four stations (2102,2133,2145 and 2164) were lower than stationary levels. In Figure 7.8, for the 100-year return period, sub-basin 2145 provided the highest negative percentage difference while sub-basin 2156 gave the highest positive percentage difference between stationary and nonstationary return levels. Generally, all three distributions in both Figures (7.7 and 7.8) have shown the similar type of impacts (i.e., positive or negative percentage difference). It means that distributions are consistent in applying the frequency analysis for high flows. However, in some cases, the magnitude of impacts is found to be different for each distribution. For example, in case of sub-basin 2102, the percentage difference value of GEV was negligible since the value was less than plus-minus 5 percent, while for same sub-basin normal distribution gave percentage difference value more than 10 percent. Similarly, for sub-basin 2124, normal distribution has shown almost zero percentage difference value while both gumbel and GEV have shown positive impacts with more than 5 percent positive difference.

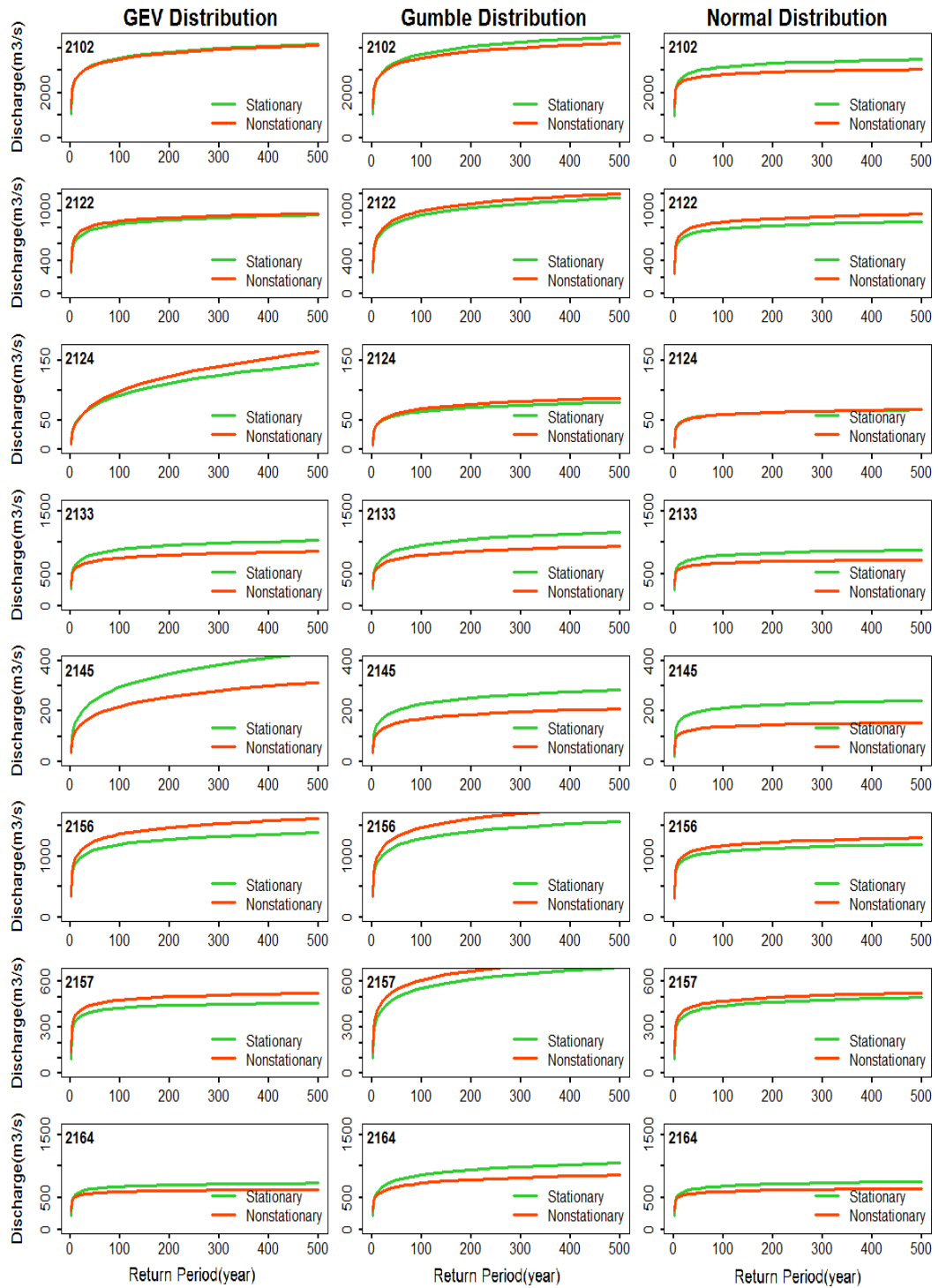


Figure 7.7 Comparison of stationary and nonstationary design discharges obtained from yearly AMFs of observed data at eight streamflow stations using GEV distribution (left column), gumbel distribution (middle column) and normal distribution (right column).

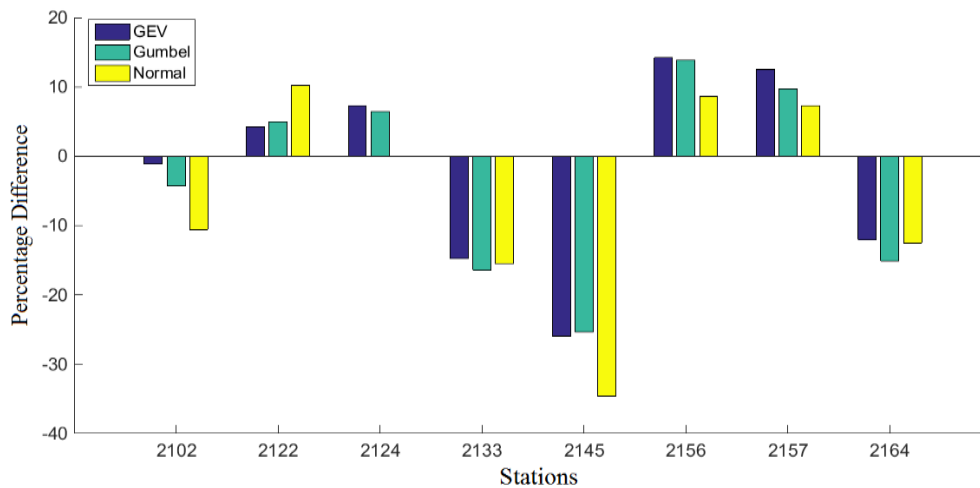


Figure 7.8 Percentage difference between 100-year stationary and nonstationary return levels for Yearly AMFs during the observation period.

Impacts of nonstationarities were also evaluated for seasonal AMFs. Percentage difference for 100-year return period between stationary and nonstationary return levels was estimated for each season for different return periods using stationary and nonstationary GEV, gumbel and normal distributions and the results are presented in Figure 7.9. It is shown that the impacts of nonstationarities are different for different seasons at different stations. There is also consistency among the three distributions in the type of impact at all stations and seasons. During winter seasons, at six stations (2102, 2124, 2133, 2156, 2156 and 2164) impacts were found to be positive from all three distributions with an exception for sub-basin 2102 where percentage difference has negative values for normal distribution. Sub-basin 2124 and 2145 have shown negative impacts for the winter season. For the spring season, at five stations (2102, 2124, 2133, 2145 and 2164) the impacts were found to be negative using all three distributions while at three stations (2122, 2156, 2157) the impacts were positive. At five stations (2124, 2133, 2145, 2157 and 2164) the impacts of nonstationarities were negative during the summer period while at three stations (2102, 2124 and 2156) the impact values were positive. During the autumn season, impacts were found to be positive at six stations (2102, 2122, 2133, 2156 and 2164)

while at remaining two stations (2124 and 2145) the impacts were negative. It is also evident from Figure 7.9 that during the autumn season, the magnitudes of impact values obtained were higher as compared to other seasons particularly using GEV distribution. At stations 2122 and 2156 impacts were positive for all seasons while at stations 2124 and 2145 impacts were negative for all seasons. At other stations at least one season shows an opposite impact type for nonstationarity. Generally, seasonal AMFs support the yearly AMF by releasing the same impact type (positive or negative) but with different magnitudes. However, at a few stations (2133, 2102, and 2124) seasonal AMFs indicated different impact (positive) from yearly AMFs (negative). Seasonality effect on the determination of high flow values with respect to yearly AMFs can be of importance at these sub-basins.

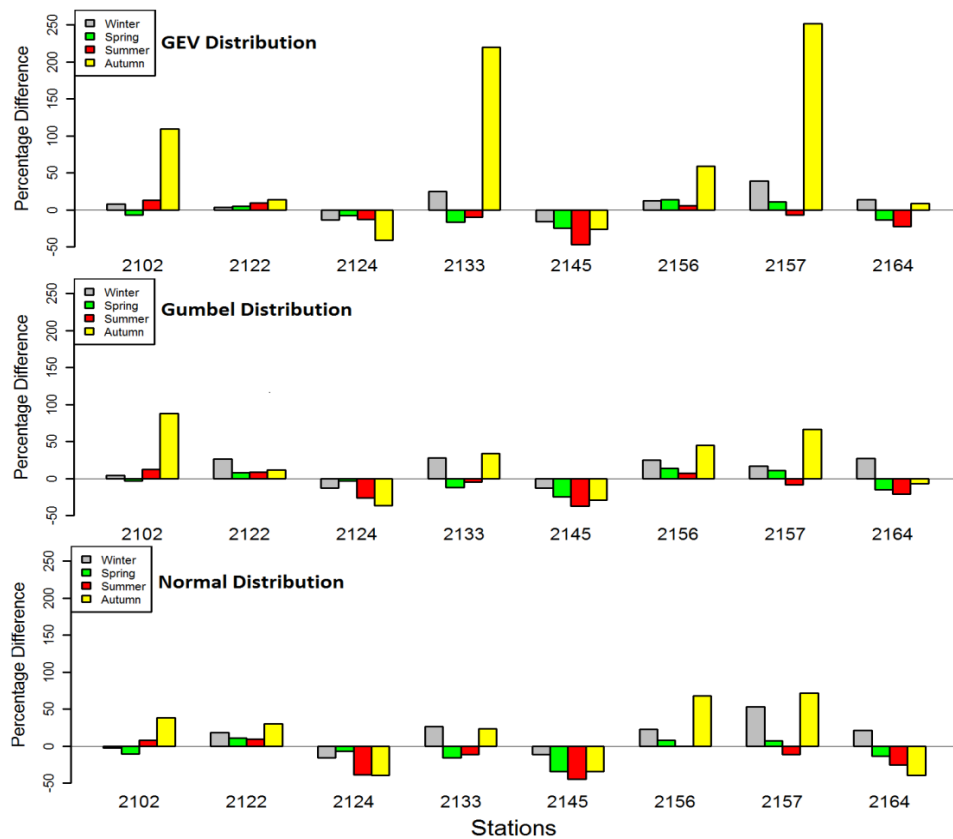


Figure 7.9 Percentage difference between 100-year stationary and nonstationary return levels for seasonal AMFs during the observation period.

## 2) Low Flows

Annual 35<sup>th</sup> percentile values are used to analyze the impacts of nonstationarities on low flows. Stationary and nonstationary forms of GEV, gumbel and normal distributions were used to estimate stationary and nonstationary return levels for different return periods. Percentage difference between stationary and nonstationary return levels for a 100-year return period of yearly ALFs are shown in Figure 7.10. In this figure, six stations (2102, 2122, 2133, 2156, 2157 and 2164) exhibit positive nonstationary impacts using all three distributions. The positive impact for sub-basin 2164 reaches 80% that is at least 60% greater than the impact at other stations (2102, 2122, 2133, and 2157). At sub-basin 2124 and 2145, results from all three distributions have shown negative impacts. It is also worth mentioning that these two stations are located at relatively downstream locations.

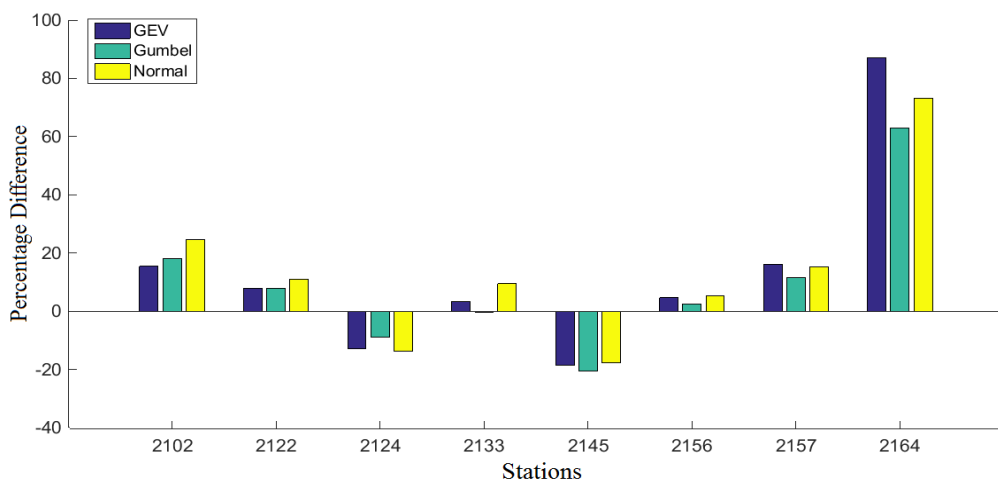


Figure 7.10 Percentage difference between 100-year stationary and nonstationary return levels for seasonal ALFs during the observation period.

Comparison of percentage difference (impact values) between 100-year stationary and nonstationary return levels obtained from observed yearly ALFs at eight stations using GEV, gumbel and Normal Distribution. A similar analysis was also carried out for

seasonal ALFs to understand the behavior of nonstationarities on a seasonal basis for seasonal 35<sup>th</sup> percentile value and results are presented in Figure 7.11. It is evident from Figure 7.11 that six stations (2102,2122,2133,2156,2157 and 2164) the impacts were positive during all seasons using all three distributions with few exceptions (e.g; impacts during winter at sub-basin 2122, spring at stations 2133 and 2157, and summer at sub-basin 2157 were slightly negative). Highest positive impacts (up to 50%) are seen at stations 2157 and 2164. Generally, in these basins, the 100-year low flow values increase with nonstationarity. At stations 2124 and 2145 which are located at relatively downstream positions, the impacts of nonstationarities were negative for all seasons. This indicates that low flow values for these two basins decrease with nonstationarity and hence, they are prone to have a possible drought condition. Seasonal ALFs supports the type of nonstationarity effect seen on yearly ALFs.

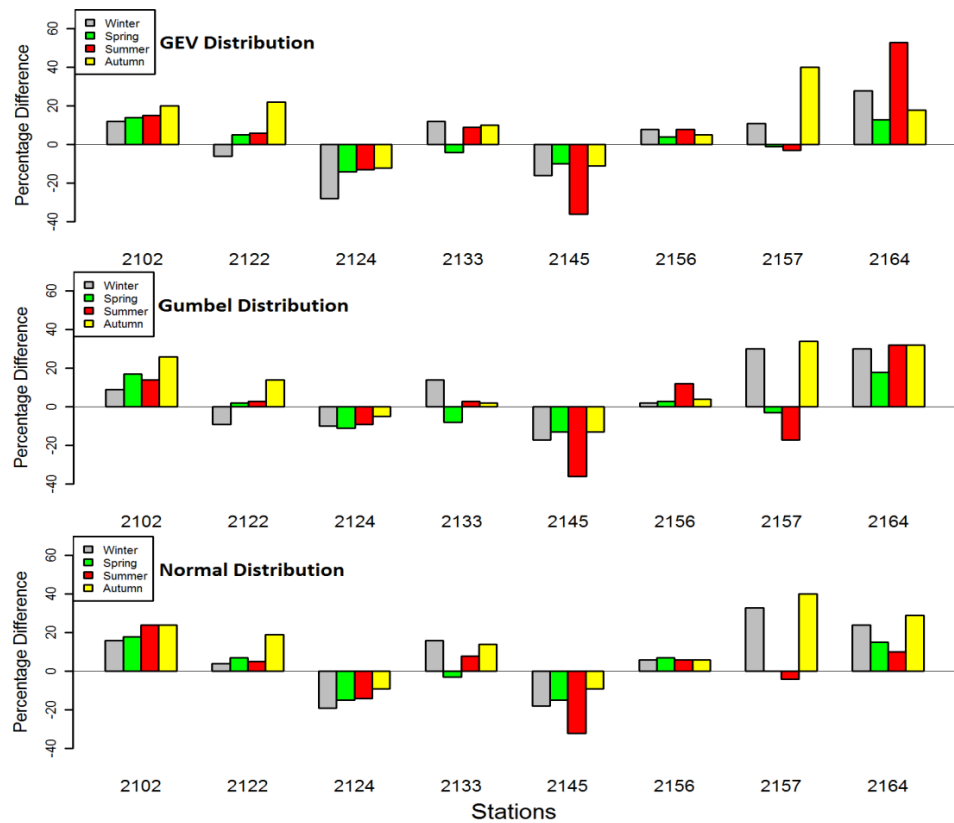


Figure 7.11 Percentage difference between 100-year stationary and nonstationary return levels for seasonal ALFs during the observation period.

### 7.1.3. Impacts of Nonstationarities for Projected Streamflow (2050-2100)

#### 1) High Flows

Stationary and nonstationary GEV distributions were applied on yearly and seasonal AMFs for three watersheds. Box plots of stationary and nonstationary return levels from 12 different ensemble members are shown in Figure 7.12 along with lines of ensemble means for both cases. Based on ensemble means, nonstationary discharges along with different return periods were less than the stationary ones particularly for sub-basin 2133. The differences are less pronounced for stations 2164 and 2157. Ensemble median also shows less nonstationary discharges that means at least half of CORDEX models has resulted in less nonstationary discharges compared to stationary ones. The uncertainty (greater box size) in estimating return levels increases as return period increases for both cases. This is more evident at stations 2133 and 2157. Also, the uncertainty for nonstationarity is greater than that for stationary at 2164. However, overall the size of the boxes of 2164 is almost the half of the boxes at stations 2133 and 2157 for all return periods.

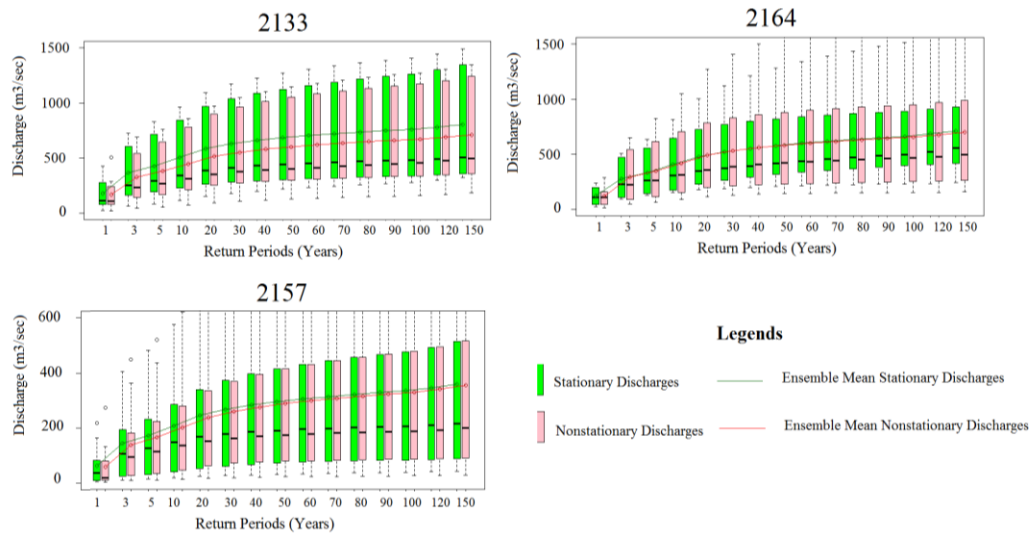


Figure 7.12 Boxplots of stationary and nonstationary return levels at three selected watersheds obtained from yearly AMFs of CORDEX driven streamflow projections. In each boxplot “—” refers to ensemble median while green and red lines represent

Stationary and nonstationary design discharges were estimated for yearly and seasonal AMFs for projections. Figure 7.13 shows the box plots that contain twelve values of the percentage difference between 100-year stationary and nonstationary discharge from each CORDEX model for yearly and seasonal AMFs at three stations. During winter and autumn seasons, the ensemble mean and median of impact values were positive at all stations meaning that 100-year nonstationary discharges were more than stationary discharges. Ensemble mean and median of impact values were negative during summer at all stations meaning lower return levels for stationary case. During the spring season, at sub-basin 2133 and 2157, the ensemble mean and median of impact values were negative indicating lower values in nonstationary case. At sub-basin 2164, the ensemble mean and median of impact values were positive during spring. Overall winter and summer were the seasons which exhibit the most positive and the most negative impacts, respectively. In addition, the seasonality effect on the difference was more significant at sub-basin 2164. All 12 models show the positive impact in winter at all stations while it was the case for summer with negative impact. Except for winter, there is a tendency of having a negative impact (decreasing trend and reducing the return levels with nonstationarity) at all the stations as it is also noticeable from yearly AMFs.

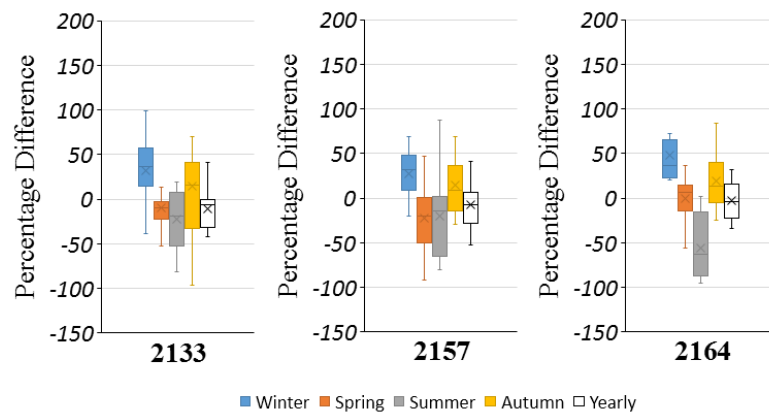


Figure 7.13 Boxplots of the percentage difference between 100-year stationary and nonstationary return levels obtained from yearly and seasonal AMFs of CORDEX driven streamflow projections for three watersheds (2133,2157 and 2164) using GEV distribution.

## 2) Low Flow

Stationary and nonstationary return levels were estimated for yearly ALFs obtained from projected streamflows of each of CORDEX model. The results are shown in Figure 7.14 as boxplots and ensemble means of both stationary and nonstationary design discharges. The ensemble results of nonstationarity impacts obtained from yearly low flow series were positive at all three stations (2133,2157, 2164). The increase in return levels with nonstationarity was very significant at sub-basin 2164 with high variability between models and it reached to 20 m<sup>3</sup>/s of median values towards higher return periods. This should be noted that this subbasin is projected to be not affected by drought. Also, the sub-basin 2157 released the least positive impact with the nonstationarity. At this station, the variability between models is the smallest.

The boxplots of percentage difference of 100-yr return period for each ensemble member are shown for seasonal ALFs in Figure 7.15. Mean and median of boxplots show positive impacts for yearly ALFs at all stations. Impacts of nonstationarities were positive for winter ALFs at all three stations. Ensemble results of spring ALFs show that stations 2133 and 2164 exhibits positive impacts while sub-basin 2157 have shown negative impacts. The results of summer ALFs have shown slightly negative impacts at stations 2133 and 2157 while positive at sub-basin 2164. Stations 2157 and 2164 shown positive impacts while sub-basin 2133 didn't show any significant impacts as the ensemble mean and median values were close to zero. Overall the impacts of nonstationarities at sub-basin 2164 were positive for all seasonal and yearly ALFs. It is an evidence from yearly ALFs and AMFs that the effect of nonstationarity decreases high flow values for given return periods while it increases low flow values for corresponding return periods at three subbasins. In addition, the seasonality shows important influence on the nonstationarity impact in estimating return levels of high and low flows.

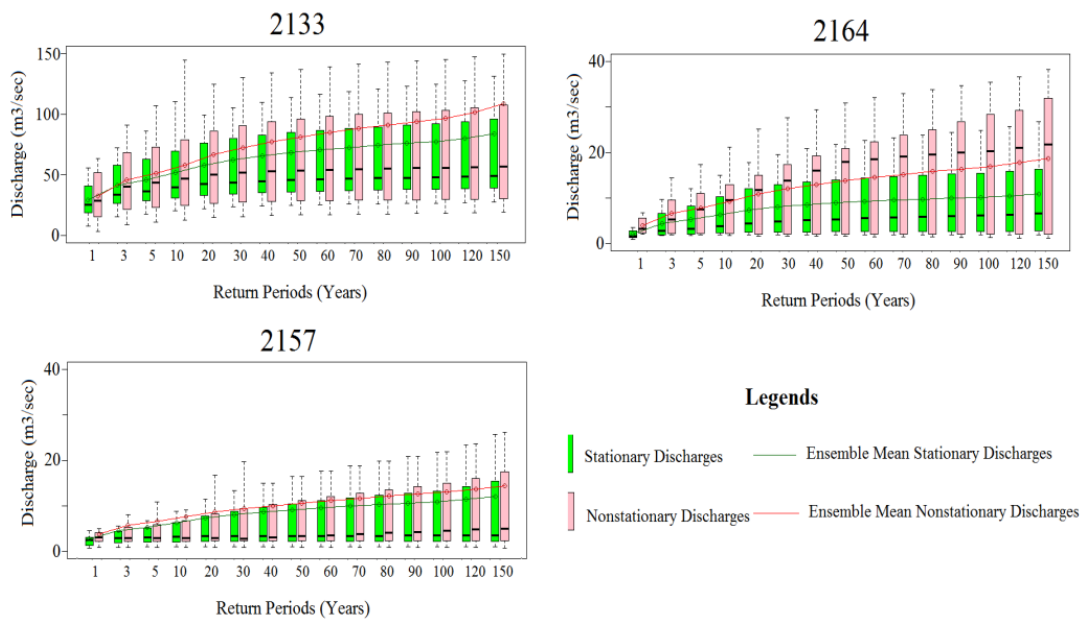


Figure 7.14 Boxplots of stationary and nonstationary return levels at three selected watersheds obtained from yearly ALFs of CORDEX driven streamflow projections.

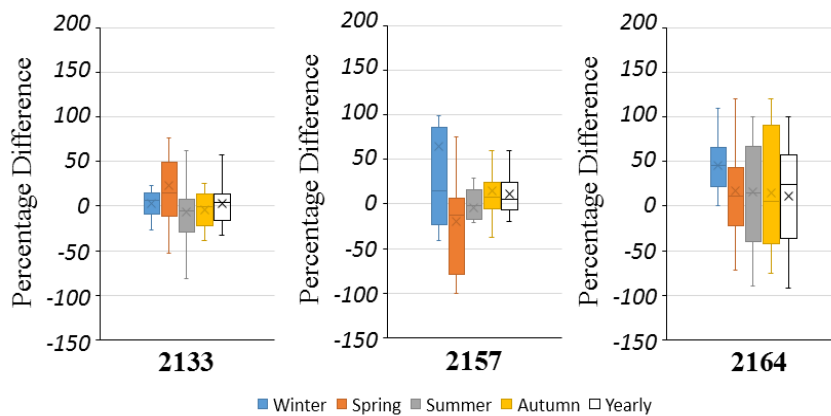


Figure 7.15 Boxplots of the percentage difference between 100-year stationary and nonstationary flows obtained from yearly and seasonal ALFs of CORDEX driven streamflow projections for three watersheds (2133,2157 and 2164) using GEV distribution.

## 7.2. Discussion

Comparison of GEV, gumbel and normal distributions shows that all three distributions have shown more or less similar results with a notable exception for yearly AMF case where impacts were considerable more for the autumn season using GEV as compared to other two distributions

Design impacts of nonstationarities were found to be significant from observed yearly AMFs for all stations as four stations have shown positive impacts while remaining four stations have shown negative impacts using all three (GEV, gumbel and normal) distributions. Nonstationarities found to have strong impacts on observed seasonal AMFs as well. Winter and autumn AMFs have shown positive impacts at most of the stations while during spring and summer, impacts were negative at most of the stations using all three distributions. Using yearly and seasonal ALFs, nonstationarities have positive impacts at most of the stations with few exceptions. Two stations located at most downstream positions, impacts were found to be negative for all seasonal and yearly ALFs. The nonstationarity effect in ALFs is more pertinent than the effect in AMFs. However, the impact of nonstationarity for both flows is substantially lower than the impact obtained through ensemble method.

Ensemble mean and median nonstationary 100-year return values of yearly AMFs of CORDEX driven projected streamflow were found to be less than stationary ones, thus, suggesting negative impacts at all three selected watersheds. Ensemble mean and medians for projected seasonal AMFs exhibits positive impacts during autumn and winter seasons while generally negative impacts during spring and summer seasons at all three watersheds. Positive impacts were obtained from ensemble results of projected yearly ALFs at all three watersheds. Results of winter ALFs of projected streamflow suggests considerable positive impacts. Generally, the results obtained from observations were found to be consistent with those obtained from

CORDEX driven projections, but there was some difference as well which suggests that present state of nonstationarities may change over longer period.

Ensemble analysis during observation period at stations 2133 and 2157 shows similar results compared to those during the projection period while at sub-basin 2164 the impacts of nonstationarities were found to be opposite. It gives a hint about the fact that the status of nonstationarities may change over a long period at some places. Similarly, few consistencies between observation and projection period can be established from seasonal AMF results. For example, winter, summer and autumn seasons show similar kind of nonstationarity impacts at stations 2157 and 2164. In the case of 2133, impacts were again similar for all seasons.

Ensemble analysis of the results obtained from observed and projected ALFs are found to be consistent. For example for yearly ALFs, all three stations show positive impacts during both observation and projection period and during the projection period, these impacts become more evident. Small et al. (2006) claimed that one of the major reason for the increase in low flows is because of increase in autumn precipitations because during the autumn season most of the precipitation is contributed towards baseflow rather than inducing floods. These positive impacts of nonstationarities on precipitation extremes during the autumn season (which are shown section 5.1.3) might increase the magnitudes of lower quantiles of flow. Nonstationarities impact results of seasonal ALFs during observation were found to be generally consistent with the results obtained during the projection period. For example, winter ALFs exhibits positive impacts at all three stations during observation and projection time period. Similarly for autumn ALFs, 2164 and 2157 shown positive impacts for both observation and projection time period. For sub-basin 2164 impacts were significantly positive during observation and projection period for spring and summer ALF.

Owing to higher elevation and low temperatures, in this region ratio of precipitation falling as snow is higher as compared to other part of Turkey (Yucel et al., 2014; Önoel and Semazzi, 2009; Önoel et al., 2014). However, increasing temperature (especially minimum temperature), as suggested by the results presented in section 7.1.3, hints towards alteration of precipitation pattern as some portion of snow might become rain in future. This kind of situation usually suggests a smaller contribution towards snowmelt runoff. The increase in temperature over mountainous regions also contributes towards early and accelerated snow-melting process (Yucel et al., 2014; Önoel and Semazzi, 2009; Önoel et al., 2014). Thus, increases in return levels of minimum temperatures might be the reason for the early snow melting which might alter the peak flow towards the earlier times. Hereby, increasing the winter and reducing the spring peak flows. The reduction in a number of wet and dry days below freezing might also be attributable towards shifting in streamflow peaks in mountainous basins where streamflow is strongly governed by snow melting.

Having said that, any potential land-use change in future may also affect the dynamics of the rainfall-runoff relationship (Zhang et al., 2012). Ensemble analysis approach used here might avoid planning that is based on pure historical record or a single “best estimate” scenario, encouraging adaptation efforts that better reflect the changing nature of the risk. Furthermore, ensemble results from CORDEX based projections show the importance of potential variation in probabilities of annual and seasonal high and low flows in future. It should be noted for engineers, decision makers and water managers to carefully design an optimized structure based on the needs of flood mitigation, hydropower generation, irrigation schemes, and water supply projects by incorporating the annual and seasonal impacts of nonstationarities during historical as well as future time periods.

Based on these results, it is important to note that the impact of climate-related nonstationarity is significant enough to incorporate it in the design and planning of

water resources development project in the study area of Euphrates basin. Furthermore, detailed risk and reliability analysis can be done for each of the individual sites by considering into account the seasonality effect for present and proposed projects so that it can be clear if the impacts of nonstationarities are within the acceptable range. Overall in the region, the magnitudes of low flows are having positive impacts while those for high flows show opposite impacts by the end of the century according to ensemble analyses. In addition, the seasonality should be considered in these analyses as the climate-related nonstationarity behaves differently at each season.



## CHAPTER 8

### ANALYSES OF BIAS-ADJUSTED CORDEX RCMS

Climate impact models need to have finer resolution with minimum uncertainties like biases. However, GCMs and RCMs generally contain uncertainties and bias. CORDEX provides the downscaled data at much finer resolutions (for example Eur-11 with approximately 12km resolution). But still, CORDEX models contains uncertainties and biases when compared to the observation data. Analyses based on multi-member ensemble approach is one way to reduce the effects of these uncertainties and biases. However, many users of climate model data apply some form of bias correction and further downscaling to get better agreement between simulation and observation data. Maraun (2016) critically reviewed the different bias correction methods and discussed the possibility of alteration of climate change trends and nonstationarity signals after bias correction. One of the main reasons for this alteration of nonstationarity signals comes from the fact that most of the bias correction methods assume the stationarity of correction function (Maraun, 2016). CORDEX provides bias-adjusted data for few models using different bias correction methods. The aim of this part of the study is to evaluate the performance of bias-adjusted models using conventional performance indicators (like *RMSE*, *MBE*, *MAE*, and *CORR*) as well as their ability to preserve the nonstationarity signals. Initially, the improvement in bias-adjusted models is evaluated by comparing the bias-adjust model performance statistics with those of the original model. Then nonstationarities impacts were estimated using bias-adjusted model data using stationary and nonstationary form of GEV distribution and these impacts were compared to those

of the original model to analyze if bias-adjust models can preserve the nonstationarity signals. Two bias-adjusted precipitation models (one with DBS correction method and other with CDF method) and two bias-adjusted temperature models (both with BDS method) are evaluated here.

## **8.1. Results**

### **8.1.1. Precipitation Analyses**

#### **1)- CNRM-CERFACS-CNRM-CM5—CCLM4-8-7 (BDS Method)**

##### **a)- Performance Evaluation**

Daily mean precipitation of raw and bias-adjusted model is plotted against observations during the reference period in Figure 8.1. The plots show that for all regions there was a considerable improvement after bias correction. A better agreement between observation and corrected model can be seen for late spring and early summer precipitation in Aegean region. Improvement can be observed winter and spring precipitation in the Black Sea and Marmara region. Similarly, the plots suggest betterment after corrections in Central Anatolia throughout the year. Similarly, much improvement is found in Eastern Anatolia throughout the year where raw RCM contained significant positive biases. Overall significant improvement is visible in the Mediterranean region particularly in the mid of the year. Similarly, in South-Eastern Anatolia, bias-adjusted RCMs shows a better representation of spring and autumn precipitation. A similar improvement can be found in performance statistics based on mean daily precipitation as well as successive monthly totals as provided in Table 8-1. The values of RMSE and MAE were less in case of the bias-adjusted model for both mean daily as well as successive monthly evaluation. Values of MBE error were much closer to zero.

CORR values show increment after correction in all regions (except for Eastern Anatolia region where the slight decrease was found for daily mean evaluation).

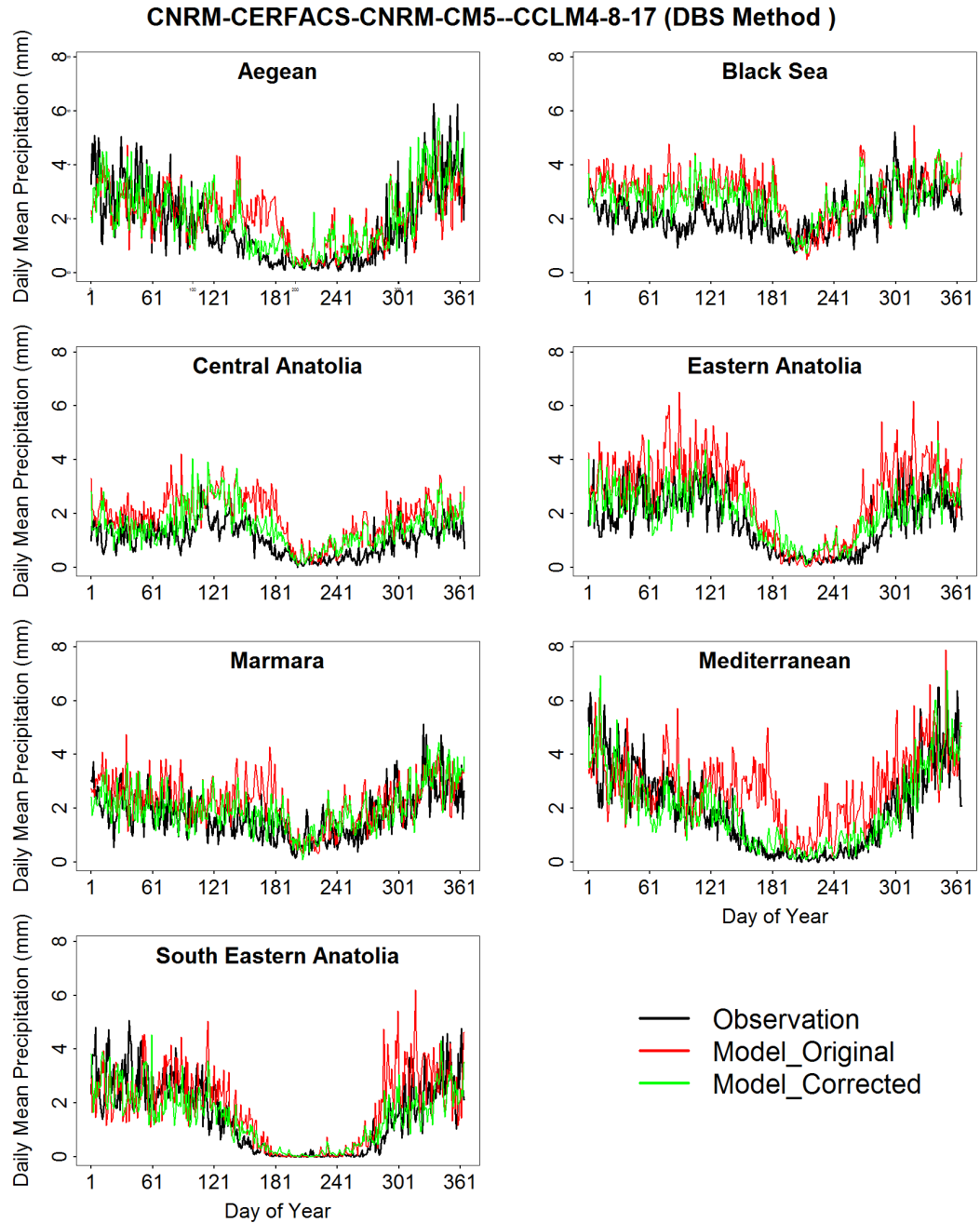


Figure 8.1 Comparison of observed daily mean precipitation with those of original and bias-adjusted RCM ( CNRM-CERFACS-CNRM-CM5—CCLM4-8-7 (BDS Method) )

Table 8-1 Performance Evaluation Statistics of Original and Bias-Adjusted RCM for precipitation.

Region Name	RMSE (mm)		MAE (mm)		MBE (mm)		CORR	
	RAW	BC	RAW	BC	RAW	BC	RAW	BC
<b>A</b>	<i>Mean Daily Precipitation Evaluation</i>							
<i>Aegean</i>	1.21	1.05	0.94	0.80	0.30	0.27	0.55	0.70
<i>Black Sea</i>	1.20	0.97	0.97	0.80	0.73	0.51	0.33	0.37
<i>Marmara</i>	1.04	0.86	0.81	0.69	0.50	0.23	0.45	0.50
<i>Central Anatolia</i>	1.07	0.77	0.87	0.60	0.82	0.46	0.58	0.59
<i>Eastern Anatolia</i>	1.52	0.87	1.22	0.69	1.13	0.30	0.71	0.70
<i>Mediterranean</i>	1.59	1.00	1.29	0.74	0.81	0.00	0.55	0.78
<i>South Eastern Anatolia</i>	1.17	0.88	0.80	0.63	0.25	-0.11	0.64	0.75
<b>B</b>	<i>Successive Monthly Total Precipitation</i>							
<i>Aegean</i>	55.50	52.35	41.31	38.47	9.16	8.15	0.30	0.42
<i>Black Sea</i>	49.20	43.20	38.55	33.40	24.67	18.05	0.17	0.18
<i>Marmara</i>	45.82	44.36	35.92	34.51	12.94	10.72	0.22	0.22
<i>Central Anatolia</i>	40.21	31.23	31.24	23.74	25.56	14.41	0.39	0.41
<i>Eastern Anatolia</i>	57.81	40.80	42.14	30.67	29.29	8.48	0.48	0.45
<i>Mediterranean</i>	70.92	52.43	53.26	35.95	24.69	-0.04	0.35	0.57
<i>South Eastern Anatolia</i>	54.88	49.12	36.29	32.63	8.33	3.39	0.42	0.53

#### b)- Nonstationarity Impact Evaluation

The impacts of nonstationarities were estimated using GEV distribution for original/raw as well as bias-adjusted RCM for yearly maximum precipitation (Yearly AMP) and interpolated maps are presented in Figure 8.2 while the impact values at individual gridded stations are presented in Figure 8.3 on regional bases in form of bar plots. The overall look of the nonstationarity impact maps of original and bias-adjusted RCM suggest that magnitudes of nonstationarity impacts are less in case of bias-adjusted RCM throughout Turkey. Particularly in Central Anatolia, Marmara and Aegean region, where original RCM shows significant positive and

negative impacts while in case of bias-adjusted RCM, the nonstationarity impacts almost vanished. In addition of the decreases in magnitudes of impacts, many gridded stations exhibited opposite impacts or no impact at all in case of bias-adjusted RCM. This can be observed from interpolated maps given in Figure 8.2 as well as bar plots are given in Figure 8.3. For example, gridded station 17034 of Black Sea region, 17152 of Marmara region, 17193, 17244 of Central Anatolia, 17199 of Eastern Anatolia, 17190 of Aegean region, 17270, 17275 and 17282 of South Eastern Anatolia exhibited positive impacts in case of bias-adjusted RCM while these stations were under the influence of negative impacts in the case of original RCM. Similarly, gridded stations 17062,17112 and 17114 of Marmara region, 17080, 17126, 17130, 17135 and 17192 of Central Anatolia, 17155, 17186,17188 and 17237 of Aegean region shown negative and positive impacts using bias-adjusted RCM and original RCM respectively.

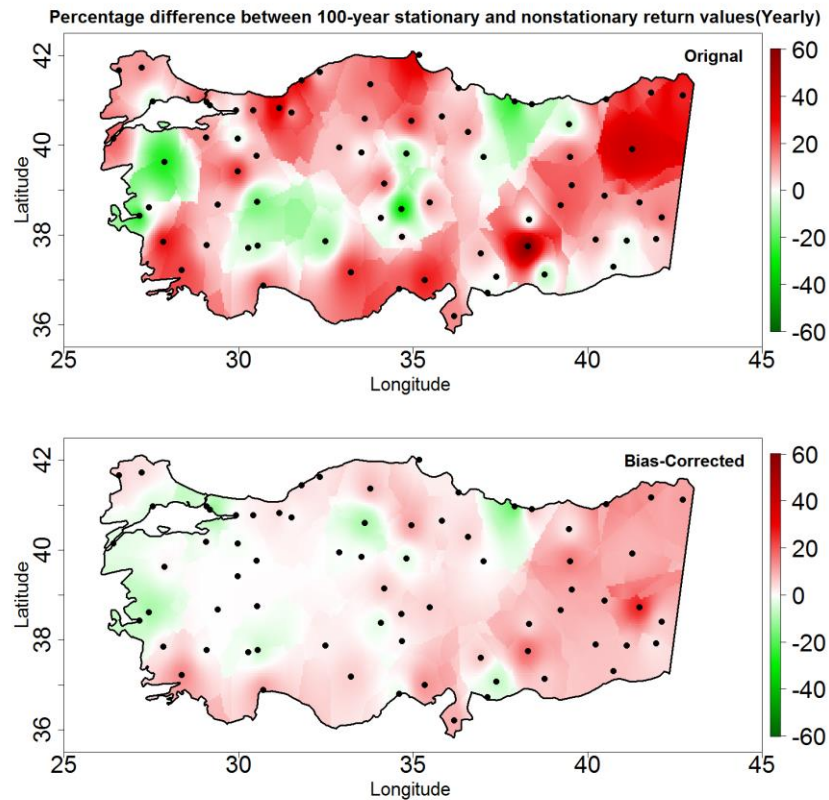


Figure 8.2 Comparison of nonstationarity impacts obtained from original and the bias-adjusted RCM for Yearly AMPs

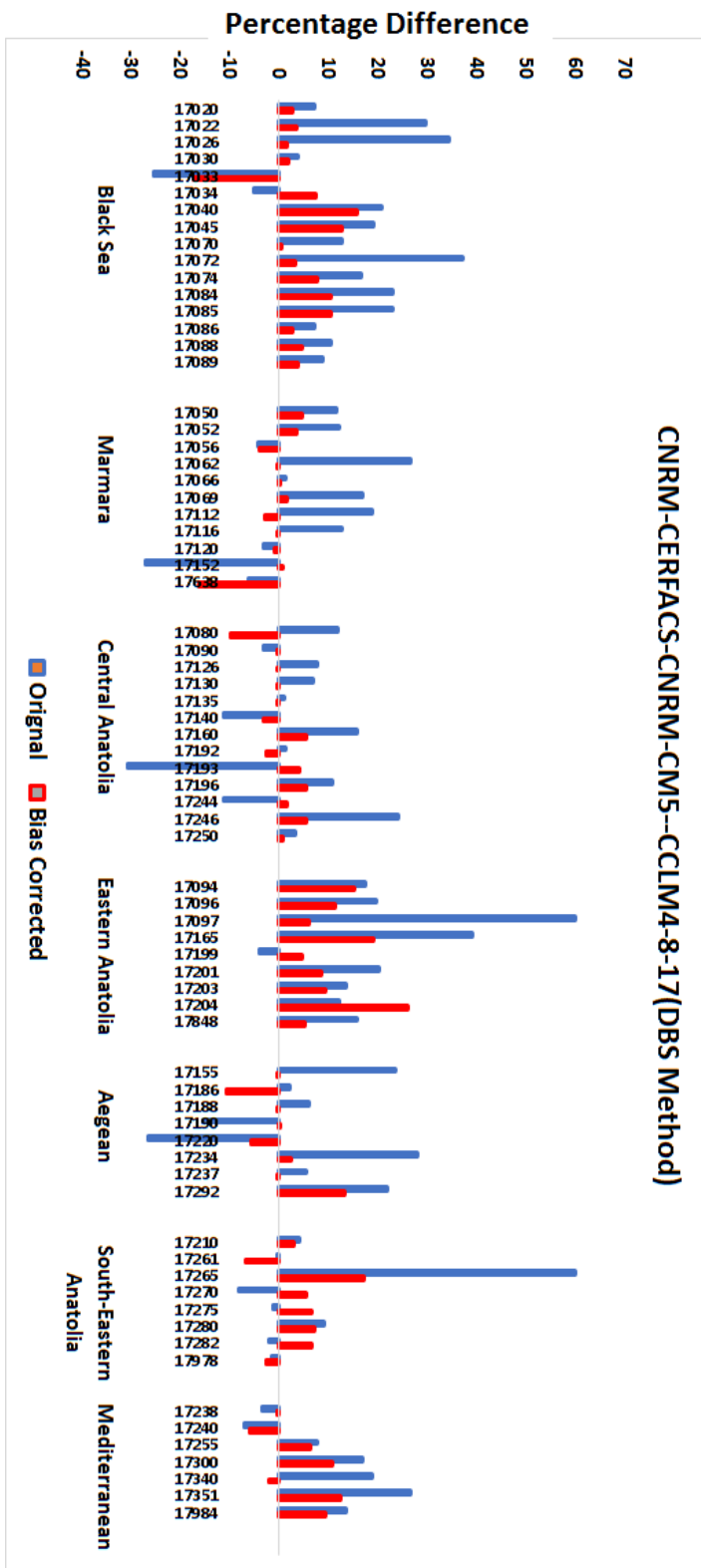


Figure 8.3 Comparison of nonstationarity impact values at gridded stations obtained using original and bias-adjust RCM for yearly AMPs

## 2)- IPSL-IPSL-CM5A-MR—*WRF331F* (CDF Method)

### 2)- Performance Evaluation

Daily mean precipitation of raw and bias-adjusted models is plotted against observations during the reference period in Figure 8.4. The plots show that for all regions there was a considerable improvement after bias correction. A better agreement between observation and corrected model can be seen for winter, spring, early summer and autumn precipitations in the Aegean region. Improvement can be observed winter and spring precipitation in the Black Sea and Marmara region. Similarly, the plots show improvement after corrections in the Central Anatolia for winter and spring precipitation. Similarly, much improvement is found in Eastern Anatolia throughout the year where raw RCM shows significant positive biases. A notable improvement is visible in the Mediterranean region particularly in the mid of the year. Similarly, in South-Eastern Anatolia, bias-adjusted RCMs shows a better representation of winter, spring and autumn precipitation where in case of original RCM, significant positive biases are present.

A similar improvement can be found in performance statistics based on mean daily precipitation as well as successive monthly totals as provided in Table 8-2. The values of RMSE and MAE were less in case of the bias-adjusted model for both mean daily as well as successive monthly evaluation. Values of MBE error were much closer to zero. CORR values show increment after correction in all regions (except for Black Sea region where a slight decrease in CORR value was found for daily mean evaluation).

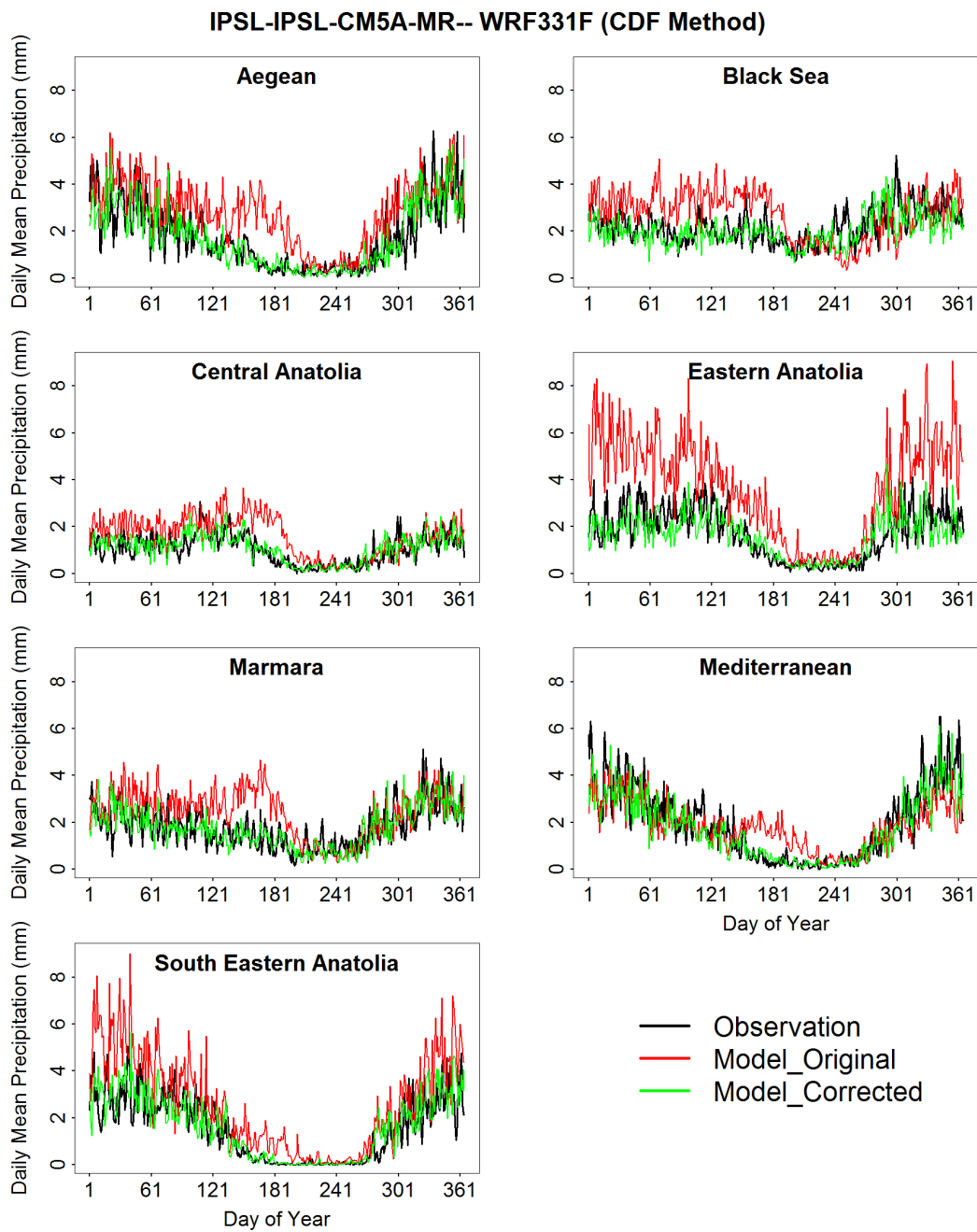


Figure 8.4 Comparison of observed mean daily precipitation with original and bias-adjusted RCM

Table 8-2 Performance evaluation statistics of original and bias-adjusted RCM

Region Name	RMSE (mm)		MAE (mm)		MBE (mm)		CORR	
	RAW	BC	RAW	BC	RAW	BC	RAW	BC
<b>A</b>	<i>Mean Daily Precipitation Evaluation</i>							
<i>Aegean</i>	1.51	0.90	1.21	0.65	1.00	-0.05	0.67	0.78
<i>Black Sea</i>	0.95	0.82	0.79	0.61	-0.17	-0.20	0.49	0.33
<i>Marmara</i>	1.22	0.75	0.98	0.58	0.67	0.01	0.42	0.61
<i>Central Anatolia</i>	0.91	0.51	0.70	0.39	0.56	0.05	0.55	0.64
<i>Eastern Anatolia</i>	3.46	0.85	2.81	0.63	2.79	-0.12	0.66	0.67
<i>Mediterranean</i>	1.13	0.93	0.87	0.63	-0.10	-0.21	0.70	0.81
<i>South Eastern Anatolia</i>	1.66	0.89	1.20	0.61	1.04	0.08	0.69	0.78
<b>B</b>	<i>Successive Monthly Total Precipitation</i>							
<i>Aegean</i>	68.17	51.61	50.70	33.72	30.93	-1.24	0.34	0.46
<i>Black Sea</i>	39.72	35.44	30.96	27.04	-2.90	-3.50	0.28	0.30
<i>Marmara</i>	54.20	38.72	43.47	30.03	24.55	1.90	0.16	0.28
<i>Central Anatolia</i>	33.55	22.78	26.21	17.42	17.40	1.93	0.39	0.43
<i>Eastern Anatolia</i>	94.12	40.63	66.04	29.96	58.10	-4.00	0.45	0.45
<i>Mediterranean</i>	55.79	53.67	38.83	34.99	-3.51	-6.68	0.43	0.54
<i>South Eastern Anatolia</i>	77.16	49.12	51.83	32.63	33.39	3.39	0.50	0.52

### Nonstationarity Impact Evaluation

The impacts of nonstationarities were estimated using GEV distribution for original/raw as well as bias-adjusted RCM for yearly maximum precipitation (Yearly AMP) and interpolated maps are presented in Figure 8.5 while the impact values at individual gridded stations are presented in Figure 8.6 on regional bases in form of bar plots. The overall look of the nonstationarity impact maps of original and bias-adjusted RCM suggest that magnitudes and direction of nonstationarity impacts more or less similar in both cases on a regional scale. However, interpolated maps given in Figure 8.5 and bar plots of the individual gridded station in Figure 8.6 shows that at grid scale, the magnitudes and direction of nonstationarities are found

to be inconsistent at many gridded stations. For example, gridded stations (17085 of Black Sea region, 17056, 17069, 17120 and 17152 of Marmara region, 17126, 17160 of Central Anatolia, 17094 of Eastern Anatolia, 17621 of South-Eastern Anatolia and 17140 of Mediterranean region) exhibited positive impacts using bias-adjusted RCM while negative impacts were found using original RCM. Similarly, few gridded stations (17052, 17116 of Marmara region, 17188, 17234 of Aegean region, 17120, 17270 and 17978 of South-Eastern Anatolia and 17240 of Mediterranean region) shows negative impacts using bias-adjusted RCM while these gridded stations were under the influence of positive impacts when using original RCM.

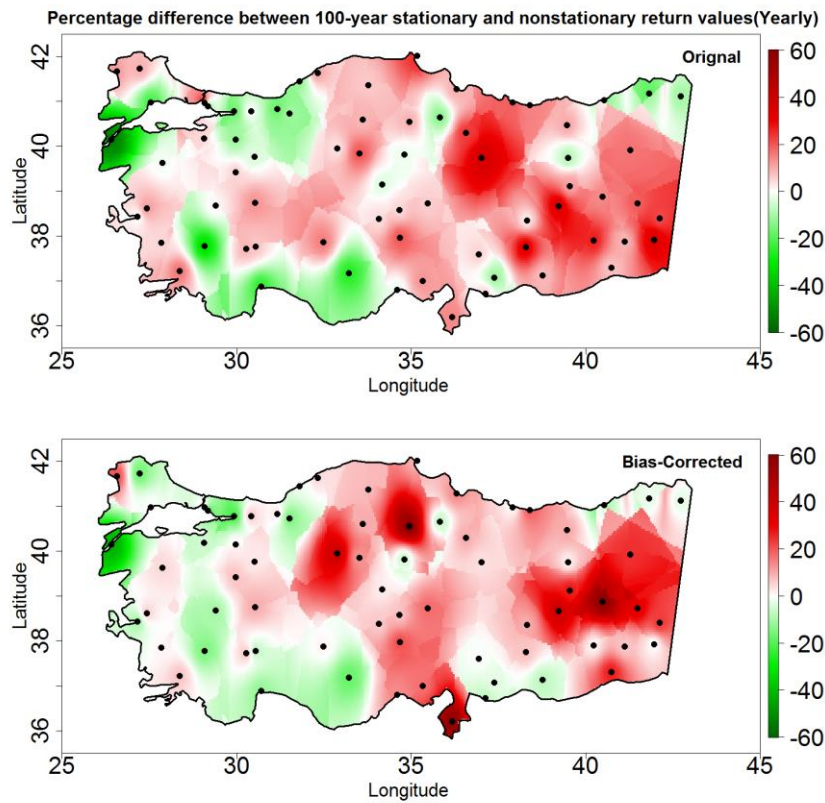


Figure 8.5 Comparison of nonstationarity impacts obtained from original and bias-adjusted RCM for Yearly AMPs

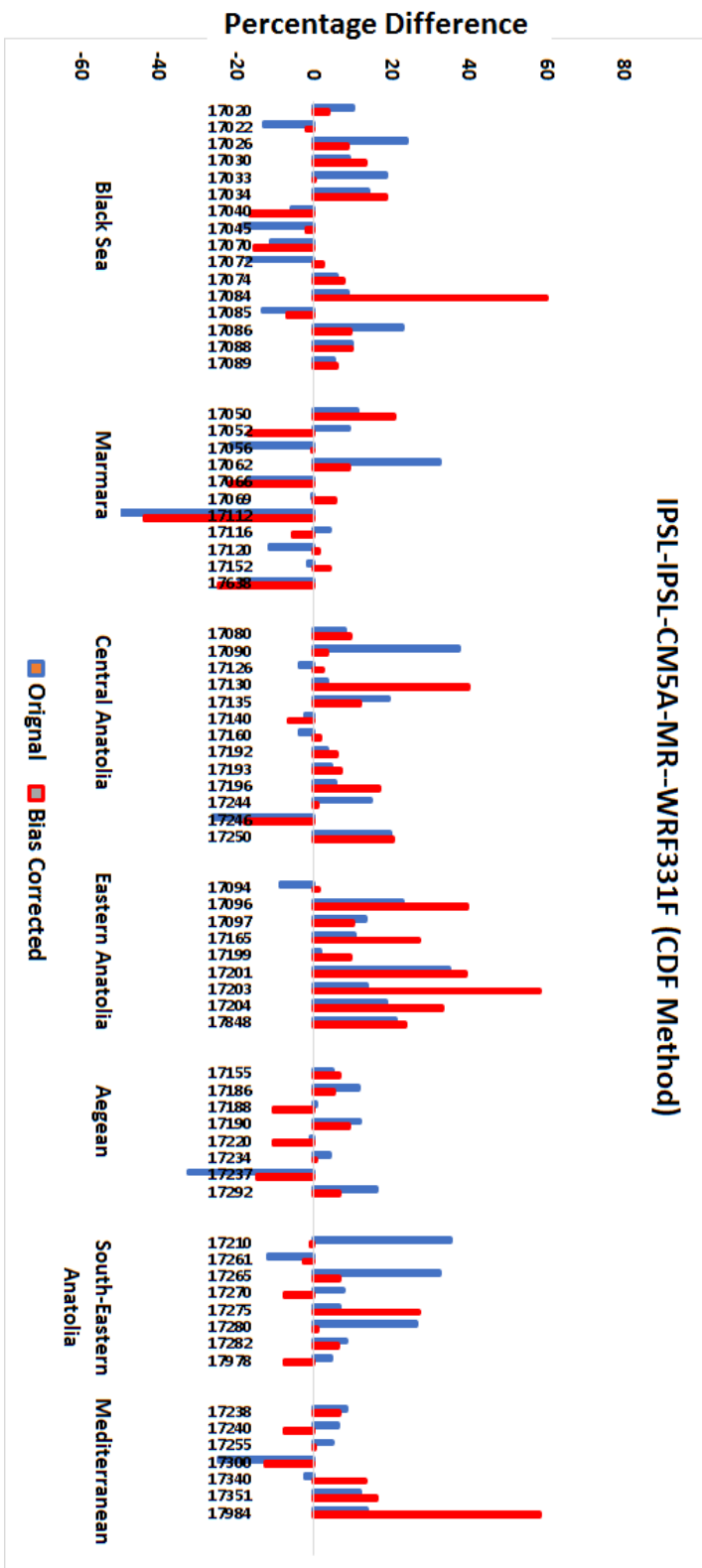


Figure 8.6 Bar charts of nonstationarity impact value at gridded stations obtained using original and bias-adjusted RCM for yearly AMPs

### 8.1.2. Temperature Analyses

#### 1)- CNRM-CERFACS-CNRM-CM5—CCLM4-8-7 (BDS Method)

##### a)- Performance Evaluation

Daily mean precipitation of raw and bias-adjusted models is plotted against observations during the reference period in Figure 8.7. The model performance statistics for original as well as bias-adjusted RCM is given in Table 8-3.

The plots show that for all regions there is a considerable improvement after bias correction throughout Turkey. The improvement was more evident during summer and mid of the year. Aegean region, Eastern Anatolia as well as Mediterranean region contained relatively more negative model biases in original RCM which were removed in case of bias-adjusted RCM. In the case of Marmara, South-Eastern Anatolia, and Black sea regions, smaller biases were present in the original RCM and after correction the biases further reduced. The performance statistics (*RMSE*, *MAE*, *MBE*, and *CORR*) also suggest improvement. Values of *RMSE* and *MAE* is found to be (approximately more than 60 percent) lower for bias-adjusted RCM than the Original RCM. Similarly, in all regions, *MBE* was relatively close to zero. However, even for bias-adjusted RCM, all negative biases were found in all regions with Marmara contained least (-0.13 and -0.55 for mean daily temperature and successive monthly average temperature respectively) negative bias values. Similarly, Eastern Anatolia contained the highest amount (-1.18 for daily mean as well as successive monthly average temperature) of negative biases. *CORR* values which were already more than 0.9 in all the regions in case of original RCM, were also found to be slightly more for bias-adjusted RCM.



Table 8-3 Performance evaluation statistic of original and bias-adjusted RCM

Region Name	RMSE (°C)		MAE (°C)		MBE (°C)		CORR	
	RAW	BC	RAW	BC	RAW	BC	RAW	BC
<b>A</b>	<b>Mean Daily Temperature Evaluation</b>							
<i>Aegean</i>	3.62	1.11	3.43	0.91	-3.43	-0.80	0.98	0.99
<i>Black Sea</i>	2.32	1.23	2.13	1.06	-2.13	-0.98	0.99	0.99
<i>Marmara</i>	1.48	0.84	1.19	0.67	-0.94	-0.13	0.98	0.99
<i>Central Anatolia</i>	2.69	1.04	2.43	0.84	-2.43	-0.56	0.99	0.99
<i>Eastern Anatolia</i>	3.82	1.41	3.58	1.25	-3.58	-1.18	0.99	0.99
<i>Mediterranean</i>	3.20	1.15	3.07	1.00	-3.07	-0.97	0.99	0.99
<i>South Eastern Anatolia</i>	2.21	1.03	2.03	0.90	-2.02	-0.84	0.99	0.99
<b>B</b>	<b>Successive Monthly Average Temperature</b>							
<i>Aegean</i>	4.27	2.33	3.70	1.82	-3.48	-0.80	0.94	0.95
<i>Black Sea</i>	3.15	2.55	2.56	1.98	-2.15	-0.99	0.94	0.94
<i>Marmara</i>	2.72	2.34	2.13	1.84	-0.99	-0.55	0.93	0.95
<i>Central Anatolia</i>	3.72	2.82	3.10	2.15	-2.45	-0.59	0.94	0.95
<i>Eastern Anatolia</i>	4.52	2.92	3.93	2.34	-3.61	-1.18	0.96	0.967
<i>Mediterranean</i>	3.80	2.14	3.29	1.72	-3.14	-0.98	0.95	0.97
<i>South Eastern Anatolia</i>	3.13	2.39	2.56	1.90	-2.07	-0.84	0.96	0.97

### b)- Nonstationarity Impact Evaluation

The impacts of nonstationarities were estimated using GEV distribution for original/raw as well as bias-adjusted RCM for yearly maximum temperature (Yearly AMTmax) and interpolated maps are presented in Figure 8.8 while the impact values at individual gridded stations are presented in Figure 8.9 on regional bases in form of bar plots.

Nonstationarity impact maps show that overall, both original and bias-adjusted RCM gave similar impacts of nonstationarities in term of direction as mostly positive

impacts were estimated in both cases. However, a few inconsistencies between magnitudes of nonstationarity impacts at few locations are evident from nonstationarity maps as well as bar plots. Also, few stations, for example, 17084 of Marmara, 17275, 17280 and 17282 of South-Eastern Anatolia exhibited opposite impacts of nonstationarities. Impacts of nonstationarities were estimated as negative in these gridded stations using bias-adjusted RCM while these gridded stations (like other stations) exhibited positive impacts when using original RCM.

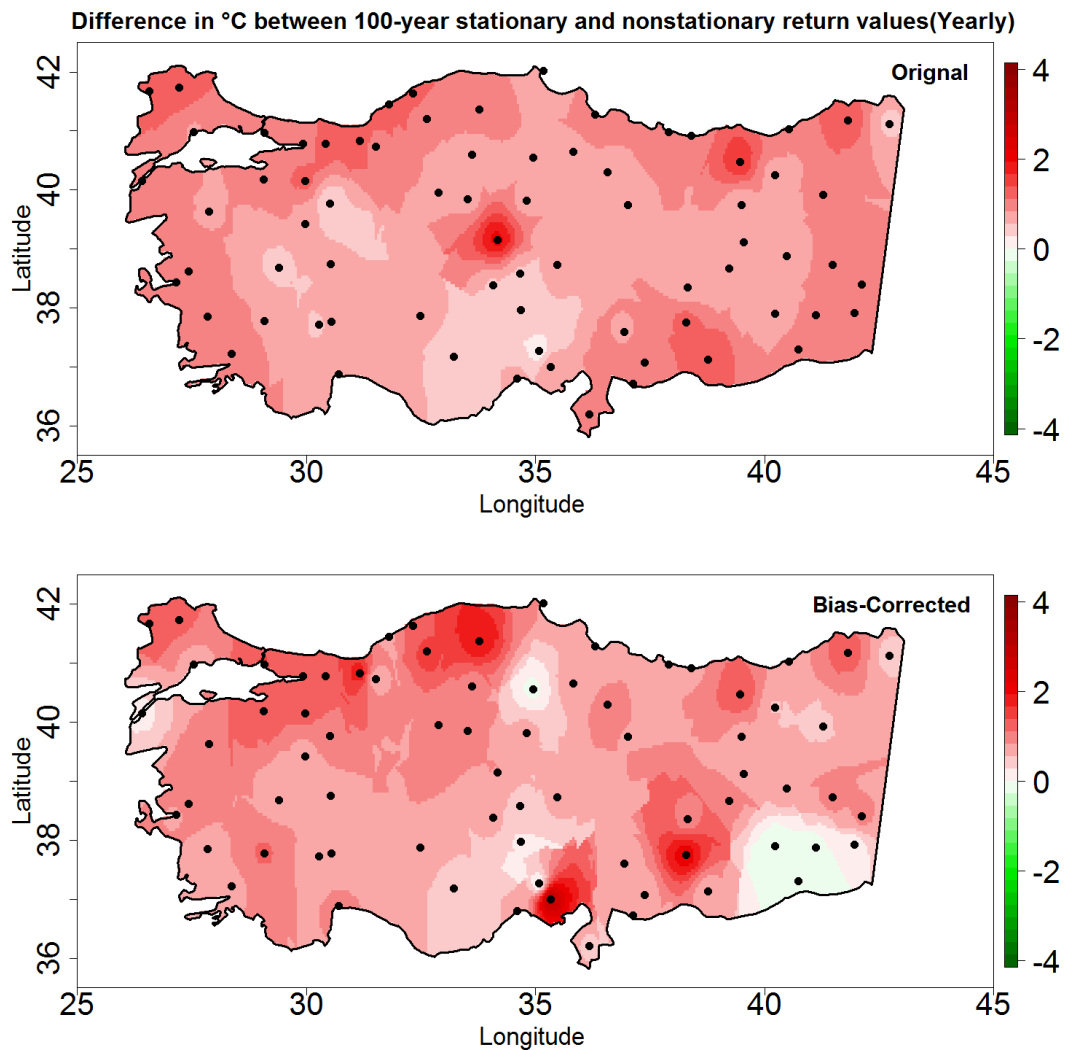


Figure 8.8 Comparison of nonstationarity impacts obtained using original and bias-adjusted RCM for Yearly AMTmax

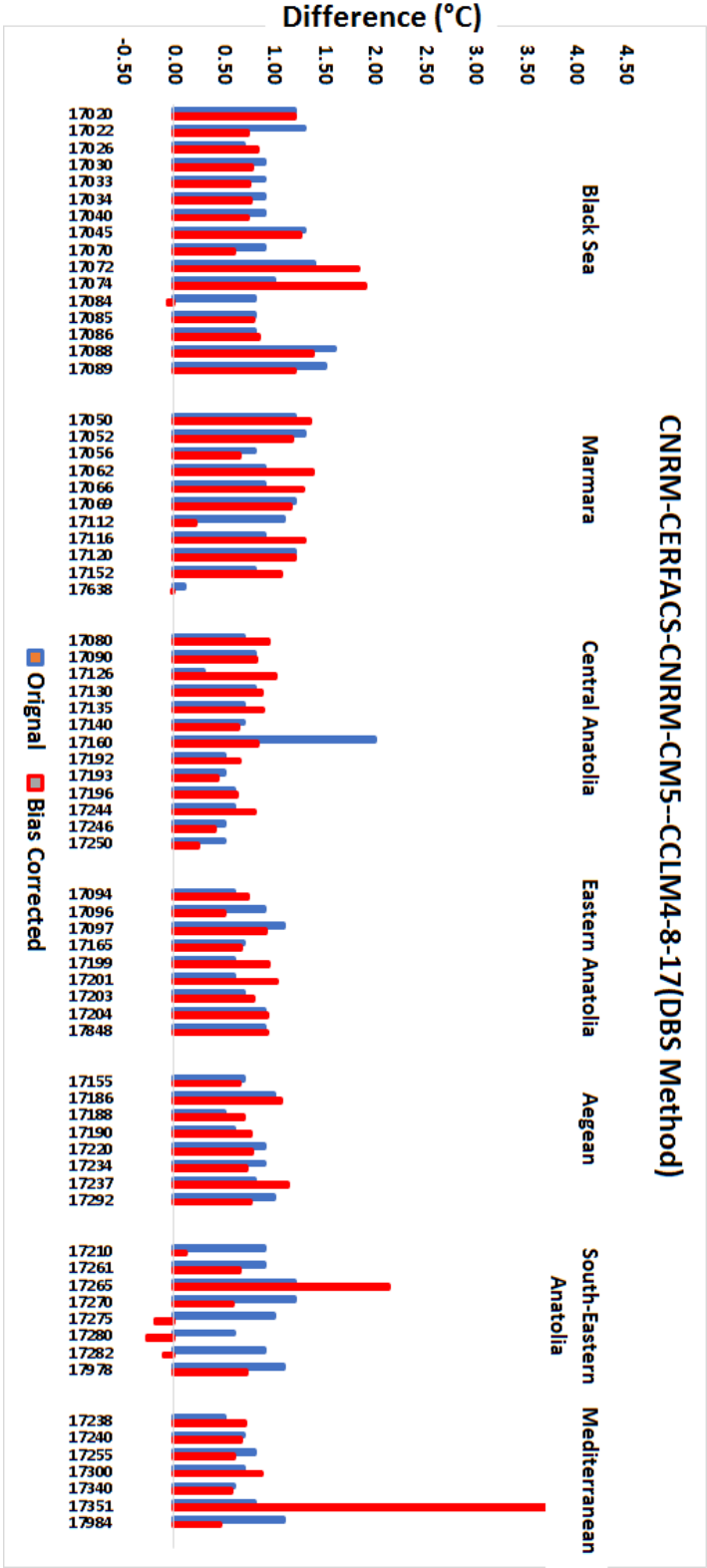


Figure 8.9 Bar chart of nonstationarity impact values at gridded stations obtained from original and bias-Adjusted RCM for AMTmax

## 2)- IPSL-IPSL-CM5A-MR—RCA4 (DBS Method)

### a)- Performance Evaluation

Daily mean precipitation of raw and bias-adjusted models is plotted against observations during reference period in Figure 8.10. The model performance statistics for original as well as bias-adjusted RCM is given in Table 8-4. The plots show that for all regions there is considerable performance enhancement after bias correction throughout Turkey. The improvement was found all over the year. In the case of Aegean, Mediterranean and South Eastern Anatolia regions, there were smaller biases found in original RCM during summer as compared to other seasons especially winter. So, most of the improvement is found in winter season from bias-adjusted RCM. Marmara region showed good agreement between observation as well as both original and bias-adjusted RCM data. Similarly, improvement in performance is clearly observable Black Sea region, Central Anatolia and Eastern Anatolia regions. Much of the betterment can be seen in Eastern Anatolia where the highest amount of negative biases was present in case of original RCM.

The performance statistics (*RMSE*, *MAE*, *MBE*, and *CORR*) also suggest improvement. Values of *RMSE* and *MAE* is found to be (approximately 50 percent) lower for bias-adjusted RCM than the Original RCM. Similarly, in all regions, *MBE* was relatively close to zero. However, even for bias-adjusted RCM, all negative biases were found in all regions with Marmara contained least (-0.34 and -0.83 for mean daily temperature and successive monthly average temperature respectively) negative bias values. Similarly, Eastern Anatolia contained the highest amount (-1.46 for daily mean as well as successive monthly average temperature) of negative biases. *CORR* values which were already more than 0.9 in all the regions in case of original RCM, were also found to be slightly more for bias-adjusted RCM.

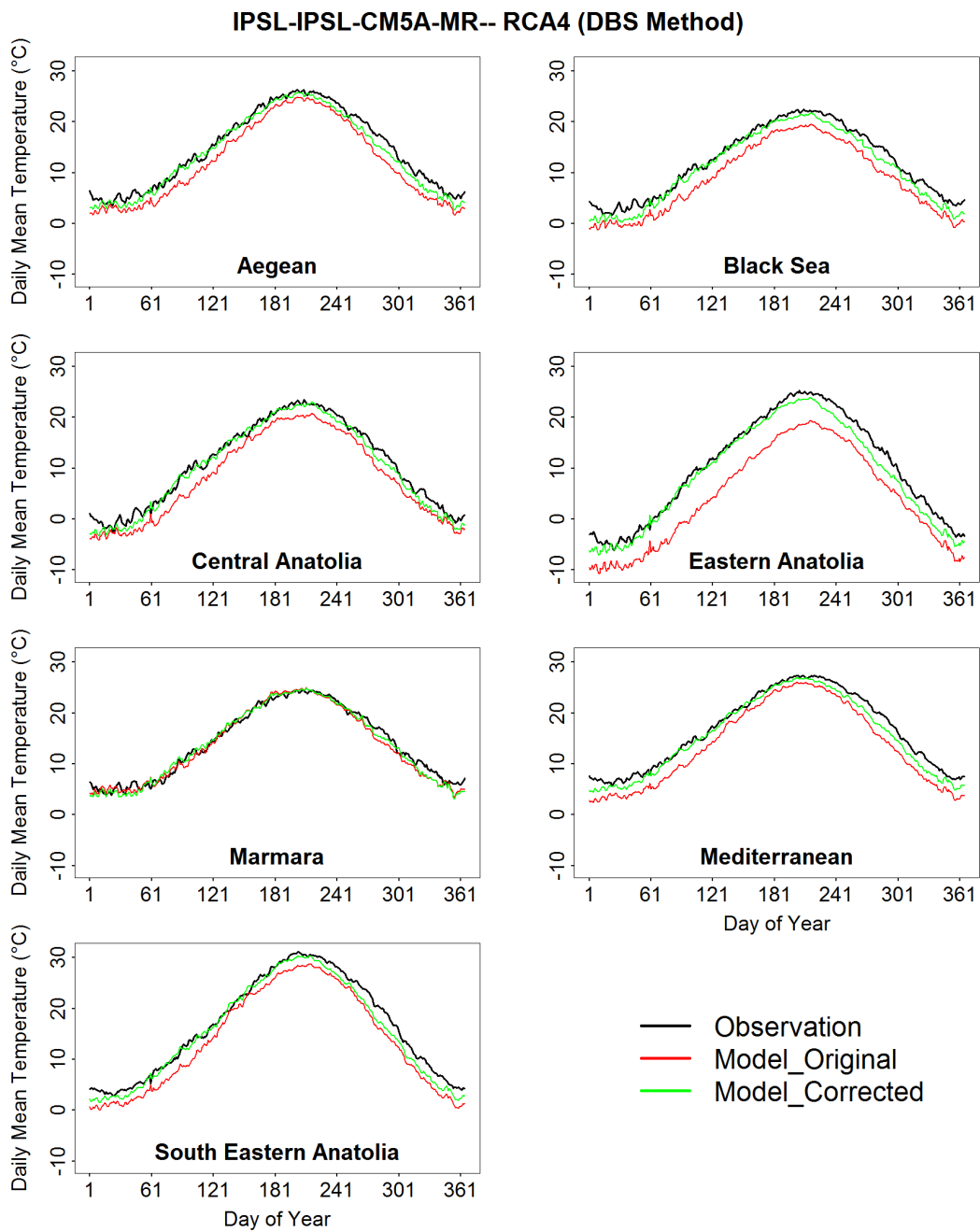


Figure 8.10 Comparison of observed mean daily temperature with original and bias-adjusted RCM

Table 8-4 Performance evaluation statistics of original and bias-adjusted RCM

Region Name	RMSE (°C)		MAE (°C)		MBE (°C)		CORR	
	RAW	BC	RAW	BC	RAW	BC	RAW	BC
<b>A</b>	<i>Mean Daily Temperature Evaluation</i>							
<i>Aegean</i>	2.77	1.35	2.58	1.12	-2.58	-0.92	0.99	0.99
<i>Black Sea</i>	3.49	1.56	3.40	1.30	-3.40	-1.22	0.99	0.99
<i>Marmara</i>	1.19	1.11	0.95	0.88	-0.49	-0.34	0.98	0.99
<i>Central Anatolia</i>	2.91	1.29	2.74	1.04	-2.73	-0.81	0.99	0.99
<i>Eastern Anatolia</i>	5.97	1.85	5.86	1.56	-5.86	-1.46	0.99	0.99
<i>Mediterranean</i>	3.15	1.42	2.96	1.20	-2.96	-1.12	0.99	0.99
<i>South Eastern Anatolia</i>	5.06	1.54	4.92	1.27	-4.92	-1.08	0.99	0.99
<b>B</b>	<i>Successive Monthly Average Temperature</i>							
<i>Aegean</i>	3.40	2.38	2.82	1.85	-2.58	-0.92	0.96	0.96
<i>Black Sea</i>	4.05	2.56	3.48	1.95	-3.39	-1.22	0.95	0.95
<i>Marmara</i>	2.33	2.40	1.79	1.83	-0.50	-0.83	0.95	0.95
<i>Central Anatolia</i>	3.86	2.86	3.15	2.16	-2.73	-0.85	0.95	0.96
<i>Eastern Anatolia</i>	6.49	3.03	5.90	2.39	-5.85	-1.46	0.96	0.97
<i>Mediterranean</i>	3.59	2.19	3.04	1.71	-2.97	-1.13	0.96	0.97
<i>South Eastern Anatolia</i>	5.44	2.51	4.93	1.96	-4.91	-1.08	0.97	0.97

### b)- Nonstationarity Impact Evaluation

The impacts of nonstationarities were estimated using GEV distribution for original/raw as well as bias-adjusted RCM for yearly maximum temperature (Yearly AMTmax) and interpolated maps are presented in Figure 8.11 while the impact values at individual gridded stations are presented in Figure 8.12 on regional bases in form of bar plots. Nonstationarity impact maps show that overall, both original and bias-adjusted RCM gave similar impacts of nonstationarities in term of direction as mostly positive impacts were estimated in both cases. However, a few inconsistencies between magnitudes of nonstationarity impacts at few locations are evident from nonstationarity maps as well as bar plots. For example, in case of

gridded stations 17020, 17074 of Black Sea region, 17135,17160 and 17193 of Central Anatolia and 17094 of Eastern Anatolia, original RCM exhibited significantly higher magnitudes of positive impacts than bias-adjusted RCM. Similarly, in case of gridded stations 17066 of Marmara, 17090 of Central Anatolia, 17203 of Eastern Anatolia and 17280 of South Eastern Anatolia, the estimated impacts of nonstationarities were much higher using bias-adjusted RCM than the original RCM.

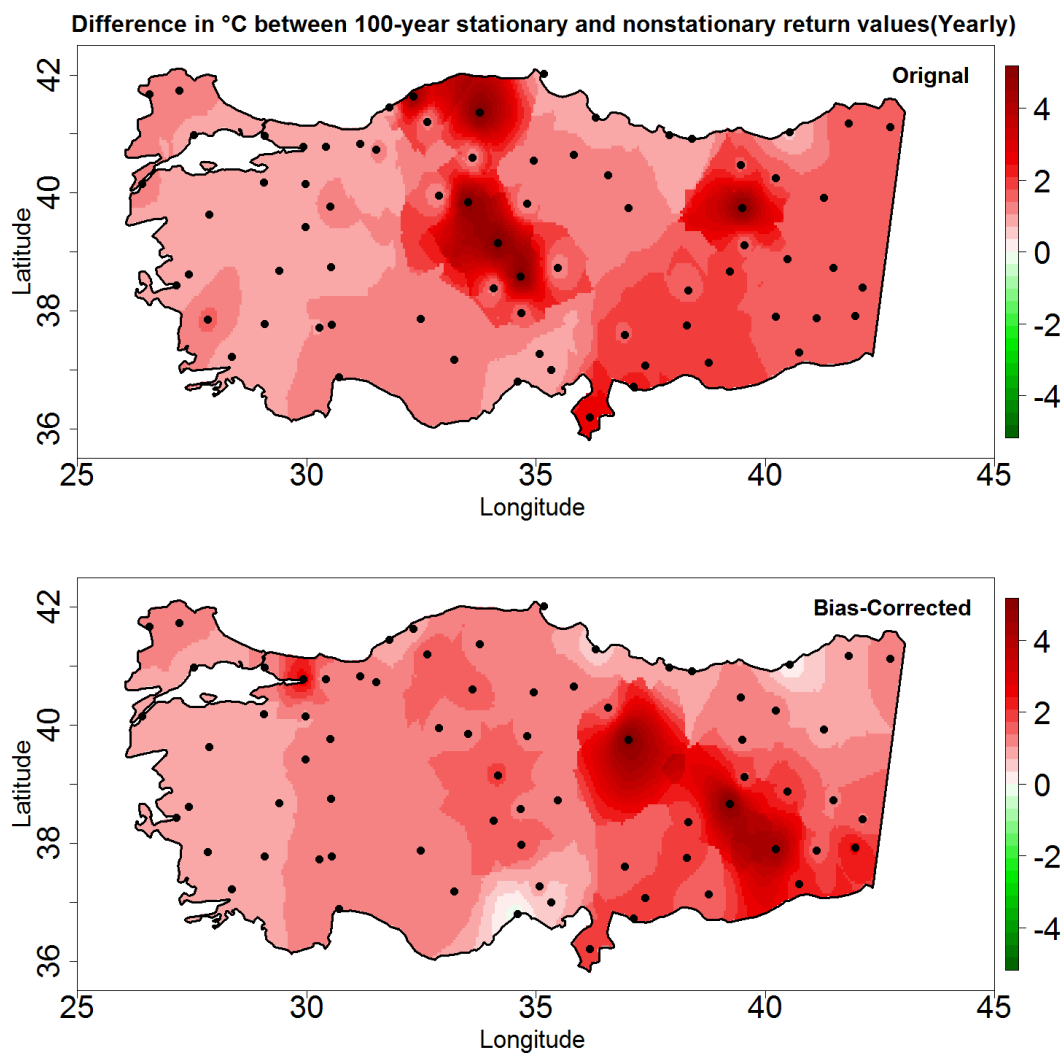


Figure 8.11 Comparison of nonstationarity impacts obtained using original and the bias-adjusted RCM for AMTmax

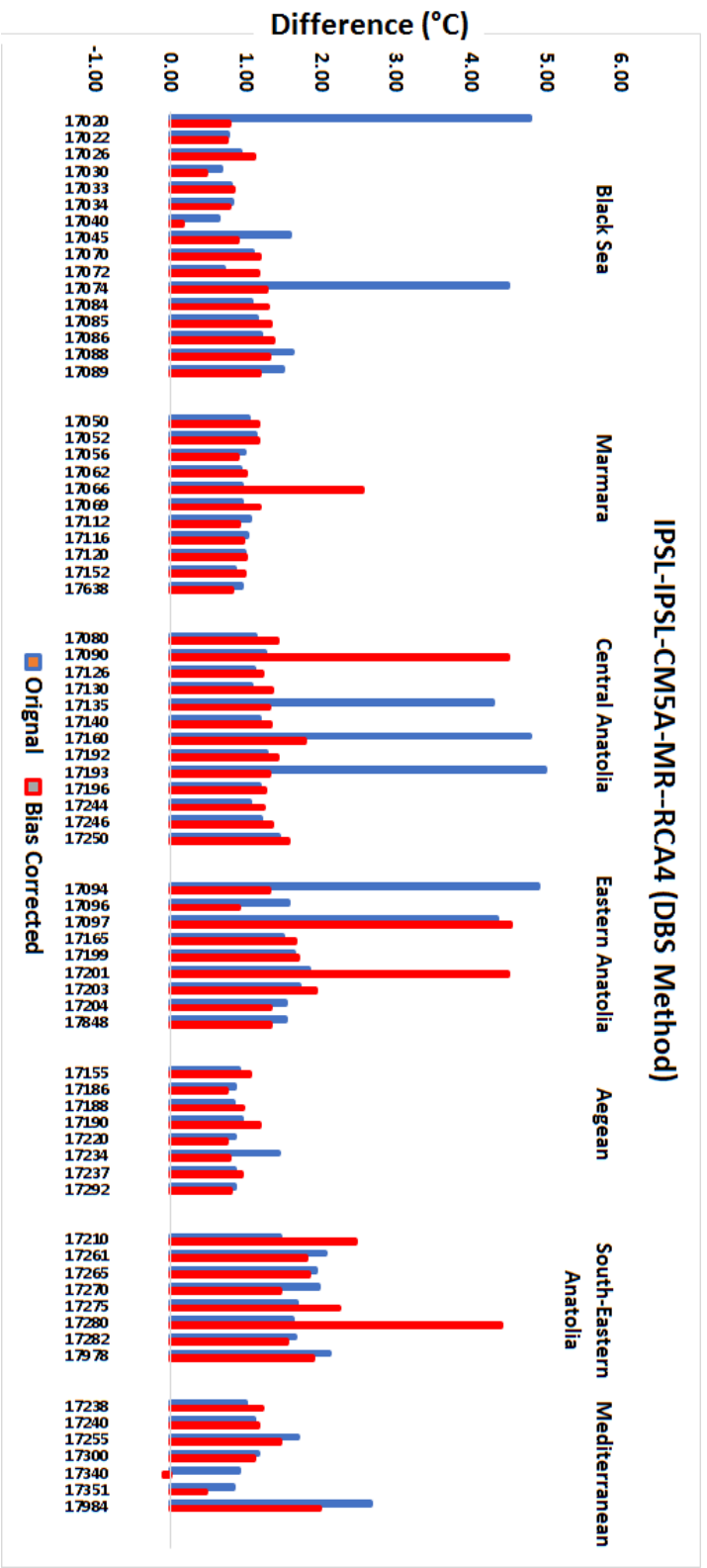


Figure 8.12 Bar charts of nonstationarity impact values at gridded stations obtained using original and bias-adjusted RCM for AMTmax

## 8.2. Discussion

Performance evaluation of bias-adjusted models using conventional performance indicators (like *RMSE*, *MBE*, *MAE*, and *CORR*) as well as their ability to preserve the nonstationarity signals. Initially, the improvement in bias-adjusted models is evaluated by comparing the bias-adjust model performance statistics with those of the original model. Then nonstationarities impacts were estimated using bias-adjusted model data using the stationary and nonstationary form of GEV distribution and these impacts were compared to those of the original model to examine if bias-adjust models can preserve the nonstationarity signals. Two bias-adjusted precipitation models (one with DBS correction method and other with CDF method) and two bias-adjusted temperature models (both with BDS method) are evaluated.

As results indicate, both bias correction methods for precipitation were able to improve the performance of RCMs. RMSE and MAE values were reduced, and MBE values were much closer to zero for bias-adjusted RCMs. Similarly, the CORR values also show significant improvement for both methods. The nonstationarity impact results show that in the case of DBS correction method, which was (applied to *CNRM-CERFACS-CNRM-CM5—CCLM4-8-7*), much of the nonstationarity signals were lost. At many gridded stations, the impacts of nonstationarity were altered to opposite direction. Even for the gridded stations where nonstationarity signals were preserved, the magnitudes were altered as results show significant decreases in the magnitude of nonstationarity impacts values. However, in case of RCM adjusted using CDF-t method (applied to model *IPSL-IPSL-CM5A-MR—WRF331F*) overall on a regional scale, the CDF-t method was able to preserve nonstationarity signal well, or at least better than DBS method. However, results suggested that for few gridded stations in different regions of Turkey, evidence was found where nonstationarity signals are lost or altered. But overall, CDF-t method preserved nonstationarity signals much better than the DBS method. It is also worth noting that there were more biases present in raw model *IPSL-IPSL-CM5A-MR—*

*WRF331F* than raw model *CNRM-CERFACS-CNRM-CM5—CCLM4-8-7*. So, CDF-t method in spite of removing more biases as compared to the DBS method, the nonstationarity signals were better preserved. This makes CDF-t method a better choice in overall reducing model biases while preserving the future climate nonstationarity signals. However, at local/station scale much care is needed while applying CDF-t method, as results are evident of the fact that inconsistencies might occur as nonstationarity signals might be lost or alter at local/ station scale.

The performance of two bias-adjusted temperature RCMs (*CNRM-CERFACS-CNRM-CM5—CCLM4-8-7* and *IPSL-IPSL-CM5A-MR—RCA4* both corrected by using DBS), was evaluated. The results indicate that unlike for precipitation, DBS method was able to preserve climate nonstationarity signals in both bias-adjusted RCMs. Magnitude and direction of nonstationarity impacts were mostly consistent in original and bias-adjusted RCM data which makes DBS method usable for temperature correction while preservation of nonstationarity signals.



## CHAPTER 9

### SUMMARY AND CONCLUSIONS

#### 9.1. Summary

This thesis describes research in which impacts of nonstationarities in minimum and maximum temperatures and precipitation were assessed at annual and seasonal scales for historical and projection periods throughout Turkey. Impact analyses within both periods were also performed for high and low streamflow of Upper Euphrates basin. The CORDEX-driven 12 ensemble model pairs were used for future projection (2051-2100) analyses. A conceptual water balance model of HBV-light was used to estimate future streamflow values using the CORDEX-driven inputs.

CORDEX performance evaluation suggests that in most of the regions in Turkey, generally RCMs originated from GCMs EC-EARTH and HadGEM2-ES were able to represent the seasonal variability of precipitation better than RCMs originated from GCMs CNRM-CM5 and IPSL-CM5A-MR. RCMs originated from GCM CNRM-CM5 and RCM WRF331F coupled with IPSL-CM5A-MR were found to be the worst models in most of the region in Turkey for precipitation. CORDEX performance evaluation suggests that in most of the regions in Turkey, generally RCMs originated from GCMs EC-EARTH and HadGEM2-ES were able to represent the seasonal variability of precipitation better than RCMs originated from

GCMs CNRM-CM5 and IPSL-CM5A-MR. RCMs originated from GCM CNRM-CM5 and RCM WRF331F coupled with IPSL-CM5A-MR were found to be the worst models in most of the region in Turkey for precipitation. For temperature, in most of the regions of Turkey, RCM CCLM4-8-17 coupled with GCM HadGEM2-ES was found to be the best model. RCMs RACMOO22E and RCA4 coupled with GCM IC-EARTH and RCMs ALADIN53 and CCLM4-8-17 coupled with GCM CNRM-CM5 performed worse for most of the regions in Turkey for temperature emulation. Most of the models underestimated temperatures in many regions.

Overall comparison of negative log-likelihood values suggests that GEV which is a three-parameter distribution provides a better fit for all hydroclimatological variables used in this study. For precipitation, amongst two parameter distributions, lognormal was better while normal was found to be worst. Similarly, in case of temperature normal distribution provided a better fit than gumbel distribution particularly for maximum temperature. The fitting performance was overall similar in yearly and seasonal scales. Even though GEV (originally with three parameters) is most commonly used distribution for such studies, however, the results of this thesis show that other simpler distributions were also able to predict nonstationarity impacts similar to those obtained using GEV for a different variable in different regions. Most of the distributions (particularly GEV and lognormal) has shown that the impacts of nonstationarities for yearly maximum precipitation were positive in most of the Aegean, Marmara, Mediterranean, and Black Sea region however mixed type of impacts were recorded for Eastern Anatolia, South-Eastern Anatolia as well as Central Anatolia regions of Turkey.

Analyses based on historical data suggest that more intense precipitation extremes are expected during winter in the eastern part of Central Anatolia, most of the Mediterranean, Aegean, and Marmara region. Eastern Anatolia (mostly positive) and South-Eastern Anatolia (mostly negative) exhibited the mixed type of impacts on winter extreme precipitation. During the spring season, impacts of nonstationary

were positive on precipitation extremes in the Aegean region, and some parts of Marmara, Black Sea region as well as central part of Turkey. Other regions like Eastern Anatolia, South-Eastern Anatolia and most of the Mediterranean regions are under negative impacts. Mixed type of impacts is present in most of the regions during summer while positive impacts were recorded during the autumn season in most of Turkey with few exceptions in Central Anatolia. The ensemble analyses during projection period (2051-2100) provided an evidence that in many regions (particularly in the eastern part of Turkey), the present status of nonstationarities (impact types and magnitude) might alter over a longer period particularly during the spring season. The inconsistencies between nonstationarity impacts during historical and projection period were also significant in Eastern Anatolia, South-Eastern Anatolia and eastern part of Central Anatolia as many stations exhibiting negative impacts during historical period released positive impacts during the projection period.

Nonstationary impacts analyses during historical period show considerable increases in return levels of yearly minimum as well as yearly maximum temperature during summer throughout Turkey (except few locations in the Black Sea and Marmara region where summer extremes of maximum temperature are reduced). This indicates the plausible hotter summers with possible more intense heat waves as time passes. Increases in return levels of maximum and minimum temperature during winter suggest that winter is expected to be more moderate through the time in many parts of Turkey. However, some locations in Marmara and Aegean region might experience slightly colder winter because of negative impacts of nonstationarities. The nonstationary impact results during the projection period showed remarkable increases in 100-year return values for yearly as well as seasonal minimum and maximum temperatures. These increases are spatially more widespread in the case of projection as compared to observation. Results also suggest that at some locations (e.g., few stations in the Black Sea and Marmara region for yearly as well as summer AMTmax, in Central Anatolia and Black Sea region during winter, some areas of

eastern Turkey as well as Aegean region during spring) the impacts from current to future period turned opposite. Similar changes are also recorded for yearly as well as seasonal AMT<sub>min</sub>. The magnitude of positive impacts was larger for minimum temperatures than that for maximum temperatures both in yearly and seasonal scales during historical as well as projection periods.

For observed yearly maximum streamflow four stations (2122,2124,2156 and 2157) have shown positive impacts while remaining four stations (2102, 2133,2145 and 2164) have shown negative impacts using all three (GEV, gumbel and normal) distributions. Nonstationarities found to have significant impacts on seasonal AMFs. Low flows with nonstationarity increase in six out of eight sub-basins in Upper Euphrates basin on yearly and four seasons. On the other hand, only in two of the sub-basins low flows decrease with nonstationarity. Ensemble analyses of annual high flows during the projection period found evidence that all three stations used in future projection analyses exhibited negative impacts. Only one sub-basin (2157) has shown opposite impact from observation to the future period while other two sub-basins have shown no change in the impact type. Ensemble analyses of high flows shown that return levels are increasing during winter and autumn in all three stations while summer has shown decreases. Positive impacts were obtained from ensemble results of projected yearly as well as seasonal low flows at all three watersheds. Results of winter low flows of projected streamflow suggest considerable positive impacts. In most of the cases, impact types were consistent for low flow during historical as well as projection periods.

After the bias-correction was applied to precipitation, nonstationarity signals were mostly preserved by CDF transformation overall in Turkey. However, BDS method was not much trustable in preserving the climate nonstationarities. Nevertheless, both methods have provided poor performance in preserving the signals after bias correction at the local scale. However, both bias-adjusted models have mostly preserved the nonstationarity signal were for temperature.

## 9.2. Conclusions

Following conclusions can be drawn from the research described in this thesis:

- Members of the ensemble approach via CORDEX can be increased for better documenting the model uncertainties in different regions. Especially increasing the number of driving models (GCM) rather than RCM is more essential for ensemble analyses as they originate the source of errors. Uncertainties coming from ensemble members are more critical as compared to the distribution related uncertainties. However, regions particularly for temperature, where most of the ensemble members provide homogenous impact, smaller ensemble size or even single model, might be useful for future impact studies.
- Planning and operational strategies of water conservation, irrigation scheduling, and hydropower generation become critically important as warming due to nonstationarities in historical and projection periods causes less snow accumulation and shift in timing of snowmelt runoff peak to earlier in mountainous regions of Turkey including Upper Euphrates basin. Besides, a possible water stress will get aggravated through evapotranspiration losses in summer.
- Results of nonstationarity impacts should be incorporated in design procedures as design values might increase or decrease over time. Risk and reliability analyses are recommended at a local scale to investigate if these nonstationarity impacts are within the safety as well the economic limits of any hydraulic structure designed using the assumption of stationarity.
- Projections provided an evidence that in many regions (particularly in the eastern part of Turkey), the present status of nonstationarities (impact types

and magnitude) might alter over a longer period. This, in turn, might affect the planning strategies of hydraulic structures in those regions.

- Adaptation to climate change under these nonstationary conditions becomes critically important as the extreme variables mostly increase and occur more frequently.

### **9.3. Recommendations**

Outputs from higher number of GCMs are recommended to make use of ensemble analyses approach in a better sense.

Even though GEV (originally with three parameters) is most commonly used distribution for such studies, however, the results of this thesis show that other simpler distributions were also able to predict nonstationarity impacts similar to those obtained using GEV for a different variable in different regions. So, these simpler distributions might be more helpful in some regions because of their simplicity.

More local/station scale studies are required as the problem might get worse because of increases in return levels of minimum and maximum temperature coupled with increased precipitation extremes at the same time.

Moderate emission scenario can be studied to limit the range of nonstationarity effects. In addition, such nonstationarity effects can be studied for the shorter time period (by the mid of the century). More attention is suggested while using bias-adjusted models since bias correction methods have a tendency to lose nonstationarity signals even though they improved the model performance substantially.

Considering the effects of seasonal variability and vulnerability to climate change, it is strongly recommended to adapt similar methodology in Pakistan for better documentation of implication of nonstationary climate conditions. This methodology might also be helpful in better understanding the temporal shifts in snowmelt runoff in response to nonstationary temperatures as well as changing precipitation patterns, frequencies and intensities in mountainous areas of the northern Pakistan.



## REFERENCES

- Aksoy, Hafzullah, N., Unal, E., Alexandrov, V., Dakova, S., and Yoon, J. (2008). Hydrometeorological analysis of northwestern Turkey with links to climate change. *International Journal of Climatology*, 28: 1047-1060
- Aniya, M. (1999). Recent glacier variations of the Hielos Patagónicos, South America, and their contribution to sea-level change. *Arctic, Antarctic, and Alpine Research*, 31: 165-173
- Bayazit, M. *Environ. Process.* (2015). 2: 527. <https://doi.org/10.1007/s40710-015-0081-7>
- Bergström, S. (1976). Development and application of a conceptual runoff model for Scandinavian catchments. SMHI RHO 7. Norrköping.
- Bergström, S. (1990). Parametervärden för HBV-modellen i Sverige, Erfarenheter från modelkalibreringar under perioden 1975-1989 (Parameter values for the HBV model in Sweden, in Swedish), SMHI Hydrologi, No.28, Norrköping.
- Bergström, S. (1992). The HBV model - its structure and applications. SMHI Reports RH, No. 4, Norrköping.
- Bozkurt, D. and Sen, O.L. (2013). Climate change impacts in the Euphrates–Tigris Basin based on different model and scenario simulations. *Journal of Hydrology*, 480 149-161. <https://doi.org/10.1016/j.jhydrol.2012.12.021>
- Bozkurt, D., Sen, O.L., Hagemann, Stefan. (2015). Projected river discharge in the Euphrates-Tigris Basin from a hydrological discharge model forced with RCM and GCM outputs. *Climate Research*. 62. 131-147. 10.3354/cr01268.
- Castillo, E. (1988). *Extreme Value Theory in Engineering* (Academic Press, San Diego, 1988).2.
- Coles, S. (2001). *An Introduction to Statistical Modeling of Extreme Values*. Springer Series in Statistics. Springer Verlag London.
- Cooley, D. (2013). Return periods and return levels under climate change. Chapter 4, *Extremes in a changing climate: Detection, analysis and uncertainty*, A. AghaKouchak, D. Easterling, and K. Hsu, eds., Vol. 65, Springer, New York. [https://doi.org/10.1007/978-94-007-4479-0\\_4](https://doi.org/10.1007/978-94-007-4479-0_4)

- Dalfes, H.N., Karaca, M., and Sen, O.L. (2007). Climate change scenarios for Turkey in "Climate Change & Turkey: Impact, Sectoral Analyses, Socio-Economic Dimensions. Ankara: United Nations Development Programme (UNDP) Turkey Office.
- Donat, G. Markus, Lowry A L, Alexander L V, O’Gorman Paul A. Maher N. (2016). More extreme precipitation in the world’s dry and wet regions. *Nature Climate Change*. <http://dx.doi.org/10.1038/nclimate2941>
- Dowdeswell, J.A., Hagen, J.O., Björnsson, H., Glazovsky, A.F., Harrison, W.D., Holmlund, P., Jania, J. (1997). The Mass Balance of Circum-Arctic Glaciers and Recent Climate Change. *Quaternary Research*, 48: 1-14. <https://doi.org/10.1006/qres.1997.1900>
- Du Tao, Lihua Xiong, Chong-Yu Xu, Christopher J. Gippel, Shenglian Guo, Pan Liu. (2015). Return period and risk analysis of nonstationary low-flow series under climate change” *Journal of Hydrology* 527 (2015) 234–250. <https://doi.org/10.1016/j.jhydrol.2015.04.041>
- Emori, S., and Brown S. J. (2005). Dynamic and thermodynamic changes in mean and extreme precipitation under changed climate, *Geophys. Res. Lett.*, 32, L17706. <https://doi.org/10.1029/2005GL023272>
- Endris, Hussen Seid & Omondi, P & Jain, Suman & Lennard, Chris & Hewitson, Bruce & Chang, Ladislaus & Awange, Joseph & Dosio, Alessandro & Ketiem, Patrick & Nikulin, Grigory & Panitz, Hans-Jürgen & Büchner, Matthias & Stordal, Frode & Tazalika, Lukiya. (2013). Assessment of the Performance of CORDEX Regional Climate Models in Simulating East African Rainfall. *Journal of Climate*. 26. 8453–8475.
- Ertürk, A., Ekdal, A., Gürel, M., Karakaya, N., Guzel, C., and Gönenç, E. (2014). Evaluating the impact of climate change on groundwater resources in a small Mediterranean watershed. *Science of the Total Environment*, xxx xxx–xxx (Article in Press). <https://doi.org/10.1016/j.scitotenv.2014.07.001>
- Ezber, Y., Sen, O.L., Kindap, T., and Karaca, M. (2007). Climatic effects of urbanization in Istanbul: a statistical and modeling analysis. *International Journal of Climatology*, 27: 667-679. <https://doi.org/10.1002/joc.1420>
- Fischer E, Knutti R. (2015). Anthropogenic contribution to global occurrence of heavy-precipitation and high-temperature extremes. *Nature Climate Change*. 5. 560–564 (2015). <http://dx.doi.org/10.1038/nclimate2617>
- Flato, Gregory & Marotzke, J & Abiodun, Babatunde & Braconnot, P & Chou, Sin Chan & Collins, W & Cox, Peter & Driouech, Fatima & Emori, S & Eyring, Veronika & Forest, Chris & Gleckler, P & Guilyardi, Eric & Jakob, C &

- Kattsov, V & Reason, C & Rummukainen, M. (2013). Evaluation of climate models. Chapter 9 in climate change 2013: the physical science basis. Contribution of Working Group I to the Fifth Assessment Report of the Intergovernmental Panel on Climate Change.
- Fujihara Y., Tanaka K, Nagano T, Watanabe T, Kojiri T. (2007). Assessing the impact of climate change on the water resources of the Seyhan river basin Turkey, Vol. 1. River Basin Management International Congress: Antalya, Turkey; 453 – 463. <https://doi.org/10.1016/j.jhydrol.2008.01.024>
- Giorgi, F., Colin, J., Asrar, G. (2008). Addressing climate information needs at the regional level: The CORDEX framework. WMO Bull. 53.
- Givati, A., and Rosenfeld, D. (2013). The Arctic Oscillation, climate change and the effects on precipitation in Israel. Atmospheric Research, 132-133: 114-124. <https://doi.org/10.1016/j.atmosres.2013.05.001>
- Gokturk OM, Bozkurt D, Sen OL, Karaca M. (2008). Quality control and homogeneity of Turkish precipitation data. Hydrol. Process. 22(16): 3210 – 3218. <https://doi.org/10.1002/hyp.6915>
- Gómez Martín, Ma. (2005). Weather, Climate and Tourism. A Geographical Perspective. Annals of Tourism Research, 32(3), 571-591. <https://doi.org/10.1016/j.annals.2004.08.004>
- Gordon, N. and Shaykewich, J. (2000). Guidelines on performance assessment of public weather services. WMO/TD No. 1023, 32 pp.
- Gumbel, E. J. (1941). "The return period of flood flows." Ann. Math. Stat., 12(2), 163–190. <http://doi:10.1214/aoms/1177731747>
- Hardwick Jones, Rhys & Westra, Seth & Sharma, Ashish. (2010). Observed relationships between extreme sub-daily precipitation, surface temperature, and relative humidity. Geophysical Research Letters. 37. 22805. <https://doi.org/10.1029/2010GL045081>
- Harmancıoğlu, N.B., Özkul, S., Fıstıkoğlu, O., Barbaros, F., Onuşluel, G., Çetinkaya, C.P., and Dalkılıç, Y. (2007). Modeling for climate change effects in the Gediz and Büyük Menderes river basins in "Climate Change & Turkey: Impacts, Sectoral Analyses, Socio-Economic Dimensions". Ankara: United Nations Development Programme.
- Hatfield, Jerry & H. Prueger, John. (2015). Temperature extremes: Effect on plant growth and development. Weather and Climate Extremes. 10. WACED1400046. <https://doi.org/10.1016/j.wace.2015.08.001>

- Heffernan J., Stephenson A. (2012). ismev: An Introduction to Statistical Modeling of Extreme Values. R package version 1.39, Original S functions written by Janet E. Heffernan with R port and R documentation provided by Alec G. Stephenson, URL <https://CRAN.R-project.org/package=ismev>.
- Hu, Y. & Ritchie, J. (1993). Measuring destination attractiveness: a contextual approach. *Journal of Travel Research*, 32(20), 25-34. <https://doi.org/10.1177/004728759303200204>
- IPCC 2007. *Climate Change 2007: Impacts, Adaptation, and Vulnerability*, Parry ML, OF Canziani, Palutikof JP, van der Linden PJ, Hanson CE (eds). Cambridge University Press: Cambridge, UK.6
- IPCC (2000). *IPCC special report: emission scenarios*. Cambridge University Press, Cambridge, United Kingdom and New York, NY, USA.
- IPCC (2012). Glossary of terms. In: *Managing the Risks of Extreme Events and Disasters to Advance Climate Change Adaptation* [Field, C.B., V. Barros, T.F. Stocker, D. Qin, D.J. Dokken, K.L. Ebi, M.D. Mastrandrea, K.J. Mach, G.-K. Plattner, S.K. Allen, M. Tignor, and P.M. Midgley (eds.)]. A Special Report of Working Groups I and II of the Intergovernmental Panel on Climate Change (IPCC). Cambridge University Press, Cambridge, UK, and New York, NY, USA, pp. 555-564.
- IPCC (2013). *Climate Change 2013: The Physical Science Basis. Contribution of Working Group I to the Fifth Assessment Report of the Intergovernmental Panel on Climate Change* [Stocker, T.F., D. Qin, G.-K. Plattner, M. Tignor, S.K. Allen, J. Boschung, A. Nauels, Y. Xia, V. Bex and P.M. Midgley (eds.)]. Cambridge University Press, Cambridge, United Kingdom and New York, NY, USA, 1535 pp.
- IPCC (2014). *Climate Change 2014: Impact, Adaptation, and Vulnerability. Contribution of Working Group II to the Fifth Assessment Report of the Intergovernmental Panel on Climate Change*. Cambridge University Press, Cambridge, United Kingdom and New York, NY, USA.
- Kadıoğlu, M. (1997). Trends in surface air temperature data over Turkey. *International Journal of Climatology*, 17: 511-520.
- Kahya, E. and Kalaycı, S. (2004). Trend analysis of streamflow in Turkey. *Journal of Hydrology*, 289: 128-144. <https://doi.org/10.1016/j.jhydrol.2003.11.006>
- Kahya, E. and Karabörk MÇ. (2001). The analysis of El Nino and La Nina signals in streamflows of Turkey. *Int. J. Climatol.* **21**: 1231 – 1250. <https://doi.org/10.1002/joc.663>

- Kara F., Yucel, I., Zuhail, A. (2016). Climate change impacts on extreme precipitation of water supply area in Istanbul: use of ensemble climate modelling and geo-statistical downscaling, *Hydrological Sciences Journal*, 61:14, 2481-2495. <https://doi.org/10.1080/02626667.2015.1133911>
- Karl, T.R., Ya Groisman, P., Knight, R.W., and Heim Jr, R.R. (1993). Recent Variations of Snow Cover and Snowfall in North America and Their Relation to Precipitation and Temperature Variations. *Journal of Climate*, 6: 1327-1344. [https://doi.org/10.1175/1520-0442\(1993\)006<1327:RVOSCA>2.0.CO;2](https://doi.org/10.1175/1520-0442(1993)006<1327:RVOSCA>2.0.CO;2)
- Karl, T. R., and Trenberth K. E. (2003). *Modern Global Climate Change*. Vol. 302, Issue 5651, pp. 1719-1723, doi:10.1126/science.1090228
- Kartz R.W., and Brown B.G. (1992). Extreme events in changing climate: variability is more important than averages, *Clim. Change*, 21(3), 289-302
- Katz, R. W. (2013). "Statistical methods for nonstationary extremes." Chapter 2, *Extremes in a changing climate: Detection, analysis and uncertainty*, A. AghaKouchak, D. Easterling, and K. Hsu, eds., Vol. 65, Springer, New York.
- katz, R.W., Parlange, M. B., and Naveau, P. (2002). "Statistics of extremes in hydrology." *Adv. Water Resour.*, 25(8), 1287–1304
- Kozak, N., Uysal, M. & Birkan, I. (2008). An analysis of cities based on tourism supply and climatic conditions in Turkey. *Tourism Geographies*, 10(1), 81-97.
- Kum, G. and Çelik, M.A. (2014). Impacts of global climate change on the Mediterranean Region: Adana as a case study. *Procedia - Social and Behavioral Sciences*, 120: 600-608.
- Lawrence, D., Haddeland, I., and Langsholt, E. (2009). Calibration of HBV hydrological models using PEST parameter estimation. OSLO: Norwegian Water Resources and Energy Directorate.
- Leadbetter, M. R. (1983). "Extremes and local dependence in stationary sequences." *Probab. Theory Related Fields*, 65(2), 291–306.
- Lenderink, Geert & van Meijgaard, Erik. (2008). Increase in hourly precipitation extremes beyond expectations from temperature. *Nature Geoscience - NAT GEOSCI.* 1. 511-514. 10.1038/ngeo262.
- Linnenluecke, M.K., Stathakis, A., and Griffiths, A. (2011). Firm relocation as adaptive response to climate change and weather extremes. *Global Environmental Change*, 21: 123-133.

- Luhunga, Philbert & Botai, Ondego & Kahimba, Frederick. (2016). Evaluation of the performance of CORDEX regional climate models in simulating present climate conditions of Tanzania. *Journal of Southern Hemisphere Earth System Science*. 66. 32-54. 10.22499/3.6601.005.
- Maraun, D. (2016). Bias correcting climate change simulations—a critical review. *Curr Clim Change Rep* 2(4):211–220. doi: 10.1007/s40641-016-0050-x
- Meier, H.E.M., Höglund, A., Döscher, R., Andersson, H., Löptien, U. and Kjellström, E. 2011. Quality assessment of atmospheric surface fields over the Baltic Sea from an ensemble of regional climate model simulations with respect to ocean dynamics, *Oceanologia*, 53(1-TI), 193–227.
- Milly, P. C. D., et al. (2008). “Stationarity is dead: Whither water management?” *Science*, 319(5863), 573–574.
- Min, E., Hazeleger, W., Oldenborgh, G.J. and Sterl, A. 2013. Evaluation of trends in high temperature extremes in northwestern Europe in regional climate models, *Environ. Res. Lett.*, 8. doi:10.1088/1748-9326/8/1/014011.
- Mirza, M.M.Q. (2003). Climate change and extreme weather events: can developing countries adapt? *Climate Policy*, 3: 233-248.
- Moglen, G. E. (2003). “Frequency analysis under nonstationary landuse conditions.” Chapter 13, *Modeling hydrologic change—Statistical methods*, R. H. McCuen, ed., Lewis Publishers, Boca Raton, FL.
- Montanari, A. and Koutsoyiannis, D. (2014). Modeling and mitigating natural hazards: stationarity is immortal! *Water Resour. Res* 50, WR016092
- O’Gorman, P. A. and T. Schneider. (2008). The hydrological cycle over a wide range of climates simulated with an idealized GCM. *J. Climate*, **21**, 3815–3832,
- O’Gorman, P. A. (2015). *Precipitation Extremes Under Climate Change*. Current Climate Change Reports. 1. 10.1007/s40641-015-0009-3.
- Olsen, J. R., Lambert, J. H., and Haines, Y. Y. (1998). Risk of extreme events under nonstationary conditions. *Risk Anal.*, 18(4), 497–510.
- Önol, B., Bozkurt, D., Ufuk, U.T., Sen, O. L., Dalfes, N. (2014). Evaluation of the twenty-first century RCM simulations driven by multiple GCMs over the Eastern Mediterranean-Black Sea region. *Climate Dynamics*. 42. 1949-1965. 10.1007/s00382-013-1966-7.

- Önol, B., Semazzi F. H. M. (2009). Regionalization of climate change simulations over the Eastern Mediterranean J. Clim., 22 (8), pp. 1944-1961, 10.1175/2008JCLI1807.1
- Ozturk, I., Ceber, Z.P., Türkeş, M., Kurnaz, M.L. (2015). Projections of climate change in the Mediterranean Basin by using downscaled global climate model outputs Int. J. Climatol., 35 (14) (2015), pp. 4276-4292,
- Pendergrass, G. Angeline & Hartmann, Dennis. (2014). Changes in the Distribution of Rain Frequency and Intensity in Response to Global Warming. Journal of Climate. 27. 8372-8383. <https://doi.org/10.1175/JCLI-D-14-00183.1>
- Read, L.K, and Vogel R.M. (2015). “Reliability, return periods and risk under nonstationarity, Water Resources Res., doi:10.1002/2015WR017089
- Robert M. H. (2010). USGS “a perspective on nonstationarity and water management” Workshop on nonstationarity, hydrological frequency analysis and water management 2010, Colorado Water Institute. P5-14
- Rummukainen, M. (2010). State-of-the-art with regional climate models. WIREs Clim Change, 1: 82-96. doi:10.1002/wcc.8
- Salas, J.D., Obeysekera, J. (2014). Revisiting the concepts of return period and risk for non-stationary hydrologic extreme events. J. Hydrol. Eng. 19, 554–568. [http:// dx.doi.org/10.1061/\(ASCE\)HE.1943-5584.0000820](http://dx.doi.org/10.1061/(ASCE)HE.1943-5584.0000820).
- Salvati, L., Sateriano, A., and Zitti, M. (2013). Long-term land cover changes and climate variations – A country-scale approach for a new policy target. Land Use Policy, 30: 401-407.
- Seibert, J. (1997). Estimation of Parameter Uncertainty in the HBV Model: Paper presented at the Nordic Hydrological Conference (Akureyri, Iceland - August 1996). *Hydrology Research* 1 August 1997; 28 (4-5): 247–262. doi: <https://doi.org/10.2166/nh.1998.15>
- Sensoy, Serhat & TÜRKOĞLU, Necla & AKÇAKAYA, Alper & Ekici, Mithat & ULUPINAR, Yusuf & Demircan, Mesut & Atay, Hakkı & TÜVAN, Arzu & DEMİRBAŞ, Hatice. (2013). Trends in Turkey Climate Indices from 1960 to 2010.
- Sensoy, Serhat & Demircan, Mesut. (2016). Climate of Turkey. Article: March 2016
- Small, D., Islam, S., and Vogel, R. M. (2006). Trends in precipitation and streamflow in the eastern US. Paradox or perception? Geophys. Res. Lett., 33, L03403, doi:10.1029/2005GL024995.

- Sönmez, I. (2013). Quality control tests for western Turkey Mesonet. *Meteorol. Appl.* 20: 330 – 337, doi: 10.1002/met.1286
- Sunyer, M. A., Hundedcha, Y., Lawrence, D., Madsen, H., Willems, P., Martinkova, M., Vormoor, K., Bürger, G., Hanel, M., Kriaučiūnienė, J., Loukas, A., Osuch, M., and Yücel, I. (2015). Inter-comparison of statistical downscaling methods for projection of extreme precipitation in Europe, *Hydrol. Earth Syst. Sci.*, 19, 1827-1847, <https://doi.org/10.5194/hess-19-1827-2015>, 2015.
- Tayanç, M., İm, U., Doğruel, M., and Karaca, M. (2009). Climate change in Turkey for the last half century. *Climatic Change*, 94: 483-502.
- Toros, H. (2012). Spatio-temporal variation of daily extreme temperatures over Turkey. *Int. J. Climatol.*, 32: 1047-1055. <https://doi.org/10.1002/joc.2325>
- Trenberth, K. E., Dai, A., Rasmussen R. M., and Parsons, D. B. (2003). The changing character of precipitation, *Bull. Am. Meteorol. Soc.*, 84, 1205–1217, doi:10.1175/BAMS-84-9-1205.
- Turgay, P., and Kahya, E. (2005). Trend analysis in Turkish precipitation data *Hydrol. Process.* 20, 2011–2026 (2006) Published online 23 December 2005 in Wiley InterScience ([www.interscience.wiley.com](http://www.interscience.wiley.com)). DOI: 10.1002/hyp.5993
- Türkeş, M. (1996). Spatial and temporal analysis of annual rainfall variations in Turkey. *International Journal of Climatology*, 16: 1057-1076.
- Türkeş, M., Koç, T., and Sariş, F. (2009). Spatiotemporal variability of precipitation total series over Turkey. *International Journal of Climatology*, 29: 1056-1074.
- Türkeş, M., Sümer, U.M., and Demir, İ. (2002). Re-evaluation of trends and changes in mean, maximum, and minimum temperatures of Turkey for the period 1929-1999. *International Journal of Climatology*, 22: 947-977.
- Türkeş, M., Yozgatlıgil, C., Batmaz, İ., İyigün, C., Kartal, Koç E., Fahmi, F. M., Aslan, S. (2016). Has the climate been changing in Turkey? Regional climate change signals based on a comparative statistical analysis of two consecutive time periods, 1950-1980 and 1981-2010. *Clim Res* 70:77-93.
- Vrac, M., Drobinski, P., Merlo, A., Herrmann, M., Lavaysse, C., Li, L., and Somot, S. (2012). Dynamical and statistical downscaling of the French Mediterranean climate: uncertainty assessment, *Nat. Hazards Earth Syst. Sci.*, 12, 2769-2784, <https://doi.org/10.5194/nhess-12-2769-2012>
- WEB1:[http://www.nasa.gov/audience/forstudents/k-4/stories/what-is-climate-change-k4.html#.VAIpS\\_mSx8E](http://www.nasa.gov/audience/forstudents/k-4/stories/what-is-climate-change-k4.html#.VAIpS_mSx8E). 14/, Last Accessed: June 05, 2018.

- WEB2:<http://www.metoffice.gov.uk/climate-guide/climate-change/>, Last Accessed: June 5, 2018.
- WEB3:<https://help.theclimatedatafactory.com/technical-documentation/limitations-in-bias-adjustment-methods/>, Last Accessed: June 05, 2018.
- WEB4:<https://www.c2es.org/content/extreme-precipitation-and-climate-change/>, Last Accessed: April 06, 2018
- WEB5:<http://sciencepolicy.colorado.edu/socas/weather1/adams.html/>, Last Accessed: August 30, 2018
- Webb, J. W., and White K. D. (2010). "Nonstationarity in water management: USACE perspective" Workshop on nonstationarity, hydrological frequency analysis and water management 2010, Colorado Water Institute. P16-19
- Wigley, T. M. L. (1988). "The effect of climate change on the frequency of absolute extreme events." *Clim. Monit.*, 17(1–2), 44–55
- Willett, K. M., Gillett, N. P., Jones, P. D., and Thorne, P. W. (2007). Attribution of observed surface humidity changes to human influence, *Nat. Lett.*, 449, 710–712, doi:10.1038/nature06207.
- Yang, Wei & Andréasson, Johan & Graham, L & Olsson, Jonas & Rosberg, Jörgen & Wetterhall, Fredrik. (2010). Distribution based scaling to improve usability of RCM regional climate model projections for hydrological climate change impacts studies. *Hydrology Research*. 41. 10.2166/nh.2010.004
- Yılmaz, K.K. and Yazıcıgil, H., (2011). Potential Impacts of Climate Change on Turkish Water Resources: A Review. In *Climate Change and its Effects on Water Resources*, by A. Baba, G. Tayfur, O. Gündüz, K.W.F. Howard, M.J. Friedel and A. Chambel, 105-114. Netherland: *Springer*
- Yucel, I., Güventürk, A. and Sen, O. L. (2015). Climate change impacts on snowmelt runoff for mountainous transboundary basins in eastern Turkey. *Int. J. Climatol.*, 35: 215–228. doi:10.1002/joc.3974
- Zhang, A., Zhang, C., Fu, G., Wang, B., Bao, Z., and Zheng, H. (2012). Assessments of impacts of climate change and human activities on runoff with SWAT for the Huifa River basin, northeast China. *Water Resour. Manage.*, 26, 2199–2217, doi:10.1007/s11269-012-0010-8



## APPENDICES

### A. PROGRAMING CODES

```
##### Normal Distribution#####  
# This file contains the following functions:  
# nor.fit  
"nor.fit"<-  
  function(xdat, ydat = NULL, mul = NULL, sigl = NULL, mulink = identity, siglink  
= identity, muinit = NULL, siginit = NULL, show = TRUE, method = "Nelder-  
Mead", maxit = 10000, ...)  
  {  
    #  
    # finds mles etc for log normal  
    #  
    z <- list()  
    npmu <- length(mul) + 1  
    npsc <- length(sigl) + 1  
    z$trans <- FALSE  
    in2 <- sqrt(6 * var(xdat))/pi  
    in1 <- mean(xdat) - 0.57722 * in2  
    if(is.null(mul)) {  
      mumat <- as.matrix(rep(1, length(xdat)))  
      if( is.null( muinit)) muinit <- in1  
    }  
    else {  
      z$trans <- TRUE  
      mumat <- cbind(rep(1, length(xdat)), ydat[, mul])  
      if( is.null( muinit)) muinit <- c(in1, rep(0, length(mul)))  
    }  
    if(is.null(sigl)) {  
      sigmat <- as.matrix(rep(1, length(xdat)))  
      if( is.null( siginit)) siginit <- in2  
    }  
    else {  
      z$trans <- TRUE  
      sigmat <- cbind(rep(1, length(xdat)), ydat[, sigl])  
      if( is.null( siginit)) siginit <- c(in2, rep(0, length(sigl)))  
    }  
    z$model <- list(mul, sigl)  
    z$link <- c(deparse(substitute(mulink)), deparse(substitute(siglink)))  
    init <- c(muinit, siginit)
```

```

nor.lik <- function(a) {
  # calculates neg log lik of normal
  mu <- mulink(mumat %**% (a[1:npmu]))
  sc <- siglink(sigmat %**% (a[seq(npmu + 1, length = npsc)]))
  if(any(sc <= 0)) return(10^6)
  y <- (xdat - mu)/sc
  sum(log(2*pi*sc^2))/2+sum((y^2)/2)
}
x <- optim(init, nor.lik, hessian = TRUE, method = method,
          control = list(maxit = maxit, ...))
z$convc <- x$convergence
if(!z$convc) {
  mu <- mulink(mumat %**% (x$par[1:npmu]))
  sc <- siglink(sigmat %**% (x$par[seq(npmu + 1, length = npsc)]))
  z$nullh <- x$value
  z$data <- xdat
  if(z$trans) {
    z$data <- as.vector((xdat - mu)/sc)
  }
  z$mle <- x$par
  z$cov <- solve(x$hessian)
  z$se <- sqrt(diag(z$cov))
  z$vals <- cbind(mu, sc)
}
if(show) {
  if(z$trans)
    print(z[c(2, 3, 4)])
  else print(z[4])
  if(!z$convc)
    print(z[c(5, 7, 9)])
}
class(z) <- "nor.fit"
invisible(z)
}

```

```

inname1="D:/ydat.txt"
Y=read.table(inname1)
y=Y[,1]
ydat=matrix(y)
inname2="D:/xdat.txt"
X1=read.table(inname2)
X=as.matrix(X1)

```

```

staall=77
param=array(NA,dim=c(staall,3))

```

```

## loop for stations ##
for(sta in 1:staall){
  xdat=X[,sta]
  aa = nor.fit(xdat, ydat = NULL, mul = NULL, sigl = NULL, mulink = identity,
siglink = identity, muinit = NULL, siginit = NULL, show = TRUE, method =
"Nelder-Mead", maxit = 10000)

  V1=aa$nullh
  V2=aa$mle
  param[sta,1:3]=c(V2,V1)

  print(paste(sta))
}

##### Lognormal Distribution#####

rm(list=ls())
# This file contains the following functions:
# log.nor.fit
"log.nor.fit"<-
function(xdat, ydat = NULL, mul = NULL, sigl = NULL, mulink = identity, siglink
= identity, muinit = NULL, siginit = NULL, show = TRUE, method = "Nelder-
Mead", maxit = 10000, ...)
{
  #
  # finds mles etc for log log.normal
  #
  z <- list()
  npmu <- length(mul) + 1
  npsc <- length(sigl) + 1
  z$trans <- FALSE
  asd=log(xdat)
  in2 <- sqrt(6 * var(asd))/pi
  in1 <- mean(asd) - 0.57722 * in2
  if(is.null(mul)) {
    mumat <- as.matrix(rep(1, length(xdat)))
    if( is.null( muinit)) muinit <- in1
  }
  else {
    z$trans <- TRUE
    mumat <- cbind(rep(1, length(xdat)), ydat[, mul])
    if( is.null( muinit)) muinit <- c(in1, rep(0, length(mul)))
  }
  if(is.null(sigl)) {
    sigmat <- as.matrix(rep(1, length(xdat)))

```

```

  if( is.null( siginit)) siginit <- in2
}
else {
  z$trans <- TRUE
  sigmat <- cbind(rep(1, length(xdat)), ydat[, sigl])
  if( is.null( siginit)) siginit <- c(in2, rep(0, length(sigl)))
}
z$model <- list(mul, sigl)
z$link <- c(deparse(substitute(mulink)), deparse(substitute(siglink)))
init <- c(muinit, siginit)
log.nor.lik <- function(a) {
  # calculates neg log lik of log.normal
  mu <- mulink(mumat %**% (a[1:npmu]))
  sc <- siglink(sigmat %**% (a[seq(npmu + 1, length = npsc)]))
  if(any(sc <= 0)) return(10^6)
  y <- (log(xdat) - mu)/sc
  sum(log(2*pi*sc^2))/2+sum(log(xdat))+sum((y^2)/2)
}
x <- optim(init, log.nor.lik, hessian = TRUE, method = method,
          control = list(maxit = maxit, ...))
z$convc <- x$convergence
if(!z$convc) {
  mu <- mulink(mumat %**% (x$par[1:npmu]))
  sc <- siglink(sigmat %**% (x$par[seq(npmu + 1, length = npsc)]))
  z$nullh <- x$value
  z$data <- xdat
  if(z$trans) {
    z$data <- as.vector((xdat - mu)/sc)
  }
  z$mle <- x$par
  z$cov <- solve(x$hessian)
  z$se <- sqrt(diag(z$cov))
  z$vals <- cbind(mu, sc)
}
if(show) {
  if(z$trans)
    print(z[c(2, 3, 4)])
  else print(z[4])
  if(!z$convc)
    print(z[c(5, 7, 9)])
}
class( z ) <- "log.nor.fit"
invisible(z)

```

## **B. MISSING DATA**

Following stations contained missing data years for daily precipitation and temperature.

1. Kartal (2005,2006,2007)
2. Eskişehir (1978,1979,1980,2013,2014)
3. Hakkari (1977)
4. Kırıkkale (1996)
5. Balıkesir (2007,2008)
6. Bitlis (2011)



## **CURRICULUM VITAE**

### **PERSONAL INFORMATION**

Surname, Rizwan Aziz  
Nationality: Pakistani(Pak)  
Date and Place of Birth: 18 June 1987, Faisalabad-Pakistan  
Marital Status: Single  
Email: rizwan.aziz@metu.edu.tr

### **EDUCATION**

Degree	Institution	Year of Graduation
M.Sc.	UET, Lahore	2011
B.Sc.	Univ. of Agriculture, Faisalabad.	2009
F.Sc.	GC University, Faisalabad	2005

### **FOREIGN LANGUAGES**

English.

### **HOBBIES**

Traveling, Football, Music